Surface modification of styrene maleic anhydride nanofibers for efficient capture of Mycobacterium tuberculosis

by

Lizl Cronje

Dissertation presented for the degree of PhD in Chemistry and Polymer Science

University of Stellenbosch
Faculty of Science
Department of Chemistry and Polymer Science

Promoter: Prof. B. Klumperman

December 2012

This work is dedicated to the people who believed in me, who supported me during this time and filled my life with joy and happiness: my dear husband, Danie, my darling daughter, Michele, and my loving parents, Alet and Flip Simpson.

Declaration

By submitting this thesis/dissertation, I declare that the entirety of the work contained therein is my own, original work, that I am the sole author thereof (save to the extent explicitly otherwise stated), that reproduction and publication thereof by Stellenbosch University will not infringe any third party rights and that I have not previously in its entirety or in part submitted it for obtaining any qualification.

Lizl Cronje December 2012

Abstract

Tuberculosis (TB) is a major cause of morbidity and mortality across the world, affecting adults and children. Children infected with TB differ from adults, as their immunological and patho-physiological response to the disease is different. Although there are a variety of tests available for TB diagnosis, they have limitations when used to diagnose paediatric TB. Children are also unable to generate sputum spontaneously when required for the use in culture or microscopy as diagnostic method. Children however do produce sputum, containing the TB bacilli, which they swallow. If the TB bacilli can therefore be retrieved from the stomach and tested, TB can be diagnosed using gastric samples.

In this thesis, a variety of styrene maleimide copolymer (SMI) derivatives were prepared as potential *M. tuberculosis*-capturing platforms. This was done by modifying poly(styrene-*co*-maleic anhydride) (SMA) with a variety of primary amine compounds, selected based on possible chemical interactions with the *M. tuberculosis* cell wall. All the prepared copolymer derivatives were electrospun into nanofibrous mats using the single needle electrospinning technique to yield SMI nanofibers, functionalized with different compounds. Some of the functionalized SMI nanofibers were prepared by surface-functionalization of the polymer nanofibers after electrospinning and some by modification of the polymer before electrospinning.

Affinity studies were conducted at neutral and low pH between the different functionalized SMI nanofibers and two mycobacterium strains, namely the bacillus Calmette-Guérin strain of *Mycobacterium bovis* (BCG) and *M. tuberculosis*, to evaluate the surfaces of the modified SMI nanofibers as mycobacterium-capturing platforms. The successful capture of BCG onto the surfaces of the various functionalized nanofibers was confirmed by SEM and fluorescence microscopy (FM). Analysis of the SEM and FM images indicated that the SMI nanofibers, functionalized with a C_{12} aliphatic quaternary ammonium moiety (SMI-qC_{12}), captured BCG the most effectively through a combination of ionic and hydrophobic interaction. Concentration and time studies revealed that the extent of this interaction was dependent on incubation time and concentration of BCG. The affinity studies with BCG also concluded that the polymer used for the nanofibrous-capturing platform should not be too hydrophobic in character as this caused poor wetting of the functionalized nanofibers, thus preventing close contact with the mycobacteria and a reduction in the capture effectivity of the polymer nanofibers.

The successful capture of *M. tuberculosis* onto the SMI-qC_{12} nanofibrous surface was confirmed by FM, light microscopy (LM) and polymerase chain reaction (PCR). The extent of this interaction was dependent on the concentration *of M. tuberculosis*. The detection of *M. tuberculosis* using FM and LM as detection methods was simplified by the tendency of *M. tuberculosis* to clump together in clusters on the hydrophobic surface of the SMI-qC_{12} nanofibers. As a result of this clustering, FM and LM were therefore regarded as feasible detection methods to image *M. tuberculosis* on the surface of the SMI-qC_{12} nanofibers, even at relatively low concentration of *M. tuberculosis*.

Opsomming

Tuberkulose (TB) is 'n groot oorsaak van morbiditeit en mortaliteit regoor die wêreld en affekteer volwassenes en kinders. Kinders wat met TB geïnfekteer is, se immunologiese en patofisiologiese reaksie op die siekte verskil van die van volwassenes en dit het belangrike implikasies vir die diagnose van TB in kinders. Alhoewel daar 'n verskeidenheid van toetse beskikbaar is vir die diagnose van TB, het hulle beperkings wanneer dit gebruik word om pediatriese TB te diagnoseer. Kinders kan ook nie spontaan sputum produseer as dit nodig is vir die gebruik in kultuur of mikroskopie as diagnostiese metode. Kinders produseer egter wel sputum, wat die TB basille bevat, wat hulle dan insluk. As die TB basille uit die maag versamel kan word en getoets kan word, kan TB gediagnoseer word met behulp van maag monsters.

In hierdie tesis is 'n verskeidenheid van stireen maleimied kopolimeer (SMI) afgeleides voorberei as potensiële *Mycobacterium tuberkulose (Mtb)*-vaslegging platforms. Dit is gedoen deur die modifikasie van poli(stireen-*ko*-maleïen anhidried) (SMA) met 'n verskeidenheid primêre amien verbindings as oppervlak-funksionaliseringsagente. Hierdie primêre amien verbindings is gekies op grond van moontlike chemiese interaksies met die *Mtb* selwand. Al die voorbereide kopolimeer afgeleides is elektrogespin in nanoveselagtige matte met behulp van die enkel-naald elektrospin tegniek om SMI nanovesels te lewer wat gefunksionaliseer is met verskillende verbindings. Sommige van die gefunksionaliseerde SMI nanovesels is berei deur oppervlak-funksionalisering van die polimeer nanovesels na elektrospin, en sommige deur die modifikasie van die polimeer voor elektrospin.

Affiniteitstudies is uitgevoer, by neutrale en lae pH, tussen die verskillende gefunksionaliseerde SMI nanovesels en twee mikobakterium rasse, naamlik die basillus Calmette-Guérin ras van *Mycobacterium bovis* (BCG) en *M. tuberculosis*, om die oppervlaktes van die gewysigde SMI nanovesels te evalueer as mikobakterium-vaslegging platforms. Ontleding van die SEM en FM beelde het aangedui dat die SMI nanovesels, gefunksionaliseer met 'n C_{12} alifatiese kwaternêre ammonium groep (SMI-qC_{12}), BCG die doeltreffendste vasgevang het deur 'n kombinasie van ioniese en hidrofobiese interaksie. Konsentrasie- en tydstudies tussen BCG en SMI-qC_{12} het aangedui dat die omvang van hierdie interaksie afhanklik is van inkubasietyd en konsentrasie van BCG. Die affiniteitstudies met BCG het ook aangedui dat die polimeer wat gebruik word vir die nanoveselagtige-vaslegging platform nie te hidrofobiese moet wees nie, aangesien dit swak benatting van die gefunksionaliseerde nanovesels veroorsaak, en dus noue kontak met die mikobakterieë voorkom met 'n gevolglike vermindering in die vasvang-effektiwiteit van die polimeer nanovesels.

Die suksesvolle vasvang van *M. tuberculosis* op die SMI-qC_{12} nanovesels is bevestig deur FM, lig mikroskopie (LM) en polimerase kettingreaksie (PKR). Die opsporing van *Mtb* deur die gebruik van FM en LM as opsporingmetodes is vergemaklik deur die tendens van *Mtb* om in groepies saam te pak op die hidrofobiese oppervlak van die SMI-qC_{12} nanovesels. As gevolg van hierdie groepering, is FM en LM dus haalbare opsporingmetodes om *M. tuberculosis* op die oppervlak van die SMI-qC_{12} nanovesels waar te neem, selfs by relatief lae konsentrasie van *M. tuberculosis*.

Table of contents

INDEX

LIST OF FIGURES

LIST OF SCHEMES

LIST OF TABLES

LIST OF SYMBOLS

E	Electric field strength
V	Voltage difference between electrodes
d	Distance between electrodes
K_i	Binding affinity
kV	Kilovolt
Đ	Dispersity
M_w	Weight average molecular weight

LIST OF ACRONYMS

TB	Tuberculosis
M. tuberculosis	*Mycobacterium tuberculosis*
SMA	Poly(styrene-*co*-maleic anhydride)
SMI	Poly(styrene-*co*-maleimide)
BCG	*Mycobacterium bovis* bacillus Calmette-Guérin
CFU	Colony-forming units
LTBI	Latent tuberculosis infection
TST	Tuberculin skin test
PPD	Purified protein derivative
IFN-γ	Interferon-gamma
IGRAs	Interferon-gamma assays
AFB	Acid-fast bacilli
ZN	Ziehl-Neelsen
NALC	*N*-acetyl-L-cysteine
NAA	Nucleic acid amplification
LED	Light emitting diode
CT	Computed tomography
MODS	Microscopic observation drug-susceptibility
TLA	Thin-layer agar
NRA	Nitrate reductase assay
PCR	Polymerase chain reaction
mAGP	Mycolyl arabinogalactan-peptidoglycan
TDM	Trehalose-6,6'-dimycolate
PGL	Phenolic glycolipids
LOS	Liposaccharides
PIMs	Phosphatidylinositol mannosides
PE	Phosphatidyl ethanolamine
LM	Lipomannan
LAM	Lipoarabinomannan

SL-1	Sulfolipid-1
HBHA	Heparin-binding haemagglutinin adhesion
MR	Macrophage mannose receptor
MBP	Mannose binding protein
DC-SIGN	Dendritic cell-specific intercellular adhesion molecule grabbing non-integrin
Sp-A	Lung surfactant protein
Sp-D	Lung surfactant protein
CRD	Carbohydrate recognition domain
GAG	Glycosaminoglycan
P(St-*alt*-MAnh)	Poly(styrene-*alt*-maleic anhydride)
P(St-*co*-MAnh)	Poly(styrene-*co*-maleic anhydride)
P(St-*alt*-MI)	Poly(styrene-*alt*-maleimide)
P(St-*co*-MI)	Poly(styrene-*co*-maleimide)
ATR-FTIR	Attenuated total reflectance Fourier transform infrared spectroscopy
SEM	Scanning electron microscopy
^{1}H-NMR	Proton nuclear magnetic resonance spectroscopy
^{13}C-NMR	Carbon nuclear magnetic resonance spectroscopy
SEC	Size exclusion chromatography
DMF	*N,N*-dimethylformamide
Gluc	Glucosamine
Man	Mannosamine
Con A	Concanavalin A
BCML	N_{α},N_{α}-bis(carboxymethyl)-L-lysine hydrate
DMSO	Dimethyl sulfoxide
Boc	Di-*tert*-butyl-dicarbonate
IR	Infrared
Ninhydrin	2,2-Dihydroxyindane-1,3-dione
HRP	Horseradish peroxidase
tC_{12}	*N*-dodecyl-*N*-propyl-propane-1,3-diamine
tC_{16}	*N*-hexadecyl-*N*-propyl-propane-1,3-diamine

qC_{24}	*N,N*-didodecyl-*N*-propyl-propane-1,3-diamine
qC_{32}	*N,N*-dihexadecyl-*N*-propyl-propane-1,3-diamine
PBS	Phosphate buffered solution
$CDCl_3$	Deuterated chloroform
SMI-tC	Styrene-[*N*-3-(*N',N'*-dimethylamino)propyl maleimide] copolymer
SMI-C_{12}	Styrene-[*N*-dodecyl-maleimide] copolymer
SMI-C_{16}	Styrene-[*N*-hexadecyl-maleimide] copolymer
SMI-qC_2	Styrene-[*N*-3-(*N'*-ethyl-*N',N'*-dimethylammonium)propyl maleimide] copolymer
SMI-qC_{12}	Styrene-[*N*-3-(*N'*-dodecyl-*N',N'*-dimethylammonium)propyl maleimide] copolymer
SMI-qC_{16}	Styrene-[*N*-3-(*N'*-hexadecyl-*N',N'*-dimethylammonium)propyl maleimide] copolymer
M. smegmatis	*Mycobacterium smegmatis*
FAP	Fibronectin-binding protein
FM	Fluorescence microscopy
LM	Light microscopy
dNTP's	Dinucleotide triphosphates
TAE buffer	Tris-acetate-EDTA buffer

Chapter 1: Introduction and objectives

1.1 Introduction

Tuberculosis (TB) is a major cause of morbidity and mortality across the world and is currently one of the most devastating diseases worldwide.[1,2] The World Health Organization estimates that more than 2 billion people are infected with *Mycobacterium tuberculosis*, the pathogen that causes TB.[3-5] Children across the world are also greatly affected by TB as it causes severe illness and death, especially in young children and infants.[2,3,6]

Young children are highly susceptible to developing the active disease following primary *Mycobacterium tuberculosis* (*M. tuberculosis)* infection due to their underdeveloped immune system. Children infected with tuberculosis differ from adults, as their immunological and patho-physiological response to the disease is different.[7-9] This has important and significant implications for the prevention, diagnosis and treatment of tuberculosis in children.[10] In addition to this, the accurate diagnosis of childhood TB is particularly problematic for a variety of reasons, such as non-specific symptoms, low bacillary yield, poor specimen collection methods and low sensitivities of the respective diagnostic tests.[11,12]

Currently, a variety of test methods are used for the diagnosis of latent and active TB, such as the tuberculin skin test and Interferon-gamma assay (latent TB) and sputum smear microscopy, chest radiography, culture and nucleic acid amplification tests (active TB).[7,8] These tests unfortunately all have limitations. Recently, many advances have been made in the research fields of biotechnology and molecular biology where several new and improved diagnostic tests for tuberculosis were introduced. However, the majority of these new and improved tests are far too costly and complicated to be of any real use to the vast majority of infected people living in resource-poor areas.[13] An easy and inexpensive diagnostic test thus remains elusive and the conventional methods of diagnosis rely on tests with limitations.

The current tests available for the diagnosis of paediatric tuberculosis also have limitations, and the complete range of tests is not always readily accessible in areas where tuberculosis infection is common and widespread.[10] Due to these reasons, the search is still on for new and/or improved specimen collection methods as well as better diagnostic methods. The sensitivity of many of the current detection methods can also be increased by improving the specimen collection methods and specimen processing procedures. For faster and more accurate diagnosis of tuberculosis in young children, it is therefore vital that the specimen collection method is improved in order to provide samples with adequate bacteriological load for fast and accurate detection.[9,14]

This study used the Entero-string test as the basic model with the aim to develop a specimen collection method for gastric samples in young children undergoing investigation for TB infection. The goal is to increase the yield of *M. tuberculosis* for faster and more accurate diagnosis of TB using conventional light microscopy or fluorescence microscopy. This could be accomplished by functionalizing a polymer with a chemical entity that can capture *M. tuberculosis* onto the

functionalized surface of the polymer under gastric conditions, thereby increasing the mycobacterial yield. An increased yield in *M. tuberculosis* should then result in faster and more accurate diagnosis of TB in young children.

Poly(styrene-*co*-maleic anhydride) (SMA) was selected as the polymer to be modified as it is an inexpensive and versatile polymer that can easily be modified via its highly reactive maleic anhydride group.[15-20] The polymer modification was done using chemical groups that were expected to aid the capture of *M. tuberculosis*. Another advantage of SMA is that it can also be electrospun with ease and functionalized before or after electrospinning.[21]

Electrospinning was selected as the polymer processing method as it is a simple and versatile technique that allows the production of continuous polymer nanofibers from a wide variety of polymers.[22-24] These polymer nanofibers have high specific surface areas and high aspect ratios that make them ideal for a wide variety of applications, such as filtration media, biomedical textiles and affinity membranes.[25-27]

These functionalized polymer nanofibers were therefore considered good candidates for the *M. tuberculosis*-capturing device.

1.2 Objectives

The basic motivation for this work was to synthesize a capturing platform for *M. tuberculosis* in a low pH environment. For this purpose, poly(styrene-*co*-maleic anhydride) (SMA) was chosen as polymer and modified with a variety of chemical groups selected based on possible chemical interactions with the *M. tuberculosis* cell wall. SMA can easily be synthesized through conventional free radical copolymerization and is also commercially available in varying grades based on molar mass and anhydride content. Modification took place via imidization of the highly reactive maleic anhydride unit of SMA to yield poly(styrene-*co*-maleimide) (SMI) derivatives.

Electrospinning was used as technique to produce continuous polymer nanofibers with a high specific surface area. SMA was thus modified with a variety of compounds to yield modified SMI derivatives and electrospun to produce functionalized polymer nanofibers. Some of the functionalized SMI nanofibers were prepared by surface-functionalization of the polymer nanofibers after electrospinning and some by modification of the polymer before electrospinning.

The functionalized SMI nanofibers were subsequently evaluated as potential capturing platforms for *Mycobacterium bovis* bacillus Calmette-Guérin (BCG) (as *M. tuberculosis*-mimic) and finally for *M. tuberculosis.*

The objectives of the study can therefore be summarized as follows:

1. To synthesize a high molar mass alternating styrene-maleic anhydride (SMA) copolymer using conventional free radical copolymerization that can be electrospun into polymer nanofibers.

2. To synthesize various functionalized poly(styrene-*alt*-maleimide) and poly(styrene-*co*-maleimide) nanofibers by first electrospinning the parent polymer into nanofibers and thereafter surface-functionalizing it with a variety of chemical compounds via nucleophilic acyl substitution.

3. To synthesize various functionalized poly(styrene-*alt*-maleimide) (SMI) nanofibers by first modifying the parent polymer with a variety of chemical compounds via nucleophilic acyl substitution and thereafter electrospinning it.

4. To evaluate the interaction between BCG as *M. tuberculosis*-mimic and all the functionalized SMI nanofibers at pH 7 and 2 to determine whether these functionalized nanofibers can capture BCG.

5. To evaluate the interaction between *M. tuberculosis* and selected SMI nanofibers at pH 2 to determine if *M. tuberculosis* can be captured onto the surface of these nanofibers.

1.3 Layout of the thesis

Chapter 1: A brief introduction to the scope of this study is offered and the objectives set out to achieve are highlighted.

Chapter 2: An overview of previous research related to tuberculosis (TB) and the diagnosis thereof is presented here. The specific problems related to the diagnosis of paediatric TB are highlighted, with particular reference to the approaches used for possible improvement. To conclude, the factors that had to be taken into account in developing a polymer as an affinity membrane for the specimen collection of *M. tuberculosis* are discussed.

Chapter 3: This chapter describes the synthesis of poly(styrene-*alt*-maleic anhydride), the electrospinning of poly(styrene-*alt*-maleic anhydride) and poly(styrene-*co*-maleic anhydride) into nanofibers, and the subsequent surface-functionalization protocols of the resultant nanofibers to yield functionalized styrene-maleimide copolymer nanofibers. The characterization of SMA and the functionalized SMI nanofibers are included.

Chapter 4: This chapter presents the synthesis and characterization of the alternating styrene-maleimide copolymer derivatives, as well as the electrospinning conditions of these SMI derivatives to yield functionalized styrene-maleimide copolymer nanofibers. The characterization of the functionalized SMI nanofibers is included.

Chapter 5: In this chapter, affinity studies between the different functionalized SMI nanofibers and two mycobacterium strains, namely BCG and *M. tuberculosis*, are presented. These affinity studies were done at different pH values and the incubated fibers were evaluated using a variety of detection methods.

Chapter 6: Conclusions and recommendations for future research are highlighted in this chapter.

1.4 References

1. Dye, C. *Lancet* **2006**, *367*, 938-940.

2. Walls, T.; Shingadia, D. *J. Infect*. **2004**, *48*, 13-22.

3. Corrigan, D.L.; Paton, J.Y. *Breathe* **2007**, *3*, 351-363.

4. Marais, B.J.; Pai, M. *Paediatr. Respir. Rev*. **2007**, *8*, 124-133.

5. Marais, B.J.; Pai, M. *Br. Med. J*. **2007**, *92*, 446-452.

6. Marais, B.J.; Gie, R.P.; Schaaf, H.S.; Beyers, N.; Donald, P.R.; Starke, J.R. *Am. J. Respir. Crit. Care Med.* **2006**, *173*, 1078-1090.

7. Pai, M.; Minion, J.; Sohn, H.; Zwerling, A.; Perkins, M.D. *Clin. Chest Med.* **2009**, *30,* 701-716.

8. Pai, M.; Minion, J.; Steingart, K.; Ramsay, A. *Curr. Opin. Pulm. Med*. **2010**, *16*, 271-284.

9. Cuevas, L.E. *Indian J. Pediatr*. **2010**, 1-7.

10. Maher, D. *Int. J. Tuberc. Lung Dis*. **2006**, *10*, 1091–1097.

11. Eamranond, P.; Jaramillo, E. *Int. J. Tuberc. Lung Dis*. **2001**, *5,* 594-603.

12. Oberhelman, R.A.; Soto-Castellares, G.; Gilman, R.H.; Caviedes, L.; Castillo, M.E.; Kolevic, L.; et al. *Lancet Infect. Dis.* **2010**, *10*, 612-620.

13. Butt, T.; Ahmad, R.N.; Kazmi, S.Y.; Afzal, R.K.; Mahmood, A. *J. Coll. Physicians Surg. Pak.* **2003**, *13*, 728-734.

14. Urbanczik, R. *Int. J. Tuberc. Lung Dis*. **2010**, *14*, 1087-1093.

15. Lai, X.; Sun, C.; Tian, H.; Zhao, W.; Gao, L. *Int. J. Pharm*. **2008**, *352*, 66-73.

16. Stoilova, O.; Ignatova, M.; Manolova, N.; Godjevargova, T.; Mita, D.; Rashkov, I. *Eur. Polym. J.* **2010**, *46*, 1966-1974.

17. Vermeesch, I.; Groeninckx, G. *J. Appl. Polym. Sci.* **1994**, *53*, 1365-1373.

18. Wang, K.; Huang, W.; Xia, P.; Gao, C.; Yan, D. *React. Funct. Polym.* **2002**, *52*, 143-148.

19. Henry, S.M.; El-Sayed, M.E.H.; Pirie, C.M.; Hoffman, A.S.; Stayton, P.S. *Biomacromolecules* **2006**, *7*, 2407-2414.

20. Donati, I.; Gamini, A.; Vetere, A.; Campa, C.; Paoletti, S. *Biomacromolecules* **2002**, *3*, 805-812.

21. Tang, C.; Ye, S.; Liu, H. *Polymer* **2007**, *48*, 4482-4491.

22. Doshi, J.; Reneker, D.H. *J. Electrostatics* **1995**, *35*, 151-160.

23. Frenot, A.; Chronakis, I.S. *Curr. Opin. Colloid Interface Sci.* **2003**, *8*, 64-75.

24. Huang, Z.M.; Zhang, Y.Z.; Kotaki, M.; Ramakrishna, S. *Compos. Sci. Technol.* **2003**, *63*, 2223-2253.

25. Reneker, D.H.; Chun, I. *Nanotechnology* **1996**, *7*, 216-223.

26. Teo, W.E.; Gopal, R.; Ramaseshan, R.; Fujihara, K.; Ramakrishna, S. *Polymer* **2007**, *48*, 3400-3405.

27. Wang, X.; Kim, Y.G.; Drew, C.; Ku, B.C.; Kumar, J. *Nano Lett.* **2004**, *4*, 331-334.

Chapter 2: Historical and theoretical background

2.1 Tuberculosis: A General Overview

Tuberculosis (TB) is a major cause of morbidity and mortality across the world and is currently one of the most devastating diseases worldwide.[1,2] The World Health Organization estimates that more than 2 billion people are infected with *Mycobacterium tuberculosis*, the pathogen that causes tuberculosis.[3,4] In 2007, 9 million people developed tuberculosis of whom 1.77 million died.[5-7] In the World Health report it is predicted that during the period from 2000 to 2020, almost 1 billion people will become infected with tuberculosis, 200 million will develop active tuberculosis and 35 million will die from the disease.[8,9]

The areas with the highest occurrence of tuberculosis are currently Asia (55%), sub-Saharan Africa (30%) and certain Eastern European countries, where the rates of infection generally surpass 100 per 100 000 people.[8,10] The spread of TB in these countries is mostly exacerbated by poverty, malnutrition, poor living conditions, war and the human immunodeficiency virus epidemic.[2,11,12] More than 90% of people infected with tuberculosis live in developing countries. The World Health Organization has designated 22 of these countries as high burden countries where approximately 5000 people die per day from tuberculosis.[1,13] South Africa is such a high burden country.[11,14]

Infection with *Mycobacterium tuberculosis* usually occurs when a previously uninfected person inhales infected airborne droplets produced by a person with active tuberculosis. These infectious droplets are distributed through coughing.[13] At this stage, the infected person shows no symptoms due to the control of the body's immune system and the *M. tuberculosis* organisms remain dormant. The person stays healthy and is not infectious. This condition is called latent tuberculosis. In some cases, the immune system is not able to fight the infection and the person progresses to active disease.[15-17]

Disease can also develop at a much later stage due to reactivation of latent tuberculosis when the body's immune system is weakened by illness, medical treatment, malnutrition and/or old age. When the condition of latent tuberculosis has changed to active tuberculosis, there may be radiological (chest x-rays) or microbiological (culture) evidence of the disease.[15,18]

If an infected person is not treated properly for tuberculosis, he can infect an average of 10 to 20 people per annum with tuberculosis.[3,15,19] This ongoing transmission of the disease will fuel the worldwide epidemic, resulting in an increase in tuberculosis cases from one year to the next.[20]

2.1.1 Paediatric Tuberculosis

Children across the world are affected by tuberculosis as it causes major morbidity and death, especially in young children and infants.[2] [3,21] In general, children account for 5 – 15% of the tuberculosis disease burden in the world, although the numbers may be a lot higher in areas with poor

epidemic control.[11,22,23] A study done in South Africa in 1999 indicated that the case notification rate of tuberculosis in children 0 – 5 years old was 3588 cases/100 000. This was 3.5 times the case notification rate in adults.[24]

Children infected with tuberculosis differ from adults, as their immunological and patho-physiological response to the disease is different.[25,26] This has important and significant implications for the prevention, diagnosis and treatment of tuberculosis in children.[5] The diagnosis and treatment of childhood tuberculosis does not always get the attention it deserves in areas with resource constraints, because it is believed that children do not contribute to the spread and maintenance of the epidemic.[21,27,28] They usually develop paucibacillary tuberculosis, which is sputum smear-negative due to the size of the bacillary population being less than 10^4 colony-forming units (CFU)/mL and 10^4 CFU/mL is the lowest limit of detection with acid-fast smears.[22,30,31] Young children are also unable to generate the necessary "coughing force" to aerosolize *M. tuberculosis* into tiny droplets.[7,21] However, childhood tuberculosis is an indicator of ongoing transmission within an area and, more importantly, infected children grow up to become infected adults, who can infect an average of 10 to 20 people per active disease episode per annum.[3,8,32]

Tuberculosis is also an important cause of death in children under 5 years of age.[4] Young children are more likely than adults to develop active TB directly after exposure and infection[2,18,22] and tend to develop very severe cases of extrapulmonary tuberculosis, e.g. meningitis and miliary tuberculosis.[3,25] Young children (<2-3 years of age) have an immune system that is not yet fully developed, and are therefore highly susceptible to developing active disease following primary *M. tuberculosis* infection.[29,33] The chances of developing tuberculosis after infection with *M. tuberculosis* decreases with age, with the youngest most at risk. An estimate of 5-10% adults, 15% adolescents, 24% children 1-5 years old and 43% infants <1 year old will develop tuberculosis after infection.[10,11,28]

Children are also most at risk of becoming infected and developing tuberculosis when exposed to a sputum smear-positive case from within the house or living area.[5,33] Exposure to a sputum smear-negative source case within the house or living area still poses a considerable risk, although significantly less than in the instance of sputum smear-positive cases. From the pre-chemotherapy literature, 60-80% of children became infected after extended household contact with a sputum smear-positive source case.[34] An average of 30-40% of children became infected after contact with a sputum smear-negative source case. A significant number of children (80%) who developed tuberculosis before 2 years of age were infected by a source case within the house or living area.[27] It is also usually this group of children (<2 years of age) who has the highest risk for disease development and death following primary infection.[22,33] The chances of children becoming infected with tuberculosis depends mainly on the infectivity of the source case together with the proximity and contact time with the source case.[34,35]

It is not easy to establish the precise number of children infected with tuberculosis, because the diagnosis of this disease in children is far less accurate than in adults.[4,10,29] There are many causes for this, namely non-specific symptoms, low bacillary yield, poor specimen collection methods and low

sensitivities of the respective diagnostic tests.[36,37] More than half of childhood tuberculosis cases are asymptomatic, and consequently a major portion is not diagnosed in resource poor countries where there is a lack of facilities, e.g. properly equipped laboratories and radiographic instruments.[31] A combination of clinical features is therefore used to diagnose paediatric tuberculosis, such as the tuberculin skin test and chest radiography, as well as contact history with an infected adult.[37] For this reason, the International Union against Tuberculosis and Lung Disease decided that only information regarding childhood tuberculosis from developed countries may be used for statistical purposes.[24] The actual worldwide paediatric tuberculosis disease burden is therefore a lot higher than reported. In 2004, a study of active case finding was conducted in South Africa in which it was found that for every nine cases of sputum smear-positive pulmonary tuberculosis identified in a community, two cases of tuberculosis were not identified. This study did not included children younger than 10 years of age.[38]

The real magnitude of paediatric tuberculosis morbidity and mortality is therefore seldom appreciated, because the figures available seriously underestimate the true disease burden due to the difficulty in diagnosing childhood TB as well as poor record keeping in many areas of the world.[3,11,18]

2.2 Diagnoses of Tuberculosis

In order to contain the spread of tuberculosis, it is essential that the disease is diagnosed accurately and in time. Tuberculosis infection can manifest in three ways, namely active pulmonary tuberculosis, extrapulmonary tuberculosis and latent tuberculosis infection (LTBI). Different methods are used to diagnose latent tuberculosis and active pulmonary tuberculosis. Recently, major advances have been made in the research fields of biotechnology and molecular biology where several new and improved diagnostic tests for tuberculosis were introduced. However, the majority of these new and improved tests are far too costly and complicated to be of any real use to the vast majority of infected people living in resource poor areas.[39] An easy and cheap diagnostic test remains elusive and the conventional methods of diagnosis rely on tests with limitations.

2.2.1 Latent tuberculosis

A third of the world's population is estimated to be infected with *M. tuberculosis*.[40] Accurate diagnosis of latent tuberculosis is crucial to the prevention of the spread of this disease amongst the people in a community. But establishing an accurate diagnostic test method for latent tuberculosis infection is a major challenge as there is no gold standard for LTBI.[17,34] A gold standard is the test used to detect a particular disease and, more specifically, to compare any other results to. The diagnosis of latent tuberculosis is further hindered by a low bacteria load that makes it extremely difficult to directly

detect *M. tuberculosis*.[40] Two test methods are used for the diagnosis of latent tuberculosis, namely the tuberculin skin test and the Interferon-gamma assay.[33] Both test methods have certain shortcomings rendering them imperfect.[17]

a) Tuberculin Skin Test

Until recently, latent tuberculosis could only be diagnosed using the tuberculin skin test (TST). This test was introduced in 1910 and is also known as the intradermal Mantoux test. It is the oldest test used for diagnostic purposes in the modern medical practice.[34] This test is performed by injecting a purified protein derivative (PPD) solution intradermally into the most superficial layer of the skin of the forearm. This injection results in a swollen wheal at the position of injection. After a period of 48-72 hours has elapsed, the reaction (wheal) is measured as millimeters of induration.[17] Purified protein derivative (PPD) is a complex mixture of mycobacterial antigens prepared from heat-killed cultures of *M. tuberculosis.*[3] Despite the test's longevity, its use and interpretation of results remain controversial and the test has several limitations.[41]

The tuberculin skin test is problematic as 10% of children with culture-proven tuberculosis do not have a positive tuberculin test result at the time of testing. On the other hand, approximately 50% of children diagnosed with tuberculosis meningitis or miliary disease have a negative skin test result.[18]

The tuberculin skin test also has poor specificity for latent tuberculosis detection in populations vaccinated with bacilli Calmette-Guérin (BCG). People who have been vaccinated with BCG but not infected with *M. tuberculosis* present with false positive tuberculin skin test results.[33,41] These false positive results can be explained by the PPD, which is a culture filtrate of tubercle bacilli containing over 200 antigens shared with the BCG vaccine and most non-tuberculous mycobacteria. People vaccinated with BCG, but not infected with *M. tuberculosis,* will thus present with a positive TST result.[42] BCG is a very popular vaccine used across the world against tuberculosis with more than 3 billion people estimated to have received it. Studies have indicated that false positive TST results have been recorded for people who had received a BCG vaccine 15 years prior to the tuberculosis test.[34] The TST is therefore imprecise and the results are often nonspecific.[39,41,43]

Another limitation of the TST is its inability to tell recent infection apart from previous infection as well as the fact that the patient must return to the clinic or test facility 48-72 hours after injection to have the test read and interpreted.[29] Correct interpretation is a skill that requires training.[3,17,39,41,43]

b) Interferon-gamma test

Another test used for the diagnosis of LTBI is an *in vitro* assay that detects antigen-specific Interferon-gamma (IFN-γ). These blood tests detect cellular immune response by measuring IFN-γ released by T-cells after stimulation by *M. tuberculosis* antigens.[3,33] This test has a high specificity and is very useful for the detection of latent tuberculosis in low prevalence, resource-rich communities where

most people would have been vaccinated against tuberculosis with the BCG vaccine.[44] Interferon-gamma assays (IGRAs) do not give false positive results in the presence of BCG, as is the case with TST.[34,43] Although the sensitivity of the IFN-γ tests and TST are inconsistent across tests and populations, the IFN-γ test proved to be as sensitive as the TST.[26,42]

The Interferon-gamma test only requires one visit to the clinic or doctor, compared to the TST that requires a follow-up visit after the 48-72 hour time period elapsed after the initial injection. Another advantage of this blood test is that the test results are usually available the day after the test was performed. The test can also be repeated numerous times as testing do not boost the subsequent blood test results.[41] It is therefore possible to do repeated screenings of people that are at recurrent risk of tuberculosis exposure, such as health care workers.[26,33,34]

A major disadvantage of immune-based tests, such as IFN-γ and TST, is that they do not detect *M. tuberculosis* directly. Even if these tests present with a positive test result, it is only indicative of a cellular immune response to recent or distant sensitization with *M. tuberculosis*. Because IFN-γ cannot differentiate between latent and active tuberculosis, a positive test result does not necessarily indicate active TB and a negative test result would not rule out active disease in a person suspected of having tuberculosis.[26,33,42]

Another disadvantage, especially in the case of high-burden and resource poor countries, is the high material cost of these tests, the need for proper equipped laboratories and the fact that the blood tests must be processed within 6 hours from venipuncture. After the lapse of 6 hours, the test results are not reliable anymore.[33]

There are numerous studies that have reported unexplained inconsistencies between TST and different IFN-γ release assay results, which suggest that the results from these assays are not always reliable.[34,43]

2.2.2 Active tuberculosis

Active tuberculosis infection has historically been diagnosed with a variety of tests, namely sputum-smear microscopy, chest radiography and culture.

a) Sputum smear microscopy

Sputum-smear microscopy was developed in the 1880s and is still used today as an essential tool for the diagnosis of active tuberculosis.[7] Microscopy entails the identification of acid-fast bacilli (AFB) in specimen smears by spreading the sputum specimen directly on a slide and then staining it with Ziehl-Neelsen (ZN), auramine or rhodamine stain for visual detection using a microscope. It is the most common method used to diagnose tuberculosis and can detect 60-70% of culture positive

samples.[8,45,46] In developing countries, such as South Africa and Pakistan, it is often the only test method available for the diagnosis of tuberculosis. The World Health Organization recommends sputum smear microscopy as the most important and key laboratory diagnostic test for resource poor countries as it is cheap, easy and fast and is able to detect the most infectious cases of tuberculosis infection.[7,39,44]

There are advantages to using sputum smear microscopy, such as the requirement of only one piece of equipment, namely a microscope, and the visual evidence of tuberculosis. In most instances, the sputum smear microscopy test is specific enough and additional confirmatory testing is not needed.[47]

Sputum smear microscopy however also has some disadvantages. It cannot detect sputum smear-negative tuberculosis. Its sensitivity is very broad and may vary from 33% to 75%,[46] because a very high bacteria concentration is required to be visible under the microscope as very small amounts of material (sputum) are examined – as little as 0.2 µL. A smear specimen only test positive if a large number of bacilli (at least 5 x 10^3 AFB/mL) are present. Consequently, this test is of limited use and can only be improved if the sensitivity is improved.[12,47] The sensitivity of the test can be improved by improving the specimen collection method or examining several specimens,[39] which means that the patients will have to make repeated visits to the clinic for specimen collection. These repeated visits can be very costly and can result in a significant number of patients dropping out.[14]

A further disadvantage is the fact that the test does not make a distinction between dead and viable mycobacteria and speciation is not possible.[11] Although it is a simple test, the outcome of the test depends on the training and diligence of the microscope operator as well as correct sample preparation.[46,47]

b) Chest Radiography

In resource-poor and developing countries, chest x-rays and clinical symptoms have traditionally been used for the diagnosis of tuberculosis. Clinical signs and symptoms are however inconsistent and non-specific and are often absent in early disease. Chest x-rays, on the other hand, have historically always played an important role in the diagnosis of tuberculosis and will continue to be seen as a cornerstone of tuberculosis diagnosis. Chest radiography is unfortunately not always reliable as it can only be used in the case of pulmonary tuberculosis and not for extrapulmonary tuberculosis. But, although pulmonary tuberculosis usually presents with abnormalities on the chest x-ray, it cannot be used on its own to differentiate between tuberculosis and other pulmonary illnesses and the diagnosis can be misleading.[44,48] Furthermore, almost 25% of all tuberculosis cases are extrapulmonary and in such cases chest x-rays are of limited use.[39,43]

c) Culture

Mycobacterium tuberculosis is a slow-growing bacterium that requires specialized solid or liquid culture media.[11] Culture is a complicated procedure whereby a definitive diagnosis of tuberculosis is

reliant upon the isolation of *M. tuberculosis*.[43,46] The sensitivity of this test method is 80-85% and the specificity around 98%. The superior sensitivity of this test method can be attributed to its ability to give a positive culture result with only a small number of bacilli (10-100 AFB/mL) present in the test specimen. Culture is therefore a more sensitive detection method for *M. tuberculosis* than sputum smear microscopy.[7]

The main disadvantage of the culture method is the lengthy incubation period needed for mycobacterial growth.[49] Growth is sometimes only visible after 8 weeks of incubation due to the bacteria's slow doubling time of 18-24 hours.[39] Culture plates must therefore be kept for 12 weeks before a test result may be indicated as negative.

Another disadvantage is that the volume of sputum required to provide optimum results for the growth detection of *M. tuberculosis* must exceed 5 mL. Studies have also indicated that the best results are achieved if the high volume of sputum is collected overnight or over 24 hours, thus increasing the risk of contamination. These sputum specimens must be decontaminated before culture to get rid of normal fast growing contaminants, such as normal flora, without killing off the mycobacteria. Unfortunately, even the mildest decontamination method, such as the frequently used N-acetyl-L-cysteine (NALC)-NaOH method, can kill up to a third of the mycobacteria in a clinical specimen.[14]

d) Nucleic Acid Amplification assays

New tests recently developed for the diagnosis of active tuberculosis are the nucleic acid amplification (NAA) tests. These tests amplify target nucleic acid regions that are unique to *M. tuberculosis* and have the advantage that it can be used directly on clinical specimens, such as sputum. Compared to conventional culture as detection method, the direct NAA test can decrease the overall turnaround time for the laboratory diagnosis of tuberculosis by 2 to 4 weeks.[14,26]

The precision and dependability of this NAA tests used for the detection of tuberculosis have been studied extensively.[31] The results of these studies indicated a low sensitivity in the paucibacillary forms of tuberculosis (i.e. sputum smear-negative tuberculosis), but higher specificity for pulmonary and extrapulmonary tuberculosis. The sensitivity of NAA tests was the best in sputum smear-positive pulmonary tuberculosis.[11,26] For these very reasons, the NAA tests cannot be used in the place of conventional tests such as microscopy and culture, but it is very useful to confirm that a positive sputum smear result is due *to M. tuberculosis* infection and not non-tuberculous mycobacterium infection, keeping in mind that these tests cannot tell between dead and viable mycobacteria. This can lead to inconsistency between sputum and NAA results.[44]

Because contamination from amplicons derived from positive specimens is a very big risk when performing NAA tests,[50] it can only be done in laboratories with adequate quality assurance systems in place, such as having three separate and dedicated rooms for the three main steps of the procedure.[14,43] This requirement increases the cost of performing NAA assays.

2.3 Diagnosis of Tuberculosis in Children

It is important to diagnose tuberculosis in children accurately in order to provide effective treatment.[51] Children with tuberculosis may develop symptoms, present with abnormal signs on examination or on chest x-rays and sometimes there may be bacteriological confirmation of the disease.[3,37] However, although there may be symptoms, these symptoms are often non-specific (such as fever, growth delay, weight loss, coughing, night sweats and chills)[38] with more than half of the children being asymptomatic with early tuberculosis disease.[8]

The tests available for the diagnosis of paediatric tuberculosis have limitations, and the complete range of tests may not be readily accessible in areas where tuberculosis infection is common and widespread.[5] The diagnosis of paediatric tuberculosis is particularly difficult and challenging and is further complicated by the lack of a practical gold standard.[30,34] (A gold standard is a test that entails confirmation of infection by demonstration of *M. tuberculosis* on direct microscopy of sputum, or culture.) The problem is that most children with active tuberculosis are rarely infectious due to the paucibacillary nature of childhood tuberculosis, i.e. sputum smear negative.[11,52] Compared with adults, children seldom have cavitatory tuberculosis (<6%) and they seldom have a forceful cough. When a cough ìs present, it is often not forceful enough to expel airborne bacteria efficiently. Cavitating pulmonary tuberculosis rarely occurs in children before puberty.[3] Bacteriological confirmation, the 'gold standard', is therefore of limited use in children, especially young children, due to poor bacteriological yields. Obtaining clinical samples are also highly problematic.[11]

Bacteriological confirmation for the diagnosis of paediatric tuberculosis is particular difficult and rarely successful. The diagnosis of paediatric tuberculosis in non-endemic areas are therefore usually based on (1) known contact with an infected adult case usually within the household or community, (2) a positive tuberculin skin test (TST) as evidence of *M. tuberculosis* infection, and (3) suggestive signs on the chest radiograph.[22,33] These pointers are usually fairly accurate indicators in the diagnosis of tuberculosis where exposure to *M. tuberculosis* is uncommon.[18,53] However, in the case where a major portion of the population has been infected with *M. tuberculosis* during childhood, and in endemic areas where the exposure to *M. tuberculosis* is common, the diagnostic accuracy of the triad is greatly reduced.[36,52] This is because a positive TST is common in healthy children in endemic areas, which limits the diagnostic value of the test. On the other hand, up to 10% of otherwise normal children with culture proven tuberculosis do not respond to tuberculin at first;[8] or children may present with a false-positive reaction to TST due to asymptomatic infection by environmental nontuberculous mycobacteria.[8,41,53] Children can also present with false-negative TST results due to associated immune-suppressive illnesses such as HIV, malnutrition, or other bacterial or viral infections.

Although the Interferon-gamma test is seen as an alternative test method for latent tuberculosis in adults with better specificity and sensitivity than the conventional TST, it is not recommended for use in young children at present, as there is no good evidence that this test actually works as a diagnostic tool for paediatric tuberculosis.[33] Paediatric studies have been limited and inconsistent and there is

not enough evidence yet to make clinical recommendations.[3,52] The use of this test in children is further limited by the large amount of blood required (4-5 mL), the high cost and the unavailability of proper laboratory equipment and infrastructure to do the test properly.[4]

There are various approaches that can be used for the diagnosis of active tuberculosis in children. The various specimen collection methods and resultant test methods are discussed below.

2.3.1 Specimen Collection Methods

a) Sputum

Older children suspected of having pulmonary tuberculosis can usually produce sputum when required for the use in culture or microscopy as diagnostic method. This is more likely to be positive than other samples.[3] The problem is that younger children less than 4 years of age are unable to produce sputum spontaneously[25] and as a result, only 5-10% of children diagnosed with pulmonary paediatric tuberculosis have a positive acid-fast smear test result based on sputum as the test specimen.[30,32,54] It is also usually this group of children that has the highest risk for disease development and death following primary infection.[34,35,55]

b) Induced Sputum

Studies done recently indicated that sputum induction is safe and well tolerated by young children. It can be performed on an outpatient basis and is superior to gastric lavage and gastric aspirates, with twice as many positive case results. Careful environmental and infection control measures are needed due to the possibility to induce an infectious airborne particle.[23,31] This specimen collection method can therefore only be performed in facilities with adequate ventilation mechanisms. Another disadvantage is the possibility of bronchospasm in the children.[3,8]

c) Gastric Aspirates

In 1898 Neunier was not successful in obtaining sufficient sputum samples and reasoned that children, who were unable to expectorate, would therefore swallow their sputum containing *Mycobacterium tuberculosis*. He became the first person to culture stomach contents for the evidence of tuberculosis infection in children.[36]

Gastric aspiration using a nasogastric feeding tube remains the most widely used modality in young children who cannot produce sputum on demand. It is an easy procedure to perform, requires no special apparatus and is very cost effective. Samples are collected on three consecutive mornings after an overnight fast period of 8-10 hours.[31,53] This sample collection process usually requires

hospitalization as it is vital that the correct technique is used and that the timing and processing of the samples are consistent. However, even under optimal conditions less than 50% of the samples will give a positive result in those with tuberculosis infection.[8,52]

The disadvantages of this method are that the gastric aspirates are uncomfortable, involve fasting and require repeated admission to a hospital or clinic[3,23] and are therefore not really an option in resource-poor countries.[31] Despite the low sensitivity of this method and the disadvantages listed above, gastric aspirates are considered amongst the better methods for collecting specimens from children suspected of having tuberculosis.[36,50,53]

The samples collected in any of the before mentioned methods can be used for tuberculosis diagnosis using sputum smear microscopy or culture as detection methods.

2.3.2 Diagnostic methods - current

a) Sputum smear microscopy

Sputum smear microscopy is often the only test method available for the diagnosis of tuberculosis in endemic areas, but is positive in as little as 10 to 15% of children suspected of having tuberculosis.[3,47,52] The main reason for these low diagnostic test results is that young children with pulmonary tuberculosis infection cannot produce sputum. As a result, early morning gastric aspirate samples are therefore often collected for diagnostic purposes. But less than 20% of children with positively diagnosed tuberculosis will have a positive sputum or gastric aspirate sample when Ziehl-Neelsen staining is used as the detection method, compared to 75% in adults.[8,53] This is however not the case with older children, as children more than 10 years of age with adult-type disease usually have a high bacteriologic yield. Sputum smear microscopy has therefore definite diagnostic value in this instance.[36]

In order to improve the diagnostic test results of sputum smear microscopy, fluorescence microscopes have been employed instead of conventional light microscopes. Studies conducted indicated that fluorescence microscopy is on average 10% more sensitive than light microscopy with similar specificity as conventional ZN staining.[26] The sensitivity of fluorescence microscopy ranged from 52 to 97%, whereas for conventional light microscopy it ranged from 32 to 94%. With fluorescence microscopy, it is possible to read the slides more efficiently as a lower magnification is used for visualization, thus covering bigger portions of the slide – this improves the laboratory throughput greatly.[56,57] Fluorescence microscopy is currently however not commonly used in low-income countries as a detection method due to the high cost of short-lived mercury vapour lamps.[14,16,46]

This was the case until the development of light emitting diode (LED) light sources for fluorescence microscopes, using acid-fast fluorochrome dyes for visualization. LED light sources are cheap, long

lasting, have less maintenance requirements, require little power and can be battery operated and will make fluorescence microscopy an economical option for low-resource settings.[16,26,31,33,58]

The World Health Organization recommended recently that LED microscopy replace fluorescence microscopy and that LED microscopy be phased in as an alternative to conventional ZN light microscopy.[16,56,57]

In spite of these changes, the yields are still low regarding detection of paediatric tuberculosis.

b) Culture

Culture yields in children suspected of having tuberculosis is low at 30-40%, but is still better than sputum smear microscopy.[21,22,52] However, culture using solid media can take up to 8 weeks to get results.[3,36] This is particularly problematic when dealing with children less than 6 years of age who can develop pulmonary, disseminated and central nervous system tuberculosis in less than 3 months after infection due to the short incubation period.[36]

Liquid culture is a new and automated system that enables the continuous monitoring of bacterial growth and is more sensitive regarding the detection of *M. tuberculosis* than solid media. It can increase the yield by 10% compared with solid media and reduces the delay in test results from weeks to days.[31,59] Liquid culture systems do have some disadvantages as it is prone to contamination and requires very strict quality assurance systems and training standards. This test method also requires sophisticated equipment and is costly to perform. [31,42]

These limitations are particularly problematic and relevant in low-income, high burden areas where facilities are seldom available for culture.[31]

2.4 New techniques

Although sputum smear microscopy and culture have historically been the primary detection methods used for paediatric TB, both methods have numerous disadvantages and limitations. The diagnosis of tuberculosis in children from endemic areas is therefore dependent primarily on clinical features and the subjective interpretation of the chest radiograph.[52] The problem is that radiological findings in tuberculosis are variable and neither specific nor diagnostic of tuberculosis except in miliary tuberculosis.[22] Diseases such as pneumonia, bronchopneumonia, asthma and congenital pulmonary anomalies can often present on a chest radiograph as tuberculosis but are not. Studies have also indicated that as many as 20% of cases of tuberculosis were missed on chest radiography.[3] The equipment required for chest radiography is also usually unavailable in many endemic areas due to

resource restrictions as well as lack of trained health practitioners to interpret these radiographs properly.[21,36]

Due to these various reasons mentioned, the search is still on for new and improved specimen collection methods as well as better diagnostic methods.

2.4.1 New specimen collection methods

The sensitivity of many of the previously mentioned detection methods can be increased by improving the specimen collection methods and specimen processing procedures. As it is difficult to collect good quality sputum specimens, other new specimen collection methods have been developed and used the last couple of years, such as a) nasopharyngeal aspirates, b) nebulized hypertonic saline-induced sputum c) bronchoalveolar lavage d) stool, e) find needle aspiration biopsies, and f) string.

Both the a) nasopharyngeal aspirate method and b) saline-induced sputum method allow recovery of sputum samples without expectoration, are non-invasive and can be easily performed on an outpatient basis. The sensitivity of these tests compared to standard gastric aspirate has however not yet been established.

c) Bronchoalveolar lavage also allows recovery of sputum samples without expectoration, but is invasive, costly, requires special equipment and trained personnel and the sensitivity of this test compared to standard gastric aspirate has not yet been established.[36]

d) Due to children swallowing their sputum rather than coughing it out, mycobacterial culture of stool was expected to give good results. These specimens must unfortunately be rigorously decontaminated to prevent overgrowth from normal bowl flora. Such procedures are likely to kill most of the mycobacteria in the sample as well, resulting in insensitive stool culture results.[25,31]

e) Fine needle aspiration is an easy, trouble-free and robust method. It has little side effects and provides rapid and excellent diagnostic results in children with superficial tuberculosis lymphadenitis. It is not commonly used for the diagnosis of pulmonary tuberculosis.[31,52]

f) A recent study from Peru used a string test as a novel approach to retrieve *M. tuberculosis* from sputum smear-negative adults infected with HIV with tuberculosis symptoms. The yield of the string test was higher than in the case of induced sputum and the procedure was safer to health workers.[3,55]

Moore also found in 2005 that better diagnostic sensitivity could be gained by the string test, compared to sputum induction. The string test may thus have a role to play in the difficult and challenging diagnosis of pulmonary tuberculosis in children as the string test procedure is well tolerated by children as young as 4 years of age suspected of having tuberculosis infection.[49] Children

younger than 12 years do not easily produce sputum, but are likely to swallow it when they do. The string can then be used as a specimen collection device in the stomach.

2.4.2 New diagnostic tests

There are a number of reasons why the methods for the diagnosis of tuberculosis in children must be improved. These are:

a) to accurately assess the influence of childhood tuberculosis on global tuberculosis,
b) to improve the efficiency of identifying and treating children with tuberculosis,
c) to reduce disease transmission caused by paediatric tuberculosis, and
d) to facilitate children's rights to basic health care.

New diagnostic tests developed the last couple of years include a) serological tests, b) nucleic acid amplification tests c) various polymerase chain reactions (PCR), d) high resolution computed tomography (CT), e) chromatography, f) mycobacteriophage-based methods and several unconventional and novel culture methods, such as microscopic observation drug-susceptibility test (MODS), thin-layer agar (TLA) and the direct nitrate reductase assay (NRA).[36,42]

a) Serological tests measure humoral immunity and are based on the detection of antibodies binding to *M. tuberculosis* antigens in serum. These tests are fast and easy and are primarily used for the detection of active tuberculosis (pulmonary and extrapulmonary).[54] Serological tests are presently unable to diagnose childhood tuberculosis with the required accuracy and thus cannot replace conventional tests, namely microscopy and culture.[60] Studies have indicated that 65% of children with active tuberculosis but negative smears had a positive serodiagnosis, but none of the infected children that are asymptomatic had a positive serodiagnosis.[51,61] Another big disadvantage of serological tests is that it is very difficult to collect blood samples in children, especially in infants, as required for these tests.[8,52]

b) A new technique used amongst adults, namely nucleic acid amplification, offer rapid, sensitive and specific results for tuberculosis diagnosis.[11,51] Nucleic acid amplification however has very low sensitivity and gives variable results when used to diagnose TB infection in children.[18] This test can therefore unfortunately not be used in children, especially in smear-negative and extrapulmonary tuberculosis infection[42] where the sensitivity of this test method in these cases can be as low as 50%.[11,31] A positive test result does not confirm tuberculosis and a negative result never eliminates tuberculosis as a diagnostic possibility.[18]

c) Sputum based polymerase chain reaction (PCR): These tests are very fast but have shown inconsistent results probably due to variations in methodology, high risk of contaminations and the presence of PCR inhibitors, giving false negative PCR results. It is unfortunately also a very expensive test. Limited information is available regarding studies done on children and therefore decisions regarding TB diagnostics cannot be made.[6,59]
Gastric aspirate PCR: Studies have indicated that same day gastric aspirate PCR may be used as a screening test for high-risk children likely to have culture-proven tuberculosis, although the routine use of PCR for the diagnosis of paediatric tuberculosis is not recommended.[37]

Stool PCR: Due to the difficulty with obtaining sputum samples from young children suspected of having culture positive pulmonary tuberculosis and since tuberculous DNA is able to survive intestinal transit, stool samples were collected and tested for the presence of *M. tuberculosis*.[62] Studies indicated that *M. tuberculosis* DNA could successfully be detected in stool specimens using PCR with a sensitivity of 38% and 100% specificity. The sensitivity was affected by the DNA extraction method used, indicating that the presence of PCR inhibitors play a major role in the quality of the test results.[63]

The advantage of stool PCR is the quick turnaround time with results available within 24 hours of receiving the stool specimens, compared to tuberculosis culture taking several weeks. Stool PCR can therefore be used for the diagnosis of pulmonary paediatric tuberculosis if the sensitivity of the test method can be improved significantly. Due to the high specificity of the test method, a positive stool PCR test result can be indicative of culture positive pulmonary tuberculosis and can thus alert clinicians to initiate treatment at an early stage. Stool PCR can thus be used as an initial screening test for tuberculosis, providing the sensitivity is improved.[62,63]

d) High resolution computed tomography is costly and requires a scanner that is not readily available in many areas.[36] These disadvantages have restricted the use of these tests.[3,8,21]

e) High-performance liquid chromatography is used to detect the signature pattern of mycolic acids present in the cell wall of mycobacterial species. Although it is a fast and very specific detection method using computer software to identify the different mycobacterial species, false positive results are quite common due to organisms other than *M. tuberculosis* also present in the specimen.[44]

f) Mycobacteriophage-based detection methods are cheap, phage-amplified biological assays that use Mycobacteriophage D29 to rapidly detect viable *M. tuberculosis* in decontaminated sputum specimens. Although this method has a high specificity of 86%, its low sensitivity of 31% makes it a poor diagnostic test for tuberculosis.[44] Further studies have also indicated that the performance of bacteriophage-based tests for the direct detection of *M. tuberculosis*

was inferior to that of smear microscopy, and that these phage-based tests are not suitable for routine diagnostic use.[14,26]

g) Another sputum-based test recently developed for the detection of tuberculosis, is the microscopic-observation drug-susceptibility (MODS) assay. This test uses an inverted light microscope to rapidly detect mycobacterial growth in liquid growth media.[4] It is an inexpensive, low technology, broth culture method that provides highly sensitive bacteriological detection of *Mycobacterium tuberculosis.*[49] The turnaround time for results is excellent since they are usually available within 7 days of performing the test.[37] The sensitivity and speed of the MODS assay is due to the culture broth used in this technique that makes microscopic detection of positive cultures possible before they are visible to the naked eye. A large volume of each specimen can also be cultured due to the increased capacity of the technique, thus increasing sensitivity.[37] These new culture methods are very promising as they use inexpensive materials with quick turnaround times

Although this test is very simple to perform, the work-up of the sputum samples requires material, laboratory equipment and trained personnel.[12] These tests are also not always consistent and require intensive training and optimization before routine clinical use. This method needs routine specimen processing before direct inoculation with sputum can be done and specimen processing is the most burdensome component of mycobacterial culture.[42] As with all culture methods, contamination can be a problem and therefore require strict quality control standards.

Not one of these methods is foolproof nor has the necessary sensitivity, specificity or reproducibility for use in the diagnosis of paediatric tuberculosis.[8]

For faster and more accurate diagnosis of tuberculosis in young children, it is vital that the specimen collection method is improved in order to provide samples with adequate bacteriological load for detection.[25,58]

2.5 Improved Specimen Collection

Most of the laboratory techniques used for the diagnosis of tuberculosis is dependent on the detection of *M. tuberculosis*. It is therefore of utmost importance that good quality specimens are obtained with the highest possible concentration of mycobacteria to enable the accurate diagnosis of tuberculosis.[11,58] It is especially difficult to collect adequate samples in young children who are unable to produce good sputum specimens and therefore gastric aspirates are normally used in young

children (<8 years). This method entails two to three fasting early morning aspirates – it is very time consuming and must usually be done in a hospital.[4,51]

Another method also used for specimen collection in children is the induced sputum method, using a single hypertonic saline solution. This test provides the same yield as gastric aspirates, but there is the risk of nosocomial transmission if infection control measures are not adequate.[4,51]

These specimens obtained by gastric aspirates or induced sputum method must be processed and decontaminated to kill or inhibit bacterial contaminants. This decontamination procedure is unfortunately also responsible for killing most of the mycobacteria as only approximately 10-20% of the mycobacteria remain viable after optimal processing.[51] These remaining mycobacteria can then be viewed under the microscope or they can be cultured.

For microscopy, the mycobacteria are stained with Ziehl-Neelsen stain and show up under the microscope as acid-fast bacilli. Although it is a fast method, a substantial number of mycobacteria is needed to be detected under the microscope and is only visible if there are 5000-10 000 bacilli per milliliter of specimen. If the concentration of the specimen can be increased, the sensitivity of the test may be improved.[51] The yield of smear microscopy may be increased by concentrating the specimens using centrifugation and ligand-coated magnetic beads, but in depth studies to ascertain the success of these concentration methods must still be conducted and documented.[31]

Culture is more sensitive than microscopy as it is able to detect as little as 10-100 bacilli per milliliter of specimen. In spite of this sensitivity, culture is still only positive in less than 50% of children diagnosed with active tuberculosis. Diagnosis by culture is much slower than microscopy as it takes 2-8 weeks for mycobacterial growth to be detected with conventional media and 1-3 weeks with the new liquid broth system.

If the specimen collection method can thus be improved to give sufficiently high yields of mycobacteria, fast and accurate diagnosis can potentially be made using microscopy. The Entero-string test is a specimen collection method that can be modified and improved to increase the yield of *M. tuberculosis* for faster and more accurate diagnosis of tuberculosis using traditional microscopy, fluorescence microscopy or MODS.

The string test is a non-evasive specimen collection method initially developed and used for the retrieval of an assortment of gastrointestinal microbes and parasites, such as *Helicobacter pylori*, *Giardia lamblia* and *Salmonella enterica*.[64,65] The string test consists of a nylon string coiled up inside a conventional gelatin capsule. A piece of the nylon string protrudes through a hole at the one end of the capsule and is taped to the cheek of the patient. The patient then swallows the rest of the weighted capsule and the string unravels through the same hole as the capsule descends into the stomach. When the gelatin capsule comes into contact with the gastric juices, it dissolves and releases the string into the stomach. After a period of 4 hours has elapsed, the string is retrieved by pulling it out via the esophagus and mouth and is tested for the presence of certain pathogens.[31,51]

Neunier proved successfully that children, who were unable to expectorate, swallowed their sputum containing *Mycobacterium tuberculosis*. He became the first person to culture stomach contents for the evidence of tuberculosis infection in children.[36]

Based on the same concept as the original string test, a paediatric string has successfully been used in children in the past to detect enteric pathogens, to diagnose gastroesophageal reflux and for the confirmation of contaminated small-bowel syndrome.[64,65] Moore conducted a study in 2006 to determine if the string test method was tolerated and acceptable to children undergoing examination for tuberculosis. The results of this study indicated that the string test is acceptable and well tolerated by the majority of children.[66] The string test can therefore be used as a novel specimen collection method for gastric samples from children undergoing investigation for tuberculosis infection. It is minimally invasive, cheap and not dependent on sophisticated and expensive equipment.[65,67] Unfortunately no microbiological diagnosis could be made during the study with the string collection method. A possible reason may be the harsh decontamination procedure using NaOH-NALC from which only 5-10% of the mycobacteria remain viable for further testing. The effect of this decontamination step is greater in children than in adults due to the lower bacillary load of children.[67]

When comparing the string test with induced sputum as specimen collection method in patients diagnosed with sputum smear-negative tuberculosis, the string test demonstrated superior sensitivity.[52] These preliminary results from previous investigations indicated that the Entero-string, as a specimen collection device for the diagnosis of tuberculosis in young children, can be used as a basis if it can be improved to optimize specimen collection for better and accurate diagnosis of tuberculosis in young children.

There are several problems with the string test that still requires optimization, namely

1. String delivery to ensure contact of the string with gastric fluids
2. String retrieval to prevent contamination of the string with upper gastrointestinal tract bacteria as the string passes the esophagus and pharynx.
3. Post collection processing of the string
4. Capture of *M. tuberculosis* by the string to increase the bacterial yield

Heymann reported in 2000 that if the number of children who entered treatment could be increased by 5%, it would lead to a 25% decrease in the number of tuberculosis cases among children and a 16% decrease in the number of tuberculosis deaths after 10 years. It is therefore of utmost importance to identify as many children as possible with tuberculosis infection in order to introduce them into an effective treatment program. This should decrease the number of adult cases as well as the mortality rate amongst children.[25,68]

The string can potentially be improved as a specimen collection device for *Mycobacterium tuberculosis* by functionalizing the string polymer with a chemical entity that can capture *M. tuberculosis* onto the functionalized surface of the polymer under gastric conditions, thereby increasing the mycobacterial yield. An increased yield in *M. tuberculosis* should then result in better and more accurate diagnosis of tuberculosis in young children.

In order to achieve this objective, chemical groups must be identified that will facilitate improved mycobacterial binding to the string. The polymer functionalized with these chemical groups must also be stable at the acid pH conditions within the stomach. In order to identify possible chemical groups that would be suitable for polymer functionalization to achieve improved mycobacterial binding, a study had to be done of the *Mycobacterium tuberculosis* cell wall to establish all the possible surface structures that would be available for binding.

2.6 *Mycobacterium tuberculosis*

Tuberculosis is caused by *Mycobacterium tuberculosis*, an intracellular pathogen that can infect human beings as the primary host, and animal species.[69] *M. tuberculosis* is an acid-fast, aerobic, non-motile and non-encapsulated bacillus, discovered by Robert Koch in 1882. It is neither gram positive nor gram negative and is described as an acid-fast bacillus since after staining the cell wall of the organism with a phenol-containing dye; it resists decolourization with acidified organic solvents.[74] *M. tuberculosis* has a lipid-rich cell wall, comprising approximately 60% of the dry weight of the cell, and functions as a physical barrier between the organism and its environment.[70,71] This waxy mycobacterial cell wall has very low permeability to hydrophilic molecules and protects the organism against long exposure to acids, bases, detergents and antibiotics.[69,72,73]

2.6.1 *Mycobacterium tuberculosis* cell wall

Refer Figure 2.1 for a schematic representation of the cell wall of *Mycobacterium tuberculosis*.[70]

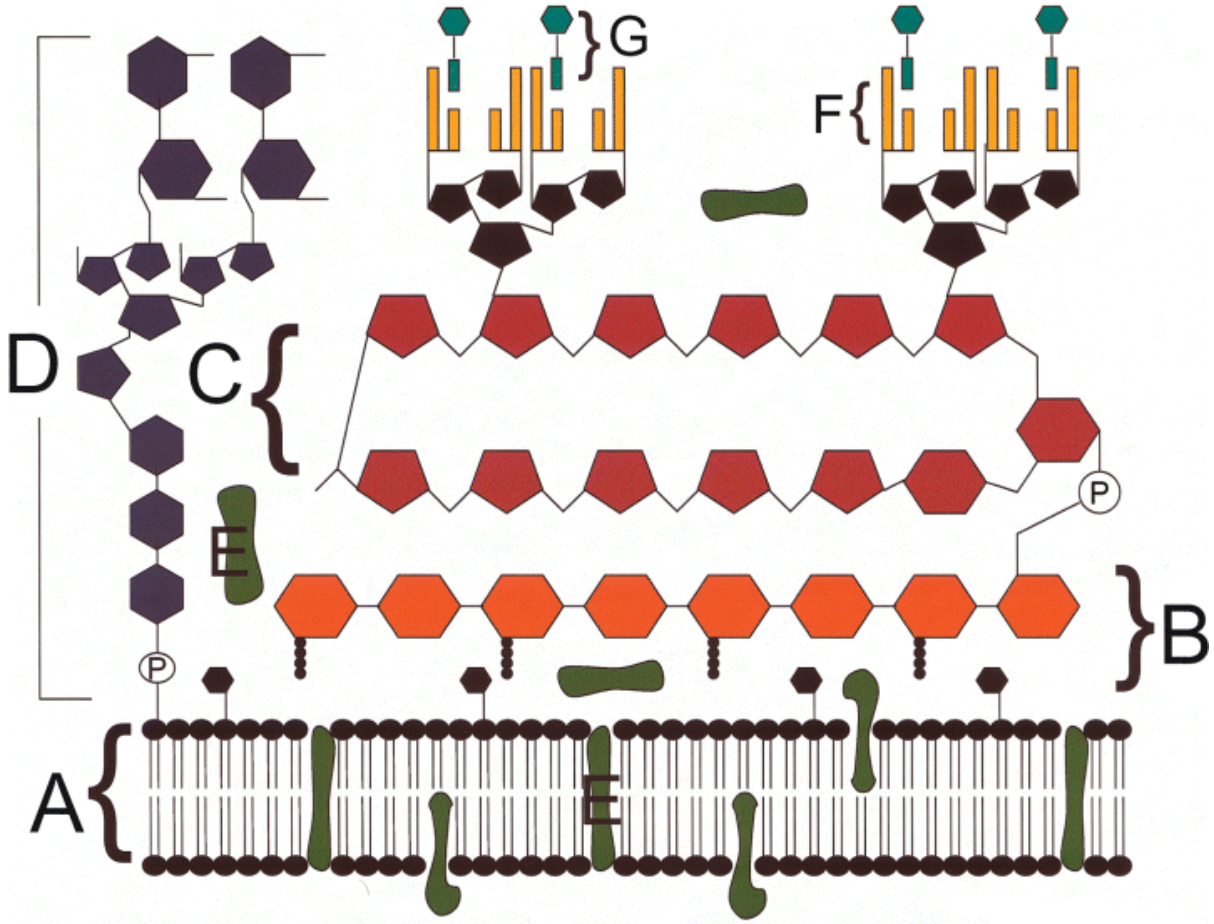

Figure 2.1 A schematic representation of the cell wall of Mycobacterium tuberculosis. The components include the (A) plasma membrane, (B) peptidoglycans, (C) arabinogalactan, (D) mannose-capped lipoarabinomannan, (E) plasma membrane- and cell envelope-associated proteins, (F) mycolic acids and (G) glycolipid surface molecules associated with the mycolic acids.[70]

The mycobacterial envelope comprises an inner plasma membrane and an outer cell wall.[75] The cell wall of *M. tuberculosis* can be divided into two segments, namely the upper and lower segments. The lower segment comprises a massive core of peptidoglycan, covalently attached to arabinogalactan, which in turn is connected to mycolic acids.[73,76] This structure is collectively known as the mycolyl arabinogalactan-peptidoglycan (mAGP) complex.[77-79] Peptidoglycan is the backbone of the mAGP complex and consists of a highly cross-linked polymer of N-acetylglucosamine and N-glycolylmuranic acid.[71] Arabinogalactan consists of D-galactofuranoses and D-arabinofuranoses and is very rare in nature.[73] The mycolic acids are complex long chain α-alkyl, β-hydroxylated fatty acids with a chain length in the range of $C_{77\text{-}80}$.[70] These hydrocarbon chains are orientated perpendicular to the plane of the cell membrane and present as tetramycolylpentaarabinofuranosyl clusters.[73] Mycolic acids are present in the *M. tuberculosis* cell wall in two forms: some are covalently bound to arabinogalactan of the cell wall, and some are loosely associated with a variety of carbohydrate-containing structures in the cell wall.[73] Mycolic acids function as a very effective lipid barrier between the cell and its environment and are the hallmark of mycobacteria.[71,74,77,80] There are also various glycolipid structures in the cell wall of *M. tuberculosis*, such as trehalose-6,6'-dimycolate (TDM), that contains

mycolic acids as part of their core.[70] The abundance of mycolic acids spread throughout the *M. tuberculosis* cell wall is the primary reason for the extreme hydrophobic character of the tubercle bacillus and their tendency to aggregate.[72,81]

The upper segment comprises a variety of free lipids, such as sulfated glycolipids, phenolic glycolipids (PGL) and liposaccharides (LOS)[82-84] with interspersed cell-wall proteins, phosphatidylinositol mannosides (PIMs), phthiocerol-containing lipids, phosphatidyl ethanolamine (PE), lipomannan (LM) and lipoarabinomannan (LAM).[70,85]

The mAGP complex of the lower segment is crucial for the viability of the cell, and the lipids, proteins and lipoglycan of the upper segment are the signaling and effector molecules in the disease process.[70,74,76] The mAGP complex is constant among mycobacterial species, but the outer segment has different molecular compositions in the different mycobacterial species.[79]

2.6.2 Surface structures of *Mycobacterium tuberculosis* cell wall

Mycobacterium tuberculosis is unique among bacterial pathogens in that it displays a wide variety of complex lipids and lipoglycans on its cell surface. The cell wall of *M. tuberculosis* is a complex structure that is responsible for many of the unique properties of the organism. The structures that are available on the outer surface of *Mycobacterium tuberculosis* include the free lipids (including the sulfated glycolipids and phenolic glycolipids), phosphatidylinositol mannosides (PIMs), phthiocerol-containing lipids, phosphatidyl ethanolamine (PE), lipomannan (LM) and lipoarabinomannan (LAM),[70,71,82,83,85] as well as a variety of mycobacterial cell wall proteins:

- Sulfated glycolipids are exclusive to *M. tuberculosis* - there are 5 structurally related sulfatides of which Sulfolipid-1 (SL-1) is the principal sulfatide of the family. This sulfolipid is 2,3,6,6'-tetraacyl-α,α'-D-trehalose 2'-sulphate.[83]

- PIM and LM are possible precursors of LAM and serves as core and anchor for LAM.[74,76,77]

- LAM is a phosphatidylinositol anchored lipoglycan with a polysaccharide backbone of D-mannan and D-arabinan and is ubiquitous molecules of mycobacteria.[86] LAM of human pathogens *M. tuberculosis, M. leprae and M. bovis BCG* are capped at the terminal arabinan residue with mannoses, a C_2-epimer of glucose.[71,84] These mannose caps allow *M. tuberculosis* to bind to various mannose receptors.[74,80] LAM extends outwards through the peptidoglycan layer to the exterior of the cell and is one of the key components of the mycobacterial cell wall.[70,77,84,87]

- Cell wall proteins available on the outer surface of *Mycobacterium tuberculosis* include fibronectin-binding proteins, heparin-binding haemagglutinin adhesion (HBHA) and laminin-binding protein.[88-93] These proteins are all available for adhesion activities with its corresponding host ligand.

Although the mycolic acids are only present in the lower segment of the cell wall and not on the outer surface, they play a very prominent role as they are responsible for the extreme hydrophobic character of the *M. tuberculosis* cell wall.[72]

2.6.3 Attachment mechanisms between *M. tuberculosis* and host

When *Mycobacterium tuberculosis* is inhaled and enters the host lung, the organism can interact with a variety of human receptors, such as mannose receptors, complement receptors, scavenger receptors; or extracellular structures such as fibronectin and heparan sulfate proteoglycans. These human receptors recognize certain ligands expressed on the surface of *M. tuberculosis*, such as mannose-capped lipoarabinomannan. These interactions between human receptors and pathogen facilitate adhesion between the extracellular organism and host cell for a) infection to occur or b) to promote phagocytosis of the mycobacterium as a host defense mechanism.[85] The innate immune response of the human body thus kicks into action to provide protection against infection and disease.

There are 2 host-bacteria attachment mechanisms that facilitate the attachment of *Mycobacterium tuberculosis* to host cells for infection to occur:

a) Mycobacterium tuberculosis has specific cell wall surface structures that can act as ligands and recognize and bind to complementary host proteins in a lectin like manner. These ligands are lipoarabinomannan.[17,85]

b) *M. tuberculosis* also has proteins expressed on its outer surface that is able to bind to ligands of the host cells. These *M. tuberculosis* proteins include fibronectin-binding proteins, heparin-binding haemagglutinin adhesion (HBHA) and laminin-binding protein.[88-92]

a) Mycobacterial ligand and host protein

The terminal mannose caps of lipoarabinomannan play a critical role and act as mycobacterial ligands that can bind to a variety of soluble and cell surface receptors,[86] such as macrophage mannose receptor (MR),[92,94,95] mannose binding protein (MBP),[96-98] concanavalin A,[99,100] dendritic cell-specific intercellular adhesion molecule grabbing non-integrin (DC-SIGN),[100-102] lung surfactant protein (Sp-A and Sp-D),[84,97,103] conglutinin, bovine collectin-43,[97,104] complement receptors and scavenger receptors,[85,105,106] to name but a few.

Most of these receptors are also collectively known as collectins and are important molecules in the innate immune defense against bacteria and other microorganisms.[96,107,108] Collectins are oligomeric proteins containing a carboxy-terminal carbohydrate recognition domain (CRD)[98,104] as a pattern recognition receptor that selectively recognize the terminal α-D-mannose caps on LAM molecules on the mycobacterial cell wall and can therefore differentiate between different mycobacterium species.[86,101] The terminal mannose cap of LAM binds the strongest to the host receptors and not mannose in the backbone of the molecule.[109] Although the lipoarabinomannan (LAM) is an abundant lipoglycan specific to the mycobacteria species, the poly-mannosylated LAM is specific only to the slow growing pathogens *M. tuberculosis, M. leprae and M. bovis BCG*[71,84] and is a key ligand of these receptors.[94,104,110-113] These receptors do not bind LAM that does not have mannose caps.[102]

For the interaction between the ligand and host receptor to be strong, it is important to have a multivalent interaction, since the carbohydrate-binding site is very small and affinity between the CRD and a single ligand is very low (K_i ~ 1mM).[98,114] These receptors bind the mannose caps of the mycobacterial components in a Ca^{2+}-dependent manner and optimally at neutral pH.[115]

b) Mycobacterial protein and host ligand

Mycobacterium tuberculosis also has proteins expressed on its outer surface that are able to bind to host ligands. One such ligand-host combination is the fibronectin-binding antigens of mycobacteria that are able to bind to human fibronectin on the host cell surface or any fibronectin-coated surface.[88,116] This fibronectin-binding protein is specific to mycobacteria.[89-91,117,118] The binding of mycobacterial antigens to fibronectin has a very high affinity and is a key process in the infection process.[119]

Another ligand-host combination is the heparin-binding haemagglutinin adhesion (HBHA) that *Mycobacterium tuberculosis* expresses on their surface that allows the organism to bind to cell surface heparan sulfate proteoglycans of epithelial cells.[92,120] The recognition domain of HBHA is a carboxy-terminal lysine-rich domain with adherence relying on the recognition of heparan sulfate proteoglycans, a complex molecule comprising a core protein with covalently linked glycosaminoglycan (GAG) chains.[120-122] The frequency and ubiquitous distribution of GAG chains on cell surfaces and in extracellular matrixes make them well suited as key ligands for mycobacterial attachment. HBHA also induces mycobacterial aggregation and bacteria-bacteria interactions that lead to mycobacterial colonization at the site of attachment.[93,116,123]

Based on the *Mycobacterium tuberculosis* cell wall structure, a variety of chemical groups has the potential to act as functionalization agents to modify the string polymer with, in order to facilitate *M. tuberculosis* capture.

2.7 Polymer

Styrene-maleic anhydride copolymer (SMA) is a cheap and versatile polymer[124] comprising nonpolar styrene and polar maleic anhydride that is easily synthesized through conventional free radical copolymerization. The polar and nonpolar combination of monomers makes the copolymer soluble in a wide variety of solvents, depending on the ratio of styrene and maleic anhydride.[125] SMA is a thermoplastic polymer with low toxicity,[126,127] high heat resistance[128] and good dimensional stability.[129]

The maleic anhydride group has high reactivity towards amidation, esterification and hydrolysis.[128,130-133] Any chemical group with a suitable reactive group can thus covalently attach to the maleic anhydride segment of SMA via a nucleophilic ring-opening reaction of the 5-membered anhydride group, making it ideal for functionalization.[126,128,134,135] Ring closure is effected by heat treatment.[136]

The hydrophobic/hydrophilic character of SMA can easily be modified by either adjusting the styrene-maleic anhydride ratio or by incorporating long hydrophobic alkyl chains or hydrophilic oxyalkalene molecules, thus making SMA an ideal platform for functionalization in order to enhance *M. tuberculosis* capture.

Another advantage to using SMA as the base polymer is the ease with which it can be electrospun.[129] SMA can also be modified before or after electrospinning. Modification of SMA before electrospinning can change the properties of the polymer considerably and thus affect the electrospinnability of the polymer. When modifying SMA before electrospinning, a new polymer is formed that may have different spinning parameters compared to pure SMA. These potential problems may be overcome by surface-functionalizing the SMA nanofibers after electrospinning. One advantage in doing that is that only the surface of the polymer nanofiber is modified; the bulk properties of the polymer remain unchanged.[128] A second advantage is that surface-active chemical groups can be used that would have made the electrospinning process difficult or impossible if functionalization was done before electrospinning. Functionalities can thus be incorporated on the surface of the polymer nanofibers that are not electrospinnable.

2.8 Electrospinning

Electrospinning is a simple but versatile technique that allows the production of continuous polymer fibers with fiber diameters in the submicron range, typically 50-500nm.[137-139] Although the process of electrospinning has been known for the last 75 years with the first patent issued in 1934,[140] it only became a topic of interest and a research area again the last couple of years. [137-139,141]

The versatility of the electrospinning process lies in the fact that it can be applied to a wide variety of polymers and produces nanofibers with high specific surface area and high aspect ratio,[142-144] making them ideal for a wide variety of applications, such as filtration media,[145-149] sensors,[150] biomedical textiles,[151,152] tissue scaffolding[144,148,151] and drug delivery systems,[141,144,151] to name but a few.[137,138,153] In addition, the electrospinning technique allows easy functionalization of the polymer nanofibers, superior mechanical properties and easy processing.[144,150,151,154] Each of these factors adds to the versatility of the process and its product.

2.8.1 Electrospinning process

Figure 2.2 is a schematic illustration of the basic electrospinning set-up.

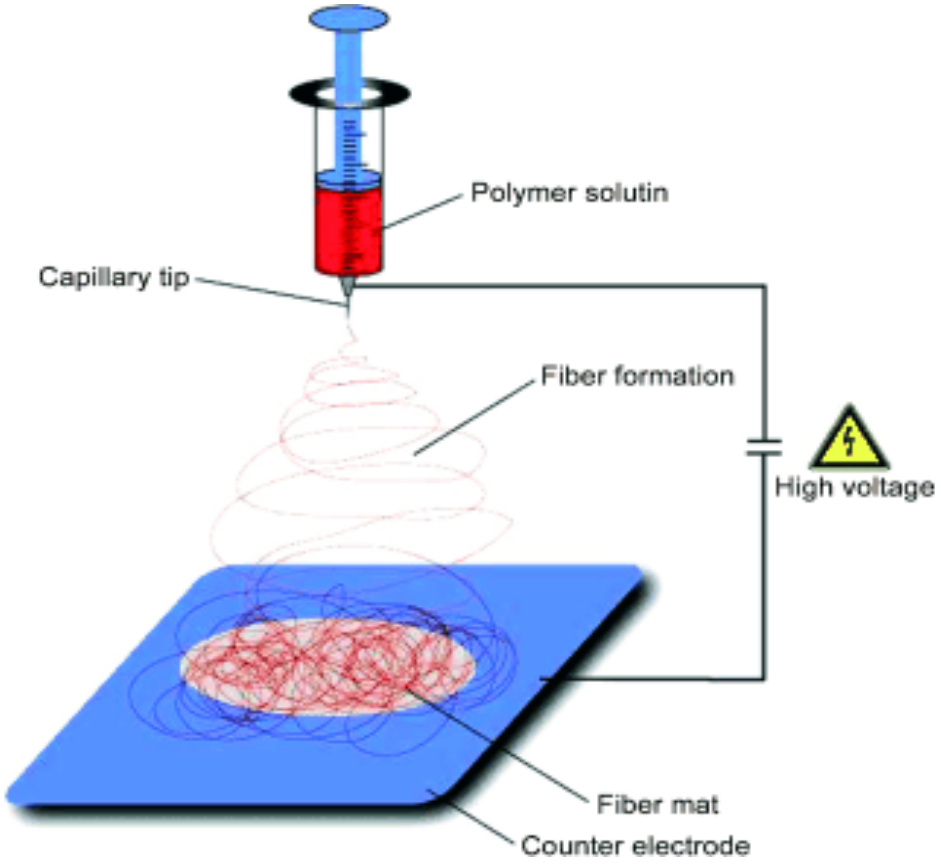

Figure 2.2 Basic electrospinning set-up.[155]

The process of electrospinning entails the following: A capillary is filled with a polymer solution. A high voltage is applied to the polymer-filled capillary using an electrode. This electrode can either be inserted into the polymer solution or it can be placed onto the tip of the capillary if a syringe with a metal needle is used. A droplet is then initiated at the tip of the capillary, either using a pump or by gravity. The electrode induces a charge on the surface of the polymer droplet. The polymer droplet is

now subjected to two opposing forces, namely the electrostatic repulsive force caused by the same charge as introduced by the electrode and the polymer solution surface tension. The charge repulsion force will aim to expand the surface area of the droplet and the solution surface tension that is a contractive force will aim to reduce the surface area of the droplet. As the intensity of the electric field is increased, the hemispherical surface of the polymer solution at the tip of the capillary elongates to form a cone, known as the Taylor cone.[156] As the electrical field increases even more, a critical point is reached where the electrostatic repulsive force overcomes the surface tension of the polymer solution and a charged jet of polymer solution is ejected from the tip of the Taylor cone. Although the jet is straight and stable near the tip of the capillary, it enters a region of instability[157] and undergoes a whipping process due to the electrostatic repulsive force from the similar charged ions within the electrospinning jet[148] before it reaches its target as dried nanofibers. During this whipping process the electrically charged jet coils onto itself repeatedly, with each coil having turns of increasing radius.[141,143] (Refer Figure 2.3) This whipping action stretches the charged jet, thereby decreasing the fiber diameter from micrometers to nanometers; whilst the solvent steadily evaporates,[137,148] resulting in dry fibers landing on the target to form a nonwoven web of nanofibers.[143,158] The target is usually a grounded collecting metal platform or oppositely charged to the capillary and placed a certain distance away from the tip of the capillary, thereby creating an electric field between the capillary and collector.[155,159]

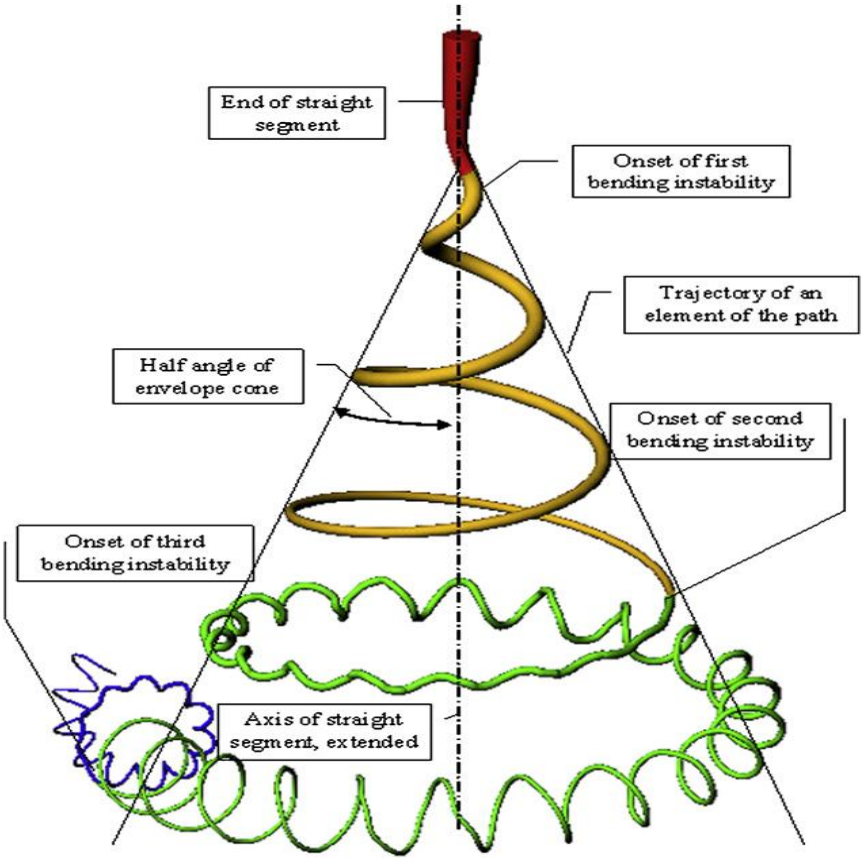

Figure 2.3 Schematic illustrating bending instability of the polymer jet to the third degree during electrospinning process.[141]

2.8.2 Electrospinning process parameters

There is a variety of parameters and processing variables that influences the electrospinning process. These are:

a) system parameters such as molar mass, molar mass distribution and polymer architecture (linear or branched),

b) solution parameters such as viscosity, conductivity and surface tension, and

c) process parameters such as electric field strength, flow rate, distance between capillary and target and ambient parameters (temperature and humidity).[138,139]

These parameters do not act or influence the electrospinning process individually. There is an interplay between them whereby changing the one parameter will have an effect on another parameter or parameters.[160] For example, fibers can only be formed during the electrospinning process if there are proper and adequate polymer chain entanglements.[161] The molar mass of the polymer and/or concentration of the polymer solution must therefore be sufficient for fibers to form, yet not so high that the resultant viscosity prevents the polymer solution jet to be induced by the electric field. In addition, the surface tension of the polymer solution must be low enough, the charge density high enough for a polymer jet to form and the viscosity high enough to prevent the jet from collapsing into droplets before solvent evaporation.[137,138]

By adjusting electrospinning process parameters like polymer solution feed rate, spinning distance and electric field strength and solution parameters like viscosity and conductivity, almost any polymer can be electrospun.[145,151]

For the purpose of this project, nanofibers had to be spun with high surface area to unit mass ratio for optimum binding of *Mycobacterium tuberculosis* to the functionalized polymer surface. Although numerous research papers have been published regarding the influence of the various parameters on the electrospinning process, only those parameters affecting fiber diameter will be discussed further.

2.8.3 Electrospinning process parameters affecting fiber diameter

Since nanofibers are the result of solvent evaporation and solidification of the polymer jets, the fiber diameter will primarily depend on the jet sizes and polymer content of the jets, i.e. a function of material and process parameters.[139] Viscosity, applied electric field strength, solution conductivity,

distance between capillary and target and polymer solution flow rate are the electrospinning parameters that have the largest influence on the diameter of the fiber formed.[138,150,152,162] Voltage and distance between capillary and target determine the strength of the electric field felt by the solution jet. As these parameters have an influence on the amount of whipping and stretching done by the solution jet, it will have a significant effect on the fiber diameter.

a) Viscosity

Viscosity refers to the resistance of a fluid to flow. The viscosity of a polymer solution is affected by the polymer solution concentration and molar mass of the polymer, with solution viscosity increasing with increasing solution concentration and molar mass of the polymer. Viscosity is a key parameter that determines electrospun fiber diameter.[163] As the viscosity of the polymer solution increases, so does the fiber diameter of the electrospun fiber due to more polymer chain entanglements and greater resistance of the viscous solution to stretch and elongate.[159,160,162,164] The jet path is also reduced since the bending instability will be smaller at higher viscosity, resulting in less whipping and stretching. If the viscosity is too high, a jet is not easily induced, even if the electric field strength is increased further.[138,139,150,152] If the viscosity however is too low, there are not enough polymer chain entanglements to stabilize the jet. The jet will break up into droplets due to Rayleigh instability that spray towards the target.[163,165] This phenomenon is known as electrospraying.[148,155,161]

Beaded fibers can also be formed when low concentration polymer solutions are electrospun due to insufficient polymer chain entanglements. As the concentration increases, beading will get less until smooth bead-free fibers are produced.[143,154,166] Bead formation is also a consequence of high surface tension since a high surface tension will aim to reduce the surface area per unit; the jet will break up and thus form beads. If a solution of higher viscosity is used, beading will be reduced due to the solution being stretched more without breaking.[143]

b) Electric field

For electrospinning to take place, an electric field is applied between the capillary (filled with polymer solution) and the target. Electric field strength is a function of the applied voltage and distance between the tip of capillary and target as defined by the following equation:

$$\mathbf{E = V/d}$$

where E = electric field strength

V = voltage difference between electrodes

d = distance between electrodes

When an electric field is applied between the polymer solution and target, the applied voltage to the solution induces charges within the solution. The mutual charges in the solution are repelled by the same charges applied via the electrode. These similar charges flow through the solution and accumulate on the surface of the polymer solution droplet, thereby increasing the charge density. The electrostatic repulsive force from the mutual charges on the droplet surface works to increase the surface area of the droplet and works against the contractive surface tension of the solution. Only when the electrostatic repulsive force overcomes the solution surface tension does a polymer jet eject from the Taylor cone.[156] This charged polymer jet undergoes whipping and stretching due to the electrostatic repulsive charges within the jet, thus decreasing the fiber diameter continuously until all solvent has evaporated and lands on the target as dry fibers in the submicron range.[159]

The higher the applied electric field, the more whipping and stretching of the polymer jet takes place due to an increase in charge density on the jet, resulting in a finer fiber diameter.[148,150,163,166] If the electric field is high, but the distance is small, thicker fibers may form due to insufficient whipping and stretching and/or wet fibers may form, as the solvent did not have sufficient time to evaporate before landing on the target.

The applied electrical field also has a strong influence on bead formation. The higher the net charge density carried by the jet (and solution viscosity of the polymer solution), the less beads are formed.[138] But, as the concentration of the polymer solution increases, the electric field required to induce a jet also needs to increase, indicating that more force is needed to form a jet from a highly viscous polymer solution.[137]

The polarity of the electric field potential does not have any effect on the jet or electrospinning process.[137,152] The jet is only driven by the high electric potential applied between the capillary and target.[142]

c) Electrical conductivity

The electrical conductivity of a solution refers to its ability to facilitate the flow of charge via the polymer molecules, solvent molecules or impurities in the solution. Solution conductivity is a key parameter in the electrospinning process since the polymer solution jet is stretched from capillary to target due to the repulsion of the mutual charges present on its surface causing whipping and stretching. More charges can be carried at higher solution conductivity, resulting in more whipping and stretching taking place, thus lower fiber diameters.[154,163] A solution with zero conductivity cannot be electrospun as no charge can flow through the solution. With an increase in the solution conductivity, lower electric field strength is required to overcome the solution surface tension and induce a polymer jet. The electrical conductivity of a solution can be increased by the addition of salt, an increase in temperature or using another solvent. Salt usually dissociates into positive and negative ions that move independently, thereby increasing the charge carrying capacity of the jet and thus the electrical conductivity of the polymer solution.[139]

d) Distance between capillary and target

The electric field strength is also influenced by the distance between the capillary and target, with an increase in distance resulting in a decrease in fiber diameter, indicating that more stretching of the polymer jet is taking place as the jet path is longer.[137,148,152]

e) Flow rate of polymer solution

Flow rate refers to the speed with which the polymer solution is pumped into the capillary. The polymer flow rate has an influence on the fiber diameter with the fiber diameter increasing with an increase in polymer solution flow rate due to more solution being drawn from the tip of the capillary.[143,148] This is the case up to a point where after the polymer solution will start dripping from the tip of the capillary as the excess solution cannot be carried away fast enough by the charge.[150,167] With an increase in flow rate there is also an increase in the variation in fiber diameter.[143]

If the flow rate is too low, the Taylor cone disappears, resulting in a discontinuous jet from the polymer solution. The flow rate is optimal if the polymer solution is carried away by the jet at the same rate as it is pumped into the capillary.

To conclude, in this chapter, TB and the diagnosis thereof have been discussed. The difficulties in diagnosing paediatric TB have also been highlighted, as well as the reasons why this is so. Various ways to address this problem have been considered, one being an improved specimen collection method in young children who are unable to expectorate. Although young children cannot produce sputum on demand, they swallow it and the sputum collects in the stomach. Incidentally, *M. tuberculosis* is one of the few bacteria that are able to survive in the extreme acidic environment of the stomach for extended periods. Neunier proved successfully that *M. tuberculosis* can be cultured from stomach contents; thus providing evidence of tuberculosis infection in children.[36]

As most of the laboratory techniques used for the diagnosis of TB are dependent on the detection of *M. tuberculosis*, it is important to obtain good quality specimens with the highest possible concentration of mycobacteria to enable the accurate diagnosis of tuberculosis. By using a polymer, task specifically functionalized to capture *M. tuberculosis* in the stomach, specimen collection can be improved by increasing the yield of *M. tuberculosis* in the specimen, thus improving the chance of successfully detecting *M. tuberculosis* and diagnosing paediatric TB.

A polymer, SMA, has been identified that is easily modified with suitable chemical moieties for increased affinity between the modified polymer and *M. tuberculosis* for the polymer to act as a *M. tuberculosis*-capturing platform. A suitable method has been identified, namely electrospinning, to produce polymer nanofibers with a high specific surface area to provide a vast surface area for *M. tuberculosis* capture.

In summary, by combining a task-specific modified polymer, electrospun into nanofibers as a specimen collection device for *Mycobacterium tuberculosis* under gastric conditions, the yield of *M. tuberculosis* in the collected specimen can be improved. This should improve the successful diagnosis of paediatric TB.

2.9 References

1. Dye, C. *Lancet* **2006**, *367*, 938-940.

2. Walls, T.; Shingadia, D. *J. Infect*. **2004**, *48*, 13-22.

3. Corrigan, D.L.; Paton, J.Y. *Breathe* **2007**, *3,* 351-363.

4. Marais, B.J.; Pai, M. *Br. Med. J*. **2007**, *92*, 446-452.

5. Maher, D. *Int. J. Tuberc. Lung Dis*. **2006**, *10*, 1091–1097.

6. Malbruny, B.; Le Marrec, G.; Courageux, K.; Leclercq, R.; Cattoir, V. *Int. J. Tuberc. Lung Dis.* **2011**, *15*, 553-555.

7. Peeling, R.W.; Mabey, D. *Clinical Microbiology and Infection* **2010**, *16*, 1062-1069.

8. Shingadia, D.; Novelli, V. *Lancet Infect. Dis.* **2003**, *3*, 624-632.

9. Dye, C. *WHO Report: Global tuberculosis control: Surveillance, planning, financing,* **2007**.

10. Nelson, L.J.; Wells, C.D. *Int. J. Tuberc. Lung Dis.* **2004**, *8*, 636-647.

11. Gray, J.W. *Clin. Biochem*. **2004**, *37*, 450-455.

12. Iseman, M.D.; Heifets, L.B. *N. Engl. J. Med.* **2006**, *355,* 1606-1608.

13. Curtis, A.B.; Ridzon, R.; Vogel, R.; McDonough, S.; Hargreaves, J.; Ferry, J.; et al. *N. Engl. J. Med*. **1999**, *341,* 1491-1495.

14. Parsons, L.M.; Somoskovi, A.; Gutierrez, C.; Lee, E.; Paramasivan, C.N.; Abimiku, A.; et al. *Clin. Microbiol. Rev*. **2011**, *24*, 314-349.

15. Lin, P.L.; Flynn, J.A.L. *J. Immunol.* **2010**, *185*, 15-22.

16. Wallis, R.S.; Pai, M.; Menzies, D.; Doherty, T.M.; Walzl, G.; Perkins, M.D.; et al. *Lancet* **2010**, *375*, 1920-1937.

17. Dheda, K.; Schwander, S.K.; Zhu, B.; Van Zyls, R.N.; Zhangy, Y. *Respirology* **2010**, *15*, 433-450.

18. Starke, J.R. *Paediatr. Infect. Dis. J*. **2000**, *19*, 1095.

19. Lixia, Z.; Xiaoxiao, H.; Dinggeng, H.; Kemin, W. *Clin. Dev. Immunol.* **2011**, *2011*, 1-8.

20. Small, P.M.; Pai, M. *N. Engl. J. Med*. **2010**, *363*, 1070-1071.

21. Marais, B.J.; Gie, R.P.; Schaaf, H.S.; Beyers, N.; Donald, P.R.; Starke, J.R. *Am. J. Respir. Crit. Care Med.* **2006**, *173*, 1078-1090.

22. Hesseling, A.C.; Schaaf, H.S.; Gie, R.P.; Starke, J.R.; Beyers, N. *Int. J. Tuberc. Lung Dis*. **2002**, 6, 1038-1045.

23. Mwinga, A. *Lancet* **2005**, *365*, 97-98.

24. Van Rie, A.; Beyers, N.; Gie, R.P.; Kunneke, M.; Zietsman, L.; Donald, P.R. *Arch. Dis. Child*. **1999**, *80*, 433-437.

25. Cuevas, L.E. *Indian J. Pediatr*. **2010**, 1-7.

26. Pai, M.; Minion, J.; Steingart, K.; Ramsay, A. *Curr. Opin. Pulm. Med*. **2010**, *16*, 271-284.

27. Marais, B.; Hesseling, A.; Gie, R.; Schaaf, H.; Beyers, N. *Int. J. Tuberc. Lung Dis.* **2006**, *10*, 259-263.

28. Donald, P.R. *Curr. Opin. Pulm. Med*. **2002**, *8*, 178-182.

29. Marais, B.J.; Obihara, C.C.; Warren, R.M.; Schaaf, H.S.; Gie, R.P.; Donald, P.R. *Int. J. Tuberc. Lung Dis*. **2005**, *9*, 1305-1313.

30. Graham, S.M. *Lancet Infect. Dis*. **2010**, *10*, 581-582.

31. Nicol, M.P.; Zar, H.J. *Paediatr. Respir. Rev.* **2011**, *12*, 16-21.

32. Starke, J.R. *Tuberculosis* **2003**, *83*, 208-212.

33. Machingaidze, S.; Wiysonge, C.S.; Gonzalez-Angulo, Y.; Hassan Mahomed, M.M. *Pediatr. Infect. Dis. J*. **2011**, *30*, 1-7.

34. Richeldi, L. *Am. J. Respir. Crit. Care Med.* **2006**, *174*, 736-742.

35. Marais, B.J.; Gie, R.P.; Schaaf, H.S.; Hesseling, A.C.; Obihara, C.C.; Nelson, L.J.; et al. *Int. J. Tuberc. Lung Dis*. **2005**, *8*, 278-285.

36. Eamranond, P.; Jaramillo, E. *Int. J. Tuberc. Lung Dis*. **2001**, *5,* 594-603.

37. Oberhelman, R.A.; Soto-Castellares, G.; Gilman, R.H.; Caviedes, L.; Castillo, M.E.; Kolevic, L.; et al. *Lancet Infect. Dis.* **2010**, *10*, 612-620.

38. Nelson, L.J.; Wells, C.D. *Sem. Paediatr. Infect. Dis.* **2004**, 150-154.

39. Butt, T.; Ahmad, R.N.; Kazmi, S.Y.; Afzal, R.K.; Mahmood, A. *J. Coll. Physicians Surg. Pak.* **2003**, *13*, 728-734.

40. Lalvani, A.; Pareek, M. *Br. Med. Bull*. **2009**, 1-16.

41. Cruz, A.T.; Geltemeyer, A.M.; Starke, J.R.; Flores, J.A.; Graviss, E.A.; Smith, K.C. *Pediatrics* **2011**, *127*, 31-41.

42. Pai, M.; Minion, J.; Sohn, H.; Zwerling, A.; Perkins, M.D. *Clin. Chest Med.* **2009**, *30,* 701-716.

43. Nahid, P.; Pai, M.; Hopewell, P.C. *Am. Thoracic Soc*. **2006**, *3*, 103-110.

44. Tiwari, R.P.; Hattikudur, N.S.; Bharmal, R.N.; Kartikeyan, S.; Deshmukh, N.M.; Bisen, P.S. *Tuberculosis* **2007**, *87*, 193-201.

45. Lemaire, J.F.; Casenghi, M. *J. Int. AIDS Soc.* **2010**, *13*, 1-7.

46. Kuhn, W.; Armstrong, D.; Atteberry, S.; Dewbrey, E.; Smith, D.; Hooper, N. *The Open Microbiology Journal* **2010**, *4*, 30-33.

47. Perkins, M.D.; Roscigno, G.; Zumla, A. *Lancet* **2006**, *367,* 942-943.

48. Eisenberg, R.L.; Pollock, N.R. *Radiology* **2010**, *256*, 998-1004.

49. Moore, D.; Evans, C.; Gilman, R.; Vargas, D.; Escombe, R. *Lancet* **2005**, *365*, 1541-1542.

50. Cho, S.N.; Brennan, P.J. *Tuberculosis* **2007**, *87*, 14-17.

51. De Charnace, G.; Delacourt, C. *Paediatr. Respir. Rev.* **2001**, *2*, 120-126.

52. Marais, B.J.; Pai, M. *Indian J. Med. Microbiol.* **2006**, *24*, 249-253.

53. Khan, E.A.; Starke, J.R. *Emerg. Infect. Dis.* **1995**, *1*, 115-123.

54. Ling, D.I.; Zwerling, A.A.; Steingart, K.R.; Pai, M. *Paediatr. Respir. Rev.* **2011**, *12*, 9-15.

55. Marais, B.J.; Graham, S.M.; Cotton, M.F.; Beyers, N. *J. Infect. Dis*. **2007**, *196*, 76-85.

56. Shenai, S.; Minion, J.; Vadwai, V.; Tipnis, T.; Shetty, S.; Salvi, A.; et al. *Int. J. Tuberc. Lung Dis*. **2011**, *15*, 483-488.

57. Minion, J.; Pai, M.; Ramsay, A.; Menzies, D.; Greenaway, C. *PloS one* **2011**, *6*, 1-6.

58. Urbanczik, R. *Int. J. Tuberc. Lung Dis*. **2010**, *14*, 1087-1093.

59. Rodrigues, C. *Indian J. Med. Microbiol.* **2011**, *29*, 2-3.

60. Steingart, K.R.; Flores, L.L.; Dendukuri, N.; Schiller, I.; Laal, S.; Ramsay, A.; et al. *PLoS Medicine* **2011**, *8*, 1-18.

61. Dowdy, D.W.; Steingart, K.R.; Pai, M. *PLoS Medicine* **2011**, *8*, 1-18.

62. Cordova, J.; Shiloh, R.; Gilman, R.H.; Sheen, P.; Martin, L.; Arenas, F.; et al. *J. Clin. Microbiol*. **2010**, *48*, 1820-1826.

63. Wolf, H.; Mendez, M.; Gilman, R.H.; Sheen, P.; Soto, G.; Velarde, A.K.; et al. *Am. J. Trop. Med. Hyg*. **2008**, *79*, 893-898.

64. Gilman, R.H.; Islam, S.; Rabbani, H.; Ghosh, H. *Lancet* **1979**, *1*, 795-796.

65. Velapatino, B.; Balqui, J.; Gilman, R.H.; Bussalleu, A.; Quino, W.; Finger, S.A.; et al. *J. Clin. Microbiol*. **2006**, *44*, 976-980.

66. Marais, B.J.; Pai, M. *Paediatr. Respir. Rev.* ***2007***, *8*, 124-133.

67. Chow, F.; Espiritu, N.; Gilman, R.H.; Gutierrez, R.; Lopez, S.; Escombe, A.R.; et al. *BMC Infect. Dis*. **2006**, *6*, 67-74.

68. Heymann, S.J.; Brewer, T.F.; Wilson, M.E.; Colditz, G.A.; Fineberg, H.V. *Pediatrics* **2000**, *106*, 1-7.

69. Kolattukudy, P.E.; Fernandes, N.D.; Azad, A.K.; Fitzmaurice, A.M.; Sirakova, T.D. *Mol. Microbiol*. **2003**, *24*, 263-270.

70. Karakousis, P.C.; Bishai, W.R.; Dorman, S.E. *Cell Microbiol*. **2004**, *6*, 105-116.

71. Bhowruth, V.; Alderwick, L.; Brown, A.; Bhatt, A.; Besra, G. *Biochem. Soc. Trans.* **2008**, *36*, 555-565.

72. Jarlier, V.; Nikaido, H. *FEMS Microbiol. Lett*. **1994**, *123*, 11-18.

73. Barry, C.E.; Lee, R.E.; Mdluli, K.; Sampson, A.E.; Schroeder, B.G.; Slayden, R.A.; et al. *Prog. Lipid Res.* **1998**, *37*, 143-179.

74. Brennan, P.J. *Tuberculosis* **2003**, *83*, 91-97.

75. Pitarque, S.; Larrouy-Maumus, G.; Payré, B.; Jackson, M.; Puzo, G.; Nigou, *J. Tuberculosis* **2008**, *88*, 560-565.

76. Alderwick, L.; Birch, H.; Mishra, A.; Eggeling, L.; Besra, G. *Biochem. Soc. Trans*. **2007**, *35*, 1325-1328.

77. Chatterjee, D. *Curr. Opin. Chem. Biol*. **1997**, *1*, 579-588.

78. McNeil, M.R.; Brennan, P.J. *Res. Microbiol*. **1991**, *142*, 451-463.

79. Rezwan, M.; Lanéelle, M.A.; Sander, P.; Daffé, M. *J. Microbiol. Methods* **2007**, *68,* 32-39.

80. Brennan, P.J. *Rev. Infect. Dis*. **1989**, *11*, 420-430.

81. Ojha, A.; Anand, M.; Bhatt, A.; Kremer, L.; Jacobs, Jr W.R.; Hatfull, G.F. *Cell* **2005**, *123*, 861-873.

82. Ortalo-Magne, A.; Lemassu, A.; Laneelle, M.A.; Bardou, F.; Silve, G.; Gounon, P.; et al. *J. Bacteriol*. **1996**, *178*, 456-461.

83. Converse, S.E.; Mougous, J.D.; Leavell, M.D.; Leary, J.A.; Bertozzi, C.R.; Cox, J.S. *Proc. Natl. Acad. Sci. U S A.* **2003**, *100*, 6121-6126.

84. Nigou, J.; Gilleron, M.; Puzo, G. *Biochimie* **2003**, *85*, 153-166.

85. Villeneuve, C.; Gilleron, M.; Maridonneau-Parini, I.; Daffe, M.; Astarie-Dequeker, C.; Etienne, G. *J. Lipid Res.* **2005**, *46*, 475-483.

86. Maeda. N.; Nigou, J.; Herrmann, J.L.; Jackson, M.; Amara, A.; Lagrange, P.H.; et al. *J. Biol. Chem*. **2003**, *278*, 5513-5516.

87. Thorson, L.M.; Doxsee, D.; Scott, M.G.; Wheeler, P.; Stokes, R.W. *Infect. Immunol*. **2001**, *69*, 2172-2179.

88. Ratliff, T.L.; McGarr, J.A.; Abou-Zeid, C.; Rook, G.A.W.; Stanford, J.L.; Aslanzadeh, J.; et al. *Microbiology* **1988**, *134*, 1307-1313.

89. Zhao, W.; Schorey, J.S.; Groger, R.; Allen, P.M.; Brown, E.J.; Ratliff, T.L. *J. Biol. Chem.* **1999**, *274*, 4521-4526.

90. Naito, M.; Ohara, N.; Matsumoto, S.; Yamada, T. *J. Biol. Chem*. **1998**, *273*, 2905.

91. Espitia, C.; Laclette, J.P.; Mondragon-Palomino, M.; Amador, A.; Campuzano, J.; Martens, A.; et al. *Microbiology* **1999**, *145*, 3487-3495.

92. Menozzi, F.D.; Rouse, J.H.; Alavi, M.; Laude-Sharp, M.; Muller, J.; Bischoff, R.; et al. *J. Exp. Med.* **1996**, *184*, 993-1001.

93. Pethe, K.; Alonso, S.; Biet, F.; Delogu, G.; Brennan, M.J.; Locht, C.; et al. *Nature* **2001**, *412*, 190-194.

94. Taylor, M.E.; Drickamer, K. *J. Biol. Chem*. **1993**, *268*, 399-404.

95. Strohmeier, G.R.; Fenton, M.J. *Microb. Infect*. **1999**, *1,* 709-717.

96. Dommett, R.M.; Klein, N.; Turner, M.W. *Tissue Antigens* **2006**, *68*, 193-209.

97. Ernst, J.D. *Infect. Immun*. **1998**, *66*, 1277-1281.

98. Ip, W.K.E.; Takahashi, K.; Ezekowitz, R.; Stuart, L.M. *Immunol. Rev.* **2009**, *230*, 9-21.

99. Brewer, C.F.; Brown, III R.D. *Biochemistry (N Y)* **1979**, *18*, 2555-2562.

100. Dinadayala, P.; Kaur, D.; Berg, S.; Amin, A.G.; Vissa, V.D.; Chatterjee, D.; et al. *J. Biol. Chem*. **2006**, *281*, 20027-20035.

101. Geijtenbeek, T.B.H.; Van Vliet, S.J.; Koppel, E.A.; Sanchez-Hernandez, M.; Vandenbroucke-Grauls, C.M.J.E.; Appelmelk, B.; et al. *J. Exp. Med*. **2003**, *197*, 7-17.

102. Van Kooyk, Y.; Geijtenbeek, T.B.H. *Nature Rev. Immunol.* **2003**, *3*, 697-709.

103. Pasula, R.; Downing, J.F.; Wright, J.R.; Kachel, D.L.; Davis, T.E.; Martin, W.J. *Am. J. Respir. Cell. Mol. Biol.* **1997**, *17*, 209-217.

104. Tailleux, L.; Schwartz, O.; Herrmann, J.L.; Pivert, E.; Jackson, M.; Amara, A.; et al. *J. Exp. Med*. **2003**, *197*, 121-127.

105. Kawai, T.; Suzuki, Y.; Eda, S.; Ohtani, K.; Kase, T.; Fujinaga, Y.; et al. *Gene* **1997**, *186*, 161-165.

106. Kilpatrick, D.C. *Immunol. Lett*. **1998**, *61*, 191-195.

107. Hoppe, H.J.; Reid, K.B.M. *Structure* **1994**, *2*, 1129-1133.

108. Weis, W.I.; Taylor, M.E.; Drickamer, K. *Immunol. Rev*. **2006**, *163,* 19-34.

109. Polotsky, V.Y.; Belisle, J.T.; Mikusova, K.; Ezekowitz, R.A.B.; Joiner, K.A. *J. Infect. Dis*. **1997**, *175*, 1159-1168.

110. Fraser, I.P.; Koziel, H.; Ezekowitz, R.A.B. *Sem. Immunol.* **1998**, 363-372.

111. Mullin, N.P.; Hitchen, P.G.; Taylor, M.E. *J. Biol. Chem*. **1997**, *272*, 5668-5681.

112. Taylor, M.E.; Brickell, P.M.; Craig, R.K.; Summerfield, J.A. *Biochem. J*. **1989**, *262*, 763-771.

113. Schweinle, J.E.; Nishiyasu, M.; Ding, T.Q.; Sastry, K.; Gillies, S.D.; Ezekowitz, R.A. *J. Biol. Chem*. **1993**, *268*, 364-370.

114. Ng, K.K.S.; Drickamer, K.; Weis, W.I. *J. Biol. Chem*. **1996**, *271*, 663-674.

115. Sastry, K.; Herman, G.A.; Day, L.; Deignan, E.; Bruns, G.; Morton, C.C.; et al. *J. Exp. Med*. **1989**, *170*, 1175-1189.

116. Brennan, M.J.; Delogu, G.; Chen, Y.; Bardarov, S.; Kriakov, J.; Alavi, M.; et al. *Infect. Immunol*. **2001**, *69*, 7326-7333.

117. Middleton, A.M.; Chadwick, M.V.; Nicholson, A.G.; Dewar, A.; Groger, R.K.; Brown, E.J.; et al. *Respir. Med*. **2004**, *98*, 1203-1206.

118. Hynes, R.O.; Yamada, K.M. *J. Cell Biol*. **1982**, *95*, 369-377.

119. Abou-Zeid, C.; Ratliff, T.L.; Wiker, H.G.; Harboe, M.; Bennedsen, J.; Rook, G.A. *Infect. Immun*. **1988**, *56*, 3046-3051.

120. Tumova, S.; Woods, A.; Couchman, J.R. *Int. J. Biochem. Cell Biol*. **2000,** *32*, 269-288.

121. Yanagishita, M.; Hascall, V.C.; Sandberg, K.; Ji, H.; Clark, A.J.; Shapira, H.; et al. *Cell* **1992**, *267*, 9451-9454.

122. David, G.; Bernfield, M. *Matrix Biol*. **1998**, *17*, 461-463.

123. Delogu, G.; Brennan, M.J. *J. Bacteriol*. **1999**, *181,* 7464-7469.

124. Lai, X.; Sun, C.; Tian, H.; Zhao, W.; Gao, L. *Int. J. Pharm*. **2008**, *352*, 66-73.

125. Shulkin, A.; Stover, H.D.H. *J. Membr. Sci.* **2002**, *209*, 421-432.

126. Ignatova, M.; Stoilova, O.; Manolova, N.; Mita, D.; Diano, N.; Nicolucci, C.; et al. *Eur. Polym. J.* **2009**, *45*, 2494-2504.

127. Lee, S.S.; Ahn, T.O. *J. Appl. Polym. Sci.* **1999**, *71*, 1187-1196.

128. Stoilova, O.; Ignatova, M.; Manolova, N.; Godjevargova, T.; Mita, D.; Rashkov, I. *Eur. Polym. J.* **2010**, *46*, 1966-1974.

129. Tang, C.; Ye, S.; Liu, H. *Polymer* **2007**, *48*, 4482-4491.

130. Vermeesch, I.; Groeninckx, G. *J. Appl. Polym. Sci.* **1994**, *53*, 1365-1373.

131. Wang, K.; Huang, W.; Xia, P.; Gao, C.; Yan, D. *React. Funct. Polym.* **2002**, *52*, 143-148.

132. Henry, S.M.; El-Sayed, M.E.H.; Pirie, C.M.; Hoffman, A.S.; Stayton, P.S. *Biomacromolecules* **2006**, *7*, 2407-2414.

133. Donati, I.; Gamini, A.; Vetere, A.; Campa, C.; Paoletti, S. *Biomacromolecules* **2002**, *3*, 805-812.

134. Jeong, J.H.; Ko, S.B. *Journal of Industrial and Engineering Chemistry* **2001**, *7*, 310-315.

135. Zhu, L.P.; Yi, Z.; Liu, F.; Wei, X.Z.; Zhu, B.K.; Xu, Y.Y. *Eur. Polym. J.* **2008**, *44,* 1907-1914.

136. Pompe, T.; Zschoche, S.; Herold, N.; Salchert, K.; Gouzy, M.F.; Sperling, C.; et al. *Biomacromolecules* **2003**, *4*, 1072-1079.

137. Doshi, J.; Reneker, D.H. *J. Electrostatics* **1995**, *35*, 151-160.

138. Frenot, A.; Chronakis, I.S. *Curr. Opin. Colloid Interface Sci.* **2003**, *8*, 64-75.

139. Huang, Z.M.; Zhang, Y.Z.; Kotaki, M.; Ramakrishna, S. *Compos. Sci. Technol.* **2003**, *63*, 2223-2253.

140. Formhals, A. Patent 1,975,504, 1934.(b) doshi, J.; Reneker, D.H. *J. Electrost*. **1995**, *35*, 151.

141. Reneker, D.H.; Yarin, A.L. *Polymer* **2008**, *49*, 2387-2425.

142. Reneker, D.H.; Chun, I. *Nanotechnology* **1996**, *7*, 216-223.

143. Teo, W.E.; Gopal, R.; Ramaseshan, R.; Fujihara, K.; Ramakrishna, S. *Polymer* **2007**, *48*, 3400-3405.

144. Ko, F.K. *Nanoengineered nanofibrous materials* **2004**, *169*, 1-18.

145. Kiekens, P.; De Vrieze, S.; Van Camp, T.; Decostere, B.; Audenaert, W.; Westbroek, P.; et al. *Proceedings of the 8th Autex conference* **2008**.

146. Grafe, T.H.; Graham, K.M. *Proceedings of the 5th international conference on non wovens in filtration*, **2003**, 1–5.

147. Graham, K.; Ouyang, M.; Raether, T.; Grafe, T.; McDonald, B.; Knauf, P. *Proceeding of the fifteen annual technical conference and expo of the American filtration and separations society*, Galveston, Texas, **2002**.

148. Subbiah, T.; Bhat, G.; Tock, R.; Parameswaran, S.; Ramkumar, S. *J. Appl. Polym. Sci*. **2005**, *96*, 557-569.

149. Wang, X.; Kim, Y.G.; Drew, C.; Ku, B.C.; Kumar, J. *Nano Lett.* **2004**, *4*, 331-334.

150. Beachley, V.; Wen, X. *Mater. Sci. Eng.* **2009**, *29*, 663-668.

151. Agarwal, S.; Wendorff, J.H.; Greiner, A. *Polymer* **2008**, *49*, 5603-5621.

152. Thompson, C.; Chase, G.; Yarin, A.; Reneker, D. *Polymer* **2007**, *48*, 6913-6922.

153. Smit, E.; Buttner, U.; Sanderson, R.D. *Polymer* **2005**, *46*, 2419-2423.

154. Uyar, T.; Besenbacher, F. *Polymer* **2008**, *49*, 5336-5343.

155. Greiner, A.; Wendorff, J.H. *Angew. Chem. Int. Ed.* **2007,** *46*, 5670-5703.

156. Taylor, G. *Proc. R. Soc. Lond. A* **1969**, *313*, 453-475.

157. Teo, W.; Ramakrishna, S. *Nanotechnology* **2006**, *17*, 89-106.

158. McKee, M.G.; Wilkes, G.L.; Colby, R.H. *Macromolecules* **2004**, *37*, 1760-1767.

159. Deitzel, J.; Kleinmeyer, J.; Harris, D.; Beck, T.N. *Polymer* **2001**, *42*, 261-272.

160. Yördem, O.; Papila, M.; Menceloglu, Y. *Mater. Des*. **2008**, *29*, 34-44.

161. Shenoy, S.L.; Bates, W.D.; Frisch, H.L.; Wnek, G.E. *Polymer* **2005**, *46*, 3372-3384.

162. Huang, C.; Chen, S.; Lai, C.; Reneker, D.H.; Qiu, H.; Ye, Y.; et al. *Nanotechnology* **2006**, *17*, 1558-1563.

163. Kilic, A.; Oruc, F.; Demir, A. *Text. Res. J*. **2008**, *78*, 532-539.

164. Dersch, R.; Steinhart, M.; Boudriot, U.; Greiner, A.; Wendorff, J. *Polym. Adv. Technol.* **2005**, *16*, 276-282.

165. Kenawy, E.R.; Layman, J.M.; Watkins, J.R.; Bowlin, G.L.; Matthews, J.A.; Simpson, D.G.; et al. *Biomaterials* **2003,** *24*, 907-913.

166. Macossay, J.; Marruffo, A.; Rincon, R.; Eubanks, T.; Kuang, A. *Polym. Adv. Technol.* **2007**, *18*, 180-183.

167. Rutledge, G.C.; Li, Y.; Fridrikh, S.; Warner, S.; Kalayci, V.; Patra, P. *National Textile Center* **2000,** 1-10.

Chapter 3: Synthesis and characterization of functionalized polymer nanofibers, modified after electrospinning

3.1 Introduction

Polymer nanofibers can be produced by electrospinning a polymer solution to yield fibers with interesting properties, one being a high surface area to volume ratio.[1,2] The modification of such polymer nanofibers has generated much interest due to the versatility of the process and unique properties of the products, e.g. biomedical devices, drug delivery carriers and tissue engineering scaffolds.[1,3] Surface modification of these polymer nanofibers can be achieved in various ways, such as plasma treatment, surface graft polymerization, co-electrospinning of surface-active agents and polymers and wet chemical methods. Chemical immobilization of surface-active agents onto the surface of electrospun nanofibers is favoured over physical immobilization due to the covalent bond formation during chemical immobilization. The covalent bond between the surface-active agent and polymer prevents the leaching out of the surface-active agent from the surface-functionalized nanofibers during use.[4,5] These covalent bonds can be formed by chemical reactions between the polymer and surface-active agents. These reactions can occur at sites on the surface of the polymer nanofibers that are susceptible to electrophilic or nucleophilic attack by the surface-active agents.[3]

A polymer can be functionalized before or after electrospinning. One advantage of surface-functionalizing polymer nanofiber mats after electrospinning is that only the surface of the polymer nanofiber mat is modified. The bulk properties of the polymer remain unchanged.[3,5,6] A second advantage is that less chemical can be used for the functionalization process, as only enough chemical is needed for the available surface to be functionalized, and not the full bulk of the polymer mat.[3] This is beneficial in terms of cost and “greener” manufacturing processes. A third advantage of surface-functionalizing polymer nanofiber mats after electrospinning is that surface-active chemical groups can be used that would have made the electrospinning process difficult or impossible if functionalization was done before electrospinning. Functionalities can thus be incorporated on the surface of polymer nanofibers that are not electrospinnable.

A prerequisite for the surface-functionalization of polymer nanofibers using covalent bonding between the polymer and surface-functionalization agent is the presence of a reactive site on the polymer and a suitable reactive group on the surface-functionalization agent.[5] Poly(styrene-*co*-maleic anhydride) (SMA) is a reactive, inexpensive, biocompatible, thermoplastic polymer with high heat resistance, good impact resistance and dimensional stability.[2,7-9] Poly(styrene-*alt*-maleic anhydride) (P(St-*alt*-MAnh)) and poly(styrene-*co*-maleic anhydride) (P(St-*co*-MAnh)) are versatile polymers for functionalization due to the presence of very reactive maleic anhydride units. P(St-*alt*-MAnh) should provide a higher degree of functionalization due to more maleic anhydride units available, compared to P(St-*co*-MAnh). Any surface-functionalization agent with a reactive group, such as a primary amine or alcohol, can thus be covalently attached to SMA through a ring-opening reaction of the maleic anhydride unit.[10,11] It is therefore possible to select various chemical compounds with a primary amine or alcohol moiety for the surface-functionalization of P(St-*alt*-MAnh) and P(St-*co*-MAnh) nanofibers to yield polymer nanofibers with new functionalities on the surface. Primary amines are better anhydride-

reactive coupling agents than alcohols due to the greater nucleophilicity of amines compared to alcohols, and were therefore the coupling agent of choice.

The surface-functionalization agents chosen in this study for the surface-functionalization of electrospun P(St-*alt*-MAnh) and P(St-*co*-MAnh) nanofibers were selected based on possible chemical interactions with the *Mycobacterium tuberculosis* cell wall. All the surface-functionalization agents had a primary amine group available for nucleophilic attack on the maleic anhydride unit, thus resulting in a ring-opening reaction of the 5-membered ring. The amide generated upon reaction of the primary amine with the maleic anhydride group was further stabilized by a heat treatment to yield the very stable 5-membered cyclic imide.

Here we report the synthesis and characterization of various functionalized poly(styrene-*alt*-maleimide) (P(St-*alt*-MI)) and poly(styrene-*co*-maleimide) (P(St-*co*-MI)) nanofibers. The general procedure entailed that P(St-*alt*-MAnh) and P(St-*co*-MAnh) were first electrospun into nanofibers and thereafter surface-functionalized with a variety of chemical compounds. The functionalized SMI nanofibers were characterized using attenuated total reflectance Fourier transform infrared spectroscopy (ATR-FTIR) and scanning electron microscopy (SEM) and the synthesized surface-functionalization agents were characterized using ^{1}H-NMR and ^{13}C-NMR spectroscopy.

3.2 Synthesis of the functionalized SMI nanofibers

3.2.1 Electrospinning of SMA

Commercially available poly(styrene-*co*-maleic anhydride) (P(St-*co*-MAnh)) (M_w = 120 000 g/mol, MAnh content: 26%) was used as polymer, as well as poly(styrene-*alt*-maleic anhydride) (P(St-*alt*-MAnh)), synthesized using conventional radical copolymerization[12] to yield SMA (M_n = 128 000 g/mol, *Đ* = 2.7, MAnh content: 50%) (refer Fig. 3.1). P(St-*co*-MAnh) and P(St-*alt*-MAnh) were both electrospun from a 1:2 DMF:acetone solution[2] to yield smooth fibers with an average fiber diameter of 675 ± 90 nm for P(St-*co*-MAnh) and 682 ± 101 nm for P(St-*alt*-MAnh). The nanofibers were dried under vacuum to remove any residual solvents.

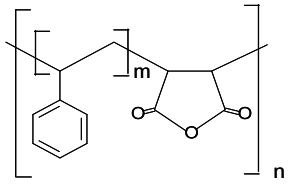

m = 1 : P(St-*alt*-MAnh)

m > 1 : P(St-*co*-MAnh)

Figure 3.1 Repeating units of SMA.

3.2.2 Functionalization of SMA nanofibers

SMA can easily undergo nucleophilic addition of a primary amine to the reactive maleic anhydride unit via a ring-opening reaction of the anhydride unit to form a secondary amide and carboxylic acid group, also known as a maleamic acid.[11] Ring closure can thereafter be achieved through the application of heat and corresponding loss of water.[10] Refer Figure 3.2 for a schematic illustration of the functionalization of the nanofibrous SMA mats via nucleophilic addition of a primary amine to the reactive maleic anhydride group.

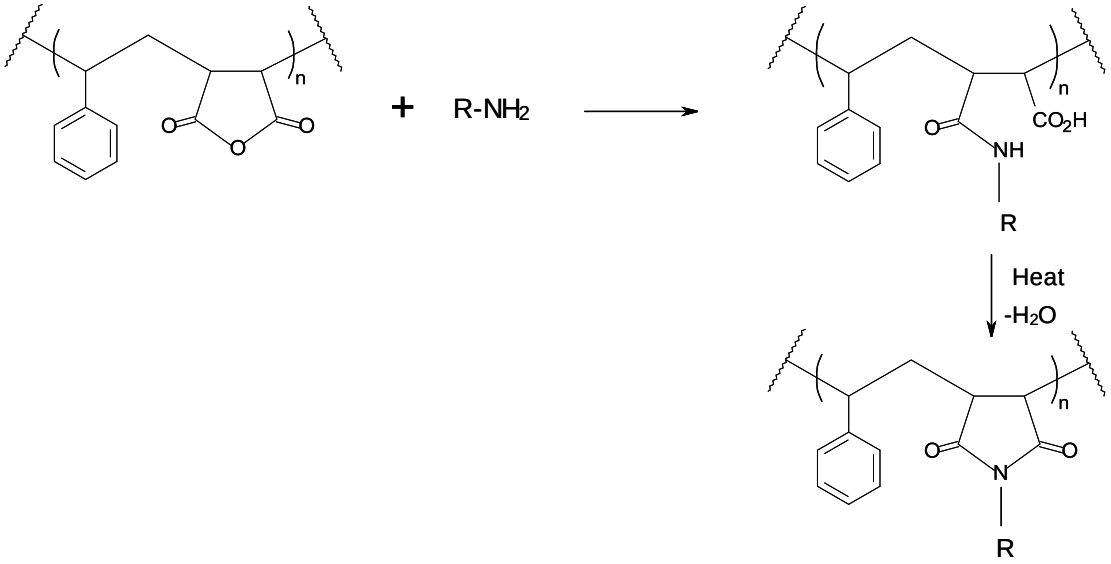

Figure 3.2 Schematic illustration of the functionalization of the nanofibrous SMA mats via nucleophilic addition of a primary amine to the reactive maleic anhydride group.

The prepared electrospun SMA nanofibrous mats were functionalized with surface-functionalization agents in a two-step reaction under mild conditions and without a catalyst. The functionalized SMI mats were thoroughly washed with water or solvent to remove unreacted surface-functionalization agent. The synthesized surface-functionalization agents used for the functionalization of the SMA nanofibers were characterized using ^{1}H-NMR and ^{13}C-NMR spectroscopy. The pristine and functionalized P(St-*alt*-MAnh) and P(St-*co*-MAnh) mats were characterized using ATR-FTIR spectroscopy, and SEM was applied to confirm the preservation of the nanofibrous structure after the functionalization procedure.

Preservation of the nanofibrous structure during the functionalization procedure proved quite a challenge in some instances, as a solvent had to be chosen which did not dissolve the pristine SMA nanofibers, dissolved the surface-functionalization agent, but not the functionalized product. This solvent system varied for the P(St-*alt*-MAnh) and P(St-*co*-MAnh) nanofibrous mats when the surface-functionalization agents were smaller, but became similar when the surface-functionalization agents

increased in molecular weight. Refer Table 3.1 for a summary of the solvents used for the surface-functionalization reaction of P(St-*alt*-MAnh) and P(St-*co*-MAnh) nanofibers with the various surface-functionalization agents.

Table 3.1 Summary of the solvents used for the surface-functionalization reaction of P(St-alt-MAnh) and P(St-co-MAnh) nanofibers with the various surface-functionalization agents

Surface-functionalization agents	**Molecular weight**	**P(St-alt-MAnh)**	**P(St-co-MAnh)**
Glucosamine	180 g/mol	Iso-propanol	Dimethyl sulfoxide
Mannosamine	180 g/mol	Iso-propanol	Dimethyl sulfoxide
Amino acid derivative	282 g/mol	Iso-propanol	Dimethyl sulfoxide
Protein	104 - 112 kDa	Phosphate buffered solution	Phosphate buffered solution
Tertiary amine groups	284 – 340 g/mol	Iso-propanol	Iso-propanol
Quaternary ammonium groups	453 – 565 g/mol	Diethyl ether	Diethyl ether

When the surface-functionalization agents had a molecular weight less than 284 g/mol, the polymer character of the surface-functionalized SMI nanofibers played the dominant role. The solvent chosen for the surface-functionalization reaction was of opposite polar character to the relevant SMA polymer, e.g. iso-propanol, with a polarity index of 3.9, was the chosen solvent when P(St-*alt*-MAnh) was surface-functionalized with the amino sugars and amino acid derivative, and dimethyl sulfoxide, with a polarity index of 7.2, was the solvent of choice when P(St-*co*-MAnh) was surface-functionalized with the said surface-functionalization agents. The polarity difference between the selected solvents and the parent polymer of the surface-functionalized SMI nanofibers was the overriding factor in order to preserve the nanofibrous structure. However, when the surface-functionalization agents increased in size and had a molecular weight above 284 g/mol, the situation changed as the polar character of the surface-functionalization agents played the dominant role. When the P(St-*alt*-MAnh) and P(St-*co*-MAnh) nanofibers were surface-functionalized with the tertiary amine moiety, iso-propanol (with a polarity index of 3.9) was the solvent of choice as it dissolved the tertiary amine but not the functionalized P(St-*alt*-MI) and P(St-*co*-MI) polymer. When the P(St-*alt*-MAnh) and P(St-*co*-MAnh) nanofibers were surface-functionalized with the quaternary ammonium moiety, diethyl ether (with a polarity index of 2.8) was used as solvent. As the polar character of the surface-functionalization agent changed from the neutral tertiary amine to the positively charged quaternary ammonium, the solvent used for the surface-functionalization reaction became less polar in order to preserve the nanofibrous structure of the modified SMI nanofibers. As the solvent chosen for the surface-

functionalization reaction did not dissolve the modified SMI nanofibrous structure, it is evident that the polarity of the surface-functionalization agents played the dominant role.

These functionalized P(St-*alt*-MAnh) and P(St-*co*-MAnh) nanofibrous mats were finally heat treated to effect ring closure to form an *N*-functionalized poly(styrene-maleimide) copolymer.[10] The ring closed maleimide compound is more stable than the ring-opened compound and less susceptible to hydrolysis. The functionalized P(St-*co*-MI) copolymers were not soluble in water after ring closure due to the hydrophobic nature of the polymer backbone. The P(St-*alt*-MI) nanofibers functionalized with a tertiary amine and quaternary ammonium moiety were however still soluble in water and warranted a further heat treatment step to achieve crosslinking of the functionalized polymer chains. Whereas the relevant functionalized P(St-*alt*-MI) nanofibers were soluble in water before heat treatment, they became insoluble after heat treatment at 130 °C under vacuum for 24 hours. The same did not apply to pristine P(St-*alt*-MAnh) nanofibers as the polymer did not cross link after the said heat treatment step. P(St-*alt*-MI) nanofibers functionalized with the amino acid derivative N_{α},N_{α}-bis(carboxymethyl)-L-lysine hydrate, the tertiary amine and quaternary ammonium compounds, therefore required an additional heat treatment step to achieve crosslinking of the polymer. This was essential for the preservation of the functionalized P(St-*alt*-MI) nanofiber structure when immersed in water for prolonged periods.

Analysis of the SEM images indicated that the average fiber diameter of the functionalized P(St-*alt*-MI) and P(St-*co*-MI) nanofibrous mats was slightly larger when compared to that of the pristine SMA mats. These results were expected considering the covalent attachment between the polymer and surface-functionalization agents and are in good agreement with literature.[3,7,13]

The chemical structures of the functionalized SMI nanofibrous mats prepared in this study using the method described are presented in Figure 3.3.

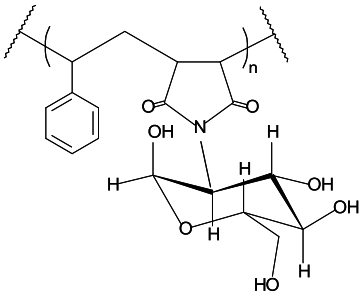

(a) SMI-Gluc/Man

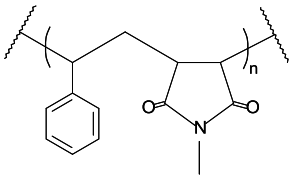

(b) SMI-Con A

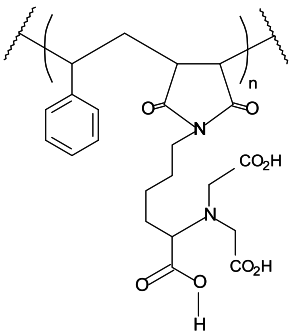

(c) SMI-BCML

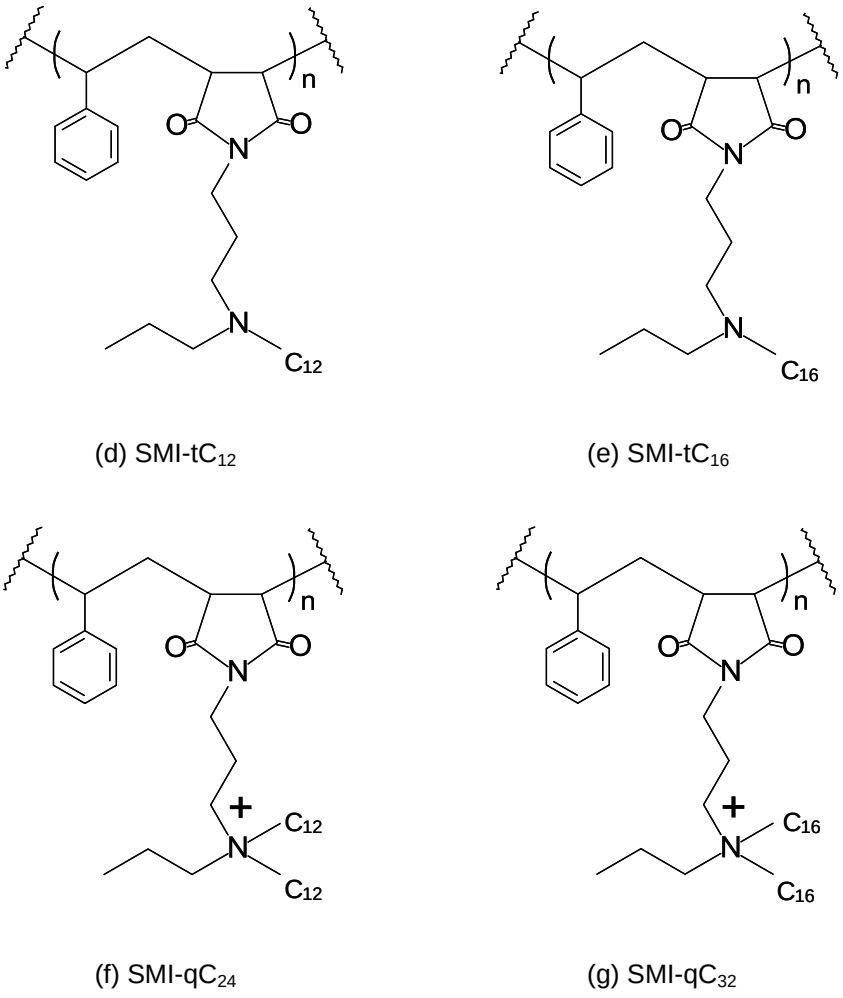

(d) SMI-tC_{12} (e) SMI-tC_{16}

(f) SMI-qC_{24} (g) SMI-qC_{32}

Figure 3.3 Chemical structures of the functionalized SMI compounds.

a) Synthesis of SMI-Man and SMI-Gluc

Mannosamine and glucosamine, the functionalization agents for SMI-Man and SMI-Gluc, respectively, (Fig. 3.3(a)), are commercially available as D-(+)-mannosamine hydrochloride and D-(+)-glucosamine hydrochloride. Since D-(+)-mannosamine and D-(+)-glucosamine decompose on storage, it is sold as the hydrochloride salt.[14] The hydrochloride salt had to be neutralized first before the nucleophilic addition reaction between the primary amine on the C_2-position of the sugar molecule and the maleic anhydride unit of SMA was possible. This was accomplished using triethylamine as the base and dimethyl sulfoxide or iso-propanol as solvent.[15]

D-(+)-glucosamine hydrochloride was used for the first set of experiments as it is an inexpensive chemical compared to D-(+)-mannosamine hydrochloride and more easily available. P(St-*alt*-MAnh) and P(St-*co*-MAnh) were initially reacted with glucosamine before electrospinning to obtain a high degree of functionalization. Ring closure was achieved with limited success using acetic anhydride, sodium acetate and triethylamine, of which the added amounts were calculated based on the mole

content of the anhydride unit in SMA.[16,17] The formation of an imide from an anhydride results in the release of a water molecule, and dehydration is therefore crucial to facilitate ring closure. These chemicals act as dehydrating agents when 2 mol acetic anhydride and 0.2 mol sodium acetate to 1 mol maleic anhydride are added to the reaction mixture. Due to the endothermic nature of the dehydration reaction accompanying the cyclization, thermal energy is required to shift the equilibrium state of the reversible reaction to the formation of the cyclic product. The optimum temperature for the cyclization reaction was determined to be 85 °C. Although some ring closure was effected, total conversion from SMA to SMI was not achieved. This result was in agreement with literature.[16,17]

Even though D-(+)-glucosamine and D-(+)-mannosamine were successfully reacted with P(St-*alt*-MAnh) and P(St-*co*-MAnh), it proved particularly problematic to dissolve and electrospin the modified polymer from a solvent suitable for electrospinning and at a concentration high enough for proper polymer chain entanglement. As soon as the concentration was sufficient for polymer chain entanglement, gelling of the solution occurred due to hydrogen bond interaction of the hydroxyl groups of the sugar molecules with each other. With the addition of solvent, the gel changed to a homogenous solution but with resultant electrospraying due to the concentration being too low for fibers to form.

Based on these results, it was decided to surface-functionalize P(St-*alt*-MAnh) and P(St-*co*-MAnh) nanofibers after electrospinning. D-(+)-mannosamine hydrochloride and D-(+)-glucosamine hydrochloride are soluble in water and not very soluble in organic solvents.[18,19] This restricted the choice of solvents for the functionalization reaction, as the chosen solvent could not dissolve the pristine SMA nanofibrous web or functionalized SMA fibers, but had to dissolve the neutralized primary amino sugar. Iso-propanol was used as solvent for the surface-functionalization reaction of P(St-*alt*-MAnh) with D-(+)-glucosamine and D-(+)-mannosamine, whilst dimethyl sulfoxide (DMSO) was the solvent of choice for the surface-functionalization reaction of P(St-*co*-MAnh) with said surface-functionalization agents. The polarity of a solvent generally determines what type of compounds it is able to dissolve and solvents usually adhere to the rule: “like dissolve like”. Amino sugars are strongly polar compounds that dissolve only in polar solvents such as water, as well as dimethyl sulfoxide. It did however dissolve in iso-propanol as well, probably due to the hydrogen bonding interaction between the solvent and hydroxyl groups of the glucosamine and mannosamine. Iso-propanol was therefore used for the surface-functionalization reaction of P(St-*alt*-MAnh) as iso-propanol dissolves non-polar compounds and thus did not dissolve the P(St-*alt*-MAnh) nanofibers with a “hydrophilic character” due to the high maleic anhydride content. DMSO was used for the surface-functionalization reaction of P(St-*co*-MAnh) as DMSO is a polar, aprotic solvent that did not dissolve the P(St-*co*-MAnh) nanofibers with a “hydrophobic character” due to the lower maleic anhydride content. The surface-functionalization reaction with the amino sugars did not change the polar character of the modified polymer sufficiently to affect the solubility thereof.

b) Synthesis of SMI-Con A and SMI-BCML

Concanavalin A (Con A), a protein, and N_{α},N_{α}-bis(carboxymethyl)-L-lysine hydrate (BCML), an amino acid derivative, are also commercially available and were used as is to surface-functionalize SMA to yield SMI-Con A (Fig. 3.3(b)) and SMI-BCML (Fig. 3.3(c)).

SMA enables the direct covalent protein immobilization of Con A in a neutral medium due to the very reactive and accessible α-amine group present on the N-terminus (of the protein) or the ϵ-amino group of the lysine residues of the protein that react spontaneously with the anhydride groups of SMA under these conditions.[1,5,20] Con A requires transition-metal ions, Mn^{2+}, and Ca^{2+} for the three-dimensional, helical and biologically active structure of the protein to remain intact, thus preventing deactivation of the protein.[21-24] Surface-functionalization of SMA with Con A therefore took place in the presence of Mn^{2+} and Ca^{2+} and phosphate buffered solution as solvent. It was essential for the function of the protein's carbohydrate recognition domain that the covalent immobilization of Con A on the surface of the SMA nanofibers took place with the biological activity of the protein still intact. The presence of protein on the surface of the SMA nanofibers was thus confirmed with a positive ninhydrin test[25] and retention of the protein's biological activity was confirmed when SMA with immobilized protein was incubated with horseradish peroxidase, a primary and a secondary antibody that catalyzed a colour change when the relevant substrate was introduced.[26,27]

c) Synthesis of SMI-tC_{12}, SMI-tC_{16}, SMI-qC_{24}, SMI-qC_{32}

This part of the study started with the synthesis of the surface-functionalization agents of SMI-tC_{12} (Fig. 3.3(d)), SMI-tC_{16} (Fig. 3.3(e)), SMI-qC_{24} (Fig. 3.3(f)) and SMI-qC_{32} (Fig. 3.3(g)). The synthetic work of Roy[28] was used as basis for the synthesis of the surface-functionalization agents schematically illustrated in Figure 3.4(a) to (d).

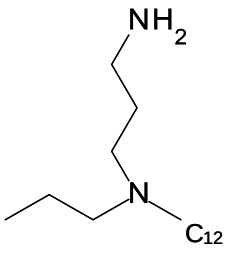

(a) tC_{12}

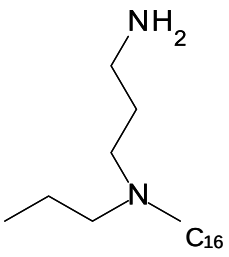

(b) tC_{16}

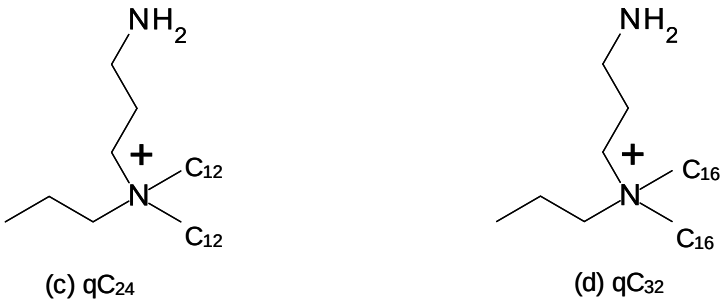

(c) qC_{24} (d) qC_{32}

Figure 3.4 Surface-functionalization agents for surface-functionalization reactions of SMA nanofibers.

Preparation of these surface-functionalization agents started with the synthesis of *N*-propyl-1,3-diaminopropane, whereafter the primary amine of this compound was protected with di-*tert*-butyl-dicarbonate (Boc) to prevent the primary amine from participating in the following nucleophilic substitution reactions. This Boc-protected aliphatic amine was then reacted with a bromoalkane in excess, whereafter the Boc-deprotection reaction of the primary amine with a strong acid produced the synthesized aliphatic tertiary amines (a) and (b) and quaternary ammonium compounds (c) and (d); ready to be used as surface-functionalization agents for the chemical modification of the electrospun SMA nanofibers.

3.3 Characterization of the functionalized SMI nanofibers

3.3.1 ATR-FTIR

Conversion of the maleic anhydride unit in SMA to the maleimide unit in the functionalized SMI nanofibrous mats was confirmed by ATR-FTIR. All the samples were used as is with no additional sample preparation before measurement.

(a) Chemical modification of SMA with glucosamine and mannosamine

P(St-*alt*-MAnh) and P(St-*co*-MAnh) nanofibers were surface-functionalized with glucosamine and mannosamine to yield SMI-Gluc and SMI-Man (Fig. 3.3(a)). As mannose is a C_2-epimer of glucose, glucosamine and mannosamine only differ in the positioning of the primary amine group on the C_2 position of the sugar molecule and does not have different infrared (IR) spectra.

Figure 3.5 shows the representative IR spectra of (a) pristine P(St-*alt*-MAnh), and P(St-*alt*-MI) surface-functionalized with glucosamine (b) and mannosamine (c).

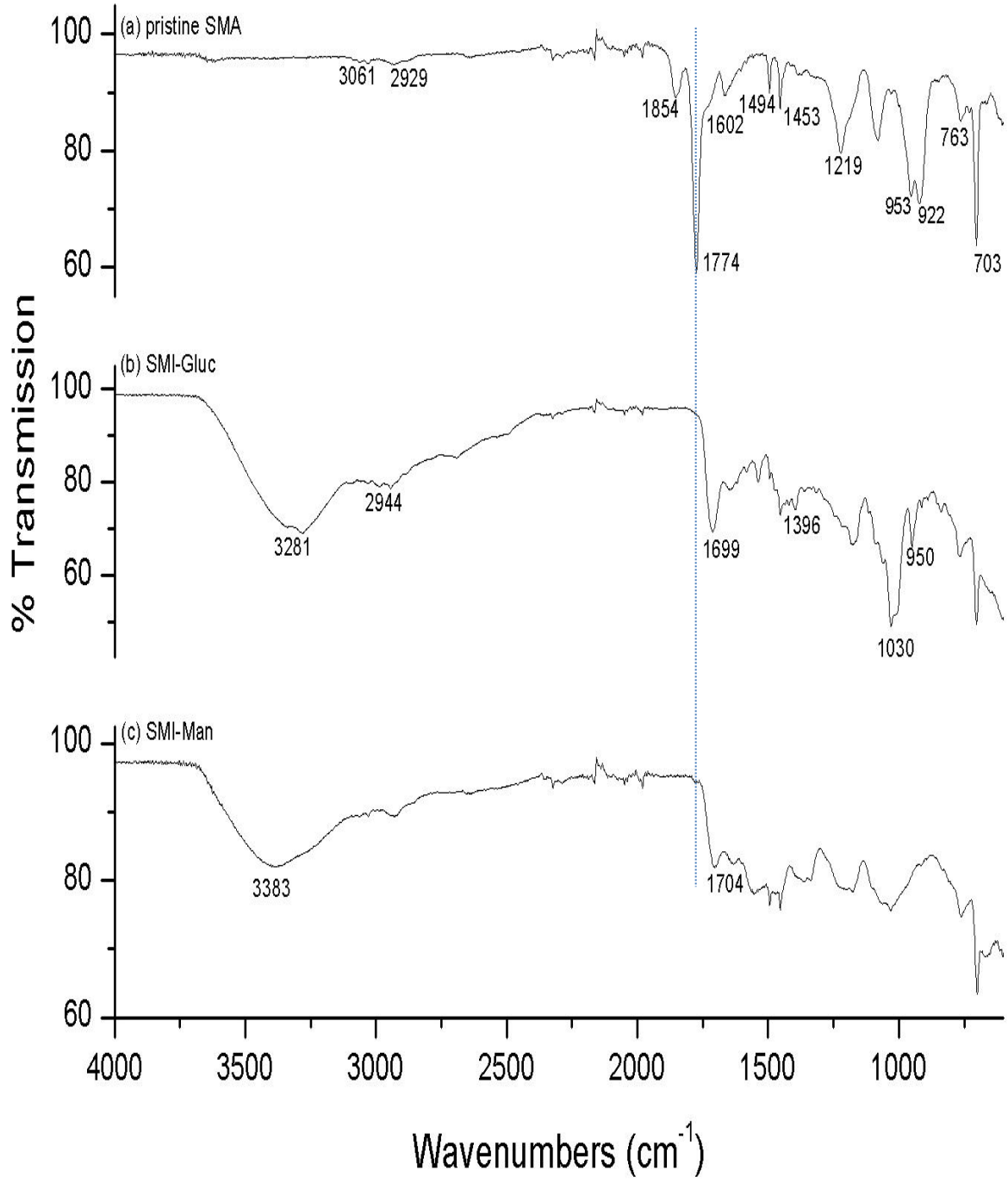

Figure 3.5 IR spectra of (a) pristine P(St-alt-MAnh), and P(St-alt-MI) surface-functionalized with glucosamine (b) and mannosamine (c).

The pair of bands of the carbonyls absorbing at 1774 cm^{-1} and 1854 cm^{-1} can be seen in Figure 3.5(a), corresponding to the symmetrical and asymmetrical carbonyl stretch vibrations of the anhydride moiety, as well as a characteristic band at 1219 cm^{-1} that corresponds to the C-O stretch vibrations of a five-membered cyclic anhydride. The peaks at 3061 cm^{-1} are due to the sp^2 aromatic C-H stretch vibrations of the styrene group and the bands at 2929 cm^{-1} are due to the sp^3 aliphatic C-H stretch vibrations of the polymer chain. The peaks at 1602 cm^{-1} and 1494 cm^{-1} correspond to the C=C stretch vibrations of the styrene aromatic ring and the peak at 1453 cm^{-1} is characteristic of the

C-H bending vibrations of the polymer chain. The peaks at 763 cm^{-1} and 703 cm^{-1} are characteristic of the C-H out-of-plane bending vibrations of a mono substituted aromatic ring of the styrene group. These results are in good agreement with literature. [2,7,10,29]

After the surface-functionalization of P(St-*alt*-MAnh) with glucosamine, followed by heat-induced ring closure, the peaks at 1854 cm^{-1} and 1774 cm^{-1} disappeared and a new ring-closed imide band appeared at 1699 cm^{-1} (refer Fig. 3.5(b)).[10,16,17] The presence of the glucose group was further confirmed by a broad peak at 3281 cm^{-1}, indicative of the hydrogen-bonded hydroxyl groups of the sugar molecule, as well as the corresponding C-O-H bending vibration appearing in the region of ~ 1400 cm^{-1} and the C-O stretch vibration at 1030 cm^{-1}. [18,30]

The IR spectrum of SMI-Man (Fig. 3.5(c)) was similar to that of SMI-Gluc (Fig. 3.5(b)). Comparison of the ATR-FTIR spectra of the functionalized P(St-*alt*-MI) nanofibers with those of the pristine P(St-*alt*-MAnh) nanofibers confirmed the successful imidization of the P(St-*alt*-MAnh) nanofibers with glucosamine and mannosamine to yield SMI-Gluc and SMI-Man (Fig. 3.3(a)).

The IR spectra of P(St-*co*-MI) functionalized with glucosamine and mannosamine were similar to those of the amino sugar functionalized P(St-*alt*-MI), but differed in terms of the amount of sugar molecules covalently attached to the polymer, as indicated by the small peak at 1774 cm^{-1} (refer Fig. 3.6(b) and (d)). Glucosamine and mannosamine surface-functionalized the P(St-*alt*-MAnh) nanofibers with 100% conversion. This observation is clear from the IR spectra (a) and (c) of Figure 3.6 where the pair of bands of the anhydride units at 1774 cm^{-1} and 1854 cm^{-1} disappeared. This result is in contrast to the surface-functionalization of P(St-*co*-MAnh) where glucosamine and mannosamine surface-functionalized the P(St-*co*-MAnh) nanofibers with 91% and 76% conversion, respectively. The conversion percentages were calculated using the ratio of the peak height of the styrene peak at 703 cm^{-1} and the anhydride carbonyl peak at 1774 cm^{-1}, before and after modification with glucosamine and mannosamine, respectively.

A possible reason why glucosamine gave a higher conversion percentage compared to mannosamine during the surface-functionalization of P(St-*co*-MAnh) nanofibers may be steric hindrance due to the positional difference of the primary amine group on the second carbon of the mannose group.

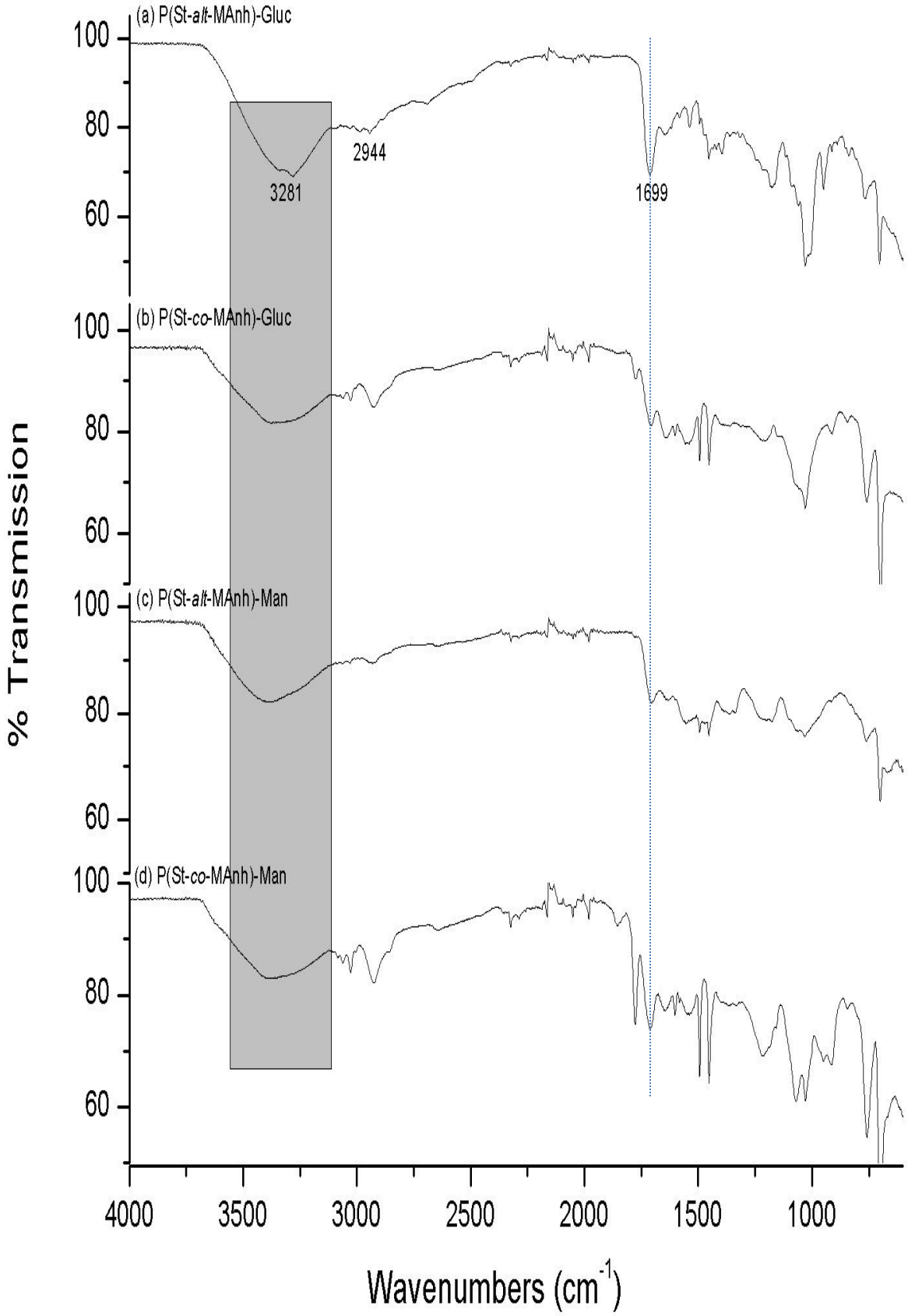

Figure 3.6 IR spectra of (a) glucose functionalized P(St-alt-MI), (b) glucose functionalized P(St-co-MI), (c) mannose functionalized P(St-alt-MI) and (d) mannose functionalized P(St-co-MI).

(b) Chemical modification of SMA with Concanavalin A (Con A)

P(St-*alt*-MAnh) and P(St-*co*-MAnh) nanofibers were surface-functionalized with Con A to yield SMI-Con A (Fig. 3.3(b)). Refer Figure 3.7 for the representative IR spectra of (a) pristine P(St-*alt*-MAnh) and (b) P(St-*alt*-MI) functionalized with Con A.

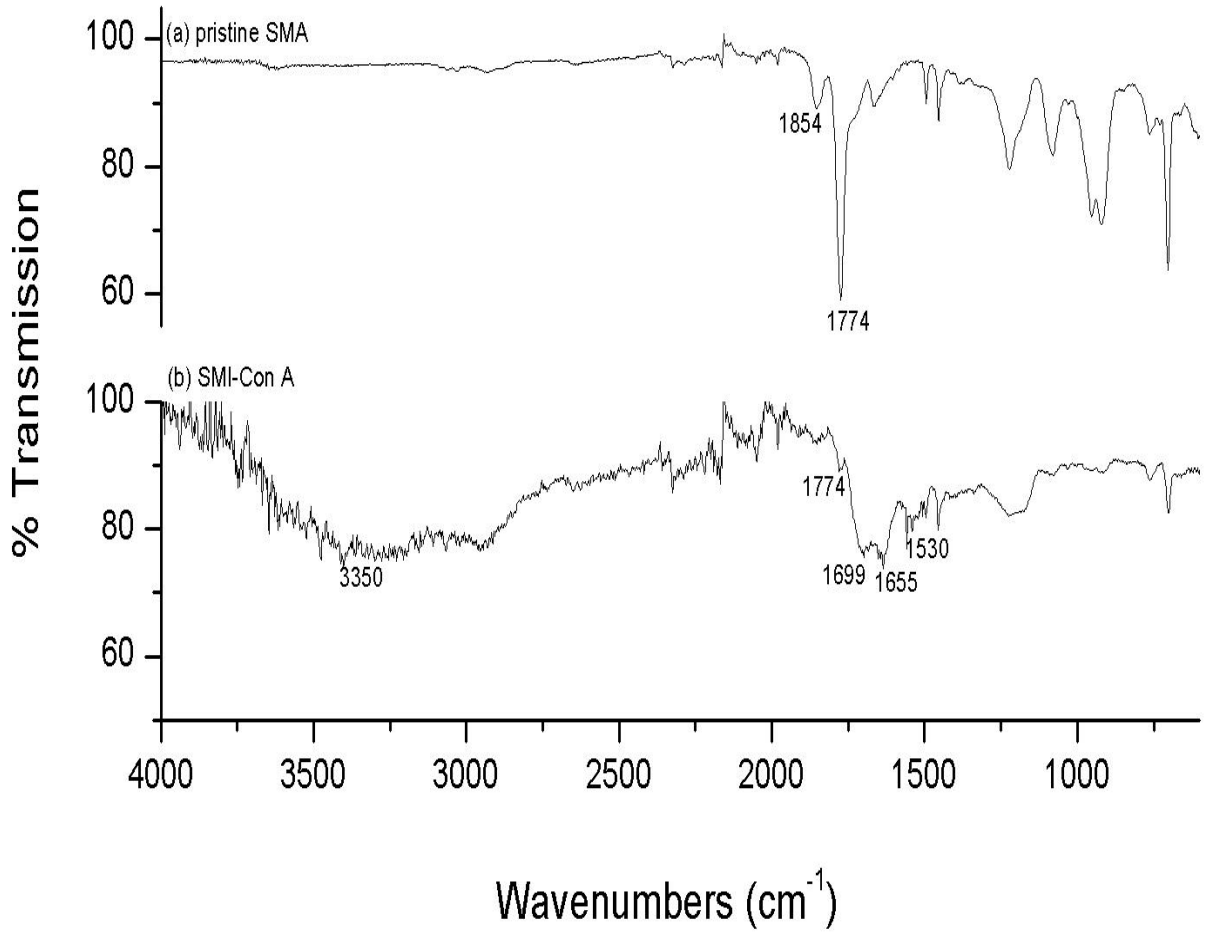

Figure 3.7 IR spectra of (a) pristine P(St-alt-MAnh) and (b) P(St-alt-MI) surface-functionalized with Concanavalin A.

After the surface-functionalization of P(St-*alt*-MAnh) with Con A, followed by heat-induced ring closure, a small peak at 1774 cm^{-1} is still visible, but a new peak appeared at 1699 cm^{-1}, indicative of a cyclic imide bond.[10,16,17] Two new bands at 1655 cm^{-1} and 1530 cm^{-1} appeared as well, and corresponds to the stretch vibration of C=O bonds and a combination of C-N stretch and N-H bending vibrations, respectively. These two new peaks are indicative of the amino acid groups in the protein backbone.[1] The broad absorption band at ~ 3350 cm^{-1} is also indicative of the N-H stretch vibration of amide bonds as well as the O-H stretch vibration of hydroxyl groups, confirming the presence of the amino acids from the protein, Concanavalin A.[1]

Comparison of the ATR-FTIR spectra of the functionalized P(St-*alt*-MI) nanofibers with those of the pristine P(St-*alt*-MAnh) nanofibers confirmed the successful covalent immobilization of Con A on the P(St-*alt*-MAnh) nanofibers to yield SMI-Con A (Fig. 3.3(b)).

The IR spectrum of P(St-*co*-MI) functionalized with Con A was similar to that of Con A functionalized P(St-*alt*-MI), but differed in terms of the amount of Con A covalently attached to the polymer, as indicated by the peak at 1774 cm^{-1}. Con A surface-functionalized the P(St-*alt*-MAnh) nanofibers with 77% conversion and P(St-*co*-MAnh) nanofibers with 51% conversion. The conversion percentages were calculated using the ratio of the peak height of the styrene peak at 703 cm^{-1} and the anhydride carbonyl peak at 1774 cm^{-1}, before and after modification with Con A, respectively. A possible reason for the difference in conversion percentages may be due to the difference in spatial orientation between the alternating maleic anhydride units of P(St-*alt*-MAnh) and the maleic anhydride units of P(St-*co*-MAnh), as explained in section 3.3.1(d).

The presence of the immobilized Con A on the surface of the polymer nanofibers was also confirmed using a ninhydrin test.[25] Ninhydrin (2,2-Dihydroxyindane-1,3-dione) is a chemical compound that is used to detect primary and secondary amines and ammonia. Refer Figure 3.8 for the chemical structure of ninhydrin.

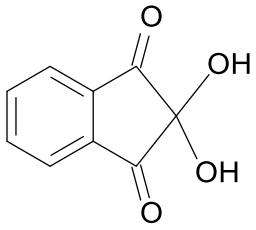

Figure 3.8 The chemical structure of ninhydrin.

When ninhydrin reacts with free amines, a deep blue colour, known as Ruhemann's purple, develops. The presence of Con A on the surface of the SMA nanofibers was tested by adding ninhydrin to SMI-Con A (Fig. 3.3(b)) and heating the mixture at 90 °C for 5 minutes. Ninhydrin reacts with the ϵ-amino group of lysine residues in the protein. The resultant complex produces a deep blue colour, thus confirming the presence of Con A immobilized on the surface of the SMA nanofibers.[25]

To confirm that Con A was covalently immobilized on the surface of the SMA nanofibers with retention of its biological activity, the SMI-Con A nanofibers were incubated in a buffered solution of horseradish peroxidase (HRP) and a primary and secondary antibody, followed by testing with an appropriate substrate solution.[26,27] Anti-HRP antibody was used as the primary antibody and anti–rabbit IgG, conjugated to alkaline phosphatase, as the secondary antibody. The substrate solution was added at room temperature and a positive result was obtained when the substrate solution changed colour from light yellow/green to dark purple, thus confirming that Con A was successfully immobilized on the surface of the polymer nanofibers with retention of its biological activity.

(c) Chemical modification of SMA with N_α,N_α-bis(carboxymethyl)-L-lysine hydrate (BCML)

P(St-*alt*-MAnh) and P(St-*co*-MAnh) nanofibers were surface-functionalized with BCML to yield SMI-BCML (fig. 3.3(c)). Refer Figure 3.9 for the representative IR spectra of (a) pristine P(St-*alt*-MAnh) and (b) P(St-*alt*-MI) functionalized with BCML.

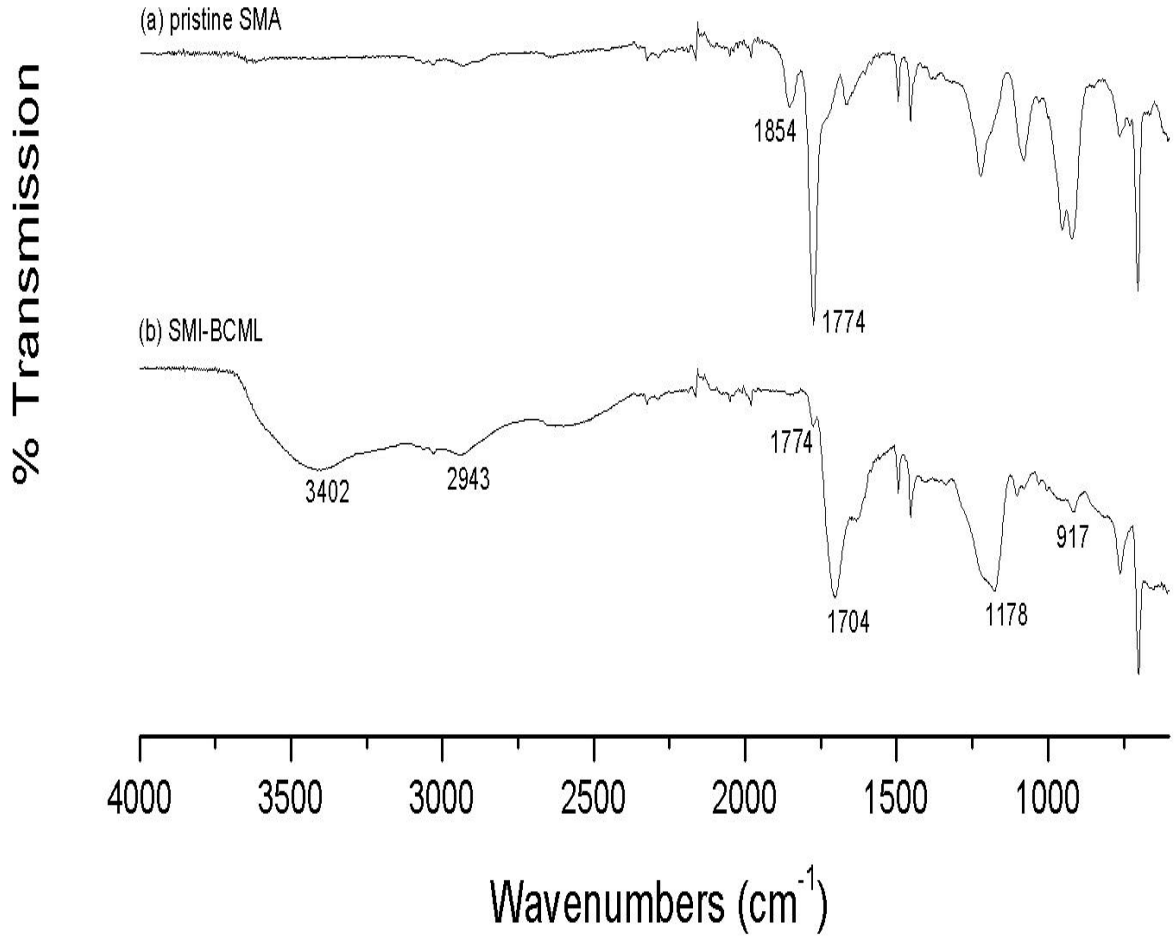

Figure 3.9 IR spectra of (a) pristine P(St-alt-MAnh) and (b) P(St-alt-MI) surface-functionalized with BCML.

After the reaction of P(St-*alt*-MAnh) with N_α,N_α-bis(carboxymethyl)-L-lysine hydrate (BCML), followed by heat-induced ring closure, the absorption peaks of the anhydride carbonyl group at 1854 cm^{-1} and 1774 cm^{-1} almost disappeared and a new strong imide peak formed at 1704 cm^{-1}. The absence of an N-H bending absorption peak of a secondary amide at ~1550 cm^{-1} is further confirmation that ring closure was complete after the initial ring opening surface-functionalization reaction.[10] The strong and broad absorption peak at 3402 cm^{-1} is indicative of hydrogen-bonded O-H groups of the multiple carboxylic acids groups of BCML. Another broad band, attributed to the hydrogen-bonded O-H out-of-plane bending vibration, is present in the region of 900 cm^{-1}. The presence of BCML is further confirmed by the C=O stretch vibration at 1704 cm^{-1} and the C-O stretch vibration of the carboxylic

acid group in the region of 1200 cm^{-1}, partially overlapped by the C-N stretch vibration of the aliphatic tertiary amine of BCML occurring at 1178 cm^{-1}. The strength of the peak at 1704 cm^{-1} is attributed to a combination of the newly formed imide stretch band and the C=O stretch vibration of the carboxylic acids of BCML.[10,18,30]

The broad O-H stretch band at 3402 cm^{-1} partially overlaps with the sp^2 C-H stretch band of the aliphatic C-H backbone of the BCML molecule, but a significant increase in the intensity of the sp^3 C-H stretch band at 2943 cm^{-1} of the modified P(St-*alt*-MI) product further confirms the imidization of the polymer with BCML when compared to the IR spectrum of pristine SMA.[29]

Comparison of the ATR-FTIR spectrum of the functionalized P(St-*alt*-MI) (Fig. 3.9(b)) with that of the pristine P(St-*alt*-MAnh) confirmed the successful imidization of P(St-*alt*-MAnh) with N_{α},N_{α}-bis(carboxymethyl)-L-lysine hydrate to yield SMI-BCML (Fig. 3.3(c)).

The IR spectrum of P(St-*co*-MI) functionalized with BCML was similar to that of the BCML functionalized P(St-*alt*-MI), but differed in terms of the amount of BCML molecules covalently attached to the polymer, as indicated by the peak at 1774 cm^{-1}. BCML surface-functionalized the P(St-*alt*-MAnh) nanofibers with 73% conversion and P(St-*co*-MAnh) nanofibers with 42% conversion. The conversion percentages were calculated using the ratio of the peak height of the styrene peak at 703 cm^{-1} and the anhydride carbonyl peak at 1774 cm^{-1}, before and after modification with BCML, respectively.

A possible reason for the difference in conversion percentages may be due to the difference in spatial orientation between the alternating maleic anhydride units of P(St-*alt*-MAnh) and the maleic anhydride units of P(St-*co*-MAnh), as explained in the next section.

(d) Chemical modification of SMA with N-alkyl compounds

P(St-*alt*-MAnh) nanofibers were surface-functionalized with a variety of aliphatic amine and ammonium compounds of varying hydrocarbon chain lengths. After the initial ring opening reaction to produce a secondary amide and free carboxylic acid group, heat-induced cyclization of the maleamic acid occurred to produce a cyclic imide bond. Refer Figure 3.10 for the representative IR spectra of (a) pristine P(St-*alt*-MAnh), (b) P(St-*alt*-MAnh) functionalized with *N*-hexadecyl-*N*-propyl-propane-1,3-diamine (tC_{16}), ring opened and (c) P(St-*alt*-MI) functionalized with *N*-hexadecyl-*N*-propyl-propane-1,3-diamine (tC_{16}), ring closed (Fig. 3.3(e)).

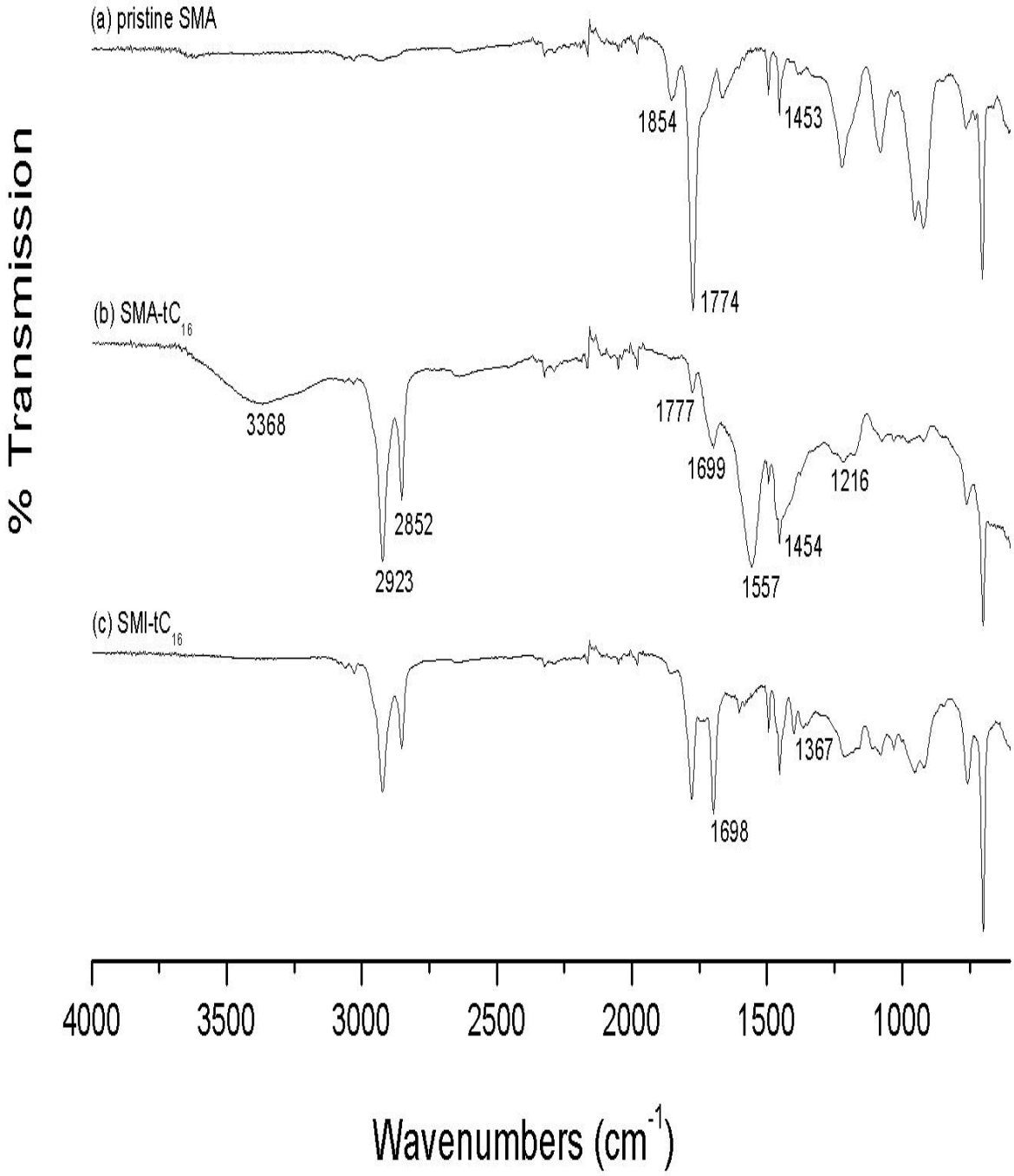

Figure 3.10 IR spectra of (a) pristine P(St-alt-MAnh), (b) P(St-alt-MAnh) surface-functionalized with N-hexadecyl-N-propyl-propane-1,3-diamine (tC_{16}), ring opened and (c) P(St-alt-MI) surface-functionalized with N-hexadecyl-N-propyl-propane-1,3-diamine (tC_{16}), ring closed.

The ring opening amidization reaction upon nucleophilic addition of the tC_{16} aliphatic amine group to the maleic anhydride unit of SMA was confirmed by the peak at 3368 cm^{-1}, attributed to the O-H stretch vibration of the free carboxylic acid and N-H stretch vibration of the secondary amide formed during the ring opening reaction, and a peak at 1557 cm^{-1}, corresponding to the N-H bending vibration and C-N stretch vibration of the secondary amide (refer Fig. 3.10(b)). This result is in good agreement

with literature.[10,16,17] The intensity of the band at 1557 cm^{-1} is attributed to a combination of the N-H bending vibration plus some C-N stretch vibration of the secondary amide. The peaks at 2923 cm^{-1} and 2852 cm^{-1} are indicative of the sp^3 C-H stretch vibrations of the hydrocarbon chains of tC_{16}; the high intensity is most probably as a result of the length of the C_{16} chain. The small peak at 1699 cm^{-1} is as a result of the carbonyl stretch vibration of the free carboxylic acid in the ring opened form and should not be confused with the vibration band of an imide bond. The peak at ~ 1216 cm^{-1} is due to the C-O stretch vibration of the cyclic anhydride moiety and the C-O-H bending vibration of the free carboxylic acid group formed during the ring opening reaction. A possible reason for the presence of this peak, as well as the small peak at 1777 cm^{-1}, is that the C_{16} aliphatic tertiary amine unit did not surface-functionalize the P(St-*alt*-MAnh) nanofibers with 100% conversion as this C_{16} group is a bulky group and steric hindrance may prevent it from reacting with every maleic anhydride unit on the surface of the nanofibrous mat. When comparing the IR spectrum of (a) pristine P(St-*alt*-MAnh) with that of the ring-opened functionalized product (b) in Figure 3.10, a significant increase in the intensity of the peak at 1454 cm^{-1} is also noticed. This is due to an increase in the characteristic bending absorption of CH_2 groups from the addition of the tC_{16} chains.[29]

When comparing the product before ring closure (b) with the product after ring closure (c), it is clear that there are no longer peaks at 3368 cm^{-1} and 1557 cm^{-1}. This observation is indicative of complete cyclization of the secondary amide to form a cyclic imide with a new peak appearing at 1698 cm^{-1}.[10,16,17] The peak at 1367 cm^{-1} is characteristic of the bending absorption of CH_3 groups, probably due to the addition of the tC_{16} chains. This peak was not noticeable in spectrum (b), possibly due to peak overlapping.

Comparison of the ATR-FTIR spectrum of the functionalized P(St-*alt*-MI) with that of the pristine P(St-*alt*-MAnh) confirmed the successful imidization of P(St-*alt*-MAnh) with *N*-hexadecyl-*N*-propyl-propane-1,3-diamine (tC_{16}) to yield SMI-tC_{16} (Fig. 3.3(e)).

The IR spectrum of P(St-*co*-MI) functionalized with tC_{16} was similar to that of the tC_{16} functionalized P(St-*alt*-MI), but differed in terms of the amount of aliphatic tertiary amine groups covalently attached to the polymer, as indicated by the peak at 1774 cm^{-1}. The tertiary amine group, tC_{16}, surface-functionalized the P(St-*alt*-MAnh) nanofibers with 84% conversion and the P(St-*co*-MAnh) nanofibers with 56% conversion. A possible reason for the difference in conversion percentages may be due to the difference in spatial orientation between the alternating maleic anhydride units of P(St-*alt*-MAnh) and the maleic anhydride units of P(St-*co*-MAnh), as explained further on in this section.

The IR spectra of P(St-*alt*-MI) functionalized with the rest of the aliphatic amine and ammonium compounds, namely tC_{12}, qC_{24} and qC_{32} are shown in Figure 3.11 in order to illustrate that a similar trend was observed when surface-functionalizing P(St-*alt*-MAnh) with the relevant compounds. The IR spectrum of SMI-tC_{16} is also included in order to compare with the spectra of SMI-tC_{12}, SMI-qC_{24} and SMI-qC_{32}.

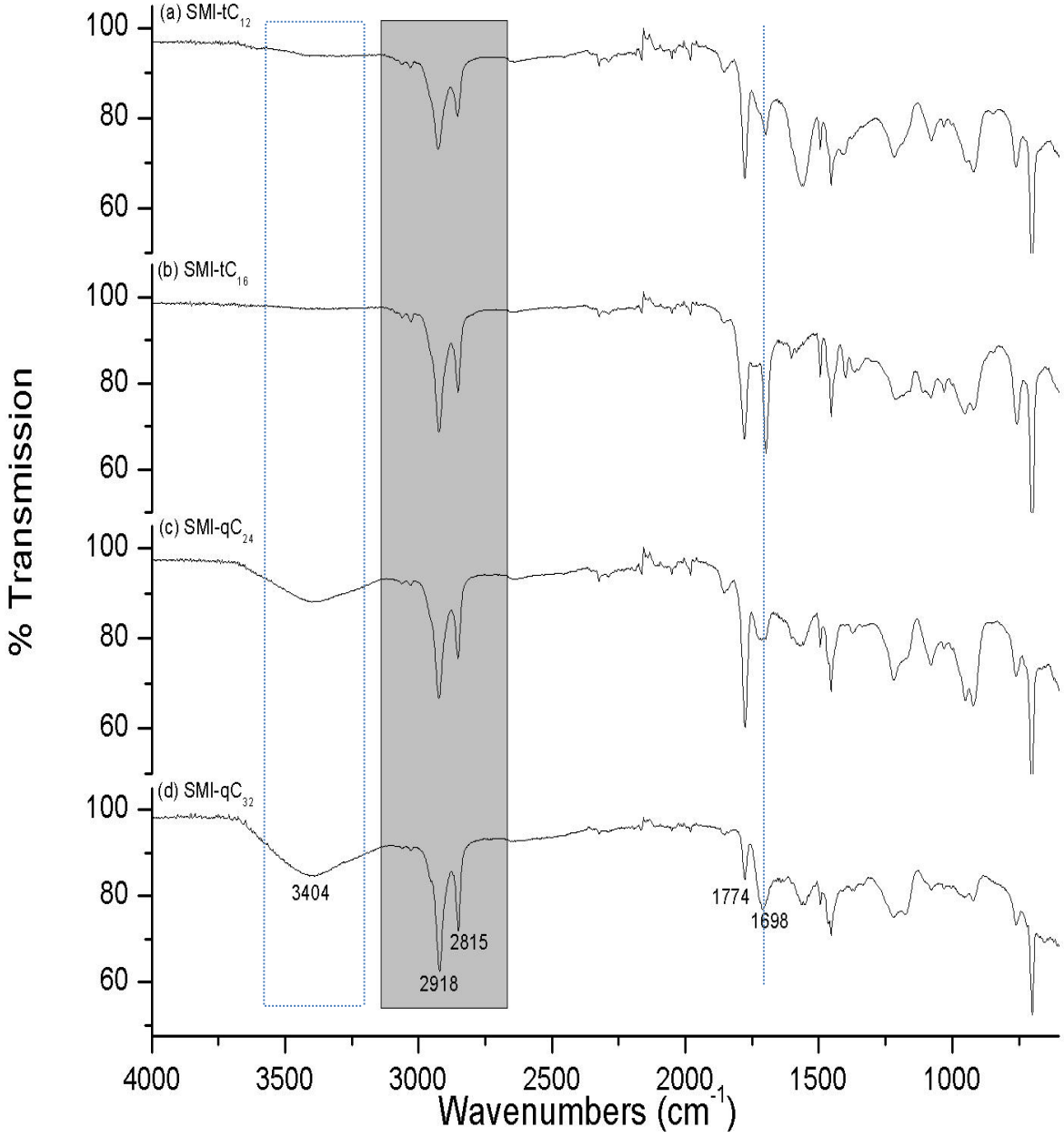

Figure 3.11 IR spectra of P(St-alt-MI) functionalized with (a) tC_{12}, (b) tC_{16} (c) qC_{24} and (d) qC_{32}.

An interesting observation from the IR spectra shown in Figure 3.11 is that there is a peak at ~ 3404 cm^{-1} in SMI-qC_{24} (c) and SMI-qC_{32} (d) that is indicative of quaternized nitrogens, as in the case of ammonium compounds.[1] As the modification of SMA with the quaternized ammonium compounds increased, i.e. an increase in the conversion percentages, the intensity of the peak at ~ 3404 cm^{-1} also increased, as expected. What is also significant is that with an increase in the alkyl chain length of the surface-functionalization agent, there is an increase in the intensities of the peaks at ~ 2918 cm^{-1} and ~ 2815 cm^{-1} due to the presence of the methylene groups of the alkyl chain. These results are expected and in good agreement with the reported data by Chen and Kim.[29,31]

It is clear from the IR spectra in Figure 3.11 that the aliphatic tertiary amine and quaternary ammonium compounds did not surface-functionalize the P(St-*alt*-MAnh) nanofibers with 100%

conversion. This is indicated by the presence of the anhydride peak at 1774 cm^{-1}. P(St-*alt*-MAnh) and P(St-*co*-MAnh) nanofibers were surface-functionalized with the relevant aliphatic tertiary amine and quaternary ammonium compounds at varying conversion percentages. These conversion percentages were calculated using the ratio of the peak height of the styrene peak at 703 cm^{-1} and the anhydride carbonyl peak at 1774 cm^{-1}, before and after modification with the relevant tertiary amine and quaternary ammonium compounds, respectively. Refer Table 3.2 for the conversion percentages of P(St-*alt*-MI) and P(St-*co*-MI) nanofibers, surface-functionalized with the tertiary amine and quaternary ammonium compounds.

Table 3.2 Conversion percentages of P(St-alt-MI) and P(St-co-MI) nanofibers, surface-functionalized with the tertiary amine and quaternary ammonium compounds

Surface active agent	**P(St-*alt*-MI): Conversion %**	**P(St-*co*-MI): Conversion %**
tC_{12}	81	58
tC_{16}	84	56
qC_{24}	84	51
qC_{32}	75	40

Two conclusions can be drawn from the conversion percentages recorded in Table 3.2. The first one being confirmation that neither P(St-*alt*-MAnh) nor P(St-*co*-MAnh) were surface-functionalized with 100% conversion and the second that P(St-*alt*-MAnh) nanofibers were surface-functionalized at higher conversion percentages than the P(St-*co*-MAnh) nanofibers. This phenomenon may possibly be explained by referring to the size of the surface-functionalization agents and the difference in spatial orientation between the alternating maleic anhydride units of P(St-*alt*-MAnh) and the maleic anhydride units of P(St-*co*-MAnh).

P(St-*co*-MAnh) has a 26% maleic anhydride content, therefore approximately three styrene units to one maleic anhydride unit. In P(St-*co*-MAnh), the single bonds of the styrene units provide flexibility around the axis of the polymer backbone. These very bulky aromatic side chains of the styrene units are therefore randomly distributed around the axis of the polymer backbone, almost concealing the maleic anhydride units.[32] This limits the accessibility to the maleic anhydride units sufficiently to prevent a significant amount of tertiary amine and quaternary ammonium surface-functionalization agents from reacting with the maleic anhydride unit, resulting in low conversion percentages. This situation is aggravated with an increase in the size of the surface-functionalization agent; thus the reason for the decrease in conversion percentages with an increase in the molecular weight from tC_{12} to qC_{32}.

This is however not the case in P(St-*alt*-MAnh), an alternating copolymer of styrene and maleic anhydride, where the maleic anhydride ring stiffens the polymer structure. Lazzara reported in 2008 that the styrene and maleic anhydride units align with respect to each other along the polymer backbone and perpendicular to each other.[33] This spatial orientation makes the maleic anhydride

units of P(St-*alt*-MAnh) more accessible for anhydride-reactive coupling agents than in the case of P(St-*co*-MAnh), thus resulting in higher conversion percentages for P(St-*alt*-MAnh).

3.3.2 NMR

The aliphatic tertiary amine and quaternary ammonium compounds synthesized and used to surface-functionalize SMA nanofibers to yield SMI fibers were characterized using ^{1}H-NMR and ^{13}C-NMR spectroscopy. Analysis of the ^{1}H-NMR spectra were quite challenging in certain instances due to the presence of the amine, ammonium and amide nitrogen in the relevant compounds synthesized for the surface-functionalization reaction of the SMA nanofibers.

Amine compounds have two characteristic types of hydrogen atoms, namely those hydrogens attached to the nitrogen of the amine, and those attached to the carbon adjacent to the nitrogen of the amine group (the α-carbon). The NH chemical shifts are usually extremely variable, appearing over a wide range of 0.5-4 ppm. The positions of these NH-peaks are usually also dependent on the solvent used, the temperature and acidity of the solution and the amount of hydrogen bonding taking place. These signals are usually quite broad and weak without any distinct coupling to hydrogens on the α-carbon. The hydrogens on the α-carbon are however slightly deshielded by the electronegative nitrogen atom, resulting in a downfield appearance. These hydrogens attached to a nitrogen atom and to the carbon atom adjacent to the nitrogen can therefore absorb over a wide range and the diagnostic use of these chemical shifts was not always possible.

The amide functional group also has an effect on the chemical shift, different to that of the amine functional groups. Amides also have two characteristic types of hydrogen atoms, namely those hydrogens attached to the amide nitrogen and those attached to the α-carbon of the amide nitrogen. The hydrogen atom attached to the amide nitrogen is variable in chemical shift and can appear from 5-9 ppm. The chemical shift is dependent on the temperature and concentration of the solution as well as solvent used. The hydrogen attached to the carbon adjacent to the amide nitrogen is also slightly deshielded by the electronegative character of the amide nitrogen. The hydrogens attached to the amide nitrogen are prone to show peak broadening and an overall reduction in intensity due to the nitrogen's moderate-size quadropole moment. It is usually only the hydrogen(s) attached to the nitrogen that is affected by quadropole broadening and will appear as a single broad peak downfield. [34]

These trends are clearly visible in Figure 3.12, showing the representative ^{1}H-NMR spectra of (a) *N*-*tert*-butoxycarbonyl-1-amino-3-chloropropane, (b) *N*-dodecyl-*N*-propane, (c) *N*-*tert*-butoxycarbonyl-*N*-dodecyl-*N*-propyl-propane-1,3-diamine, (d) *N*-dodecyl-*N*-propyl-propane-1,3-diamine and the assignments of the relevant peaks.

(a)

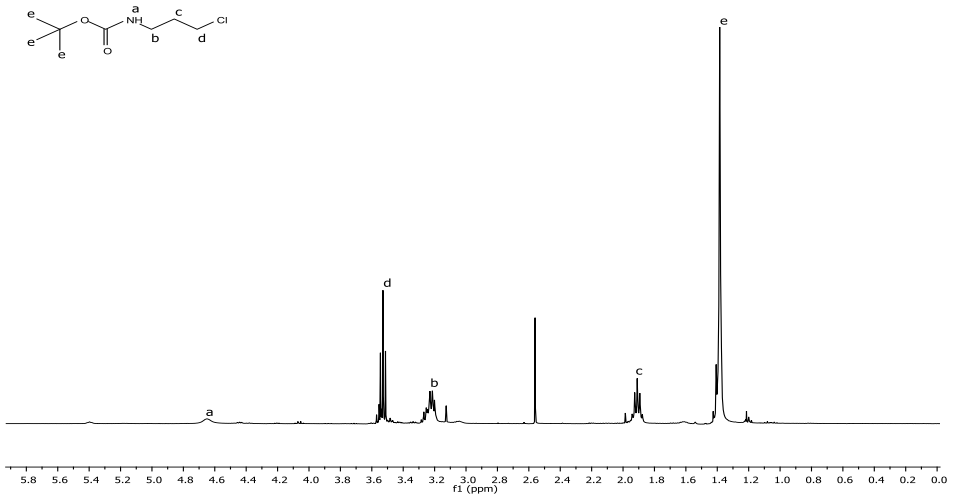

(b)

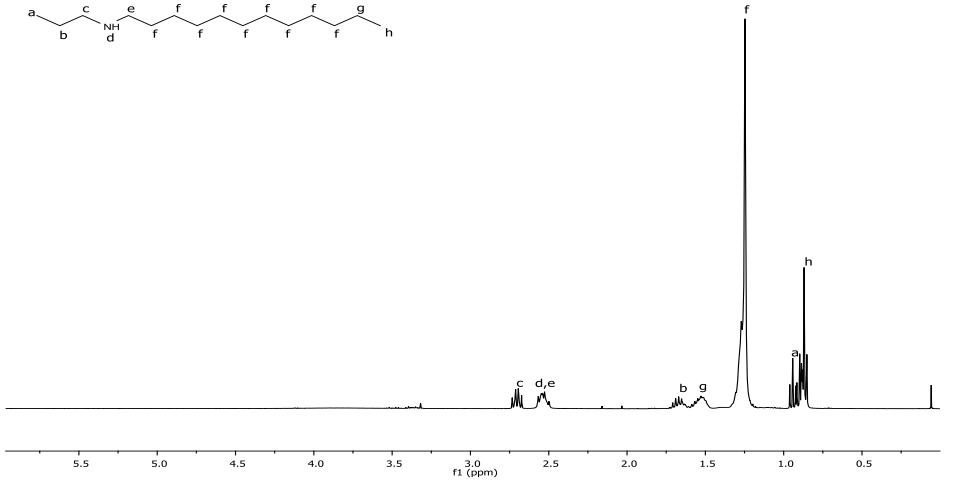

(c)

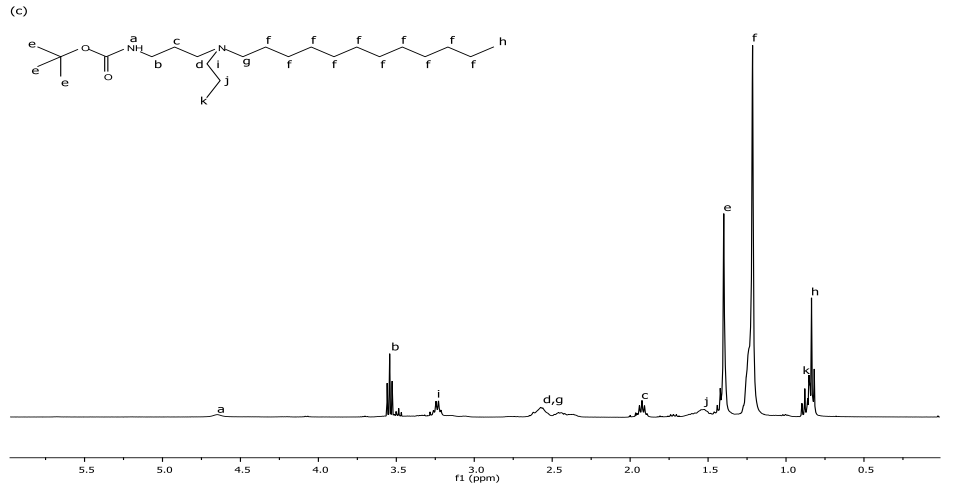

(d)

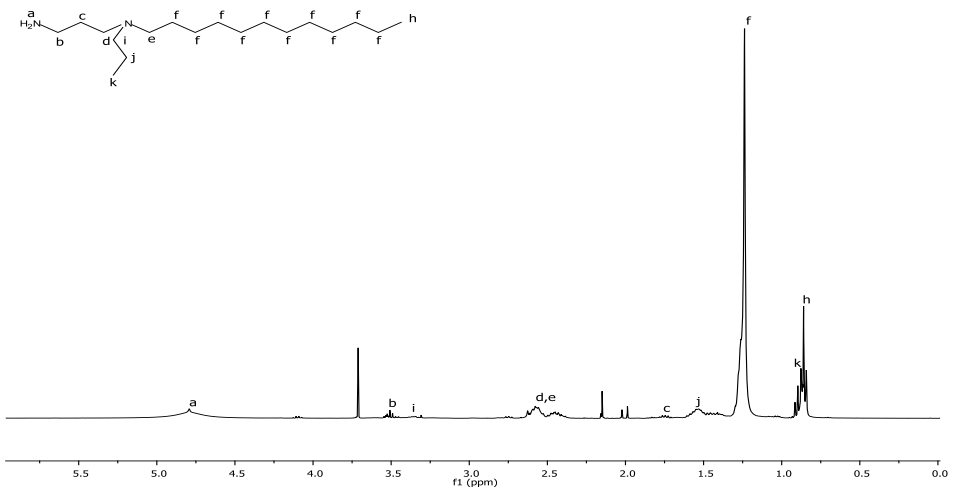

Figure 3.12 ^{1}H-NMR spectra of (a) N-tert-butoxycarbonyl-1-amino-3-chloropropane, (b) N-dodecyl-N-propane, (c) N-tert-butoxycarbonyl-N-dodecyl-N-propyl-propane-1,3-diamine, (d) N-dodecyl-N-propyl-propane-1,3-diamine (tC_{12}).

The ^{1}H-NMR spectra of the *N-tert*-butoxycarbonyl (Boc) protected compounds (a) and (c) of Figure 3.12 are characterized by a single broad peak at ~ 4.65 ppm, corresponding to the amide hydrogen, and a single peak at ~ 1.4 ppm, designated to the $–C(CH_3)_3$ group of the Boc functional group, used as protection for the primary amine. After removal of the Boc functional group via acid hydrolysis, the single broad peak at 4.65 ppm (1H integration) shifted downfield to ~ 4.8 ppm (2H integration), corresponding to the chemical shift of a primary amine, and the single peak at ~1.4 ppm disappeared, thereby confirming the deprotection of the primary amine (refer Fig. 3.12(d)).

The ^{1}H-NMR spectrum of the tC_{12} surface-functionalization agent (d) is further characterized by the single peak at ~ 1.25 ppm, designated to the C_{12} hydrocarbon chains, as well as the characteristic triplet of the methyl groups of the C_{12} hydrocarbon and propyl chains at ~ 0.86 ppm. The methylene groups of the aliphatic C_{12} chain (refer Fig. 3.12(d) – f) appear upfield from the methylene groups adjacent to the amide, amine and ammonium nitrogen (refer Fig. 3.12(d) – b,d,e,i) due to the deshielding effect of the electronegative character of nitrogen. These values correspond well to those found in literature for N-containing compounds. [2,35-37]

Some of the spectra showed other smaller peaks due to small amounts of starting material still present in the product. These were not necessarily removed, as they would not have been able to react with the maleic anhydride unit of SMA or would not be as reactive as the primary amine of the functionalization agents (d) and would not have interfered with the surface-functionalization reaction of the SMA nanofibers.

A complicating factor during the analysis and integration of the ^{1}H-NMR spectra of tC_{12}, tC_{16}, qC_{24} and qC_{32} was the intensity of the hydrocarbon peak at ~ 1.4 ppm that increased in intensity with an increase in the number of $–CH_2$- groups and overshadowed most of the other peaks.

The results of the ^{1}H-NMR spectra were confirmed by ^{13}C-NMR spectroscopy. Figure 3.13 shows the representative ^{13}C-NMR spectra of (a) *N-tert*-butoxycarbonyl-*N*-dodecyl-*N*-propyl-propane-1,3-diamine and *N*-dodecyl-*N*-propyl-propane-1,3-diamine and the assignments of the relevant peaks.

(a)

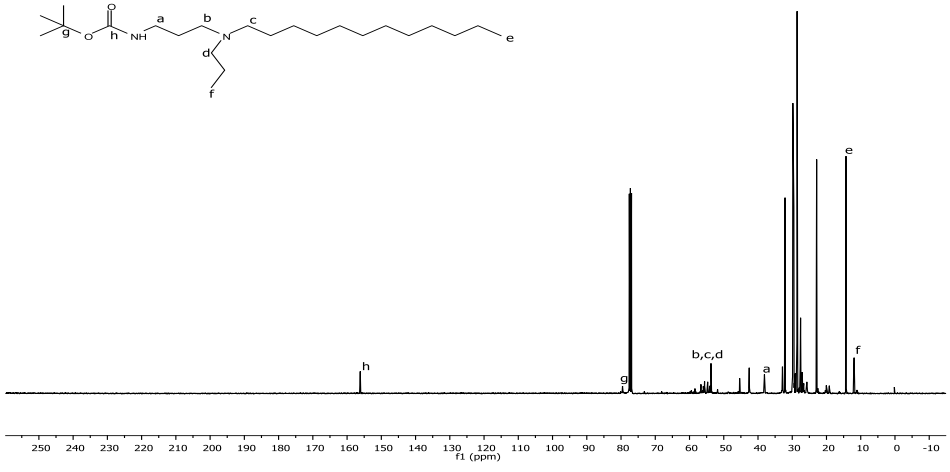

(b)

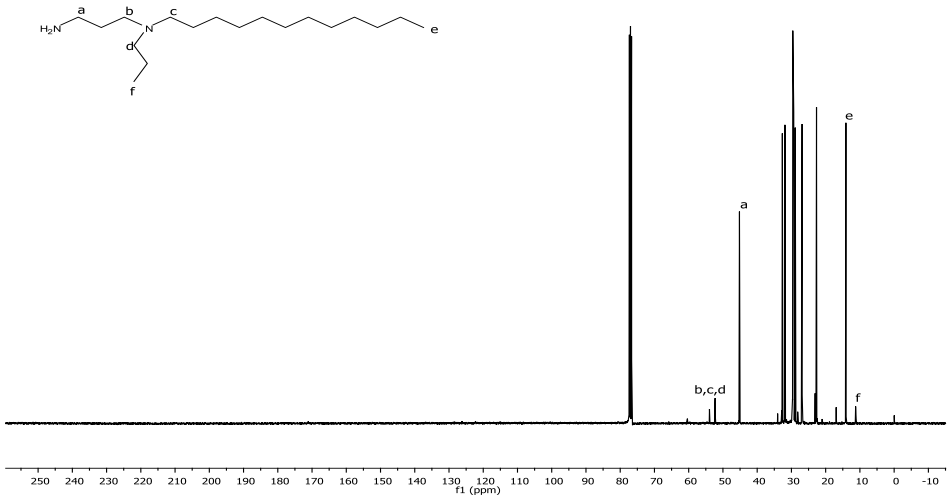

Figure 3.13 ^{13}C-NMR spectra of (a) N-tert-butoxycarbonyl-N-dodecyl-N-propyl-propane-1,3-diamine and (b) N-dodecyl-N-propyl-propane-1,3-diamine.

The ^{13}C-NMR spectra of all Boc-protected products are characterized by a peak at ~ 156 ppm, designated to an amide carbon (refer Fig. 3.13(a) – h), and a peak at ~ 80 ppm, designated to a quaternary carbon (refer Fig. 3.13(a) – g). These two peaks confirmed the presence of a *tert*-

butoxycarbonyl functional group attached to the aliphatic primary amine via an amide bond. After acid-hydrolysis of the Boc-protected compounds to deprotect the primary amine, the two peaks at ~ 156 ppm and ~ 80 ppm disappeared with a new peak appearing at ~ 45 ppm (refer Fig. 3.13(b) – a). This new peak coincides with the chemical shift of a methylene group adjacent to a primary amine, thereby confirming the deprotection of the Boc-protected products.

The ^{13}C-NMR spectra are also characterized by peaks at ~ 29 ppm, confirming the presence of methylene groups from hydrocarbon chains, peaks at 11 and 14 ppm, confirming the presence of 2 types of methyl groups (refer Fig. 3.13(b) – e,f) and peaks at ~ 54 ppm, confirming the presence of methylene groups adjacent to an electronegative atom (refer Fig. 3.13(b) – b,c,d).

The ^{1}H-NMR and ^{13}C-NMR spectra of the surface-functionalization agents confirmed the successful synthesis of the tertiary amine compounds, tC_{12} and tC_{16}, and the quaternary ammonium compounds, qC_{24} and qC_{32}, for the surface-functionalization of SMA nanofibers to incorporate new N-aliphatic functionalities on the surface of the functionalized SMA fibers.

3.3.3 SEM

Different concentrations of P(St-*alt*-MAnh) and P(St-*co*-MAnh) in 2:1 acetone:DMF were prepared and electrospun using conditions varying in electric field strength and spinning distance. Analysis of the SEM images with regard to fiber diameter and fiber morphology indicated that the optimum electrospinning concentration was 15% for P(St-*alt*-MAnh) and 20% for P(St-*co*-MAnh) yielding smooth fibers without any beads.

Further analysis of the SEM images revealed that the average fiber diameter of the electrospun pristine P(St-*co*-MAnh) and P(St-*alt*-MAnh) was 675 ± 90 nm and 682 ± 101 nm, respectively.

When the P(St-*co*-MAnh) nanofibers were surface-functionalized with the amino sugars, namely glucosamine and mannosamine, the fiber diameters increased from an average of 675 nm to an average of 737 ± 97 nm for glucosamine and 755 ± 116 nm for mannosamine, respectively. No changes were noticed regarding the morphology of the fibers as they remained round and smooth. Refer Figure 3.14 for a representative SEM image of (a) pristine P(St-*co*-MAnh), and P(St-*co*-MI) functionalized with (b) glucosamine and (c) mannosamine, respectively. It is clear from the SEM images that the nanofibrous structure was preserved during functionalization. This was vital for the benefit of the high surface area to volume ratio of the functionalized fibers.

(a)

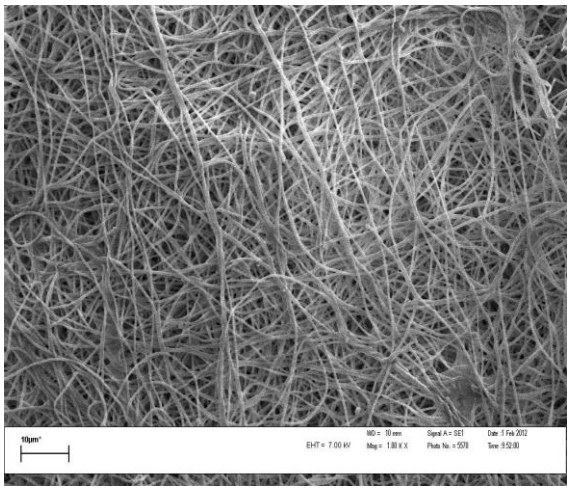

(b)

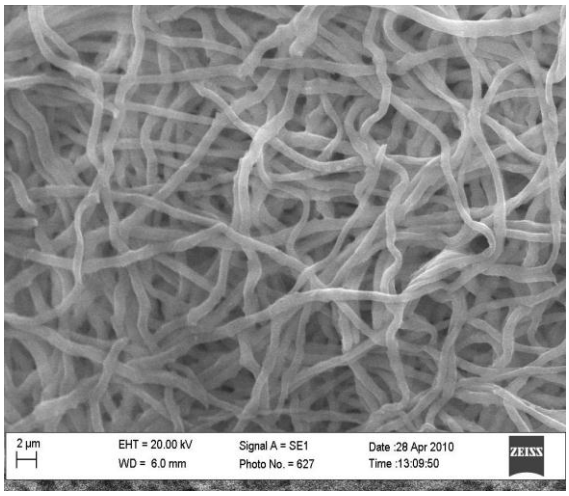

(c)

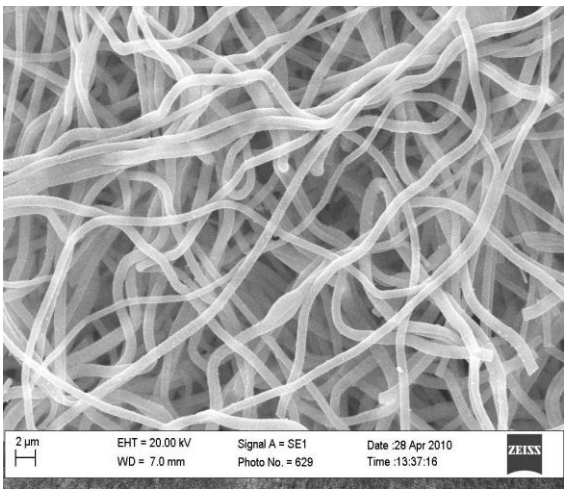

Figure 3.14 SEM images of (a) pristine P(St-co-MAnh), and P(St-co-MI) surface-functionalized with (b) glucosamine and (c) mannosamine.

The same trend was noticed after the surface-functionalization of P(St-*alt*-MAnh) with glucosamine and mannosamine where the average fiber diameter increased from 682 nm to 766 ± 106 nm in glucosamine and 728 ± 99 nm in mannosamine, respectively. The morphology of the functionalized fibers remained unchanged, namely smooth and round, with preservation of the nanofibrous structure after functionalization.

The slight increase in fiber diameter of the functionalized P(St-*co*-MI) and P(St-*alt*-MI) nanofibrous mats when compared to that of pristine P(St-*co*-MAnh) and P(St-*alt*-MAnh) nanofibrous mats is possibly due to the covalent bond formed between the reactive maleic anhydride units of SMA and the primary amine of glucosamine and mannosamine, respectively. The average fiber diameter of pristine P(St-*co*-MAnh) increased by 9-12% after surface-functionalization with the amino sugar molecules and the average fiber diameter of pristine P(St-*alt*-MAnh) increased by 7-12% after surface-functionalization. These increases in fiber diameter after surface-functionalization are

however only marginal and fall within the standard deviation of the measured average fiber diameter and is therefore not considered significant. These results were expected and are in good agreement with literature.[3,7,13]

With regard to the surface-functionalization of P(St-*co*-MAnh) and P(St-*alt*-MAnh) nanofibers with the rest of the surface-functionalization agents, the same trend was observed as with the surface-functionalization of SMA with the amino sugar molecules. Refer Table 3.3 for the average fiber diameter of the functionalized P(St-*co*-MI) and P(St-*alt*-MI) fibers and the percentage increase in average fiber diameter after surface-functionalization.

Table 3.3 The average fiber diameter of functionalized P(St-co-MI) and P(St-alt-MI) nanofibers and percentage increase in fiber diameter after surface-functionalization

Surface-functionalization agents	**P(St-*alt*-MI): average fiber diameter (nm)**	**% increase in average fiber diameter**	**P(St-*co*-MI): average fiber diameter (nm)**	**% increase in average fiber diameter**
Pristine SMA	682 ± 101	-	675 ± 90	-
BCML	745 ± 99	9	733 ± 91	9
Con A	774 ± 147	13	763 ± 99	13
tC_{12}	746 ± 81	9	737 ± 109	9
tC_{16}	752 ± 85	10	704 ± 70	4
qC_{24}	755 ± 148	11	735 ± 107	8
qC_{32}	744 ± 91	9	785 ± 107	15

The results as recorded in Table 3.3 clearly indicate that there is a slight increase in the average fiber diameter of the functionalized P(St-*co*-MI) and P(St-*alt*-MI) fibers, to the same extent as in the case of the amino sugar functionalized SMI fibers. These increases in fiber diameter after functionalization fall within the standard deviation of the measured average fiber diameter and are therefore not considered significant. The morphology of the functionalized SMI nanofibers remained unchanged, namely round and smooth. These results are in good agreement with literature.[3,5,7,13]

3.4 Conclusion

P(St-*alt*-MAnh), synthesized using conventional radical copolymerization, and commercial P(St-*co*-MAnh) were electrospun into nanofibrous mats with fiber diameters in the region of 680 nm. These pristine polymer nanofibers were subsequently successfully surface-functionalized with a variety of surface-functionalization agents via nucleophilic acyl substitution. These surface-functionalization agents were very reactive towards the maleic anhydride unit of SMA and included amino sugars, an

amino acid derivative, a protein and a variety of synthesized aliphatic tertiary amines and quaternary ammonium compounds. All the functionalized P(St-*alt*-MAnh) and P(St-*co*-MAnh) nanofibers were heat treated to achieve ring closure of the secondary amide formed upon reaction of the surface-functionalization agent with the maleic anhydride unit of SMA to form a stable cyclic imide. The P(St-*alt*-MAnh) nanofibers functionalized with BCML, tertiary amine and quaternary ammonium compounds underwent an additional heat treatment step at 130 °C under vacuum to achieve crosslinking of the functionalized polymer chains. This additional heat treatment step rendered the functionalized P(St-*alt*-MAnh) nanofibers insoluble in water, a necessity for the preservation of the nanofibrous structure when exposed to water for extended periods. The functionalized P(St-*co*-MAnh) nanofibers were already insoluble in water due to the hydrophobic nature of the polymer backbone and did not require the additional heat-induced crosslinking step.

The successful functionalization of the P(St-*alt*-MAnh) and P(St-*co*-MAnh) nanofibers was confirmed with ATR-FTIR. SEM was used to confirm the preservation of the nanofibrous structure after functionalization, which is critical for the benefit of the high surface area to volume ratio of nanofibers.

The fiber diameter of the pristine SMA fibers increased slightly after surface-functionalization, *i.e.* 4-15% in the case of functionalized P(St-*co*-MAnh) and 9-13% in the case of functionalized P(St-*alt*-MAnh). This fiber diameter increase is a result of the covalent bond formed between the polymer and surface-functionalization agent. These increases are however only marginal and fall within the standard deviation of the measured average fiber diameter and are therefore not considered significant.

The work discussed in this chapter thus confirms that polymer nanofibers can successfully be surface-functionalized with a variety of surface-functionalization agents by combining a polymer with a reactive site and a surface-functionalization agent with a suitable reactive group.

3.5 Experimental

3.5.1 Chemicals

Styrene-*co*-maleic anhydride (M_n = 120 000 g/mol, MA: 26%, grade SZ 26120, Polyscope), dichloromethane 98% (Kimix), sodium chloride 98% (Sigma-Aldrich), acetone (Protea Chemicals), glucosamine hydrochloride 99.5% (Calbiochem), mannosamine hydrochloride 99.5% (Calbiochem), dimethyl sulfoxide (Kimix), styrene 99.5% (Fluka Chemika), maleic anhydride 99% (Acros organics), methyl ethyl ketone 99.7% (Sigma-Aldrich), iso-propanol (Kimix), n-hexane (Kimix), horseradish peroxidase (Sigma), anti-HRP antibodies (Sigma), anti-rabbit IgG (Sigma), 5-bromo-4-chloro-3-indoyl

phosphate p-toluidine salt (Sigma), nitro blue tetrazolium (Sigma), concanavalin A (Sigma), ninhydrin (Sigma), Tween 20 (Sigma), phenol (Sigma), potassium cyanide 98% (Fluka), casein (Sigma), thimerosal (Sigma), N_{α},N_{α}-bis(carboxymethyl)-L-lysine hydrate 97% (Aldrich), 1-amino-3-chloropropane hydrochloride 98% (Aldrich), 4-dimethylaminopyridine 99% (Sigma), dichloromethane (Kimix), 1,2-dichloroethane (Sigma), chloroform (Kimix), di-*tert*-butyl-dicarbonate 97% (Aldrich), acetonitrile (Sigma), 1-propylamine 99% (Sigma), 1-bromododecane 97% (Aldrich), 1-bromohexadecane 97% (Aldrich), ammonia solution (Merck) and diethyl ether (Kimix) were used without further purification. 2,2' Azobis(isobutyronitrile) (AIBN) (Riedel de Haen) was recrystallized twice from methanol and dried under vacuum before use. *N*,*N*-dimethylformamide 97% (Fluka), triethylamine 99.5% (Sigma-Aldrich), ethanol (Sasol), pyridine 99% (Sigma), ethyl acetate (Sasol) and methanol (Sasol) were distilled and kept on 4 Å molecular sieve before use. Sodium acetate 99% (Sigma), manganese(II) chloride 98% (Sigma), calcium chloride (Merck), potassium chloride (Merck), sodium hydrogen phosphate 99% (Sigma), potassium dihydrogen phosphate 99% (Holpro) and potassium carbonate 99.5% (Unilab), received in a moisture-free state, was further dried at 120 °C for 24 hours just before use.

3.5.2 Characterization techniques

a) Nuclear magnetic resonance spectroscopy (NMR)

^{1}H-NMR and ^{13}C-NMR spectra were obtained using a Varian VXR 400 MHz instrument equipped with a Varian magnet (7.0 T). Depending on the solubility of the synthesized compounds, deuterated chloroform ($CDCl_3$) and deuterated dimethyl sulfoxide (DMSO-d_6) were used as solvents. All chemical shifts are reported in ppm downfield from tetramethylsilane (TMS), used as an internal standard (δ = 0 ppm).

b) Attenuated total reflectance Fourier transform infrared (ATR-FTIR) spectroscopy

Infrared spectra were recorded using a Nicolet FTIR spectrometer (model Nexus) from Thermo-Fischer equipped with a Smart Golden Gate ATR accessory with a diamond/ZnSe internal reflection crystal. The spectra were recorded from 4000 cm^{-1} to 600 cm^{-1} with a spectral resolution of 4 cm^{-1} and were the sum of 64 individual scans. No sample preparation was necessary and samples were in solid state. Omnic software was used for data acquisition and processing.

Conversion Calculation: The calculation of the conversion percentage when SMA was functionalized with a surface-functionalization agent to yield the corresponding functionalized SMI was done as follows. The mode of each relevant IR spectrum was changed from transmission to

absorbance and the baseline was corrected. The absorbance band from the aromatic styrene unit at 703 cm^{-1} was used as internal standard as the styrene group did not partake in the surface-functionalization reaction and was deemed a constant. The absorbance band from the carbonyl group of the anhydride unit at 1774 cm^{-1} was used to determine the extent of the functionalization reaction as the anhydride unit reacted with the primary amine of the surface-functionalization agent to form an imide, thus giving rise to a new band at ~ 1700 cm^{-1} with a corresponding decrease in the peak at 1774 cm^{-1}.

The heights of the styrene peak at 703 cm^{-1} and the carbonyl peak at 1774 cm^{-1} were taken, before and after functionalization, as measure of the fraction of carbonyls converted to imides by calculating the decrease in the height of the carbonyl peak of the functionalized SMI in relation to that of pristine SMA where the styrene peak at 703 cm^{-1} is constant.

c) Scanning electron microscopy (SEM)

Images of the pristine and functionalized SMI fibers were obtained using a Leo® 1430VP Scanning Electron Microscope (SEM). The sample fibers were cut into approximately 1 cm x 1 cm squares and attached onto the SEM stub with double sided carbon tape. The SEM stubs were then sputter coated with gold under vacuum prior to imaging. The images were analyzed using an imaging analysis program, SEM Image Studio, to obtain data regarding fiber diameters. An average of 100 fiber diameters was measured per sample. The average fiber diameter and the standard deviation were calculated using Microsoft Excel 2010.

d) Size exclusion chromatography (SEC)

Molar mass and dispersity (*Đ*) were obtained using size exclusion chromatography (SEC). Size exclusion chromatography (SEC) analysis was carried out on a DMAc solvent system using a flow rate of 1.0 mL/min. The instrument setup consisted of a Shimadzu LC-10AD pump, a Waters 717Plus autosampler, a column system fitted with a 50x8 mm guard column in series with three 300x8 mm, 10 µm particle size GRAM columns (2 x 3000Å and 100Å) obtained from PSS, a Waters 2487 dual wavelength UV detector and a Waters 410 differential refractive index (DRI) detector all in series. 100 µL injection volumes are sampled individually with the oven temperature of the column and DRI detector kept at 40 °C. The solvent was stabilized with 0.05% BHT (*w/v*) and 0.03% LiCl (*w/v*), and samples were filtered through a 0.45 µm GHP filter to prevent any impurities entering the system. Calibration was done using PMMA standards (Polymer Laboratories) ranging from 690 to 1.2 x 10^6 g/mol. Data acquisition was done using Millennium software, version 4.

3.5.3 Synthesis of poly(styrene-*alt*-maleic anhydride) (P(St-*alt*-MAnh))

Conventional radical copolymerization was used to synthesize an alternating copolymer of styrene and maleic anhydride in a 1:1 molar ratio styrene:maleic anhydride.[12]

Maleic anhydride (MAnh) (14 g, 0.14 mol), styrene monomer (15 g, 0.14 mol) and 2,2' azobis(isobutyronitrile) (AIBN, 0.1182 g, $7.20*10^{-4}$ mol) were dissolved in 200 mL methyl ethyl ketone (MEK). The reaction mixture was degassed with N_2 for 30 minutes and stirred overnight (16 hours) at 60 °C. The reaction mixture was cooled to room temperature, precipitated in 500 mL iso-propanol and washed with n-hexane. The polymer was dried under vacuum at room temperature to remove any unreacted monomer and residual solvent and then analyzed using SEC. M_n = 128 000 g/mol, $Đ$ = 2.7

Major IR absorptions: 3061, 2929, 1854, 1774, 1602, 1494, 1453, 1219, 1079, 953, 922, 763, 703 cm^{-1}.

3.5.4 Electrospinning of SMA

a) Electrospinning of P(St-*alt*-MAnh)

P(St-*alt*-MAnh) was dissolved in a 1:2 DMF:acetone solution (15 wt. %).[2] The prepared solution was placed in a 1 mL plastic syringe connected to a syringe pump (Harvard, Model 33 Twin Syringe Pump). An electrode lead of a high voltage power supply capable of generating positive DC voltages from 0 to 25 kV was connected to the blunt metal needle of the syringe. The positive charge was set at 7.5 kV. The flow rate was set at 0.01 mL/min and the needle diameter was 21 gauge. A stationary foil covered collector was placed 15 cm from the needle tip and connected to a negative electrode. The negative charge was set at 7.5 kV. The collected electrospun fibers were placed under vacuum at 50 °C to remove any residual solvents.

b) Electrospinning of P(St-*co*-MAnh)

The same method was followed as 3.5.4 a) with a 20 wt. % solution, electric field strength of 20 kV and 18 cm spinning distance.

3.5.5 Surface-functionalization of SMA nanofibers with amino sugars (glucosamine and mannosamine)

a) Synthesis of S-*alt*-MI-Gluc

Glucosamine hydrochloride (344 mg, 1.6 mmol)) and triethylamine (TEA, 162 mg, 1.6 mmol) in 2.5 mL iso-propanol was stirred at 60 °C until dissolved.[15] The glucosamine solution was cooled to room temperature. The electrospun P(St-*alt*-MAnh) fibers (215 mg) were placed in a petri dish and covered with the prepared glucosamine solution.[10,11] The petri dish was closed and rotated on a belly dancer laboratory shaker for 3 hours at ambient conditions. The functionalized fibers were removed and washed with iso-propanol three times. The fibers were air dried, followed by heating under vacuum at 60 °C for 24 hours. The dried fibers were washed with distilled water three times and dried at room temperature.

Major IR absorptions: 3281, 2944, 1699, 1645, 1538, 1454, 1396, 1176, 1030, 950, 838, 766, 703 cm^{-1}.

b) Synthesis of S-*co*-MI-Gluc

Glucosamine hydrochloride (172 mg, 0.8 mmol)) and triethylamine (TEA, 81 mg, 0.8 mmol) in 2.5 mL DMSO was stirred at 60 °C until dissolved.[15] The glucosamine solution was cooled to room temperature. The electrospun P(St-*co*-MAnh) fibers (215 mg) were placed in a petri dish and covered with the prepared glucosamine solution.[10,11] The petri dish was closed and rotated on a belly dancer laboratory shaker for 3 hours at ambient conditions. The functionalized fibers were removed and washed with DMSO three times. The fibers were air dried, followed by heating under vacuum at 60 °C for 24 hours. The dried fibers were washed with distilled water three times and dried at room temperature.

Major IR absorptions: 3379, 2926, 1774, 1706, 1644, 1540, 1494, 1453, 1204, 1029 759, 699 cm^{-1}.

c) Synthesis of S-*alt*-MI-Man

The same method was followed as 3.5.5 a) using 344 mg mannosamine hydrochloride (1.6 mmol) and 162 mg TEA (1.6 mmol).

Major IR absorptions: 3383, 2925, 1704, 1553, 1494, 1454, 1360, 1175, 1030, 762, 700 cm^{-1}.

d) Synthesis of S-*co*-MI-Man

The same method was followed as 3.5.5 b) using 172 mg mannosamine hydrochloride (0.8 mmol) and 81 mg TEA (0.8 mmol).

Major IR absorptions: 3377, 2926, 1777, 1712, 1602, 1538, 1494, 1453, 1217, 1071, 1029, 915, 758, 698 cm^{-1}.

3.5.6 Surface-functionalization of SMA nanofibers with protein

a) Synthesis of S-*alt*-MI-Con A

A 4 mg/mL solution of Concanavalin A in PBS buffer (8 g NaCl, 0.2 g KCl, 11.5 g Na_2HPO_4, 0.2 g KH_2PO_4, pH 7.4) was prepared. $MnCl_2$ (0.013 mg/mL) and $CaCl_2$ (0.011 mg/mL) were added to the solution.[21-24] The electrospun P(St-*alt*-MAnh) fibers (36 mg) were placed in a petri dish and covered with the Con A/PBS solution.[10,11] It was incubated for one hour at 37 °C on a belly dancer laboratory shaker. The fibers were subsequently washed three times, for 10 min at a time, with PBS-Tween buffer (PBS, 0.01% Tween 20) to remove any unreacted protein adsorbed on the nanofibrous surface. The fibers were air dried, followed by heating under vacuum at 60 °C for 24 hours.

Major IR absorptions: 3350, 2930, 2649, 1774, 1699, 1655, 1539, 1495, 1456, 1393, 1068, 1034, 766, 702 cm^{-1}.

b) Synthesis of S-*co*-MI-Con A

The same method was followed as 3.5.6 a) using electrospun P(St-*co*-MAnh) fibers.

Major IR absorptions: 3365, 2920, 2650, 1778, 1699, 1656, 1558, 1495, 1455, 764, 700 cm^{-1}.

3.5.7 Ninhydrin test

A ninhydrin test was performed to verify that the protein, Concanavalin A, was immobilized on the electrospun SMA fibers in experiment 3.5.6.[25]

An 0.5 mg sample of SMI-Con A was placed in a polytop. To the polytop was added 50 µL ninhydrin in ethanol solution (500 mg ninhydrin in 10 mL 95% absolute ethanol), 50 µL phenol in ethanol solution (40 g phenol in 10 mL 95% absolute ethanol) and 50 µL KCN in pyridine solution (2 mL

0.001M KCN solution in distilled water, diluted to 100 mL with distilled pyridine). The polytop was heated at 90 °C for 5 minutes and a colour change was observed from colourless to dark blue. This colour change is indicative of a positive test result for the presence of protein.

Pristine electrospun SMA fibers and ninhydrin reagents (without SMA) were used as negative control and Con A was used as positive control.

3.5.8 Immobilization of Horseradish peroxidase (HRP) on SMI-Con A

This test was performed to verify that the protein, Concanavalin A, was immobilized on the electrospun SMA fibers in experiment 3.5.6 with its biological activity still intact.[26,27]

The SMI-Con A nanofibers were incubated in casein buffer (10 mM TRIS, pH 7.6, 0.15 M NaCl, 0.5% Casein, 0.02% Thimerosal) for 20 minutes at 37 °C in order to block all non-specific sites. The fibers were subsequently washed three times, for 10 min at a time, with PBS-Tween buffer (PBS, 0.01% Tween 20). The casein blocked SMI-Con A nanofibers were now incubated with HRP (4 mg/mL solution of HRP in PBS buffer) for 60 minutes at 37 °C followed by wash steps as previously described. The fibers were now incubated with anti-HRP antibodies (1:10 000 in casein buffer) for 2 hours at 37 °C followed by wash steps as previously described. A secondary antibody (anti-rabbit IgG, 1:20 000) was then added to the fibers and incubated for 2 hours at 37 °C followed by wash steps as previously described. The substrate was now added to the washed fibers, consisting of 5-bromo-4-chloro-3-indoyl phosphate p-toluidine salt/nitro blue tetrazolium (BCIP-T/NBT): 33 µL of BCIP-T(50 mg/mL in DMF) and 44 µL of NBT (75 mg/mL in 70% DMF) in 10 mL of alkaline phosphatase buffer (100 mM TRIS, pH 9.5, 100 mM NaCl, 10 mM $MgCl_2$) and incubated at room temperature. A colour change was observed from light green to dark blue. This colour change is indicative of a positive test result for the presence of biologically active Con A.

Pristine electrospun SMA fibers were used as negative control and Con A as positive control.

3.5.9 Surface-functionalization of SMA nanofibers with amino acid derivative (BCML)

a) Synthesis of S-*alt*-MI-BCML

N_α,N_α-bis(carboxymethyl)-L-lysine hydrate (BCML, 330 mg, 1.26 mmol) and TEA (128 mg, 1.28 mmol) were dissolved in 2 mL iso-propanol. The electrospun P(St-*alt*-MAnh) fibers (170 mg) were placed in

a petri dish and covered with the prepared BCML solution.[10,11] The petri dish was closed and rotated on a belly dancer laboratory shaker for 2 hours at ambient conditions. The functionalized fibers were removed and washed with iso-propanol three times. The fibers were air dried, followed by heating under vacuum at 130 °C for 24 hours. The dried fibers were washed with distilled water three times and dried at room temperature.

Major IR absorptions: 3402, 2943, 1704, 1495, 1454, 1178, 1103, 917, 762, 701 cm^{-1}.

b) Synthesis of S-*co*-MI-BCML

N_α,N_α-bis(carboxymethyl)-L-lysine hydrate (BCML, 170 mg, 0.65 mmol) and TEA (66 mg, 0.65 mmol) were dissolved in 2 mL DMSO. The electrospun P(St-*co*-MAnh) fibers (170 mg) were placed in a petri dish and covered with the prepared BCML solution.[10,11] The petri dish was closed and rotated on a belly dancer laboratory shaker for 2 hours at ambient conditions. The functionalized fibers were removed and washed with DMSO three times. The fibers were air dried, followed by heating under vacuum at 60 °C for 24 hours. The dried fibers were washed with distilled water three times and dried at room temperature.

Major IR absorptions: 3408, 2923, 1856, 1777, 1703, 1633, 1494, 1454, 1403, 1222, 1017, 951, 760, 701 cm^{-1}.

3.5.10 Surface-functionalization of SMA nanofibers with *N*-dodecyl-*N*-propyl-propane-1,3-diamine (SMI-tC_{12})

a) Boc protection of 1-amino-3-chloropropane

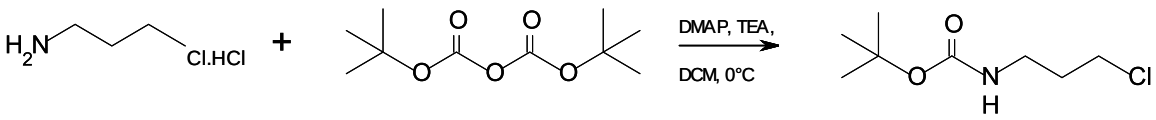

Scheme 3.1 Synthesis of N-tert-butoxycarbonyl-1-amino-3-chloropropane.

1-Amino-3-chloropropane hydrochloride (5 g, 38 mmol), 4-dimethylaminopyridine (DMAP, 0.24 g, 19 mmol) and triethylamine (TEA, 8.44 g, 84 mmol) in 7.5 mL dichloromethane (DCM) was stirred at room temperature until dissolved. To this solution was added dropwise a solution of di-*tert*-butyl-dicarbonate (t-Boc, 12.4 g, 57 mmol) in 7.5 mL DCM at 0 °C over 1 hour. The reaction was stirred for 24 hours at room temperature whereafter it was concentrated under vacuum. The residue was taken

up in ethyl acetate and washed twice with saturated NaCl. The organic phase was dried over K_2CO_3, filtered and concentrated under vacuum to give the *N-tert*-butoxycarbonyl derivative in 79% yield.

^{1}H-NMR ($CDCl_3$): δ (ppm) = 4.65 (s broad, 1H, -CO-N**H**-CH_2-), 3.53 (t, 2H, Cl-C**H$_2$**-CH_2-), 3.22 (quartet, 2H, -NH-C**H$_2$**-CH_2-), 1.91 (quintet, 2H, -CH_2-C**H$_2$**-CH_2-), 1.38 (s, 9H, -C(C**H$_3$**)$_3$)

^{13}C-NMR ($CDCl_3$): δ (ppm) = 155.98 (-**C**=O), 79.25 (-**C**(CH_3)$_3$), 42.42 (-**C**H_2-Cl), 37.97 (-**C**H_2-NH-), 32.63 (-CH_2-**C**H_2-CH_2-), 28.44 (-C(**C**H_3)$_3$)

b) Synthesis of *N*-propyldodecyl-1-amine

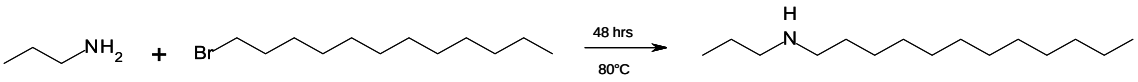

Scheme 3.2 Synthesis of N-propyldodecyl-1-amine.

Propylamine (2 g, 33 mmol) was added dropwise to a solution of 1-bromododecane (10.13 g, 40 mmol) in 11 mL 1:2 methanol:acetonitrile at room temperature. The reaction was refluxed at 80 °C for 48 hours whereafter it was concentrated under vacuum. The ammonium salt obtained was basified with ammonia and extracted with diethyl ether. The ether layer was washed with saturated NaCl solution to neutrality, dried over $CaCl_2$, filtered and concentrated under vacuum to yield 8.57 g of product.[28]

^{1}H-NMR ($CDCl_3$): δ (ppm) = 2.7 (quartet, 2H, -CH_2-C**H$_2$**-NH-), 2.53 (m, 3H, -N**H**-C**H$_2$**-CH_2-), 1.67 (sextet, 2H, CH_3-C**H$_2$**-CH_2-), 1.54 (sextet, 2H, -CH_2-C**H$_2$**-CH_3), 1.25 (s, 18H, -(C**H$_2$**)$_9$-), 0.94 (t, 3H, C**H$_3$**-CH_2-), 0.87 (t, 3H, CH_2-C**H$_3$**)

^{13}C-NMR ($CDCl_3$): δ (ppm) = 50.92 (-**C**H_2-NH-), 49.16 (-**C**H_2-NH-), 31.97 (-**C**H_2-), 29.71 (-**C**H_2-), 29.69 (-**C**H_2-), 29.66 (-**C**H_2-), 29.58 (-**C**H_2-), 29.38 (-**C**H_2-), 27.52 (-**C**H_2-), 22.74 (-**C**H_2-CH_3), 14.16 (-CH_2-**C**H_3), 11.90 (-CH_2-**C**H_3)

c) Synthesis of *N-tert*-butoxycarbonyl-*N'*-dodecyl-*N'*-propyl-propane-1,3-diamine

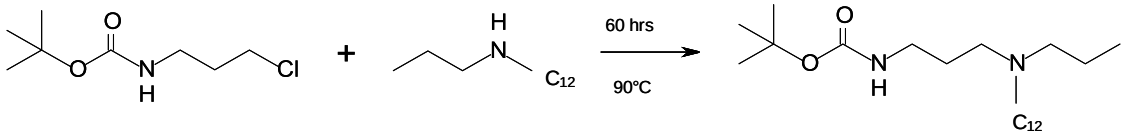

Scheme 3.3 Synthesis of N-tert-butoxycarbonyl-N'-dodecyl-N'-propyl-propane-1,3-diamine.

To a solution of *N*-propyldodecyl-1-amine (2 g, 8.8 mmol) in 10 mL 1,2-dichloroethane was added dropwise a solution of *N-tert*-butoxycarbonyl-1-amino-3-chloropropane (1.9 g, 10.6 mmol) in 5 mL 1,2-dichloroethane at room temperature. The reaction was refluxed at 90 °C for 60 hours whereafter it was concentrated under vacuum. The ammonium salt obtained was basified with ammonia and extracted with chloroform. The chloroform layer was washed with saturated NaCl solution to neutrality, dried over $CaCl_2$, filtered and concentrated under vacuum to yield 3.09 g of *N-tert*-butoxycarbonyl-*N'*-dodecyl-*N'*-propyl-propane-1,3-diamine.[28]

^{1}H-NMR ($CDCl_3$): δ (ppm) = 4.67 (s broad, 1H, -CO-N**H**-CH_2-), 3.56 (t, 2H, -CO-NH-C**H$_2$**-), 3.24 (m, 2H, -N-C**H$_2$**-CH_2-), 2.57 (m, 2Hx2, -CH_2-C**H$_2$**-N-), 1.92 (quintet, 2H, -CH_2-C**H$_2$**-CH_2-), 1.56 (m, 2H, C**H$_2$**-CH_3), 1.4 (s, 9H, -C(C**H$_3$**)$_3$), 1.22 (s, 20H, -(C**H$_2$**)$_{10}$-), 0.88 (t, 3H, C**H$_3$**-CH_2-), 0.83 (t, 3H, CH_2-C**H$_3$**)

^{13}C-NMR ($CDCl_3$): δ (ppm) = 156.23 (-**C**=O), 79.40 (-**C**(CH_3)$_3$), 55.56 (-**C**H_2-N-), 53.72 (-**C**H_2-N-x2), 38.14 (-**C**H_2-NH-), 32.08 (-**C**H_2-), 29.82 (-**C**H_2-x2), 29.77 (-**C**H_2-x2), 29.61 (-**C**H_2-), 29.53 (-**C**H_2-), 28.58 (-C(**C**H_3)$_3$), 27.68 (-**C**H_2-), 27.57 (-**C**H_2-), 25.71 (-**C**H_2-), 22.85 (-**C**H_2-CH_3x2), 14.30 (CH_2-**C**H_3), 11.90 (-CH_2-**C**H_3)

d) Surface-functionalization of P(St-*alt*-MAnh) nanofibers with *N*-dodecyl-*N*-propyl-propane-1,3-diamine

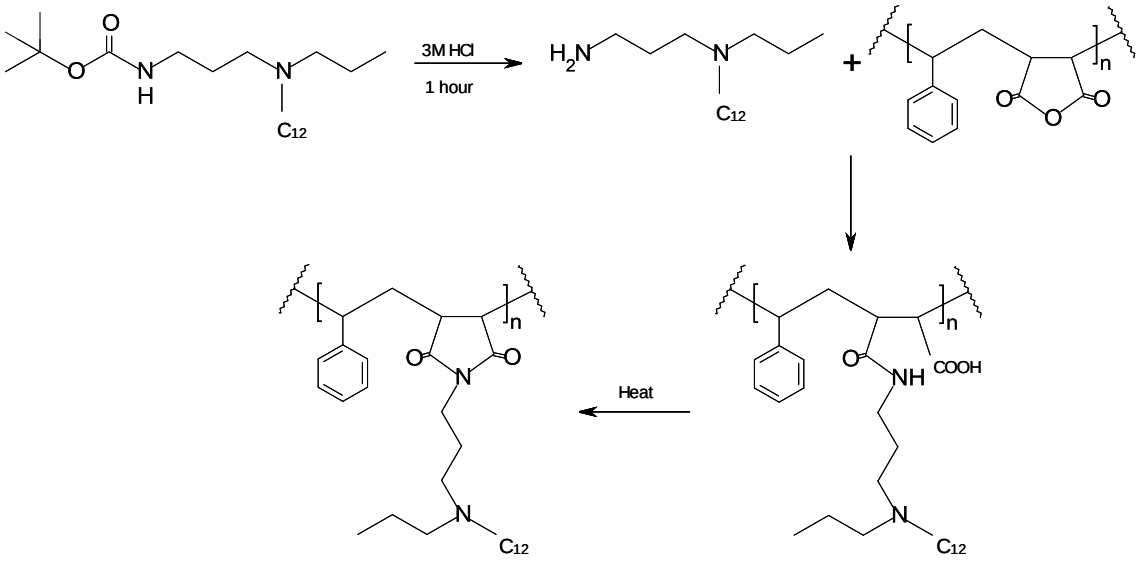

Scheme 3.4 Surface-functionalization of SMA nanofibers with N-dodecyl-N-propyl-propane-1,3-diamine.

N-tert-butoxycarbonyl-*N'*-dodecyl-*N'*-propyl-propane-1,3-diamine (1 g, 2.7 mmol) was dissolved in 5 mL 3 M HCl-EtOAc (1:1).[38] After stirring the reaction mixture for 1 hour, the solvent was removed under vacuum and diethyl ether was added to the remaining water layer. The organic phase was

extracted, dried over $CaCl_2$, filtered and concentrated under vacuum to yield the unprotected primary amine.

^{1}H-NMR ($CDCl_3$): δ (ppm) = 4.8 (s broad, 2H, N**H$_2$**-CH_2-), 3.51 (t, 2H, NH_2-C**H$_2$**-), 3.35 (m, 2H, -N-C**H$_2$**-CH_2-), 2.58 (m, 2H, -CH_2-C**H$_2$**-N-), 2.45 (m, 2H, -CH_2-C**H$_2$**-N-), 1.75 (quintet, 2H, -CH_2-C**H$_2$**-CH_2-), 1.54 (m, 2H, -CH_2-C**H$_2$**-CH_3), 1.43 (m, 2H, -CH_2-C**H$_2$**-CH_3), 1.21 (s, 18H, -(C**H$_2$**)$_9$-), 0.86 (t, 3H, C**H$_3$**-CH_2-), 0.83 (t, 3H, CH_2-C**H$_3$**)

^{13}C-NMR ($CDCl_3$): δ (ppm) = 54.16 (-**C**H_2-N-), 52.48 (-**C**H_2-N-x2), 45.27 (-**C**H_2-NH_2), 31.95 (-**C**H_2-), 29.64 (-**C**H_2-), 29.63 (-**C**H_2-), 29.53 (-**C**H_2-), 29.48 (-**C**H_2-), 29.37 (-**C**H_2-), 29.14 (-**C**H_2-), 26.99 (-**C**H_2-x3), 22.72 (-**C**H_2-CH_3), 14.17 (-CH_2-**C**H_3), 11.36 (-CH_2-**C**H_3)

The electrospun P(St-*alt*-MAnh) fibers (100 mg) were placed in a petri dish and covered with a solution of *N*-dodecyl-*N*-propyl-propane-1,3-diamine (140 mg, 0.5 mmol) in 5 mL iso-propanol.[10,11] The petri dish was closed and rotated on a belly dancer laboratory shaker for 2 hours at ambient conditions. The functionalized fibers were removed and washed with iso-propanol three times. The fibers were air dried, followed by heating under vacuum at 130 °C for 24 hours.

Major IR absorptions: 2926, 2854, 1856, 1778, 1699, 1558, 1495, 1454, 1217, 1077, 920, 761, 700 cm^{-1}.

e) Surface-functionalization of P(St-*co*-MAnh) nanofibers with *N*-dodecyl-*N*-propyl-propane-1,3-diamine

The same method was followed as 3.5.10 d) using electrospun P(St-*co*-MAnh) fibers, with *N*-dodecyl-*N*-propyl-propane-1,3-diamine (73 mg, 0.26 mmol) in 5 mL iso-propanol.

Major IR absorptions: 2923, 2852, 1779, 1699, 1583, 1494, 1454, 1366, 1217, 1079, 952, 759, 701 cm^{-1}.

3.5.11 Surface-functionalization of SMA nanofibers with *N*-hexadecyl-*N*-propyl-propane-1,3-diamine (SMI-tC_{16})

a) Synthesis of *N*-propylhexadecyl-1-amine

Propylamine (2 g, 33 mmol) was added dropwise to a solution of 1-bromohexadecane (12.2 g, 40 mmol) in 10 mL 1,2-dichloroethane at room temperature. The reaction was refluxed at 90 °C for 48 hours whereafter it was concentrated under vacuum. The ammonium salt obtained was basified with ammonia and extracted with diethyl ether. The ether layer was washed with saturated NaCl solution to neutrality, dried over $CaCl_2$, filtered and concentrated under vacuum to yield 8.57 g of product.[28]

^{1}H-NMR ($CDCl_3$): δ (ppm) = 2.6 (quartet, 2H, -CH_2-C**H$_2$**-NH-), 2.36 (m, 3H, -N**H**-C**H$_2$**-CH_2-), 1.53 (sextet, 2H, CH_3-C**H$_2$**-CH_2-), 1.4 (m, 2Hx2, -CH_2-C**H$_2$**-), 1.24 (s, 24H, -(C**H$_2$**)$_{12}$-), 0.9 (t, 3H, C**H$_3$**-CH_2-), 0.86 (t, 3H, CH_2-C**H$_3$**)

^{13}C-NMR ($CDCl_3$): δ (ppm) = 51.60 (-**C**H_2-NH-), 49.75 (-**C**H_2-NH-), 31.89 (-**C**H_2-), 30.90 (-**C**H_2-x2), 29.69 (-**C**H_2-x2), 29.68 (-**C**H_2-x2), 29.65 (-**C**H_2-x2), 29.60 (-**C**H_2-), 29.59 (-**C**H_2-), 29.35 (-**C**H_2-), 27.60 (-**C**H_2-), 22.66 (-**C**H_2-CH_3x2), 14.08 (-CH_2-**C**H_3), 11.73 (-CH_2-**C**H_3)

b) Synthesis of *N-tert*-butoxycarbonyl-*N'*-hexadecyl-*N'*-propyl-propane-1,3-diamine

To a solution of *N*-propylhexadecyl-1-amine (2 g, 7 mmol) in 10 mL 1,2-dichloroethane was added dropwise a solution of N-*tert*-butoxycarbonyl-1-amino-3-chloropropane (1.62 g, 8.4 mmol) in 5 mL 1,2-dichloroethane at room temperature. The reaction was refluxed at 90 °C for 48 hours whereafter it was concentrated under vacuum. The ammonium salt obtained was basified with ammonia and extracted with chloroform. The chloroform layer was washed with saturated NaCl solution to neutrality, dried over $CaCl_2$, filtered and concentrated under vacuum to yield 2.17 g of *N-tert*-butoxycarbonyl-*N*'-hexadecyl-*N*'-propyl-propane-1,3-diamine.[28]

^{1}H-NMR ($CDCl_3$): δ (ppm) = 4.67 (s broad, 1H, -CO-N**H**-CH_2-), 3.56 (t, 2H, -CO-NH-C**H$_2$**-), 3.24 (m, 2H, -N-C**H$_2$**-CH_2-), 2.59 (m, 2H, -CH_2-C**H$_2$**-N-), 2.43 (m, 2H, -CH_2-C**H$_2$**-N-), 1.94 (quintet, 2H, -CH_2-C**H$_2$**-CH_2-), 1.42 (s, 9H, -C(C**H$_3$**)$_3$), 1.26 (s, 30H, -(C**H$_2$**)$_{15}$-), 0.89 (t, 3H, C**H$_3$**-CH_2-), 0.87 (t, 3H, CH_2-C**H$_3$**)

^{13}C-NMR ($CDCl_3$): δ (ppm) = 155.97 (-**C**=O), 79.50 (-**C**$(CH_3)_3$), 56.95 (-**C**H_2-N-), 54.32 (-**C**H_2-N-x2), 37.98 (-**C**H_2-NH-), 31.97 (-**C**H_2-), 29.72 (-**C**H_2-x9), 28.43 (-**C**H_2-), 28.40 (-C(**C**$H_3)_3$), 27.73 (-**C**H_2-), 26.49 (-**C**H_2-), 22.70 (-**C**H_2-CH_3x2), 14.11 (-CH_2-**C**H_3), 12.03 (-CH_2-**C**H_3)

c) Surface-functionalization of P(St-*alt*-MAnh) nanofibers with *N*-hexadecyl-*N*-propyl-propane-1,3-diamine

N-tert-butoxycarbonyl-*N'*-hexadecyl-*N'*-propyl-propane-1,3-diamine (1 g) was deprotected in the same manner as 3.5.10d).

^{1}H-NMR ($CDCl_3$): δ (ppm) = 4.75 (s broad, 2H, N**H$_2$**-CH_2-), 3.47 (m, 2H, NH_2-C**H$_2$**-CH_2-), 3.37 (m, 2H, -CH_2-C**H$_2$**-N-), 3.05 (m, 2H, -CH_2-C**H$_2$**-N-), 2.94 (m, 2H, -CH_2-C**H$_2$**-N-), 1.86 (m, 2H, -CH_2-C**H$_2$**-CH_2-), 1.76 (m, 2H, -CH_2-C**H$_2$**-CH_2-), 1.24 (s, 26H, -(C**H$_2$**)$_{13}$-), 1.0 (t, 3H, C**H$_3$**-CH_2-), 0.86 (t, 3H, CH_2-C**H$_3$**)

^{13}C-NMR ($CDCl_3$): δ (ppm) = 54.21 (-**C**H_2-N-), 52.58 (-**C**H_2-N-x2), 45.48 (-**C**H_2-NH_2), 32.21 (-**C**H_2-), 29.31 (-**C**H_2-), 29.97 (-**C**H_2-), 29.96 (-**C**H_2-), 29.94 (-**C**H_2-), 29.93 (-**C**H_2-), 29.85 (-**C**H_2-), 29.75 (-**C**H_2-),

29.68 (-**C**H_2-), 29.63 (-**C**H_2-x2), 27.00 (-**C**H_2-), 27.14 (-**C**H_2-), 26.11 (-**C**H_2-), 22.98 (-**C**H_2-CH_3x2), 14.32 (-CH_2-**C**H_3), 11.52 (-CH_2-**C**H_3),

The electrospun P(St-*alt*-MAnh) fibers (100 mg) were placed in a petri dish and covered with a solution of *N*-hexadecyl-*N*-propyl-propane-1,3-diamine (180 mg, 0.5 mmol) in 5 mL iso-propanol.[10,11] The petri dish was closed and rotated on a belly dancer laboratory shaker for 2 hours at ambient conditions. The functionalized fibers were removed and washed with iso-propanol three times. The fibers were air dried, followed by heating under vacuum at 130 °C for 24 hours.

Major IR absorptions: 2925, 2853, 1855, 1778, 1698, 1494, 1454, 1367, 1250, 1167, 1077, 923, 761, 700 cm^{-1}.

d) Surface-functionalization of P(St-*co*-MAnh) nanofibers with *N*-hexadecyl-*N*-propyl-propane-1,3-diamine

The same method was followed as 3.5.11 c) using electrospun P(St-*co*-MAnh) fibers, with *N*-hexadecyl-*N*-propyl-propane-1,3-diamine (88 mg, 0.26 mmol) in 5 mL iso-propanol

Major IR absorptions: 2918, 2850, 1857, 1776, 1703, 1494, 1453, 1365, 1220, 1168, 1078, 919, 759, 699 cm^{-1}.

3.5.12 Surface-functionalization of SMA nanofibers with *N*,*N*-didodecyl-*N*-propyl-propane-1,3-diamine (SMI-qC_{24})

a) Synthesis of *N-tert*-butoxycarbonyl-*N'*,*N'*-didodecyl-*N'*-propyl-propane-1,3-diamine

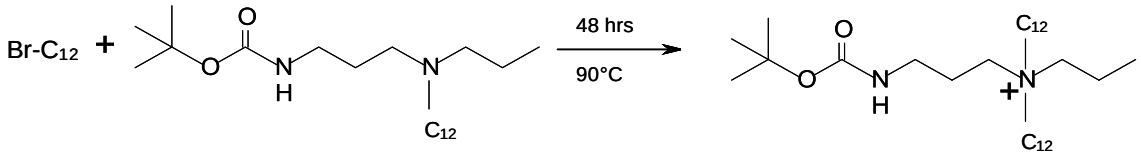

Scheme 3.5 Synthesis of N-tert-butoxycarbonyl-N',N'-didodecyl-N'-propyl-propane-1,3-diamine.

1-Bromododecane (1.88 g, 7.5 mmol) was added dropwise to a solution of *N-tert*-butoxycarbonyl-*N'*-dodecyl-*N'*-propyl-propane-1,3-diamine (1.4 g, 3.77 mmol) in 10 mL 1,2-dichloroethane at room temperature. The reaction mixture was refluxed at 90 °C for 48 hours whereafter it was concentrated under vacuum. The mixture was crystallized from methanol/diethyl ether three times to get a pure product in 83% yield.[28]

^{1}H-NMR ($CDCl_3$): δ (ppm) = 4.65 (s broad, 1H, -CO-N**H**-CH_2-), 3.51 (t, 2Hx2, -N-C**H$_2$**-CH_2-), 3.26 (m, 2H, -N-C**H$_2$**-CH_2-), 2.83 (m, 2H, -CH_2-C**H$_2$**-N-), 2.62 (m, 2H, -CH_2-C**H$_2$**-N-), 1.94 (quintet, 2H, -CH_2-C**H$_2$**-CH_2-), 1.75 (sextet, 2Hx3, -C**H$_2$**-CH_3), 1.42 (s, 9H, -C(C**H$_3$**)$_3$), 1.24 (s, 36H, -(C**H$_2$**)$_{18}$-), 0.87 (t, 3Hx3, C**H$_3$**-CH_2-)

^{13}C-NMR ($CDCl_3$): δ (ppm) = 155.90 (-**C**=O), 79.17 (-**C**(CH_3)$_3$), 56.11 (-**C**H_2-N-), 54.09 (-**C**H_2-N-x3), 37.89 (-**C**H_2-NH-), 32.64 (-**C**H_2-x2), 31.88 (-**C**H_2-x2), 29.61 (-**C**H_2-x2), 29.60 (-**C**H_2-x2), 29.58 (-**C**H_2-x2), 29.53 (-**C**H_2-x2), 29.45 (-**C**H_2-x2), 28.36 (-C(**C**H_3)$_3$), 27.60 (-**C**H_2-x2), 26.86 (-**C**H_2-x2), 25.33 (-**C**H_2-), 22.66 (-**C**H_2-CH_3x3), 14.09 (-CH_2-**C**H_3x2), 11.91 (-CH_2-**C**H_3)

b) Surface-functionalization of P(St-*alt*-MAnh) nanofibers with *N*,*N*-didodecyl-*N*-propyl-propane-1,3-diamine

N-*tert*-butoxycarbonyl-*N'*,*N'*-didodecyl-*N'*-propyl-propane-1,3-diamine (1 g) was deprotected in the same manner as 3.5.10d).

^{1}H-NMR ($CDCl_3$): δ (ppm) = 4.79 (s broad, 2H, N**H$_2$**-CH_2-), 3.53 (t, 2Hx2, N-C**H$_2$**-CH_2-), 3.4 (t, 2H, -CH_2-C**H$_2$**-N-), 2.94 (m, 2Hx2, -CH_2-C**H$_2$**-N-), 1.86 (quintet, 2H, -CH_2-C**H$_2$**-CH_2-), 1.75 (sextet, 2Hx3, -CH_2-C**H$_3$**), 1.25 (s, 36H, -(C**H$_2$**)$_{18}$-), 0.89 (t, 3Hx3, C**H$_3$**-CH_2-)

^{13}C-NMR ($CDCl_3$): δ (ppm) = 53.93 (-**C**H_2-N-), 52.26 (-**C**H_2-N-x3), 45.17 (-**C**H_2-NH_2), 32.62 (-**C**H_2-x2), 31.89 (-**C**H_2-x2), 29.61 (-**C**H_2-x2), 29.60 (-**C**H_2-x2), 29.53 (-**C**H_2-x2), 29.45 (-**C**H_2-x2), 29.32 (-**C**H_2-x2), 28.88 (-**C**H_2-x2), 26.86 (-**C**H_2-x3), 22.53 (-**C**H_2-CH_3x3), 14.09 (-CH_2-**C**H_3x2), 11.20 (-CH_2-**C**H_3)

The electrospun P(St-*alt*-MAnh) fibers (100 mg) were placed in a petri dish and covered with a solution of *N*,*N*-didodecyl-*N*-propyl-propane-1,3-diamine (220 mg, 0.5 mmol) in 5 mL diethyl ether.[10,11] The petri dish was closed and rotated on a belly dancer laboratory shaker for 2 hours at ambient conditions. The functionalized fibers were removed and washed with diethyl ether three times. The fibers were air dried, followed by heating under vacuum at 130 °C for 24 hours.

Major IR absorptions: 3398, 2926, 2854, 1856, 1777, 1698, 1568, 1495, 1454, 1402, 1218, 1078, 920, 761, 701 cm^{-1}.

c) Surface-functionalization of P(St-*co*-MAnh) nanofibers with *N*,*N*-didodecyl-*N*-propyl-propane-1,3-diamine

The same method was followed as 3.5.12 b) using electrospun P(St-*co*-MAnh) fibers, with *N*,*N*-didodecyl-*N*-propyl-propane-1,3-diamine (117 mg, 0.26 mmol) in 5 mL diethyl ether.

Major IR absorptions: 3402, 2925, 2854, 1856, 1777, 1700, 1601, 1494, 1453, 1375, 1218, 1076, 1030, 919, 758, 699 cm^{-1}.

3.5.13 Surface-functionalization of SMA nanofibers with *N*,*N*-dihexadecyl-*N*-propyl-propane-1,3-diamine (SMI-qC_{32})

a) Synthesis of *N-tert*-butoxycarbonyl-*N*',*N*'-dihexadecyl-*N'*-propyl-propane-1,3-diamine

1-Bromohexadecane (2.08 g, 6.8 mmol) was added dropwise to a solution of *N-tert*-butoxycarbonyl-*N*'-hexadecyl-*N*'-propyl-propane-1,3-diamine (1.5 g, 3.4 mmol) in 10 mL 1,2-dichloroethane at room temperature. The reaction was refluxed at 90 °C for 48 hours whereafter it was concentrated under vacuum. The mixture was crystallized from methanol/diethyl ether three times to get a pure product in 78% yield.[28]

^{1}H-NMR ($CDCl_3$): δ (ppm) = 4.65 (s broad, 1H, -CO-N**H**-CH_2-), 3.51 (t, 2Hx2, -N-C**H$_2$**-CH_2-), 3.36 (m, 2H, -N-C**H$_2$**-CH_2-), 2.81 (m, 2Hx2, -CH_2-C**H$_2$**-N-), 1.95 (quintet, 2H, -CH_2-C**H$_2$**-CH_2-), 1.75 (sextet, 2Hx3, -C**H$_2$**-CH_3), 1.43 (s, 9H, -C(C**H$_3$**)$_3$), 1.24 (s, 52H, -(C**H$_2$**)$_{26}$-), 0.86 (t, 3Hx3, C**H$_3$**-CH_2-)

^{13}C-NMR ($CDCl_3$): δ (ppm) = 155.89 (-**C**=O), 79.43 (-**C**(CH_3)$_3$), 56.83 (-**C**H_2-N-), 54.24 (-**C**H_2-N-x3), 37.85 (-**C**H_2-NH-), 32.61 (-**C**H_2-x2), 31.90 (-**C**H_2-x2), 29.67 (-**C**H_2-x2), 29.66 (-**C**H_2-x2), 29.65 (-**C**H_2-x2), 29.63 (-**C**H_2-x4), 29.60 (-**C**H_2-x2), 29.53 (-**C**H_2-x2), 29.45 (-**C**H_2-x2), 29.34 (-**C**H_2-x2), 28.88 (-C(**C**H_3)$_3$), 28.87 (-**C**H_2-x2), 28.37 (-**C**H_2-x2), 26.87 (-**C**H_2-), 22.68 (-**C**H_2-CH_3x3), 14.09 (-CH_2-**C**H_3x2), 11.94 (-CH_2-**C**H_3)

b) Surface-functionalization of P(St-*alt*-MAnh) nanofibers with *N*,*N*-dihexadecyl-*N*-propyl-propane-1,3-diamine

N-tert-butoxycarbonyl-*N'*,*N'*-dihexadecyl-*N*'-propyl-propane-1,3-diamine (1 g) was deprotected in the same manner as 3.5.10d).

^{1}H-NMR ($CDCl_3$): δ (ppm) = 4.76 (s broad, 2H, N**H$_2$**-CH_2-), 3.51 (t, 2Hx2, N-C**H$_2$**-CH_2-), 3.38 (m, 2H, -CH_2-C**H$_2$**-N-), 2.85 (m, 2Hx2, -CH_2-C**H$_2$**-N-), 1.84 (m, 2H, -CH_2-C**H$_2$**-CH_2-), 1.75 (sextet, 2Hx3, -CH_2-C**H$_3$**), 1.24 (s, 52H, -(C**H$_2$**)$_{26}$-), 0.87 (t, 3Hx3, C**H$_3$**-CH_2-)

^{13}C-NMR ($CDCl_3$): δ (ppm) = 56.14 (-**C**H_2-N-), 54.73 (-**C**H_2-N-x3), 45.15 (-**C**H_2-NH_2), 32.62 (-**C**H_2-x2), 31.92 (-**C**H_2-x2), 29.68 (-**C**H_2-x2), 29.67 (-**C**H_2-x4), 29.64 (-**C**H_2-x4), 29.61 (-**C**H_2-x2), 29.54 (-**C**H_2-x2),

29.46 (-**C**H_2-x2), 29.35 (-**C**H_2-x2), 28.89 (-**C**H_2-x2), 28.35 (-**C**H_2-x2), 26.87 (-**C**H_2-), 22.65 (-**C**H_2-CH_3x3), 14.10 (-CH_2-**C**H_3x2), 11.80 (-CH_2-**C**H_3)

The electrospun P(St-*alt*-MAnh) fibers (100 mg) were placed in a petri dish and covered with a solution of *N',N'*-dihexadecyl-*N'*-propyl-propane-1,3-diamine (268 mg, 0.5 mmol) in 5 mL diethyl ether.[10,11] The petri dish was closed and rotated on a belly dancer laboratory shaker for 2 hours at ambient conditions. The functionalized fibers were removed and washed with diethyl ether three times. The fibers were air dried, followed by heating under vacuum at 130 °C for 24 hours.

Major IR absorptions: 3390, 2921, 2851, 1777, 1710, 1563, 1494, 1454, 1220, 922, 760, 700 cm^{-1}.

c) Surface-functionalization of P(St-*co*-MAnh) nanofibers with *N*,*N*-dihexadecyl-*N*-propyl-propane-1,3-diamine

The same method was followed as 3.5.13 b) using electrospun P(St-*co*-MAnh) fibers, with *N*,*N*-dihexadecyl-*N*-propyl-propane-1,3-diamine (145 mg, 0.26 mmol) in 5 mL diethyl ether.

Major IR absorptions: 3404, 2918, 2815, 1857, 1776, 1705, 1603, 1494, 1466, 1454, 1367, 1220, 1077, 919, 756, 700 cm^{-1}.

3.6 References

1. Kim, T.G.; Park, T.G. *Biotechnol. Progr*. **2006**, *22*, 1108-1113.

2. Tang, C.; Ye, S.; Liu, H. *Polymer* **2007**, *48*, 4482-4491.

3. Yao, C.; Li, X.; Neoh, K.; Shi, Z.; Kang, E. *J. Membr. Sci.* **2008**, *320*, 259-267.

4. Agarwal, S.; Wendorff, J.H.; Greiner, A. *Polymer* **2008**, *49*, 5603-5621.

5. Yoo, H.S.; Kim, T.G.; Park, T.G.; *Adv. Drug Deliv. Rev.* **2009**, *61*, 1033-1042.

6. Chronakis, I.S. *J. Mater. Process Technol.* **2005**, *167*, 283-293.

7. Stoilova, O.; Ignatova, M.; Manolova, N.; Godjevargova, T.; Mita, D.; Rashkov, I. *Eur. Polym. J.* **2010**, *46*, 1966-1974.

8. Donati, I.; Gamini, A.; Vetere, A.; Campa, C.; Paoletti, S. *Biomacromolecules* **2002**, *3*, 805-812.

9. Lai, X.; Sun, C.; Tian, H.; Zhao, W.; Gao, L. *Int. J. Pharm*. **2008**, *352*, 66-73.

10. Vermeesch, I.; Groeninckx, G. *J. Appl. Polym. Sci*. **1994**, *53*, 1365-1373.

11. Evenson, S.; Badyal, J. *J. Phys. Chem. B*. **1998**, *102*, 5500-5502.

12. Jeong, J.H.; Ko, S.B. *Journal of Industrial and Engineering Chemistry* **2001**, *7*, 310-315.

13. Gopal, R.; Zuwei, M.; Kaur, S.; Ramakrishna, S. *Molecular Building Blocks for Nanotechnology* **2007**, 72-91.

14. Dikusar, E.; Potkin, V.; Kozlov, N. *Russ. J. Gen. Chem.* **2009**, *79*, 2655-2657.

15. García-Oteiza, M.C.; Sánchez-Chaves, M.; Arranz, F. *Macromol. Chem. Phys.* **1997**, *198*, 2237-2247.

16. Lee, S.S.; Ahn, T.O. *J. Appl. Polym. Sci.* **1999**, *71*, 1187-1196.

17. Wang, K.; Huang, W.; Xia, P.; Gao, C.; Yan, D. *React. Funct. Polym.* **2002**, *52*, 143-148.

18. Bahulekar, R.; Tokiwa, T.; Kano, J.; Matsumura, T.; Kojima, I.; Kodama, M. *Carbohydr. Polym*. **1998**, *37*, 71-78.

19. Bahulekar, R.; Tokiwa, T.; Kano, J.; Matsumura, T.; Kojima, I.; Kodama, M. *Biotechnol. Tech*. **1998**, *12*, 721-724.

20. Pompe, T.; Zschoche, S.; Herold, N.; Salchert, K.; Gouzy, M.F.; Sperling, C.; et al. *Biomacromolecules* **2003**, *4,* 1072-1079.

21. Swaminathan, C.P.; Surolia, N.; Surolia, A. *J. Am. Chem. Soc*. **1998**, *120*, 5153-5159.

22. Sato, K.; Imoto, Y.; Sugama, J.; Seki, S.; Inoue, H.; Odagiri, T.; et al. *Langmuir* **2005**, *21*, 797-799.

23. Köhn, M.; Benito, J.M.; Ortiz Mellet, C.; Lindhorst, T.K.; García Fernández, J.M. *Chem. BioChem. Eng. Q*. **2004**, *5,* 771-777.

24. Chern, C.S.; Lee, C.K.; Tsai, Y.J. *Colloid. Polym. Sci.* **2001**, *279*, 420-426.

25. Friedman, M. *J. Agric. Food Chem*. **2004**, *52*, 385-406.

26. Cloete, W.J.; Adriaanse, C.; Swart, P.; Klumperman, B. *Polym. Chem*. **2011**, *2*, 1479-1481.

27 Stott, D.I. *J. Immunol. Methods* **1989**, *119*, 153.

28. Roy, S.; Dasgupta, A.; Das, P.K. *Langmuir* **2006**, *22*, 4567-4573.

29. Chen, G.; Zhang, Y.; Zhou, X.; Xu, J. *Appl. Surf. Sci.* **2006**, *253*, 1107-1110.

30. Galgali, P.; Agashe, M.; Varma, A. *Carbohydr. Polym*. **2007**, *67,* 576-585.

31. Kim, C.H.; Choi, J.W.; Chun, H.J.; Choi, K.S. *Polym. Bull.* **1997**, *38*, 387-393.

32. Moscatelli, D.; Cavallotti, C.; Morbidelli, M. *Macromolecules* **2006**, *39*, 9641-9653.

33. Lazzara, T.D.; Whitehead, M.A.; van de Ven, T.G.M. *J. Phys. Chem.* B. **2008**, *112*, 4892-3899.

34. Pavia, D.L. *Introduction to spectroscopy*. Brooks/Cole Pub Co; **2009**.

35. Albertin, L.; Stenzel, M.H.; Barner-Kowollik, C.; Foster, L.J.R.; Davis, T.P. *Macromolecules* **2005**, *38*, 9075-9084.

36. Huang, F.; Wu, H.; Wang, D.; Yang, W.; Cao, Y. *Chem. Mater.* **2004**, *16*, 708-716.

37. Qin, C.; Xiao, Q.; Li, H.; Fang, M.; Liu, Y.; Chen, X.; et al. *Int. J. Biol. Macromol*. **2004**, *34*, 121-126.

38. Stahl, G.L.; Walter, R.; Smith, C.W. *J. Org. Chem*. **1978**, *43*, 2285-2286.

Chapter 4: Synthesis and characterization of functionalized polymer nanofibers, modified before electrospinning

4.1 Introduction

This chapter describes the preparation of functionalized polymer nanofibers that have been modified before electrospinning, whereas the previous chapter dealt with surface-functionalizing polymer nanofibers after electrospinning. Electrospinning is a highly versatile method for producing polymer nanofibers with a high surface area to volume ratio.[1,2] Although it appears to be a straightforward process, electrospinning is actually a rather intricate process that is dependent on a variety of molecular, process and technical parameters.[2] Modification of a polymer can change the properties of that polymer considerably and thus affect the electrospinnability of that polymer. When modifying a polymer before electrospinning, a new polymer is formed that may have different spinning parameters compared to the parent polymer. By adjusting the electrospinning parameters, such as voltage, spinning distance and solution flow rate, and the polymer solution properties, such as viscosity, conductivity and surface tension, most polymers should be electrospinnable.[2,3]

When modifying a polymer before electrospinning, covalent bond formation between the parent polymer and modification agent is preferred to ensure effective durability of the modified polymer's new properties. These covalent bonds can be formed by chemical reactions between the polymer and modification agent and can for example be achieved if the polymer is susceptible to electrophilic or nucleophilic attack by the modification agent.[4,5] The polymer to be modified must therefore have a reactive site and the modification agent a suitable reactive group to enable polymer modification via covalent bonding. As discussed in the previous chapter, poly(styrene-*co*-maleic anhydride) (SMA) was chosen as the polymer to be modified due to the very reactive maleic anhydride unit of SMA, which is available for nucleophilic attack by a primary amine moiety. [1,6-8] Primary amines were chosen as the preferred anhydride-reactive coupling agents because of their very nucleophilic character.[9,10] Due to the higher conversion percentages obtained when poly(styrene-*alt*-maleic anhydride) (P(St-*alt*-MAnh)) was reacted with primary amine moieties in the previous chapter, compared to poly(styrene-*co*-maleic anhydride) (P(St-*co*-MAnh)), as well as the higher degree of modification obtainable due to more maleic anhydride units available, it was decided to continue with P(St-*alt*-MAnh) as the parent polymer for modification before electrospinning.

The chemical groups chosen in this study for the modification of P(St-*alt*-MAnh) were selected based on possible chemical interactions with the *Mycobacterium tuberculosis* cell wall. All the modification agents had a primary amine group available for nucleophilic attack on the maleic anhydride unit, thus resulting in a ring-opening reaction of the 5-membered ring. The half amide generated upon reaction of the primary amine with the maleic anhydride group was stabilized by heat to yield the stable 5-membered cyclic imide.[9-11]

Here we report the synthesis, characterization and electrospinning of various modified poly(styrene-*alt*-maleimide) (P(St-*alt*-MI)) polymers. The general procedure entailed that P(St-*alt*-MAnh) was first modified with a variety of chemical compounds, then dissolved in a suitable solvent and electrospun into polymer nanofibers. The various modified P(St-*alt*-MI) (SMI) polymers were characterized using

^{1}H-NMR and ^{13}C-NMR spectroscopy and the electrospun functionalized SMI nanofibers were characterized using attenuated total reflectance Fourier transform infrared spectroscopy (ATR-FTIR) and scanning electron microscopy (SEM).

4.2 Synthesis of the functionalized SMI nanofibers

4.2.1 Modification of SMA

Poly(styrene-*alt*-maleic anhydride) (P(St-*alt*-MAnh)), synthesized using conventional radical copolymerization[12] to yield SMA (M_n = 128 000 g/mol, $Đ$ = 2.7, MAnh content: 50%) (refer Fig. 4.1), was modified via the nucleophilic addition reaction of a primary N-alkylamine to the reactive maleic anhydride unit of SMA.

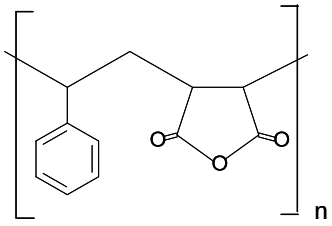

Figure 4.1 Repeating units of SMA.

The cyclic maleic anhydride underwent ring opening to form a secondary amide and carboxylic acid group, also known as maleamic acid.[9] Ring closure was achieved with the application of heat and corresponding loss of water. The ring-closed maleimide is more stable than the ring-opened compound and less susceptible to hydrolysis.[10,11,13] Refer Figure 4.2 for the schematic illustration of the modification of SMA via nucleophilic addition of a primary N-alkylamine to the reactive maleic anhydride group of SMA.

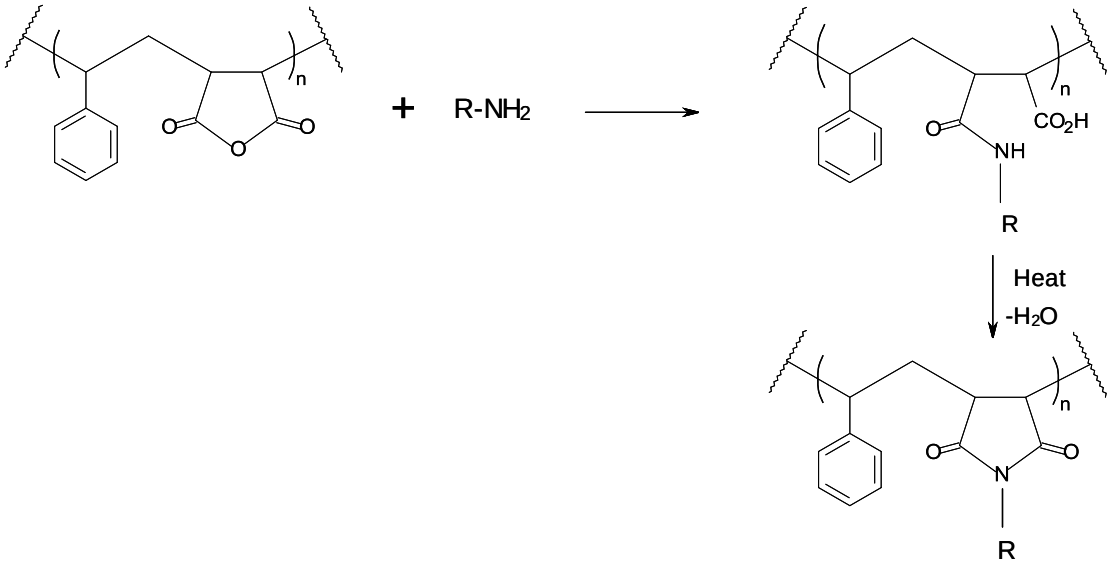

Figure 4.2 Schematic illustration of the modification of SMA via nucleophilic addition of primary N-alkylamines to the reactive maleic anhydride group.

P(St-*alt*-MAnh) was dissolved in dimethylformamide (DMF) and chemically reacted with a variety of primary N-alkylamines.[9] This ring-opening amidization reaction took place at room temperature and without a catalyst. A combination of commercially available and synthesized N-alkylamines were used for the modification reaction.

The ring-open N-alkyl modified SMA synthesized in this study was insoluble in DMF at room temperature and formed a white precipitate upon addition of the N-alkylamine to a solution of SMA in DMF. With an increase in temperature, the white precipitate started to dissolve at ~ 120 °C and the reaction mixture was subsequently refluxed at 170 °C for 1 hour to achieve ring closure to form the cyclic maleimide.[10,14] After precipitation of the modified SMI polymer in a suitable solvent, the polymer was washed and dried to remove any residual solvent or unreacted monomer. Some of the N-alkyl modified SMI polymers underwent an additional substitution reaction with suitable bromoalkane compounds[15] to yield SMI modified with an aliphatic quaternized ammonium moiety. These modified SMI polymers were subsequently dissolved in a suitable solvent and electrospun to yield functionalized polymer nanofibers.

The chemical structures of the modified SMI polymers prepared in this study using the method described are presented in Figure 4.3.

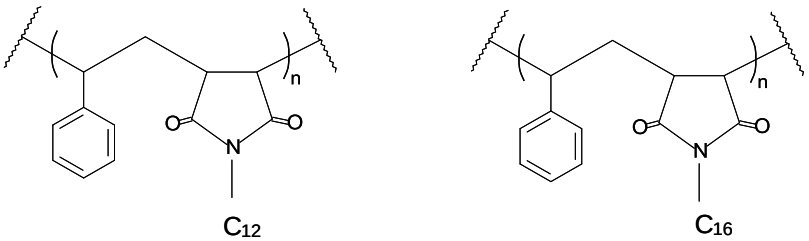

(a) SMI-C_{12} (b) SMI-C_{16}

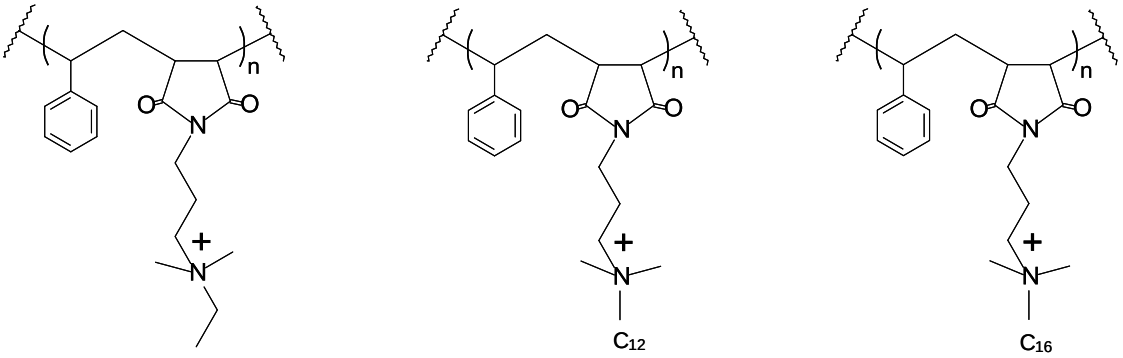

(c) SMI-qC_2 (d) SMI-qC_{12} (e) SMI-qC_{16}

Figure 4.3 Chemical structures of the modified SMI polymers.

a) Synthesis of SMI-C_{12} and SMI-C_{16}

The preparation of SMI-C_{12} (Fig. 4.3(a)) and SMI-C_{16} (Fig. 4.3(b)) entailed a straightforward ring-opening amidization reaction between the maleic anhydride unit of SMA and a C_{12} or C_{16} aliphatic primary amine compound at room temperature and without a catalyst to form the relevant maleamic acid. Ring closure of the half amide was subsequently achieved by applying heat, with the corresponding loss of water, to form the stable cyclic imide.[9,10,14]

b) Synthesis of SMI-qC_2, SMI-qC_{12} and SMI-qC_{16}

SMI-qC_2 (Fig. 4.3(c)), SMI-qC_{12} (Fig. 4.3(d)) and SMI-qC_{16} (Fig. 4.3(e)) were prepared via a precursor, namely styrene-[*N*-3-*(N',N'*-dimethylamino)propyl maleimide] copolymer (SMI-tC). This precursor was formed upon reaction of the maleic anhydride unit of P(St-*alt*-MAnh) with 3-(*N,N*-dimethylamino)-1-propylamine at room temperature and without a catalyst to form the ring-opened secondary amide and carboxylic acid, followed by heat-induced cyclization.[9,10] SMI-tC was subsequently reacted with suitable bromoalkane compounds in excess[15] which resulted in the quaternization of the tertiary amine moiety of SMI-tC to yield the relevant modified styrene-maleimide copolymers, ready for electrospinning into polymer nanofibers.

Refer Figure 4.4 for a schematic illustration of the modification of P(St-*alt*-MAnh) via the precursor to yield the relevant modified styrene-maleimide copolymers.

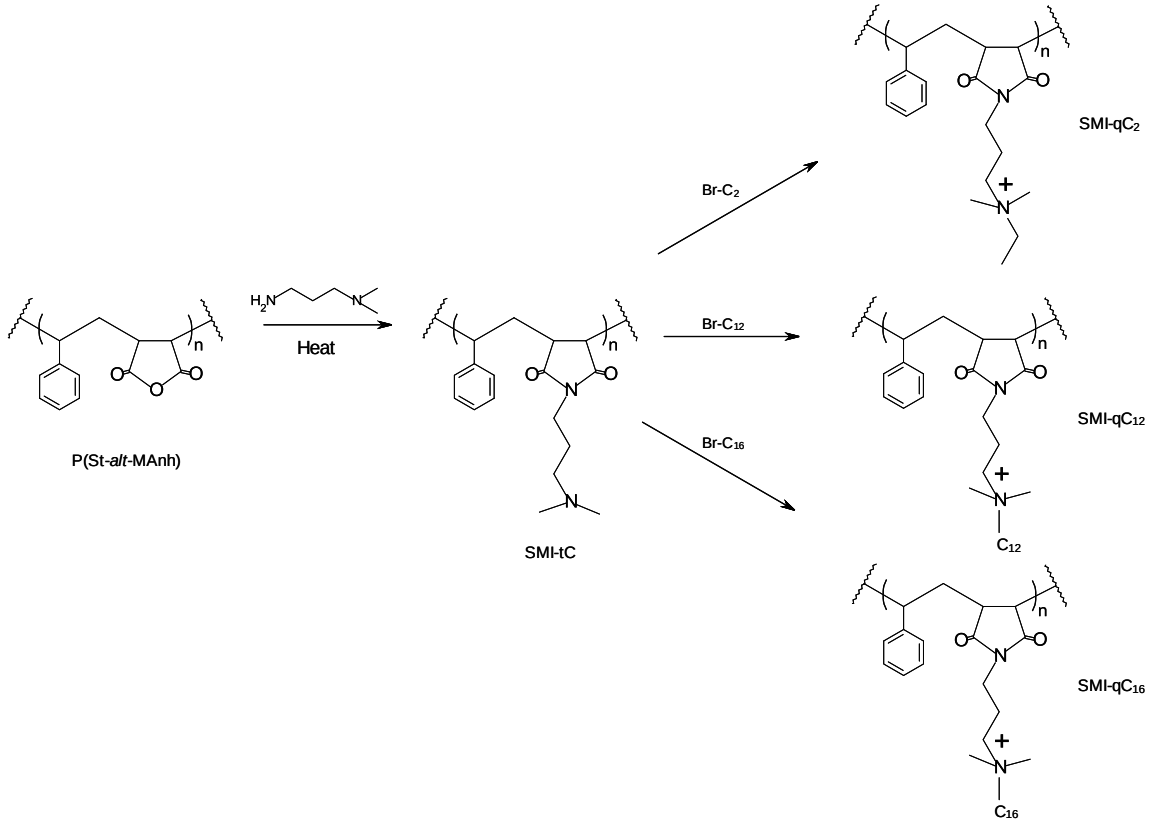

Figure 4.4 Schematic illustration of the modification of P(St-alt-MAnh) via a precursor (SMI-tC) to yield the relevant modified styrene-maleimide copolymers.

4.2.2 Electrospinning of modified SMI polymers

The modified SMI polymers were dissolved in a suitable solvent for electrospinning and electrospun at a polymer concentration that was sufficient for adequate polymer chain entanglements[16] to yield fibers with an average fiber diameter in the range of 520-755 nm. The fibers were dried under vacuum to remove any residual solvent. The choice of solvent or solvent combination is of great importance to the electrospinning process as the ideal solvent should have the proper balance between a variety of parameters, such as surface tension, vapour pressure and solution conductivity.[17,18] These parameters do not act or influence the electrospinning process individually. There is an interplay between them whereby changing the one parameter will have an effect on another parameter or parameters.[1] For a jet to form, the electrostatic repulsive force from the mutual charges induced by the electrode on the droplet surface of the polymer solution must overcome the surface tension of the polymer solution. The charge repulsion force will aim to expand the surface area of the droplet and the solution surface tension, which is a contractive force, will aim to reduce the surface area of the droplet. Only when the electrostatic repulsive force overcomes the solution surface tension does a

charged jet of polymer solution eject from the tip of the Taylor cone.[19] This charged jet undergoes whipping and stretching due to the electrostatic repulsive charges from the similar charged ions within the electrospinning jet, thus stretching the charged jet and decreasing the fiber diameter continuously until all solvent has evaporated, resulting in dry fibers landing on the collector.[20,21] Solution parameters therefore play a critical role in the electrospinning process and resultant fibers formed.[22-25]

For example, if the vapour pressure of the solvent is too high, the solvent will evaporate too quickly for proper stretching of the electrospinning jet to have taken place. Stretching of the jet will be stopped prematurely due to its solidification and fibers in the nanometer range may not be achieved. If the surface tension is too high, beaded fibers will be formed because the high surface tension will aim to reduce the surface area per unit, causing the jet to break up.[26] The choice of solvent or solvent combination also affects the solution conductivity and is a key parameter in the electrospinning process since the polymer solution jet is stretched from capillary to target due to the repulsion of mutual charges present on the surface of the jet, causing whipping and stretching. More charges can be carried at higher solution conductivity, resulting in more whipping and stretching taking place, thus yielding lower fiber diameters. A solution with zero conductivity cannot be electrospun as no charge can flow through the solution.[27,28] A solvent or solvent combination must therefore be chosen that will allow proper jets to form and be maintained and will allow proper fiber elongation during the electrospinning process.[3,19,23]

All the modified SMI polymers were dissolved in either DMF or a combination of DMF and another solvent, such as acetone, chloroform and methanol. Refer Table 4.1 for the solvents selected for electrospinning of the modified SMI polymers, as well as the electrospinning conditions used to obtain these polymer nanofibers.

Table 4.1 Solvents selected for electrospinning of the modified SMI polymers and electrospinning conditions used to obtain these polymer nanofibers

Polymer	Solvent	Concentration (wt %)	Electric field strength (kV)	Spinning distance (cm)	Flow rate (mL/min)
SMI-C_{12}	DMF	20	15	15	0.01
SMI-C_{16}	1:1 DMF:$CHCL_3$	20	15	15	0.015
SMI-qC_2	7:3 DMF:MeOH	30	15	15	0.015
SMI-qC_{12}	1:1 DMF:MeOH	25	15	15	0.0025
SMI-qC_{16}	1:1 DMF:MeOH	22	15	15	0.005

The advantage of DMF as electrospinning solvent is its slow rate of evaporation, resulting in thinner fibers due to ample whipping and stretching of the electrospinning jet. The use of DMF as solvent also prevented blockage of the needle tip during the electrospinning process. As DMF was not the best electrospinning solvent for all the modified SMI polymers, other solvents such as acetone, chloroform

and methanol were used in combination with DMF. As acetone, chloroform and methanol all have a low solvent vapour pressure, they will evaporate faster from the jet during the electrospinning process, thus possibly affecting the resultant fiber diameter. Although SEM analysis of the electrospun fibers indicated that there was a slight increase in the average fiber diameter with a decrease in the amount of DMF in the solvent mix, the increase was only marginal and fell within the standard deviation of the measured average fiber diameter. It was therefore not considered significant. The polymer solution concentration and flow rate also varied among the different modified SMI polymers, which could influence the fiber diameter of the electrospun polymer fibers as well.

All the modified SMI polymers electrospun smoothly, with the exception of SMI-qC_{16}, which spun with difficulty. This was not expected as the polymer carried a positive charge that should have aided the electrospinning process. A possible reason for the difficulty in electrospinning the SMI-qC_{16} solution may be the length of the aliphatic chain used for the quaternization of the precursor, SMI-tC, which changed the character of the modified polymer to such an extent that it became difficult to electrospin. This explanation is supported by work done in this study but not discussed in this thesis where another polymer was made when SMI-tC was successfully quaternized with 1-bromoeicosane (Br-C_{20}). This polymer was dissolved in a variety of solvents and at different concentrations and electrospinning attempted using different electrospinning parameters, but the polymer was not electrospinnable. Based on these results it may be concluded that if the aliphatic chain becomes too long and hydrophobic, the character of the polymer is modified sufficiently for electrospinning of the modified polymer to become difficult or impossible.

The electrospun N-alkyl functionalized SMI nanofibers, modified with the quaternary ammonium moiety, were soluble in water and required an additional heat treatment step to achieve crosslinking of the modified polymer chains. Whereas the functionalized SMI nanofibers were soluble in water before heat treatment, they became insoluble after heat treatment at 130 °C under vacuum for 24 hours. This was essential for the preservation of the functionalized SMI nanofibrous structure when immersed in water for prolonged periods. The mechanism by which crosslinking occurs has not yet been established.

4.3 Characterization of SMA and the modified SMI polymers

P(St-*alt*-MAnh) and the modified SMI polymers were characterized using ^{1}H-NMR and ^{13}C-NMR spectroscopy and the electrospun nanofibrous mats were characterized using ATR-FTIR and SEM. Interpretations of the NMR spectra were quite challenging in certain instances due to the presence of the amine, ammonium and imide nitrogen in the relevant modified styrene-maleimide copolymers and their influence on the chemical shifts of the carbons and protons attached to them. In chapter 3, section 3.3.2, a detailed description is given regarding the behaviour of hydrogens attached to the carbon adjacent to the nitrogen of the amine and ammonium group. The same also applies to

hydrogens attached to the carbon adjacent to the nitrogen of the imide group.[29] Quantitative analysis of the spectra of the copolymer products was also difficult in some instances due to the overlap of peaks in both ^{1}H and ^{13}C-NMR spectra.[30]

4.3.1 Characterization of P(St-*alt*-MAnh)

P(St-*alt*-MAnh) was synthesized using conventional radical copolymerization.[12]

(a) ^{1}H-NMR

Figure 4.5 shows the representative ^{1}H-NMR spectrum of P(St-*alt*-MAnh) and the assignments of the relevant peaks.

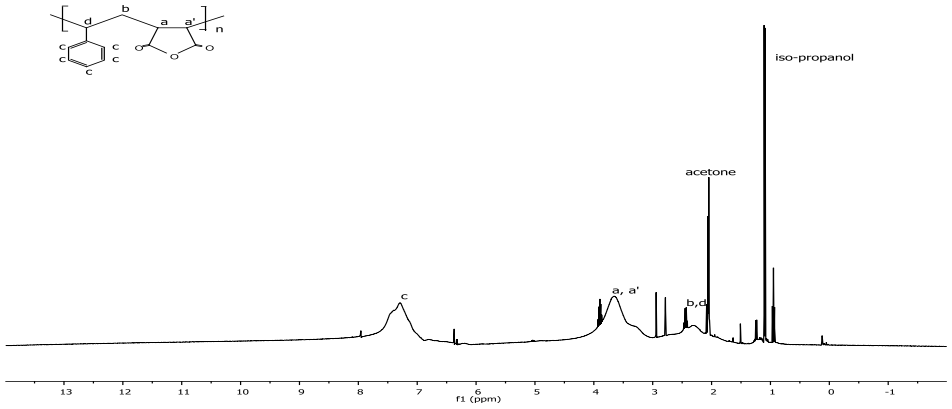

Figure 4.5 ^{1}H-NMR spectrum of P(St-alt-MAnh).

The ^{1}H-NMR spectrum of P(St-*alt*-MAnh) (Fig. 4.5) is characterized by a single broad peak in the chemical shift range of 6.9-7.7 ppm, corresponding to the aromatic ring protons of the styrene unit (c), while two broad and poorly resolved peaks at 3.66 ppm and 2.29 ppm belong to the methine and methylene protons of the maleic anhydride and styrene polymer backbone (a,a',b,d), respectively.[1] The methine hydrogens of the maleic anhydride unit are deshielded by the anisotropy of the adjacent carbonyl groups, whereas the methine hydrogen of the styrene unit is deshielded by the anisotropic field of the aromatic ring, but as the proton is removed by one carbon from the aromatic ring, the deshielding effect is smaller. The methine and methylene protons of the styrene unit therefore present as a single broad peak due to peak overlapping. These results are in good agreement with literature.[12]

The fraction of maleic anhydride in P(St-*alt*-MAnh) was calculated from the respective ^{1}H-NMR spectrum of P(St-*alt*-MAnh) (Fig. 4.5) since the resonance of the phenyl group of styrene is well

resolved from the others. The mole fraction of maleic anhydride was calculated from the integration ratio of the aromatic protons (5) of the styrene unit and the methine protons (2) of the maleic anhydride unit.[12,13,31] On the basis of the calculation, it was concluded that an alternating SMA with a maleic anhydride content of 50% was synthesized in this study.[12]

(b) ^{13}C-NMR

The results of the ^{1}H-NMR spectrum of P(St-*alt*-MAnh) were confirmed by the ^{13}C-NMR spectrum of P(St-*alt*-MAnh). Figure 4.6 shows the representative ^{13}C-NMR spectrum of P(St-*alt*-MAnh) and the assignments of the relevant peaks.

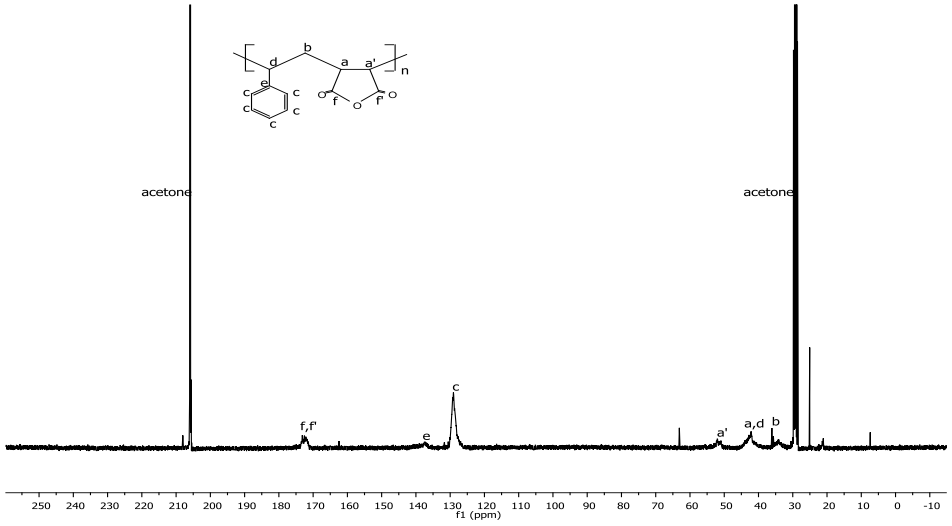

Figure 4.6 ^{13}C-NMR spectrum of P(St-alt-MAnh).

The ^{13}C-NMR spectrum of P(St-*alt*-MAnh) (Fig. 4.6) is characterized by a peak at 172 ppm, designated to the carbonyl carbons of the maleic anhydride unit (f,f'), peaks at 129 ppm and 137 ppm, corresponding to the aromatic ring carbons of the styrene unit (e,c) and peaks at 52 ppm, 42 ppm and 35 ppm, designated to the methylene and methine carbons of the SMA backbone (a,a',b,d). The ^{13}C-NMR spectrum of P(St-*alt*-MAnh) is in good agreement with literature.[10]

4.3.2 Characterization of SMI-C_{12} and SMI-C_{16}

P(St-*alt*-MAnh) was modified with dodecylamine (C_{12}-NH_2) and hexadecylamine (C_{16}-NH_2) in a straightforward ring-opening amidization reaction between the maleic anhydride unit of SMA and the primary amine group of the C_{12} and C_{16} aliphatic primary amine compound, followed by heat-induced cyclization to form the stable cyclic imide. Since the ^{1}H-NMR spectra of SMI-C_{12} and SMI-C_{16} are similar, with the exception of the integration intensity of the peak at ~ 1.26 ppm, corresponding to the

methylene protons of the aliphatic chain, only one ^{1}H-NMR spectrum will be discussed, namely that of SMI-C_{16}.

(a) ^{1}H-NMR

Figure 4.7 shows the representative ^{1}H-NMR spectrum of SMI-C_{16} and the assignments of the relevant peaks.

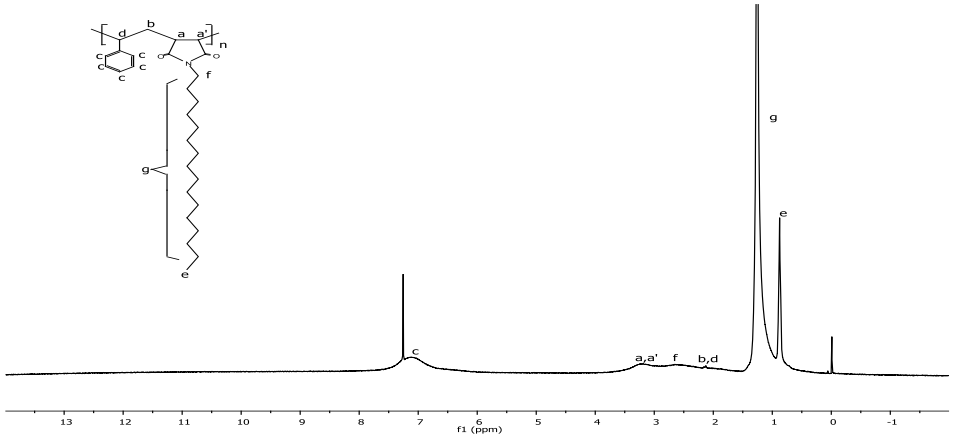

Figure 4.7 ^{1}H-NMR spectrum of SMI-C_{16}.

After the imidization of P(St-*alt*-MAnh) with hexadecylamine, three new peaks appeared in the ^{1}H-NMR spectrum of SMI-C_{16} at 0.87 ppm, 1.26 ppm and 2.95 ppm (refer Fig. 4.7), compared to that of SMA (Fig. 4.5). These new peaks correspond to the methyl protons of the C_{16} chain (e), the methylene protons of the C_{16} chain (g) and the methylene protons adjacent to the imide nitrogen (f), respectively.[15,32] These methylene protons (f) appear downfield from the other methylene protons (g) of the C_{16} chain due to the deshielding effect of the imide nitrogen.[1,32-34] The chemical shift of these methylene protons (f) correlate with those of a methylene group adjacent to an imide nitrogen, thus confirming the complete ring closure of the maleamic acid derivative formed upon the ring-opening amidization reaction.[11] The ^{1}H-NMR spectrum of SMI-C_{16} thus confirms the successful imidization of P(St-*alt*-MAnh) with hexadecylamine to yield styrene-[*N*-hexadecyl-maleimide] copolymer (SMI-C_{16}) (Fig. 4.3(b)).

The ^{1}H-NMR spectrum of SMI-C_{12} was similar to that of SMI-C_{16}, but differed in terms of the integration intensity of the peak at ~ 1.26 ppm. This is expected as the C_{16} chain has more methylene protons than the C_{12} chain.[15,32] The spectrum of SMI-C_{12} thus confirms the successful imidization of P(St-*alt*-MAnh) with dodecylamine to yield styrene-[*N*-dodecyl-maleimide] copolymer (SMI-C_{12}) (Fig. 4.3(a)).

(b) ^{13}C-NMR

The results of the ^{1}H-NMR spectrum of SMI-C_{16} were confirmed by the ^{13}C-NMR spectrum of SMI-C_{16}. Figure 4.8 shows the representative ^{13}C-NMR spectrum of SMI-C_{16} and the assignments of the relevant peaks.

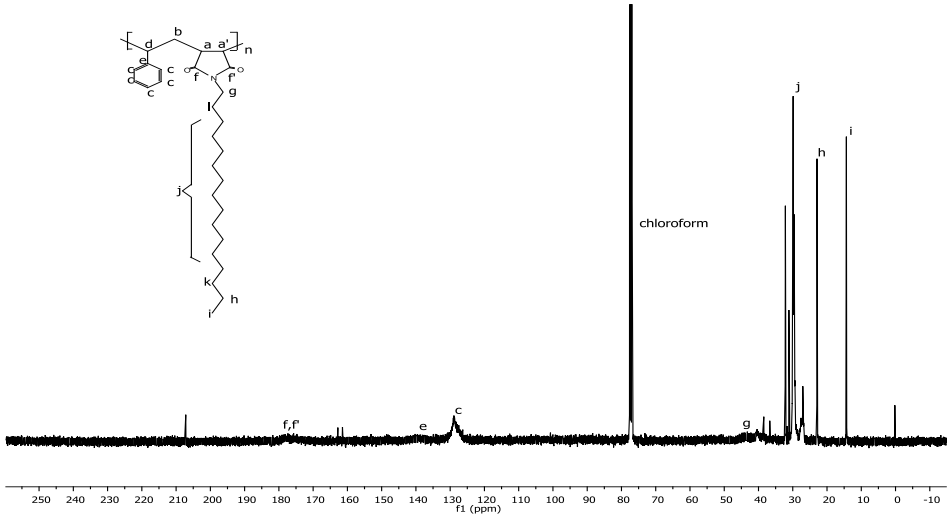

Figure 4.8 ^{13}C-NMR spectrum of SMI-C_{16}.

After the imidization of P(St-*alt*-MAnh) with hexadecylamine, the peak at 172 ppm, corresponding to the carbonyl carbons of the maleic anhydride unit of SMA, shifted downfield to 177 ppm (f,f'). This shift is consistent with the substitution of the maleic anhydride of SMA by the maleimide of the modified SMI polymer and confirms the successful imidization of SMA. The downfield shift of the imide carbonyl compared to the anhydride carbonyl is due to the larger electronegative character of the oxygen atom in the cyclic maleic anhydride ring.[10,11] The ^{13}C-NMR spectrum of SMI-C_{16} is further characterized by a peak at 29 ppm, indicative of the methylene carbons (j) of the C_{16} chain, a peak at 14 ppm, characteristic of the methyl carbon (i) of the C_{16} aliphatic chain and a peak at 38 ppm, attributed to the methylene carbon (g) adjacent to the imide nitrogen. This peak (g) appears downfield from the methylene carbon peak (j) due to the deshielding effect of the electronegative character of the imide nitrogen and serves as further confirmation that the imidization reaction of P(St-*alt*-MAnh) with hexadecylamine was successful to yield styrene-[*N*-hexadecyl-maleimide] copolymer (SMI-C_{16}) (Fig. 4.3(b)).[29]

The ^{13}C-NMR spectrum of SMI-C_{12} was similar to that of SMI-C_{16}. The ^{13}C-NMR spectrum of SMI-C_{12} thus confirms the successful imidization of P(St-*alt*-MAnh) with dodecylamine to yield styrene-[*N*-dodecyl-maleimide] copolymer (SMI-C_{12}) (Fig. 4.3(a)).

(c) ATR-FTIR

SMI-C_{12} and SMI-C_{16} were dissolved in a suitable solvent and electrospun into nanofiber mats. The nanofiber mats were dried at 60 °C under vacuum to remove any residual solvent and characterized using ATR-FTIR. Refer Figure 4.9 for the representative infrared (IR) spectra of (a) pristine P(St-*alt*-MAnh), (b) SMI-C_{12} and (c) SMI-C_{16}.

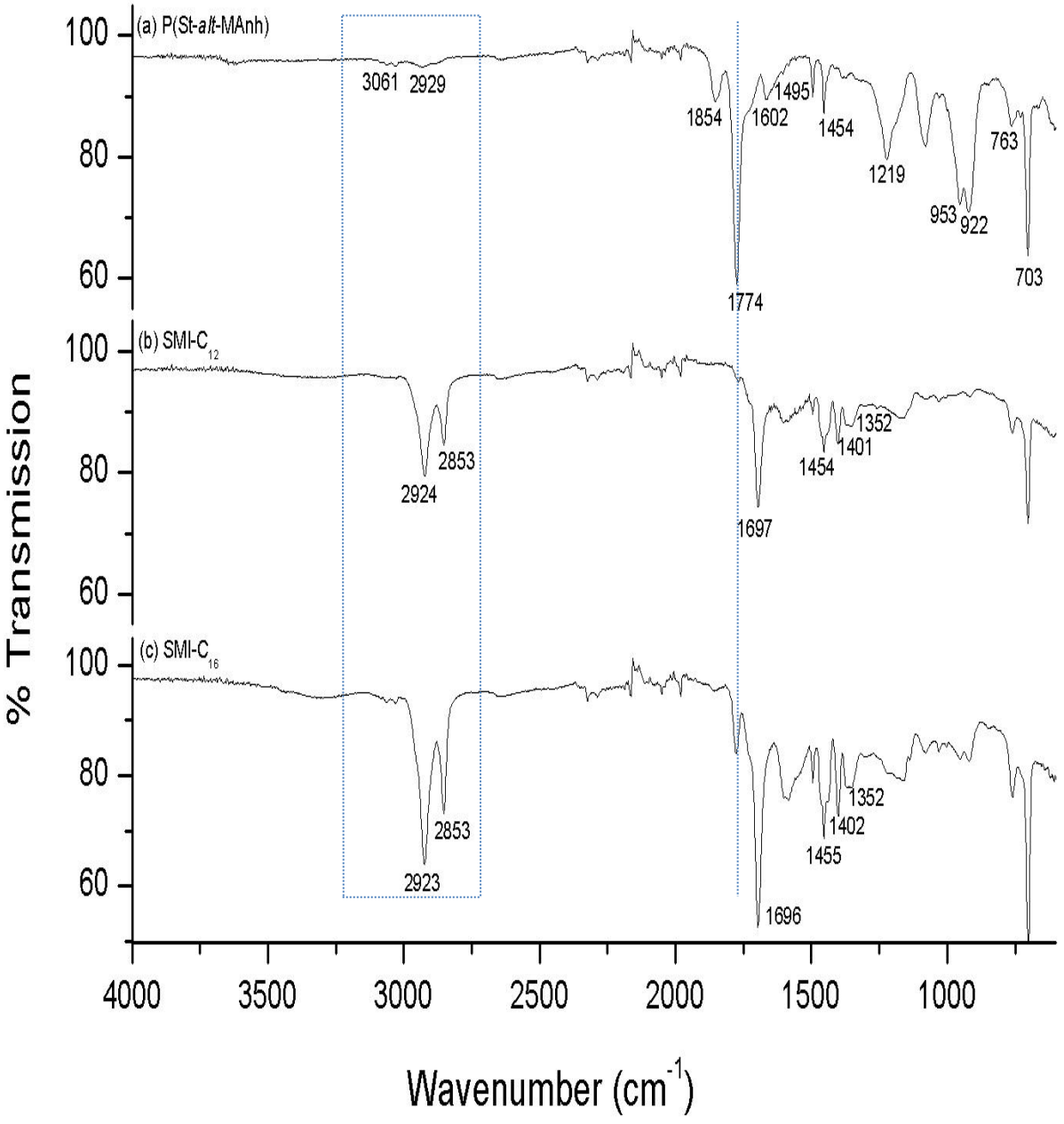

Figure 4.9 IR spectra of (a) pristine P(St-alt-MAnh), (b) SMI-C_{12} and (c) SMI-C_{16}.

The pair of bands of the carbonyls absorbing at 1774 cm^{-1} and 1854 cm^{-1} can be seen in Figure 4.9(a), corresponding to the symmetrical and asymmetrical carbonyl stretch vibrations of the anhydride moiety, as well as a characteristic band at 1219 cm^{-1} that corresponds to the C-O stretch vibrations of a five-membered cyclic anhydride. The peaks at 3061 cm^{-1} are due to the sp^2 aromatic

C-H stretch vibrations of the styrene group and the bands at 2929 cm^{-1} are due to the sp^3 aliphatic C-H stretch vibrations of the polymer chain. The peaks at 1602 cm^{-1} and 1494 cm^{-1} correspond to the C=C stretch vibrations of the styrene aromatic ring and the peak at 1453 cm^{-1} is characteristic of the C-H bending vibrations of the polymer chain. The peaks at 763 cm^{-1} and 703 cm^{-1} are characteristic of the C-H out-of-plane bending vibrations of a mono substituted aromatic ring of the styrene group. These results are in good agreement with literature.[1,6,10,35]

After the imidization of P(St-*alt*-MAnh) with dodecylamine, followed by heat-induced ring closure, the band at 1854 cm^{-1} disappeared and a small band at 1774 cm^{-1} is still visible, but a new strong peak appeared at 1697 cm^{-1}, indicative of the C-N stretch vibration of a cyclic imide bond (refer Fig 4.9(b)). The absence of an N-H bending absorption band of a secondary amide at ~ 1550 cm^{-1}, is further confirmation that ring closure was complete after the initial ring opening amidization reaction.[10,36,37] The presence of the aliphatic dodecyl chain is confirmed by new peaks at 2924 cm^{-1} and 2853 cm^{-1} that are indicative of the sp^3 C-H stretch vibration of a hydrocarbon chain. The high intensity is most probably due to the length of the C_{12}-chain. When comparing the spectrum of pristine P(St-*alt*-MAnh) (Fig. 4.9(a)) with that of the C_{12}-modified styrene-maleimide copolymer (Fig. 4.9(b)), a significant increase in the intensity of the peak at 1401 cm^{-1} is noticeable. This is due to an increase in the characteristic bending vibration of methylene groups as a result of the addition of the C_{12} moiety. A new peak at 1352 cm^{-1} is also visible in the spectrum of SMI-C_{12}, which is characteristic of the bending absorption of the methyl groups of the newly attached C_{12} chain. These results are in good agreement with literature.[35,38,39]

The IR spectrum of SMI-C_{16} (Fig. 4.9(c)) was similar to that of SMI-C_{12} (Fig. 4.9(b)), but differed in terms of the amount of primary N-alkylamines covalently attached to the maleic anhydride unit of the polymer, as indicated by the small peak at 1774 cm^{-1}. Dodecylamine and hexadecylamine modified P(St-*alt*-MAnh) with 96% and 87%, respectively. The conversion percentage was calculated using the ratio of the peak height of the styrene peak at 703 cm^{-1} and the anhydride carbonyl peak at 1774 cm^{-1}, before and after modification with the aliphatic primary amine, respectively.[11,37,40] A possible reason why the C_{12}-primary amine moiety gave a higher modification percentage than the C_{16}-primary amine moiety may be steric hindrance due to the longer aliphatic chain of the C_{16} compound, preventing more hexadecylamine compounds from reacting with SMA.

When comparing the spectrum of SMI-C_{12} (Fig. 4.9(b)) with that of SMI-C_{16} (Fig. 4.9(c)), a significant increase in the intensity of the peaks at 2924 cm^{-1} and 2853 cm^{-1} is noticeable. These peaks are characteristic of the sp^3 aliphatic C-H stretch vibrations of methylene groups and the increase in the peak intensities are due to the increased amount of CH_2-groups in the C_{16}-chain, compared to the C_{12}-chain. These results are in good agreement with literature.[2,35,38,39]

Comparison of the ATR-FTIR spectra of the C_{12} and C_{16} modified styrene-maleimide copolymers with that of pristine P(St-*alt*-MAnh) confirmed the successful imidization of SMA with dodecylamine and hexadecylamine to yield SMI-C_{12} (Fig. 4.3(a)) and SMI-C_{16} (Fig. 4.3(b)), respectively.

4.3.3 Characterization of SMI-qC$_2$, SMI-qC$_{12}$ and SMI-qC$_{16}$

The rest of the modified styrene-maleimide copolymers, namely SMI-qC$_2$ (Fig. 4.3(c)), SMI-qC$_{12}$ (Fig. 4.3(d)) and SMI-qC$_{16}$ (Fig. 4.3(e)) were synthesized via a precursor, SMI-tC (Fig. 4.4). The characterization of the precursor will be discussed first in section 4.3.3.1, followed by the characterization of the remaining modified styrene-maleimide copolymers, SMI-qC$_2$, SMI-qC$_{12}$ and SMI-qC$_{16}$ in section 4.3.3.2.

4.3.3.1 Characterization of SMI-tC

P(St-*alt*-MAnh) was modified with 3-(*N,N*-dimethylamino)-1-propylamine in a ring-opening amidization reaction, followed by heat-induced cyclization to yield the stable cyclic imide, SMI-tC.

(a) ^{1}H-NMR

Refer Figure 4.10 for the representative ^{1}H-NMR spectrum of SMI-tC and the assignments of the relevant peaks.

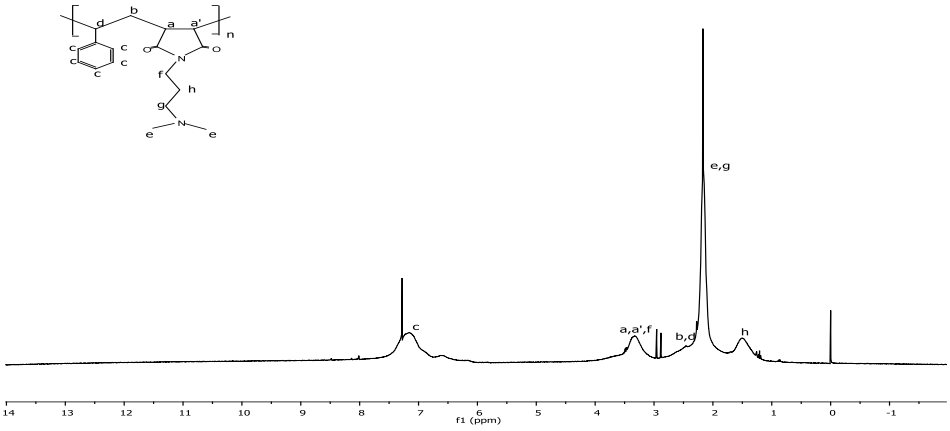

Figure 4.10 ^{1}H-NMR spectrum of SMI-tC.

The ^{1}H-NMR spectrum of SMI-tC (Fig. 4.10) is characterized by broad peaks at 6.7-7.5 ppm, 3.33 ppm and 2.28 ppm, corresponding to the aromatic ring protons of the styrene unit of SMA (c) and the methylene and methine protons of the SMA polymer backbone (a,a',b,d), as well as two new peaks at 2.17 ppm and 1.5 ppm. The broad peak at 1.5 ppm is characteristic of the methylene protons (h) of the propyl chain, whereas the peak at 2.17 ppm corresponds to the methyl protons (e) and methylene protons (g) adjacent to the tertiary amine.[15,32] These protons (g) appear downfield from the other methylene protons (h) due to the deshielding effect of the electronegative character of nitrogen of the

tertiary amine moiety. The methylene protons (f) adjacent to the imide nitrogen are also affected by the deshielding effect of the imide nitrogen resulting in the respective peak shifting downfield and overlapping with the peak of the methine protons of the maleic anhydride unit.[11,29]

The ^{1}H-NMR spectrum of SMI-tC thus confirms the successful imidization of P(St-*alt*-MAnh) with 3-(*N,N*-dimethylamino)-1-propylamine to yield styrene-[*N*-3-(*N',N'*-dimethylamino)propyl maleimide] copolymer (SMI-tC) (Fig. 4.4).

(b) ^{13}C-NMR

The results of the ^{1}H-NMR spectrum of SMI-tC were confirmed by the ^{13}C-NMR spectrum of SMI-tC. Figure 4.11 shows the representative ^{13}C-NMR spectrum of SMI-tC and the assignments of the relevant peaks.

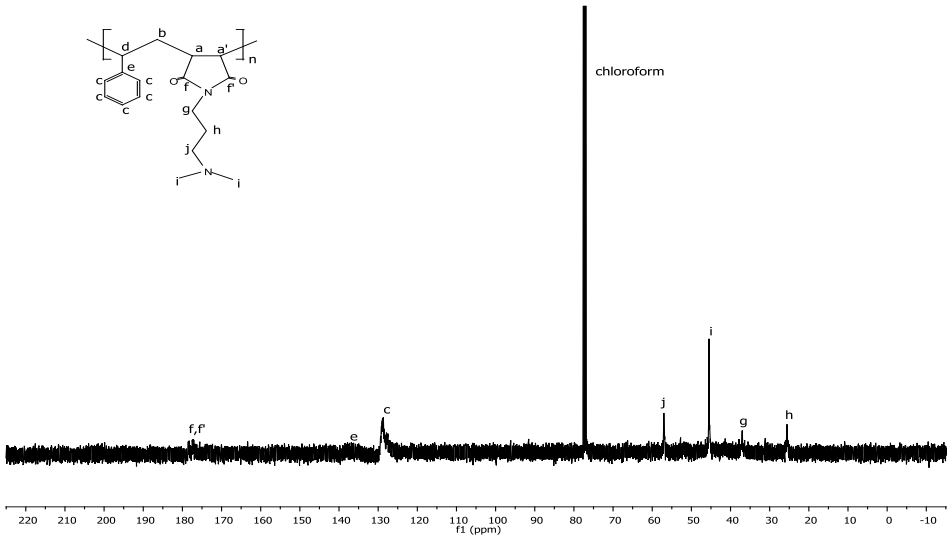

Figure 4.11 ^{13}C-NMR spectrum of SMI-tC.

The ^{13}C-NMR spectrum of SMI-tC (Fig. 4.11) is characterized by a peak at 177 ppm, indicative of the imide carbons (f, f'), a peak at 128 ppm, characteristic of the aromatic ring carbons of the styrene unit (c) and a peak at 37 ppm, attributed to the methylene carbon (g) adjacent to the imide nitrogen. The peaks at 177 ppm and 37 ppm serve as confirmation that an imidization reaction took place to substitute the maleic anhydride of SMA with a maleimide unit as discussed in section 4.3.2(b).[11] Further confirmation of the imidization reaction of P(St-*alt*-MAnh) with the primary N-alkylamine is provided by the peaks at 45 ppm and 57 ppm, corresponding to the methyl carbons (i) and methylene carbons (j) adjacent to the nitrogen of the tertiary amine, respectively, and the peak at 25 ppm, characteristic of the methylene carbon of an aliphatic chain (h). [32,34,39]

The ^{13}C-NMR spectrum of SMI-tC thus confirms the successful imidization of P(St-*alt*-MAnh) with 3-(*N,N*-dimethylamino)-1-propylamine to yield styrene-[*N*-3-(*N',N'*-dimethylamino)propyl maleimide] copolymer (SMI-tC) (Fig. 4.4).

4.3.3.2 Characterization of SMI-qC$_2$, SMI-qC$_{12}$ and SMI-qC$_{16}$

SMI-tC was subsequently reacted with suitable bromoalkane compounds in excess,[15] which resulted in the quaternization of the tertiary amine moiety of SMI-tC to yield the relevant modified styrene-maleimide copolymers, SMI-qC$_2$, SMI-qC$_{12}$ and SMI-qC$_{16}$. As the ^{1}H-NMR and ^{13}C-NMR spectra of these modified polymers were similar, they will be discussed as a group.

(a) ^{1}H-NMR

Refer Figure 4.12 for the representative ^{1}H-NMR spectra of (a) SMI-qC$_2$ and (b) SMI-qC$_{12}$ and the assignments of the relevant peaks. (Since the ^{1}H-NMR spectra of SMI-qC$_{12}$ and SMI-qC$_{16}$ are similar, with the exception of the integration intensity of the peak at ~ 1.22 ppm, corresponding to the methylene protons of the aliphatic chain, only one ^{1}H-NMR spectrum will be discussed, namely that of SMI-qC$_{12}$.)

(a)

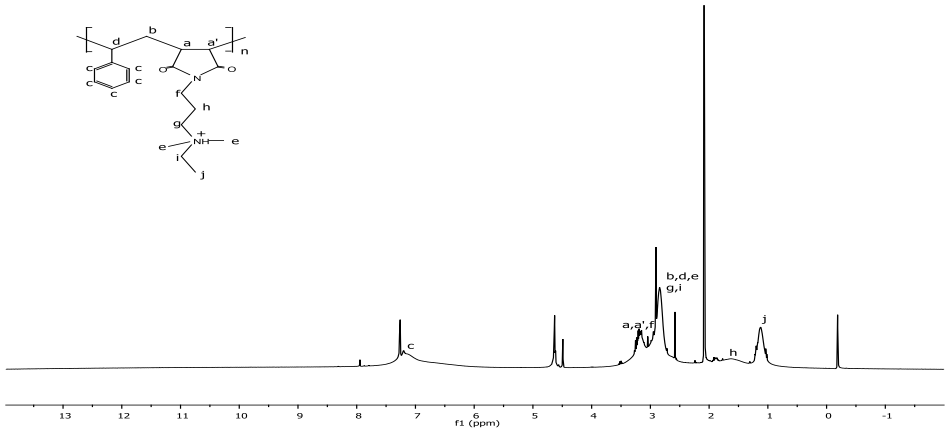

(b)

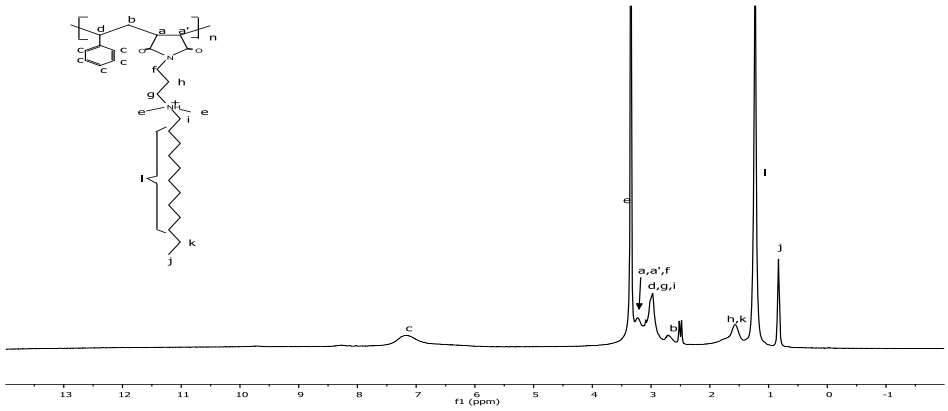

Figure 4.12 ^{1}H-NMR spectra of (a) SMI-qC$_2$ and (b) SMI-qC$_{12}$.

After quaternization of the tertiary amine moiety of SMI-tC with bromoethane, the peak at 2.17 ppm, corresponding to the methylene protons (g) and methyl protons (e) adjacent to the tertiary amine moiety of SMI-tC, shifted downfield to 2.8 ppm (refer Fig. 4.12(a)). As this chemical shift position is characteristic of methyl and methylene protons attached to an ammonium moiety,[15,32] this peak shift serves as confirmation that quaternization of SMI-tC did occur. Another confirmation that the quaternization reaction of SMI-tC with bromoethane was successful, is the presence of a new peak at 1.1 ppm, indicative of the methyl protons (j) of the ethyl side chain attached after the substitution reaction with bromoethane.[15,32]

The ^{1}H-NMR spectrum of SMI-qC_2 thus confirms the successful quaternization of styrene-[*N*-3-(*N',N'*-dimethylamino)propyl maleimide] copolymer (SMI-tC) with bromoethane to yield styrene-[*N-3*-(*N*'-ethyl-*N',N'*-dimethylammonium)propyl maleimide] copolymer (SMI-qC_2) (Fig. 4.3(c)).

SMI-tC was also quaternized with two long chain aliphatic bromoalkanes, namely 1-bromododecane (Br-C_{12}) and 1-bromohexadecane (Br-C_{16}). Only the ^{1}H-NMR spectrum of SMI-qC_{12} will be discussed. The ^{1}H-NMR spectrum of SMI-qC_{12} (Fig. 4.12(b)) is characterized by a peak at 3.34 ppm, corresponding to the methyl protons (e) adjacent to the quaternary ammonium moiety of SMI-qC_{12}, a peak at 0.83 ppm, attributed to the methyl protons (j) of the C_{12} aliphatic chain and a strong peak at 1.23 ppm, corresponding to the methylene protons (l) of the C_{12} aliphatic chain. These three peaks confirm the successful quaternization of styrene-[*N*-3-(*N',N'*-dimethylamino)propyl maleimide] copolymer (SMI-tC) with 1-bromododecane to yield styrene-[*N-3*-(*N*'-dodecyl-*N',N'*-dimethylammonium)propyl maleimide] copolymer (SMI-qC_{12}) (Fig. 4.3(d)).[15,32]

The ^{1}H-NMR spectrum of SMI-qC_{16} was similar to that of SMI-qC_{12}, but differed in terms of the integration intensity of the peak at ~ 1.23 ppm. This is expected as the C_{16} chain has more methylene protons than the C_{12} chain.[15,32] The spectrum of SMI-qC_{16} thus confirms the successful quaternization of styrene-[*N*-3-(*N',N'*-dimethylamino)propyl maleimide] copolymer (SMI-tC) with 1-bromohexadecane to yield styrene-[*N-3*-(*N*'-hexadecyl-*N',N'*-dimethylammonium)propyl maleimide] copolymer (SMI-qC_{16}) (Fig. 4.3(e)).

(b) ^{13}C-NMR

The results of the ^{1}H-NMR spectra were confirmed by the ^{13}C-NMR spectra of the relevant modified styrene-maleimide copolymers. Figure 4.13 shows the representative ^{13}C-NMR spectra of (a) SMI-qC_2 and (b) SMI-qC_{12}, and the assignments of the relevant peaks. (Since the ^{13}C-NMR spectrum of SMI-qC_{12} and SMI-qC_{16} is similar, only one ^{13}C-NMR spectrum will be discussed, namely that of SMI-qC_{12}.)

(a)

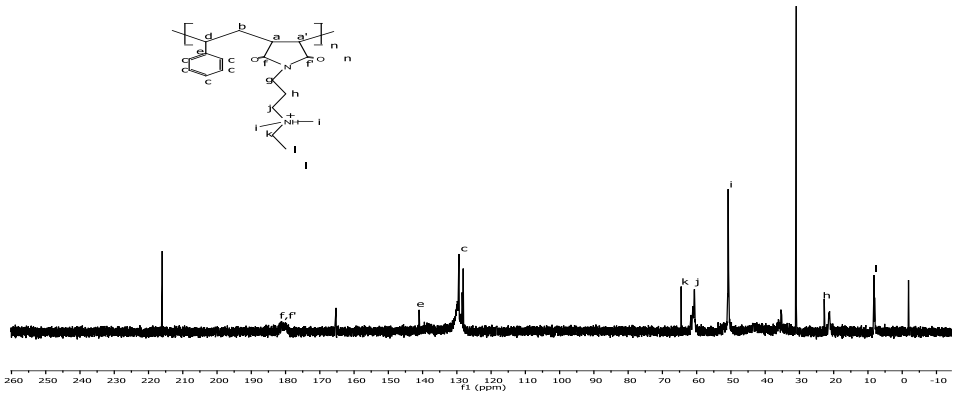

(b)

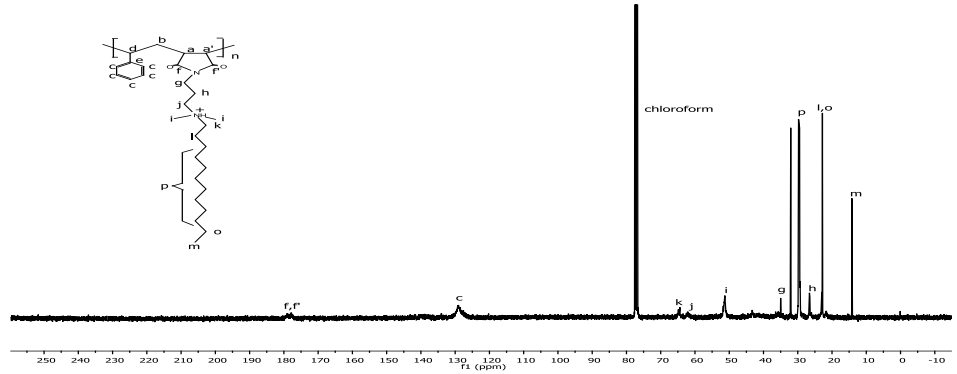

Figure 4.13 ^{13}C-NMR spectra of (a) SMI-qC$_2$ and (b) SMI-qC$_{12}$.

After quaternization of the tertiary amine moiety of SMI-tC with bromoethane, the peaks at 45 ppm and 57 ppm, corresponding to the methyl carbons (i) and methylene carbon (j) adjacent to the nitrogen of the tertiary amine moiety of SMI-tC, shifted downfield to 50 ppm and 64 ppm, respectively (Fig. 4.13(a)). As these chemical shift positions are characteristic of a methyl and methylene carbon adjacent to an ammonium moiety,[34,39,41] these peak shifts serve as confirmation that the quaternization of SMI-tC did occur. Another confirmation that the quaternization reaction of SMI-tC with bromoethane was successful is the presence of two new peaks at 60 ppm and 8 ppm, corresponding to the methylene carbon (k) of the ethyl chain attached to the ammonium nitrogen and the methyl carbon (l) of the same ethyl chain,[29] respectively.

The ^{13}C-NMR spectrum of SMI-qC$_2$ thus confirms the successful quaternization of styrene-[*N*-3-(*N',N'*-dimethylamino)propyl maleimide] copolymer (SMI-tC) with bromoethane to yield styrene-[*N-3*-(*N*'-ethyl-*N',N'*-dimethylammonium)propyl maleimide] copolymer (SMI-qC$_2$) (Fig. 4.3(c)).

SMI-tC was also quaternized with two long chain aliphatic bromoalkanes namely 1-bromododecane (Br-C$_{12}$) and 1-bromohexadecane (Br-C$_{16}$). Only the ^{13}C-NMR spectrum of SMI-qC$_{12}$ will be discussed. The ^{13}C-NMR spectrum of SMI-qC$_{12}$ (Fig. 4.13(b)) is similar to that of SMI-qC$_2$ (Fig. 4.13(a)), with the exception that there are additional peaks corresponding to the C$_{12}$ aliphatic chain of SMI-qC$_{12}$. The

most prominent of these additional peaks are the peaks at 29 ppm and 14 ppm, attributable to the methylene carbons (p) and the methyl carbon (m) of the C_{12} aliphatic chain. These peaks serve as confirmation that the quaternization of SMI-tC with 1-bromododecane was successful to yield styrene-[*N-3-*(*N*'-dodecyl-*N',N'*-dimethylammonium)propyl maleimide] copolymer (SMI-qC_{12}) (Fig. 4.3(d)).[29]

The ^{13}C-NMR spectrum of SMI-qC_{12} was similar to that of SMI-qC_{16}. The ^{13}C-NMR spectrum of SMI-qC_{16} thus confirms the successful quaternization of styrene-[*N*-3-(*N',N'*-dimethylamino)propyl maleimide] copolymer (SMI-tC) with 1-bromohexadecane to yield styrene-[*N-3-*(*N*'-hexadecyl-*N',N'*-dimethylammonium)propyl maleimide] copolymer (SMI-qC_{16}) (Fig. 4.3(e)).[29]

(c) ATR-FTIR

SMI-qC_2, SMI-qC_{12} and SMI-qC_{16} were dissolved in a suitable solvent and electrospun into nanofiber mats. The nanofiber mats were dried at 60 °C under vacuum to remove any residual solvent and characterized using ATR-FTIR. Refer Figure 4.14 for the representative IR spectra of (a) SMI-tC, (b) SMI-qC_2, (c) SMI-qC_{12} and (d) SMI-qC_{16}. The IR spectrum of the SMI-tC precursor is included in order to compare with the spectra of SMI-qC_2, SMI-qC_{12} and SMI-qC_{16}.

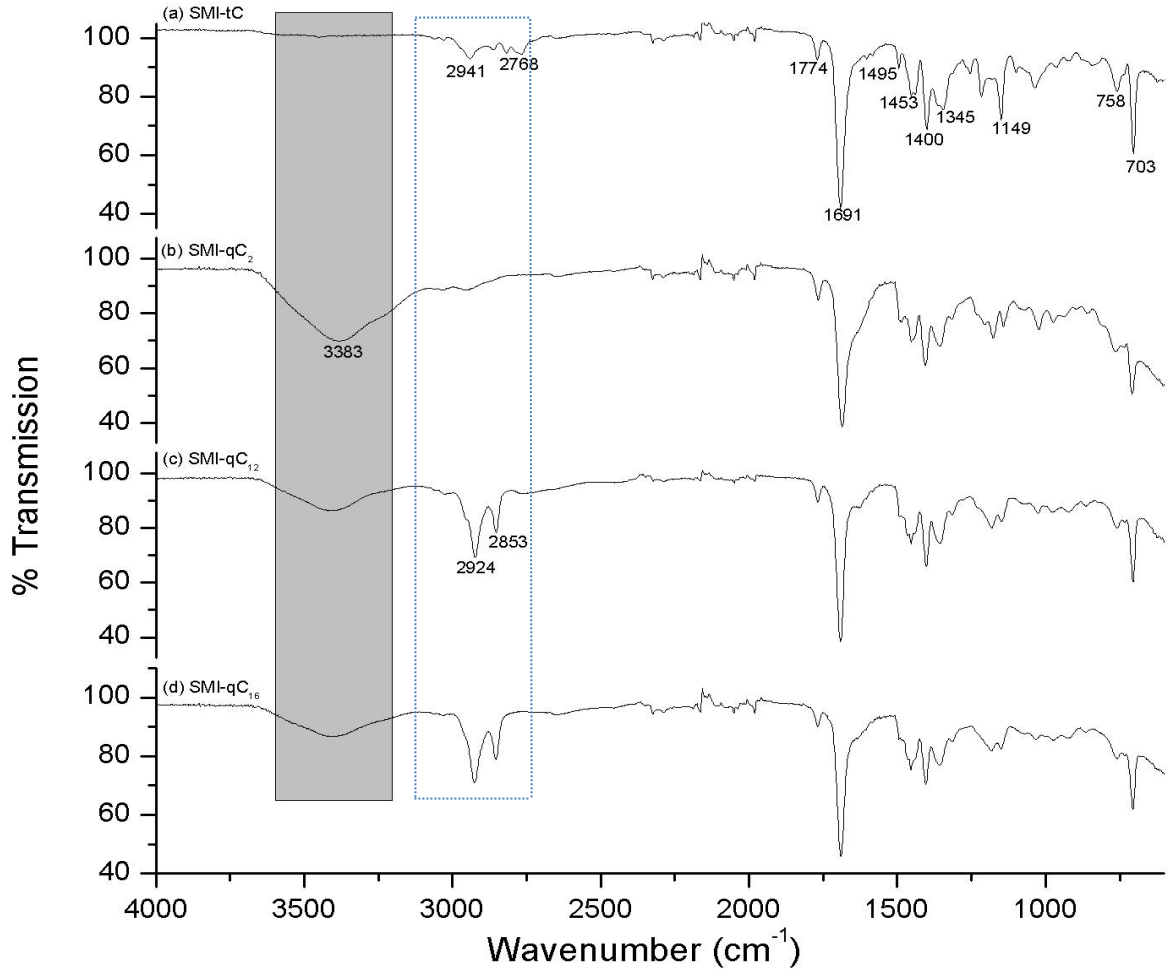

Figure 4.14 IR spectra of (a) SMI-tC, (b) SMI-qC_2, (c) SMI-qC_{12} and (d) SMI-qC_{16}.

When comparing the IR spectrum of the precursor, SMI-tC (Fig. 4.14(a)), with that of pristine P(St-*alt*-MAnh) (Fig. 4.9(a)), it is evident that the peak at 1854 cm^{-1} disappeared and only a small peak at 1774 cm^{-1} is still visible of the pair of bands of the anhydride units of SMA. A new strong band at 1691 cm^{-1} appeared, indicative of the cyclic imide bond that formed after the heat-induced ring closure of the maleamic acid that formed after the ring opening amidization reaction between the maleic anhydride unit of SMA and the aliphatic primary amine, 3-(*N,N*-dimethylamino)-1-propylamine. The absence of a band at ~ 1550 cm^{-1}, designated to the N-H bending absorption of a secondary amine, is further confirmation that ring closure was complete.[10,36,37]

3-(*N,N*-dimethylamino)-1-propylamine modified P(St-*alt*-MAnh) with 89% conversion. The conversion percentage was calculated using the ratio of the peak height of the styrene peak at 703 cm^{-1} and the anhydride carbonyl peak at 1774 cm^{-1}, before and after modification with the aliphatic primary amine, respectively.[11,37,40]

Comparison of the ATR-FTIR spectrum of the modified styrene-maleimide copolymer (SMI-tC) (Fig. 4.14(a)) with that of pristine P(St-*alt*-MAnh) (Fig. 4.9(a)) confirmed the successful imidization of SMA with 3-(*N,N*-dimethylamino)-1-propylamine to yield SMI-tC (Fig. 4.4).

When comparing the IR spectra of SMI-qC_2 (Fig. 4.14(b)), SMI-qC_{12} (Fig. 4.14(c)) and SMI-qC_{16} (Fig. 4.14(d)) with that of SMI-tC (Fig. 4.14(a)), a new peak at ~ 3400 cm^{-1} is evident and is indicative of quaternized ammonium nitrogens, as in the case of ammonium compounds.[2] The presence of this peak thus confirms the successful quaternization of the precursor, SMI-tC. As the degree of quaternization increases, the intensity of the peak at ~ 3400 cm^{-1} also increases.[2] As evident from the intensity of the peak at ~ 3400 cm^{-1}, the highest degree of quaternization is observed in SMI-qC_2 (Fig. 4.14(b)), followed by SMI-qC_{12} (Fig. 4.14(c)) and then SMI-qC_{16} (Fig. 4.14(d)). The degree of quaternization is thus decreasing with an increase in the aliphatic chain length of the bromoalkane compound. A possible reason for this trend may be that steric hindrance from the hydrocarbon chain of the bromoalkane compound is preventing more 1-bromohexadecane (Br-C_{16}) from reacting with SMI-tC than 1-bromododecane (Br-C_{12}). The same can be said for the decrease in the degree of quaternization from SMI-qC_{12} to SMI-qC_2.

When comparing the IR spectrum of the precursor with those of SMI-qC_{12} (Fig. 4.14(b)) and SMI-qC_{16} (Fig. 4.14(c)), the intensity of the peaks at ~ 2924 cm^{-1} and 2853 cm^{-1} increased after the substitution reaction of the precursor copolymer, SMI-tC, with the various bromoalkane compounds. These peaks at ~ 2924 cm^{-1} and 2853 cm^{-1} are indicative of the sp^3 C-H stretch vibrations of the C_{12} and C_{16} hydrocarbon chains of the SMI-qC_{12} and SMI-qC_{16} copolymers, respectively. These peaks are not as evident in the spectrum of SMI-qC_2, probably because the attached ethyl chain only has two additional methylene groups, which would not increase the intensity of the peaks at 2924 cm^{-1} and 2853 cm^{-1} significantly.

A significant increase in the intensity of the peak at 1400 cm^{-1} is also noticed in the spectra of SMI-qC_2 (Fig. 4.14(b)), SMI-qC_{12} (Fig. 4.14(c)) and SMI-qC_{16} (Fig. 4.14(d)). This is due to an increase in

the characteristic bending absorption of the methylene groups because of the addition of the C_2, C_{12} and C_{16} chains in SMI-qC_2, SMI-qC_{12} and SMI-qC_{16}, respectively.

A new peak at 1356 cm^{-1} is also visible in the spectra of SMI-qC_2 (Fig. 4.14(b)), SMI-qC_{12} (Fig. 4.14(c)) and SMI-qC_{16} (Fig. 4.14(d)). This peak is characteristic of the bending absorption of methyl groups, probably due to the presence of the C_2, C_{12} and C_{16} chains, respectively.[2,35,38,39]

Comparison of the ATR-FTIR spectra of the modified styrene-maleimide copolymers with that of the precursor (SMI-tC) (Fig. 4.14(a)) confirmed the successful quarternization of SMI-tC with the relevant bromoalkane compounds to yield SMI-qC_2 (Fig. 4.3(c)), SMI-qC_{12} (Fig. 4.3(d)) and SMI-qC_{16} (Fig. 4.3(e)).

The ^{1}H-NMR, ^{13}C-NMR and ATR-FTIR spectra of SMI-C_{12}, SMI-C_{16}, SMI-qC_2, SMI-qC_{12} and SMI-qC_{16} confirmed the successful synthesis of the relevant modified styrene-maleimide copolymers.

4.3.4 SEM

The modified SMI polymers were dissolved in a suitable solvent system for electrospinning and at a concentration that is sufficient for adequate polymer chain entanglements and electrospun into polymer nanofibers using varying flow rate conditions. The electric field strength and spinning distance were kept constant at 15 kV and 15 cm, respectively. Analysis of the SEM images with regard to fiber diameter indicated that nanofibers were obtained with an average fiber diameter in the range of 521-755 nm. Refer Table 4.2 for the average fiber diameters of the functionalized styrene-maleimide nanofibers.

Table 4.2 Average fiber diameters of the functionalized styrene-maleimide nanofibers

Modified SMI polymers	**Average fiber diameter (nm)**
SMI-C_{12}	549 ± 79
SMI-C_{16}	555 ± 111
SMI-qC_2	521 ± 90
SMI-qC_{12}	625 ± 90
SMI-qC_{16}	755 ± 429

It is clear from the data recorded in table 4.2 that the average fiber diameter and standard deviation of the different modified SMI polymers did not differ significantly, with the exception of SMI-qC_{16}. The average fiber diameter of SMI-qC_{16} was slightly larger when compared to the other modified SMI polymers, but the standard deviation was big. A possible explanation for this phenomenon is provided further below.

Further analysis of the SEM images with regard to fiber morphology indicated that smooth fibers with circular cross sections without any beads were obtained, with the exception of SMI-qC$_{16}$. The fibers spun from the solution of SMI-qC$_{16}$ had a combination of round fibers and fibers with a flat ribbon appearance. Refer Figure 4.15 for the representative SEM images of the functionalized styrene-maleimide fibers.

(a) (b)

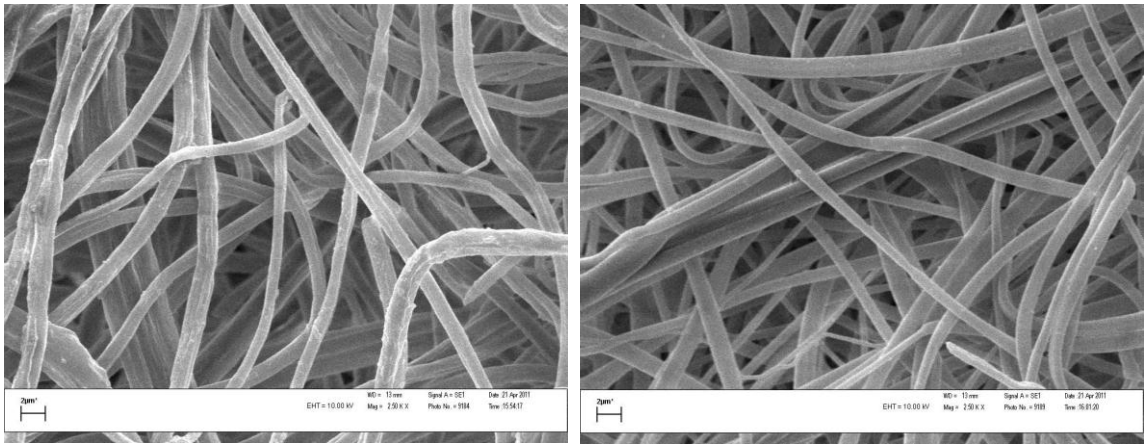

(c) (d)

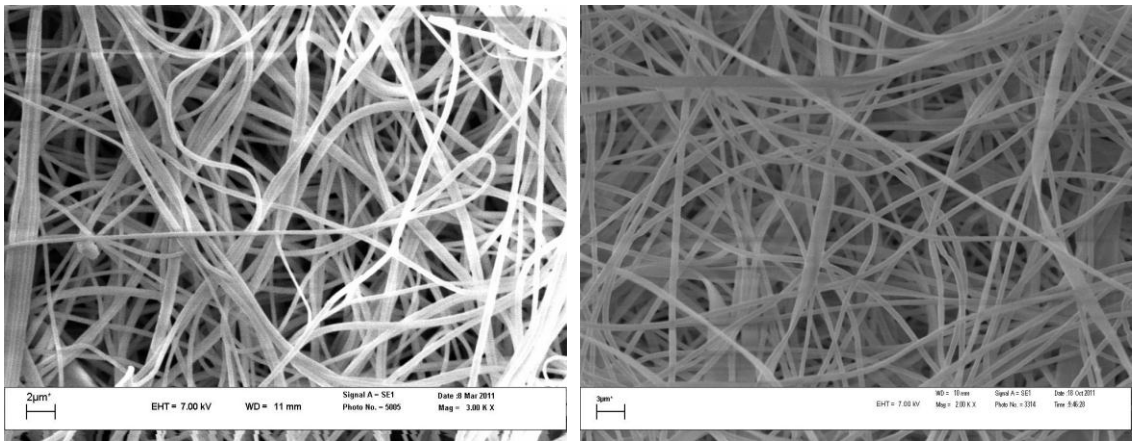

(e)

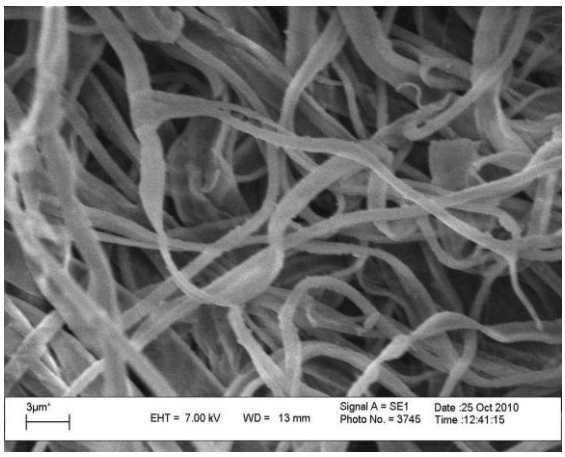

Figure 4.15 SEM images of (a) SMI-C$_{12}$, (b) SMI-C$_{16}$, (c) SMI-qC$_2$, (d) SMI-qC$_{12}$ and (e) SMI-qC$_{16}$.

The round fibers of SMI-C_{12} (Fig. 4.15(a)), SMI-C_{16} (Fig. 4.15(b)), SMI-qC_2 (Fig. 4.15(c)) and SMI-qC_{12} (Fig. 4.15(d)) are evident, compared to the flat ribbon fibers of SMI-qC_{16} (Fig. 4.15(e)). A detailed study by Koombhongse[42] concluded that flat ribbon fibers are formed when a polymer skin is formed on the outside of the electrospinning jet due to rapid solvent evaporation. A tube is formed by the outside polymer skin with residual solvent still on the inside. As this remaining solvent diffuses through the skin in order to evaporate, atmospheric pressure collapses the empty tube. The collapsing tube becomes elongated and then flat, forming a ribbon with a cross-sectional diameter slightly wider than the diameter of the jet, thus the reason for the slightly larger fibers formed. Sometimes small tubes formed at each edge of the flat ribbon and a web made from the polymer skin connects the two tubes. The ribbons also have a tendency to bend in a regular way as a result of the electrically driven bending instability.[42] Refer Figure 4.16 for a schematic illustration of the formation of flat ribbon fibers.

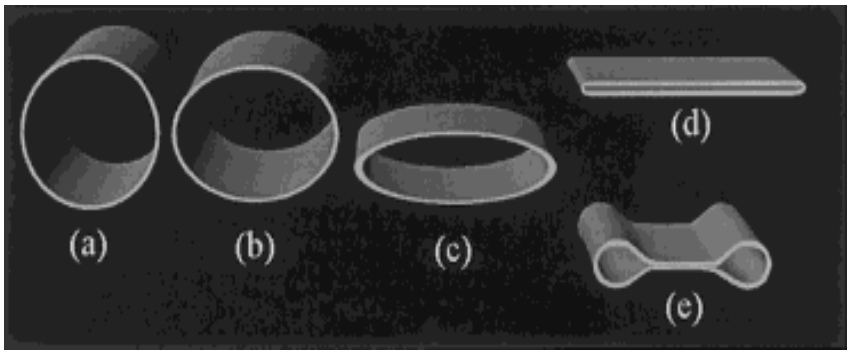

Figure 4.16 Schematic illustration of the collapse of the skin on a jet. This can happen two ways to yield fiber (d) or fiber (e).[42]

The formation of skins on polymer fibers spun from polymer solutions is a well-known phenomenon that has also been observed during the manufacture of textile fibers from viscose and other polymers.[43,44]

Based on Koombhongse's study, the flat ribbon fibers of SMI-qC_{16} are therefore possibly formed because of the rapid evaporation of methanol, leading to the formation of a skin on the electrospinning jet, whilst the remaining solvent, DMF, escaped by diffusion through the skin and evaporated. This "empty" tube formed by the skin collapsed due to atmospheric pressure, thus forming flat ribbon fibers. The disadvantage of flat ribbon fibers is that fibers are formed with a larger fiber diameter compared to fibers with a round cross section. Although only some fibers were flat ribbons, their larger fiber diameter influenced the average fiber diameter and standard deviation significantly, as indicated by the measured average fiber diameter and standard deviation of the fibers spun from the solution of SMI-qC_{16}.

4.4 Conclusion

P(St-*alt*-MAnh), synthesized using conventional radical copolymerization, was successfully modified with a variety of modification agents via nucleophilic acyl substitution. These modification agents were very reactive towards the maleic anhydride unit of SMA and included a variety of primary N-alkylamine compounds. All the modified SMI polymers were heat treated to achieve ring closure of the secondary amide formed upon reaction of the modification agent with the maleic anhydride unit of SMA to form a stable cyclic imide. Some of the N-alkyl substituted maleimide copolymers underwent an additional substitution reaction with suitable bromoalkane compounds to yield SMI modified with an aliphatic quaternary ammonium moiety.

These modified SMI polymers were dissolved in a suitable solvent and electrospun at a polymer concentration that was sufficient for adequate polymer chain entanglements to yield functionalized polymer nanofibrous mats with average fiber diameters in the region of 580 nm, with the exception of SMI-qC_{16} that spun with difficulty and formed flat ribbon fibers with an average fiber diameter of 755 ± 429 nm. The electrospun N-alkyl functionalized SMI nanofibers, modified with the quaternary ammonium moiety, underwent an additional heat treatment step at 130 °C under vacuum to achieve crosslinking of the functionalized polymer chains. This additional heat treatment step rendered the relevant functionalized SMI nanofibers insoluble in water, a necessity for the preservation of the nanofibrous structure when exposed to water for extended periods.

The successful modification of P(St-*alt*-MAnh) was confirmed with ^{1}H-NMR and ^{13}C-NMR spectroscopy and the electrospun nanofibrous mats were characterized using ATR-FTIR and SEM.

The work discussed in this chapter thus confirms that a polymer can be successfully modified with a variety of modification agents by combining a polymer with a reactive site and a modification agent with a suitable reactive group and electrospun into functionalized polymer nanofibers.

4.5 Experimental

4.5.1 Chemicals

Acetone (Protea Chemicals), styrene 99.5% (Fluka Chemika), maleic anhydride 99% (Acros organics), methyl ethyl ketone 99.7% (Sigma-Aldrich), iso-propanol (Kimix), n-hexane (Kimix), chloroform (Kimix), acetonitrile (Sigma), tetrahydrofuran (Kimix), pentane (Kimix), 1-bromododecane 97% (Aldrich), 1-bromohexadecane 97% (Aldrich), dodecylamine 99% (Aldrich), hexadecylamine 98%

(Aldrich), 3-(*N,N*-dimethylamino)-1-propylamine 99% (Aldrich), bromoethane 99% (Merck) and diethyl ether (Kimix) were used without further purification. 2,2' Azobis(isobutyronitrile) (AIBN) (Riedel de Haen) was recrystallized twice from methanol and dried under vacuum before use. *N,N*-dimethylformamide 97% (Fluka) and methanol (Sasol) were distilled and kept on 4 Å molecular sieve before use.

4.5.2 Characterization techniques

a) Nuclear magnetic resonance spectroscopy (NMR)

^{1}H-NMR and ^{13}C-NMR spectra were obtained using a Varian VXR 400 MHz instrument equipped with a Varian magnet (7.0 T). Depending on the solubility of the synthesized compounds, deuterated chloroform ($CDCL_3$) and deuterated acetone (acetone-d_6) were used as solvents. All chemical shifts are reported in ppm downfield from tetramethylsilane (TMS), used as an internal standard (δ= 0 ppm).

b) Attenuated total reflectance Fourier transform infrared (ATR-FTIR) spectroscopy

Infrared spectra were recorded using a Nicolet FTIR spectrometer (model Nexus) from Thermo-Fischer equipped with a Smart Golden Gate ATR accessory with a diamond/ZnSe internal reflection crystal. The spectra were recorded from 4000 cm^{-1} to 600 cm^{-1} with a spectral resolution of 4 cm^{-1} and were the sum of 64 individual scans. No sample preparation was necessary and samples were in solid state. Omnic software was used for data acquisition and processing.

Conversion Calculation: The calculation of the conversion percentage when SMA was modified with a primary N-alkylamine to yield the corresponding modified SMI was done as follows. The mode of each relevant IR spectrum was changed from transmission to absorbance and the baseline was corrected. The absorbance band from the aromatic styrene unit at 703 cm^{-1} was used as internal standard as the styrene group did not partake in the modification reaction and was deemed a constant. The absorbance band from the carbonyl group of the anhydride unit at 1774 cm^{-1} was used to determine the extent of the modification reaction as the anhydride unit reacted with the primary amine of the N-alkylamine to form an imide, thus giving rise to a new band at ~ 1700 cm^{-1} with a corresponding decrease in the peak at 1774 cm^{-1}.

The heights of the styrene peak at 703 cm^{-1} and the carbonyl peak at 1774 cm^{-1} were taken, before and after modification, as measure of the fraction of carbonyls converted to imides by calculating the decrease in the height of the carbonyl peak of the modified SMI in relation to that of SMA where the styrene peak at 703 cm^{-1} is constant.[11,37,40]

c) Scanning electron microscopy (SEM)

Images of the functionalized SMI fibers were obtained using a Leo® 1430VP Scanning Electron Microscope (SEM). The sample fibers were cut into approximately 1 cm x 1 cm squares and attached onto the SEM stub with double-sided carbon tape. The SEM stubs were then sputter coated with gold under vacuum prior to imaging. The images were analyzed using an imaging analysis program, SEM Image Studio, to obtain data regarding fiber diameters. An average of 100 fiber diameters was measured per sample. The average fiber diameter and the standard deviation were calculated using Microsoft Excel 2010.

d) Size exclusion chromatography (SEC)

Molar mass and dispersity (*Đ*) were obtained using size exclusion chromatography (SEC). Size exclusion chromatography (SEC) analysis was carried out on a DMAc solvent system using a flow rate of 1.0 mL/min. The instrument setup consisted of a Shimadzu LC-10AD pump, a Waters 717Plus autosampler, a column system fitted with a 50x8 mm guard column in series with three 300x8 mm, 10 µm particle size GRAM columns (2 x 3000Å and 100Å) obtained from PSS, a Waters 2487 dual wavelength UV detector and a Waters 410 differential refractive index (DRI) detector all in series. 100 µL injection volumes are sampled individually with the oven temperature of the column and DRI detector kept at 40 °C. The solvent was stabilized with 0.05% BHT (*w/v*) and 0.03% LiCl (*w/v*), and samples were filtered through a 0.45 µm GHP filter to prevent any impurities entering the system. Calibration was done using PMMA standards (Polymer Laboratories) ranging from 690 to 1.2 x 10^6 g/mol. Data acquisition was done using Millennium software, version 4.

4.5.3 Synthesis of poly(styrene-*alt*-maleic anhydride) (P(St-*alt*-MAnh))

Conventional radical copolymerization was used to synthesize an alternating copolymer of styrene and maleic anhydride in a 1:1 molar ratio styrene:maleic anhydride.[12]

Maleic anhydride (MAnh) (14 g, 0.14 mol), styrene monomer (15 g, 0.14 mol) and 2,2' azobis(isobutyronitrile) (AIBN, 0.1182 g, $7.20*10^{-4}$ mol) were dissolved in 200 mL methyl ethyl ketone (MEK). The reaction mixture was degassed with N_2 for 30 minutes and stirred overnight (16 hours) at 60 °C. The reaction mixture was cooled to room temperature, precipitated in 500 mL iso-propanol and washed with n-hexane. The polymer was dried under vacuum at room temperature to remove any unreacted monomer and residual solvent and then analyzed using SEC. M_n = 128 000 g/mol, *Đ* =2.7

Major IR absorptions: 3061, 2929, 1854, 1774, 1602, 1495, 1454, 1219, 1079, 953, 922, 763, 703 cm^{-1}.

^{1}H-NMR (acetone-d_6): δ (ppm) = 6.9-7.7 (s broad, 5H aromatic), 3.66 (s broad, 2H, C**H**-C**H**-), 2.29 (s broad, 3H, -C**H$_2$**-C**H**-)

^{13}C-NMR (acetone-d_6): δ (ppm) = 172.55 (-O-**C**=O), 137.61 (aromatic -**C**-), 129.05 (aromatic -**C**-), 52.04 (-**C**H-), 42.13 (-**C**H-), 35.65 (-**C**H$_2$-)

4.5.4 Synthesis of styrene-[*N*-dodecyl-maleimide] copolymer (SMI-C_{12})

The synthetic work of Vermeesch and Evenson was used as basis for this procedure.[9,10]

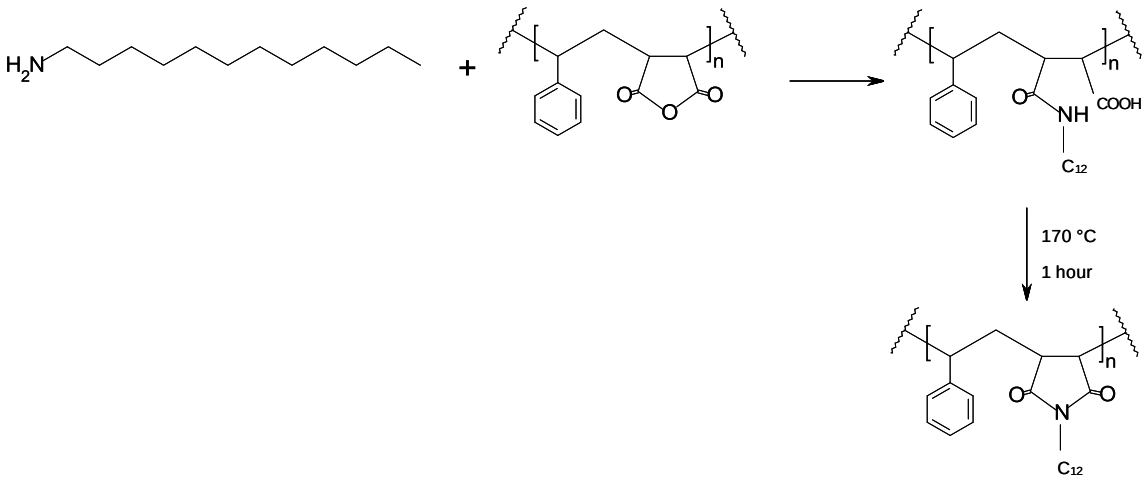

Scheme 4.1 Synthesis of styrene-[N-dodecyl-maleimide] copolymer.

Dodecylamine (3.66 g, 20 mmol) was dissolved in DMF and added dropwise to a solution of P(St-*alt*-MAnh) (2 g, 10 mmol) in 16 mL DMF at room temperature. The reaction was heated and refluxed at 170 °C for 1 hour whereafter the reaction was cooled, the polymer was precipitated in acetonitrile and filtered. The product was dried under vacuum at 60 °C for 24 hours to remove any residual solvent.

Major IR absorptions: 2924, 2853, 1697, 1584, 1495, 1454, 1401, 1352, 1159, 1079, 760, 702 cm^{-1}.

^{1}H-NMR ($CDCl_3$): δ (ppm) = 6.8-7.4 (s broad, 5H, aromatic), 3.29 (s broad, 2H, -C**H**-C**H**-), 3.21 (s broad, 2H, -$(CO)_2$N-C**H$_2$**-), 2.32 (s broad, 3H, -C**H$_2$**-C**H**-), 1.25 (s, 20H, -(C**H$_2$)$_{10}$**-), 0.88 (s, 3H, C**H$_3$**-CH_2-)

^{13}C-NMR ($CDCl_3$): δ (ppm) = 177.58 (-N-**C**=O), 138.13 (aromatic -**C**-), 128.93 (aromatic -**C**-), 50.59 (-**C**H-), 40.37 (-**C**H-), 38.45 ($(CO)_2$N-**C**H$_2$-), 36.75 (-**C**H-), 32.15 (-**C**H$_2$-), 31.14 (-**C**H$_2$-), 29.88 (-**C**H$_2$-), 27.07 (-**C**H$_2$-), 22.92 (-**C**H$_2$-CH_3), 14.35 (-CH_2-**C**H$_3$)

4.5.5 Synthesis of styrene-[*N*-hexadecyl-maleimide] copolymer (SMI-C_{16})

The same method was followed as 4.5.4 using hexadecylamine (4.8 g, 20 mmol).

Major IR absorptions: 2923, 2853, 1696, 1602, 1495, 1455, 1402, 1352, 1161, 1032, 760, 703 cm^{-1}.

^{1}H-NMR ($CDCl_3$): δ (ppm) = 6.8-7.5 (s broad, 5H, aromatic), 3.21 (s broad, 2H, -C**H**-), 2.95 (s broad, 2H, -$(CO)_2$N-C$\mathbf{H_2}$-), 2.28 (s broad, 3H, -C$\mathbf{H_2}$-C**H**-), 1.26 (s, 28H, -(C$\mathbf{H_2})_{14}$-), 0.87 (s, 3H, C$\mathbf{H_3}$-CH_2-)

^{13}C-NMR ($CDCl_3$): δ (ppm) = 177.62 (-N-**C**=O), 138.74 (aromatic -**C**-), 128.76 (aromatic -**C**-), 51.62 (-**C**H-), 40.36 (-**C**H-), 38.88 ($(CO)_2$N-**C**H_2-), 32.16 (-**C**H_2-), 29.60 (-**C**H_2-), 29.96 (**C**H_2-), 26.98 (-**C**H_2-), 22.92 (-**C**H_2-CH_3), 14.35 (-CH_2-**C**H_3)

4.5.6 Synthesis of styrene-[*N*-3-(*N*'-ethyl-*N',N'*-dimethylammonium)propyl maleimide] copolymer (SMI-qC_2)

(a) Synthesis of styrene-[*N*-3-(*N',N'*-dimethylamino)propyl maleimide] copolymer (SMI-tC)

The synthetic work of Vermeesch and Evenson was used as basis for this procedure.[9,10]

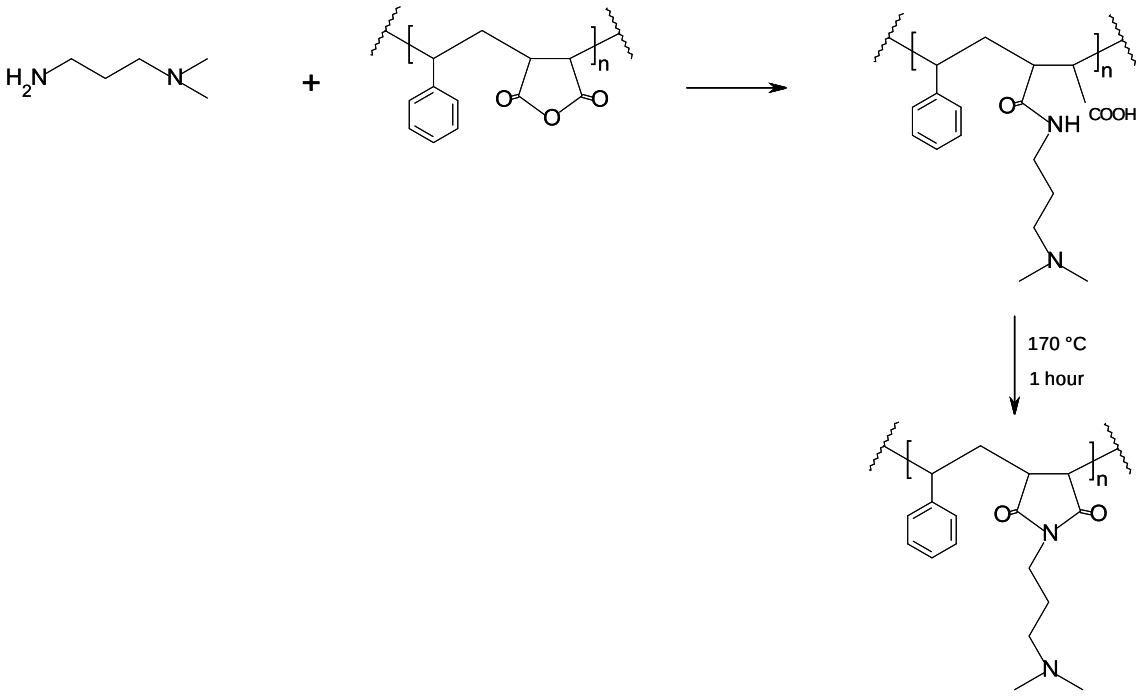

Scheme 4.2 Synthesis of styrene-[N-3-(N',N'-dimethylamino)propyl maleimide] copolymer.

3-(*N,N*-dimethylamino)-1-propylamine (3.3 g, 33 mmol) was added dropwise to a solution of P(St-*alt*-MAnh) (5 g, 25 mmol) in 25 mL DMF at room temperature. The reaction was heated and refluxed at 170 °C for 1 hour whereafter the reaction was cooled, the polymer was precipitated in diethyl ether and filtered. The product was dissolved in methanol/THF, precipitated into diethyl ether, filtered and dried under vacuum at 60 °C for 24 hours to remove any residual solvent.

Major IR absorptions: 2941, 2768, 1744, 1691, 1495, 1453, 1400, 1345, 1216, 1149, 1036, 758, 703 cm^{-1}.

^{1}H-NMR ($CDCl_3$): δ (ppm) = 6.7-7.5 (s broad, 5H, aromatic), 3.33 (s broad, 4H, -C**H**-C**H**-, -$(CO)_2$N-C$\mathbf{H_2}$-), 2.28 (s broad, 3H, -C**H**-C$\mathbf{H_2}$-), 2.17 (s, 8H, -N-C$\mathbf{H_2}$-, -N-C$\mathbf{H_3}$x2,), 1.5 (s, 2H, -CH_2-)

^{13}C-NMR ($CDCl_3$): δ (ppm) = 177.27 (-N-**C**=O), 136.87 (aromatic -**C**-), 128.67 (aromatic -**C**-), 57.03 (-N-**C**H_2-), 52.84 (-**C**H-), 45.50 (-N-**C**H_3), 37.88 ($(CO)_2$N-**C**H_2-), 37.09 (-**C**H-), 31.13 (-**C**H_2-), 25.38 (-**C**H_2-)

(b) Synthesis of styrene-[*N*-3-(*N*'-ethyl-*N',N'*-dimethylammonium)propyl maleimide] copolymer (SMI-qC_2)

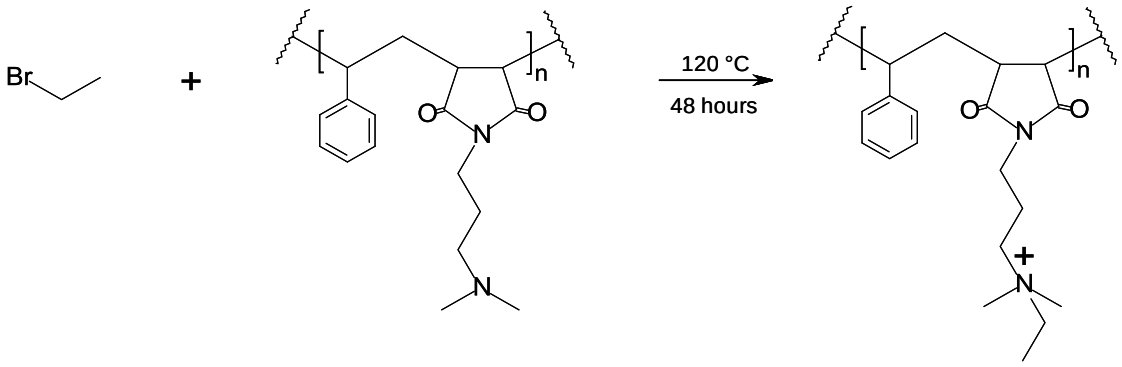

Scheme 4.3 Synthesis of styrene-[*N*-3-(*N*'-ethyl-*N',N'*-dimethylammonium)propyl maleimide] *copolymer.*

Bromoethane (0.73 g, 6.7 mmol) was added dropwise to a solution of styrene-[*N*-3-(*N',N'*-dimethylamino)propyl maleimide] copolymer (1.5 g, 5.3 mmol) in 12 mL DMF at room temperature. The reaction was heated to 120 °C for 48 hours[15] whereafter the reaction was cooled, the polymer was precipitated in acetone and filtered. The polymer was dried under vacuum at 60 °C for 24 hours to remove any residual solvent.

Major IR absorptions: 3383, 1686, 1495, 1453, 1405, 1356, 1177, 1022, 763, 708 cm^{-1}.

^{1}H-NMR ($CDCl_3$): δ (ppm) = 6.7-7.5 (s broad, 5H, aromatic), 3.21 (s broad, 4H, -C**H**-C**H**-, -$(CO)_2$N-C$\mathbf{H_2}$-), 2.84 (s broad, 13H, -N-C$\mathbf{H_3}$x2, -N-C$\mathbf{H_2}$-x2), 1.60 (s, 2H, -C$\mathbf{H_2}$-), 1.12 (s, 3H, C$\mathbf{H_3}$-CH_2-)

^{13}C-NMR ($CDCl_3$): δ (ppm) = 180.97 (-N-**C**=O), 141.01 (aromatic -**C**-), 128.45 (aromatic -**C**-), 64.52 (-N-**C**H_2-), 60.60 (-N-**C**H_2-), 50.80 (-N-**C**H_3), 42.38 (-**C**H-), 35.41 ($(CO)_2$N-**C**H_2-), 22.71 (-**C**H_2-), 8.23 (-**C**H_3)

4.5.7 Synthesis of styrene-[*N*-3-(*N*'-dodecyl-*N',N'*-dimethylammonium)propyl maleimide] copolymer (SMI-qC_{12})

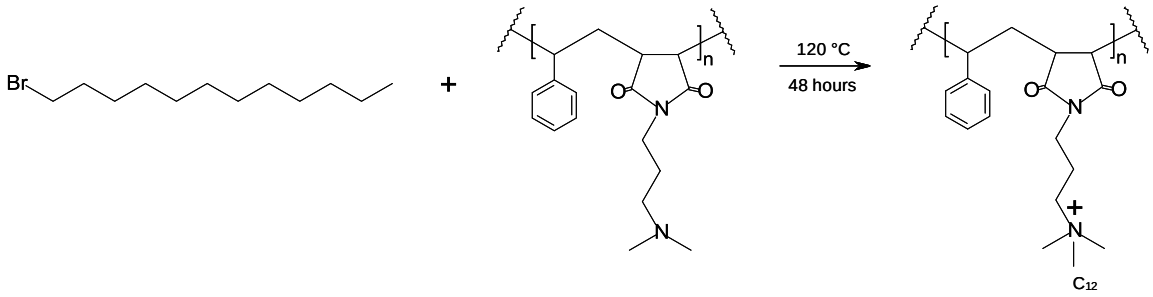

Scheme 4.4 Synthesis of styrene-[N-3-(N'-dodecyl-N',N'-dimethylammonium)propyl maleimide] copolymer.

1-Bromododecane (1.15 g, 4.6 mmol) was added dropwise to a solution of styrene-[*N*-3-(*N',N'*-dimethylamino)propyl maleimide] copolymer (1.0 g, 3.5 mmol) in 18 mL DMF at room temperature. The reaction was heated to 110 °C for 48 hours[15] whereafter the reaction was cooled, the polymer was precipitated in diethyl ether, filtered and washed thoroughly three times with pentane. The polymer was dried under vacuum at 60 °C for 24 hours to remove any residual solvent.

Major IR absorptions: 3419, 2924, 2853, 1692, 1454, 1402, 1356, 1182, 1025, 758, 705 cm^{-1}.

^{1}H-NMR ($CDCl_3$): δ (ppm) = 6.8-7.5 (s broad, 5H, aromatic), 3.34 (s, 6H, -N($C\mathbf{H_3}$)$_2$), 3.23 (s, 4H, -C**H**-C**H**-, -$(CO)_2$N-C$\mathbf{H_2}$-), 2.97 (s broad, 5H, -N-C$\mathbf{H_2}$-x2, -C**H**-), 2.71 (s, 2H, -C$\mathbf{H_2}$-), 1.57 (s, 4H, -C$\mathbf{H_2}$-x2), 1.23 (s, 18H, -($C\mathbf{H_2}$)$_9$-), 0.83 (s, 3H, C$\mathbf{H_3}$-CH_2-)

^{13}C-NMR ($CDCl_3$): δ (ppm) = 178.09 (-N-**C**=O), 138.98 (aromatic -**C**-), 129.10 (aromatic -**C**-), 64.39 (-N-**C**H_2-), 62.26 (-N-**C**H_2-), 51.28 (-N-**C**H_3), 45.99 (-**C**H-), 35.00 ($(CO)_2$N-**C**H_2-), 32.05 (-**C**H_2-), 29.77 (-**C**H_2-), 26.59 (-**C**H_2-), 22.99 (-**C**H_2-), 22.80 (-**C**H_2-), 14.20 (-**C**H_3)

4.5.8 Synthesis of styrene-[*N*-3-(*N*'-hexadecyl-*N',N'*-dimethylammonium)propyl maleimide] copolymer (SMI-qC_{16})

The same method was followed as 4.5.7 using 1-bromohexadecane (1.4 g, 4.6 mmol).

Major IR absorptions: 3400, 2926, 2854, 1690, 1455, 1404, 1356, 1183, 766, 706 cm^{-1}.

^{1}H-NMR ($CDCl_3$): δ (ppm) = 6.8-7.5 (s broad, 5H, aromatic), 3.34 (s, 6H, -N(C**H$_3$**)$_2$), 3.24 (s, 4H, -C**H**-C**H**-, -(CO)$_2$N-C**H$_2$**-), 2.98 (s broad, 5H, -N-C**H$_2$**-x2, -C**H**-), 2.70 (s, 2H, -C**H$_2$**-), 1.56 (s, 4H, -C**H$_2$**-x2), 1.21 (s, 16H, -(C**H$_2$**)$_{13}$-), 0.82 (s, 3H, C**H$_3$**-CH$_2$-)

^{13}C-NMR ($CDCl_3$): δ (ppm) = 178.61 (-N-**C**=O), 138.48 (aromatic -**C**-), 129.03 (aromatic -**C**-), 64.33 (-N-**C**H$_2$-), 63.18 (-N-**C**H$_2$-), 51.48 (-N-**C**H$_3$), 45.40 (-**C**H-), 36.70 ((CO)$_2$N-**C**H$_2$-), 32.13 (-**C**H$_2$-), 29.99 (-**C**H$_2$-), 26.60 (-**C**H$_2$-), 23.04 (-**C**H$_2$-), 22.89 (-**C**H$_2$-), 14.34 (-**C**H$_3$)

4.5.9 Electrospinning of styrene-[*N*-dodecyl-maleimide] copolymer (SMI-C_{12})

SMI-C_{12} was dissolved in DMF (20 wt. %). The prepared solution was placed in a 1 mL plastic syringe connected to a syringe pump (Harvard, Model 33 Twin Syringe Pump). An electrode lead of a high voltage power supply capable of generating positive DC voltages from 0 to 25 kV was connected to the blunt metal needle of the syringe. The positive charge was set at 7.5 kV. The flow rate was set at 0.01 mL/min and the needle diameter was 21 gauge. A stationary foil covered collector was placed 15 cm from the needle tip and connected to a negative electrode. The negative charge was set at 7.5 kV. The collected electrospun fibers were placed under vacuum at 60 °C to remove any residual solvents.

4.5.10 Electrospinning of styrene-[*N*-hexadecyl-maleimide] copolymer (SMI-C_{16})

The same method was followed as 4.5.9, using 1:1 chloroform: DMF as solvent and a flow rate of 0.015 mL/min.

4.5.11 Electrospinning of styrene-[*N*-3-(*N'*-ethyl-*N',N'*-dimethyl ammonium)propyl maleimide] copolymer (SMI-qC_2)

The same method was followed as 4.5.9, using 7:3 DMF:methanol as solvent to prepare a 30 wt. % solution, and a flow rate of 0.015 mL/min.

4.5.12 Electrospinning of styrene-[*N*-3-(*N*'-dodecyl-*N',N'*-dimethyl ammonium)propyl maleimide] copolymer (SMI-qC_{12})

The same method was followed as 4.5.9, using 1:1 DMF:methanol as solvent to prepare a 25 wt. % solution, and a flow rate of 0.0025 mL/min.

4.5.13 Electrospinning of styrene-[*N*-3-(*N*'-hexadecyl-*N',N'*-dimethyl ammonium)propyl maleimide] copolymer (SMI-qC_{16})

The same method was followed as 4.5.9, using 1:1 DMF:methanol as solvent to prepare a 22 wt. % solution, and a flow rate of 0.005 mL/min.

4.6 References

1. Tang, C.; Ye, S.; Liu, H. *Polymer* **2007**, *48*, 4482-4491.

2. Kim, T.G.; Park, T.G. *Biotechnol. Progr*. **2006**, *22*, 1108-1113.

3. Greiner, A.; Wendorff, J.H. *Angew. Chem. Int. Ed.* **2007,** *46*, 5670-5703.

4. Yao, C.; Li, X.; Neoh, K.; Shi, Z.; Kang, E. *J. Membr. Sci.* **2008**, *320*, 259-267.

5. Yoo, H.S.; Kim, T.G.; Park, T.G.; *Adv. Drug Deliv. Rev.* **2009**, *61*, 1033-1042.

6. Stoilova, O.; Ignatova, M.; Manolova, N.; Godjevargova, T.; Mita, D.; Rashkov, I. *Eur. Polym. J.* **2010**, *46*, 1966-1974.

7. Lai, X.; Sun, C.; Tian, H.; Zhao, W.; Gao, L. *Int. J. Pharm*. **2008**, *352*, 66-73.

8. Donati, I.; Gamini, A.; Vetere, A.; Campa, C.; Paoletti, S. *Biomacromolecules* **2002**, *3*, 805-812.

9. Evenson, S.; Badyal, J. *J. Phys. Chem. B*. **1998**, *102*, 5500-5502.

10. Vermeesch, I.; Groeninckx, G. *J. Appl. Polym. Sci*. **1994**, *53*, 1365-1373.

11. Soer, W.J.; Ming, W.; Klumperman, B.; Koning, C.; van Benthem, R. *Polymer* **2006**, *47*, 7621-7627.

12. Jeong, J.H.; Ko, S.B. *Journal of Industrial and Engineering Chemistry* **2001**, *7*, 310-315.

13. Henry, S.M.; El-Sayed, M.E.H.; Pirie, C.M.; Hoffman, A.S.; Stayton, P.S. *Biomacromolecules* **2006**, *7*, 2407-2414.

14. Pompe, T.; Zschoche, S.; Herold, N.; Salchert, K.; Gouzy, M.F.; Sperling, C.; et al. *Biomacromolecules* **2003**, *4,* 1072-1079.

15. Roy, S.; Dasgupta, A.; Das, P.K. *Langmuir* **2006**, *22*, 4567-4573.

16. Shenoy, S.L.; Bates, W.D.; Frisch, H.L.; Wnek, G.E. *Polymer* **2005**, *46*, 3372-3384.

17. Kiekens, P.; De Vrieze, S.; Van Camp, T.; Decostere, B.; Audenaert, W.; Westbroek, P.; et al. *Proceedings of the 8th Autex conference* **2008**.

18. Agarwal, S.; Wendorff, J.H.; Greiner, A. *Polymer* **2008**, *49*, 5603-5621.

19. Taylor, G. *Proc. R. Soc. Lond. A* **1969**, *313*, 453-475.

20. Deitzel, J.; Kosik, W.; McKnight, S.; Beck, N.; DeSimone, J.; Crette, S. *Polymer* **2002**, *43*, 1025-1029.

21. Deitzel, J.; Kleinmeyer, J.; Harris, D.; Beck, T.N. *Polymer* **2001**, *42*, 261-272.

22. Doshi, J.; Reneker, D.H. *J. Electrostatics* **1995**, *35*, 151-160.

23. McKee, M.G.; Wilkes, G.L.; Colby, R.H. *Macromolecules* **2004**, *37*, 1760-1767.

24. Subbiah, T.; Bhat, G.; Tock, R.; Parameswaran, S.; Ramkumar, S. *J. Appl. Polym. Sci*. **2005**, *96*, 557-569.

25. Teo, W.; Ramakrishna, S. *Nanotechnology* **2006**, *17*, 89-106.

26. Teo, W.E.; Gopal, R.; Ramaseshan, R.; Fujihara, K.; Ramakrishna, S. *Polymer* **2007**, *48*, 3400-3405.

27. Uyar, T.; Besenbacher, F. *Polymer* **2008**, *49*, 5336-5343.

28. Kilic, A.; Oruc, F.; Demir, A. *Text. Res. J*. **2008**, *78*, 532-539.

29. Pavia, D.L. *Introduction to spectroscopy*. Brooks/Cole Pub Co; **2009**.

30. Feng, X.S.; Pan, C.Y. *Macromolecules* **2002**, *35*, 4888-4893.

31. Zhu, L.P.; Yi, Z.; Liu, F.; Wei, X.Z.; Zhu, B.K.; Xu, Y.Y. *Eur. Polym. J.* **2008**, *44,* 1907-1914.

32. Huang, F.; Wu, H.; Wang, D.; Yang, W.; Cao, Y. *Chem. Mater.* **2004**, *16*, 708-716.

33. Albertin, L.; Stenzel, M.H.; Barner-Kowollik, C.; Foster, L.J.R.; Davis, T.P. *Macromolecules* **2005**, *38*, 9075-9084.

34. Qin, C.; Xiao, Q.; Li, H.; Fang, M.; Liu, Y.; Chen, X.; et al. *Int. J. Biol. Macromol*. **2004**, *34*, 121-126.

35. Chen, G.; Zhang, Y.; Zhou, X.; Xu, *J. Appl. Surf. Sci.* **2006**, *253*, 1107-1110.

36. Wang, K.; Huang, W.; Xia, P.; Gao, C.; Yan, D. *React. Funct. Polym.* **2002**, *52*, 143-148.

37. Lee, S.S.; Ahn, T.O. *J. Appl. Polym. Sci.* **1999**, *71*, 1187-1196.

38. Snyder, R.; Schachtschneider, J. *Spectrochimica Acta*. **1963**, *19*, 85-116.

39. Kim, C.H.; Choi, J.W.; Chun, H.J.; Choi, K.S. *Polym. Bull.* **1997**, *38*, 387-393.

40. Fang, H.; Mighri, F.; Ajji, A. *J. Appl. Polym. Sci*. **2008**, *109*, 3938-3943.

41. Domard, A.; Gey, C.; Rinaudo, M.; Terrassin, C. *Int. J. Biol. Macromol.* **1987**, *9*, 233-237.

42. Koombhongse, S.; Liu, W.; Reneker, D.H. *J. Polym. Sci., Part B: Polym. Phys.* **2001**, *39*, 2598-2606.

43. Cumberbirch, R.; Ford, J.; Gee, R. *J. Text. Inst. Proc.* **1961**, *52*, 288.

44. Capone, G. *Acrylic fiber technology and applications* Mercel Dekker Inc. **1995**.

Chapter 5: Affinity studies between modified polymers and mycobacteria

5.1 Introduction

Poly(styrene-*co*-maleic anhydride) (SMA) was functionalized with a variety of compounds to yield modified poly(styrene-*co*-maleimide) (SMI) and electrospun to produce functionalized polymer nanofibers. Some of the modified SMI polymers were prepared by surface-functionalization of the polymer nanofibers after electrospinning (as described in Chapter 3) and some by modification of the polymer before electrospinning (as described in Chapter 4). Both procedures yielded functionalized SMI nanofibers with an average fiber diameter in the range of ~ 550 - 750 nm.

The compounds chosen in this study for the functionalization of SMA were selected based on possible chemical interaction with the *Mycobacterium tuberculosis* (*M. tuberculosis)* cell wall and comprised amino sugars, an amino acid derivative, a protein and a variety of N-alkylamines of varying aliphatic chain lengths and N-functionalities. These functionalized polymer nanofibers were developed as a potential capturing platform for *M. tuberculosis* under gastric conditions (low pH) to improve the collection thereof as specimen for further diagnostic tests. Affinity studies were therefore carried out using the different functionalized SMI nanofibrous mats and mycobacteria to ascertain whether mycobacteria could be captured by the modified SMI nanofibers in a low pH environment.

Here we report the affinity studies between the functionalized SMI nanofibers and two mycobacterium strains, namely BCG and *M. tuberculosis*. BCG was initially used as a mimic for *M. tuberculosis*[1-4], as BCG is non-pathogenic and genetically closely related to *M. tuberculosis*.[5-10] Interaction between the functionalized SMI nanofibers and BCG was initially investigated at pH 7 and 2, with the pH 2 value selected to simulate the acidic environment of the stomach. These affinity studies performed at low pH using BCG as mycobacterium strain were repeated with *M. tuberculosis*. The general procedure entailed that the functionalized polymer nanofibers were incubated with the relevant mycobacterium strain at a certain pH value, washed and then analyzed. A variety of detection methods were used to evaluate the interaction between the mycobacterium strains and the surfaces of the functionalized SMI nanofibers with varying success. The process by which the mycobacteria interacted with the functionalized nanofibrous surfaces and attached to it will be referred to as ‘capture’ for the remainder of the chapter. Scanning electron microscopy (SEM), fluorescence microscopy (FM), light microscopy (LM) and polymerase chain reaction (PCR) were used as detection methods for measuring the interaction between the mycobacteria and the surfaces of the functionalized polymer nanofibers. FM and PCR were finally selected as the most reliable detection methods with FM being a visual and PCR a molecular detection method.

To conclude this study, a comparison was done between the original Entero-string test and the functionalized SMI polymer that appeared to be the most effective mycobacteria-capturing platform. FM, LM and PCR were used as detection methods to evaluate the extent of interaction between *M. tuberculosis* and the relevant capturing platform.

5.2 Affinity studies

The affinity studies between the functionalized SMI nanofibers and the two mycobacterium strains were carried out using a kanamycin-resistant strain of BCG and a rifampicin-resistant strain of *M. tuberculosis*, respectively. Kanamycin is an aminoglycoside antibiotic that is widely used in molecular biology to prevent the growth of contaminating bacteria and rifampicin is a bactericidal antibiotic used for the same purpose.[11,12] The respective antibiotics were therefore included in the corresponding growth mediums to prevent contaminating bacteria, present on the non-sterile polymer nanofibrous mats, from overgrowing the input mycobacteria due to their different growth rates, thereby possibly masking the presence of the input mycobacteria. This ensured that only the respective antibiotic-resistant strains of BCG or *M. tuberculosis* would grow and not any other contaminating bacteria.

5.2.1 Affinity studies with BCG at neutral pH

Affinity studies were initially done at neutral pH between BCG and the polymer nanofibers functionalized with amino sugars (SMI-Gluc/Man), an amino acid derivative (SMI-BCML), a protein (SMI-Con A) and a C_{12} aliphatic quaternary ammonium group (SMI-qC_{12}) to ascertain which functional moiety could potentially interact with BCG and capture it onto the functionalized nanofibrous surface. Refer to Figure 5.1 for the chemical structures of the functionalized SMI nanofibers used for the affinity test with BCG at neutral pH.

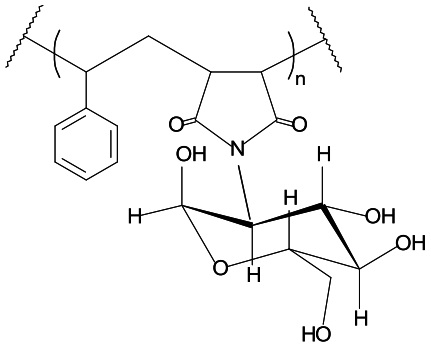

(a) SMI-Gluc/Man

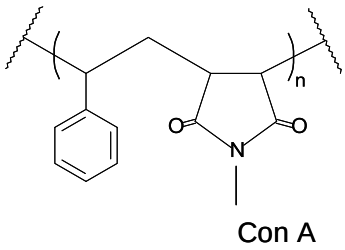

(b) SMI-Con A

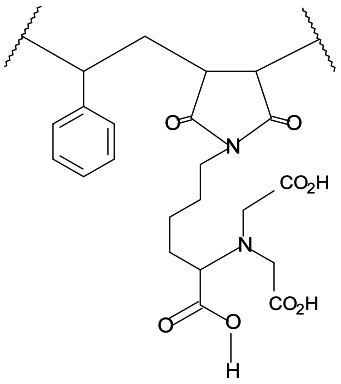

(c) SMI-BCML

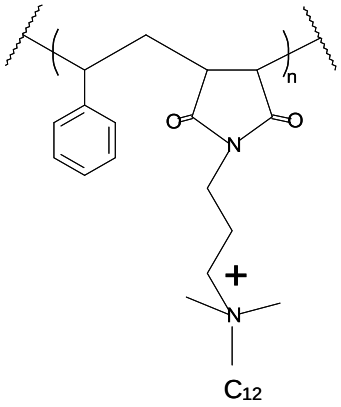

(d) SMI-qC$_{12}$

Figure 5.1 Chemical structures of the functionalized SMI nanofibers used for the affinity test with BCG at neutral pH.

Due to the fact that BCG is a slow-growing mycobacterium strain, a pilot study was done using *Mycobacterium smegmatis (M. smegmatis),* a fast-growing strain. This pilot study entailed adding a specific weight (10 mg) of the functionalized polymer nanofibers detailed in Figure 5.1 to a specific volume (10 mL) of *M. smegmatis* culture (grown to an optical density (OD_{600}) of 0.68) and incubating it at 37 °C for one hour, whilst agitating. The polymer nanofibers were subsequently removed from the tubes containing the *M. smegmatis* culture and washed twice with phosphate buffered solution (PBS) to remove any loosely adhered mycobacteria not properly captured onto the surfaces of the functionalized polymer nanofibers.

The interaction between *M. smegmatis* and the functionalized polymer nanofibers was initially visualized using conventional light microscopy and Ziehl-Neelsen (ZN) staining as it is a simple test and the most common method used to check for the presence of *M. tuberculosis*.[13-15] This test method entailed placing the washed nanofibers onto a microscope slide and staining it using the ZN staining protocol. The stained samples were observed using a 100x oil immersion objective.[13-15] Although this method worked, it was difficult to detect mycobacteria on the surfaces of the functionalized polymer nanofibers with the untrained eye, especially at low concentrations of *M. smegmatis*. It was thus not considered a robust detection method to evaluate the interaction between the mycobacteria and the functionalized SMI nanofibers.

Subsequently, liquid culture was investigated as an alternative detection method to light microscopy as the method has a higher sensitivity.[16] This test method entailed adding the relevant washed nanofibers to separate tubes containing sterile liquid growth medium. The supposition was that if *M. smegmatis* was carried over from the test culture into the sterile growth medium via the functionalized polymer nanofibers, it would grow in the sterile growth medium and serve as evidence that *M. smegmatis* was indeed captured onto the polymer nanofibrous surface. The liquid in the tubes containing the washed SMI-Gluc/Man, SMI-BCML and SMI-Con A nanofibrous mats became turbid, possibly due to growth of the mycobacteria that was carried over from the test culture on the

nanofibrous surfaces into the sterile growth medium. The tubes containing the washed SMI-qC_{12} nanofibers however did not become turbid, indicating that the SMI-qC_{12} nanofibrous surface did not capture *M. smegmatis*. However, subsequent SEM images taken of the washed SMI-qC_{12} nanofibers suggested that *M. smegmatis* was captured onto the SMI-qC_{12} nanofibrous surface, as indicated by wart-like structures visible on the SEM images. A possible explanation for this result was that SMI-qC_{12} appeared to have mycobacteriostatic and/or mycobacteriocidal properties. It thus killed or inactivated the mycobacteria captured onto the polymer nanofibrous surface; consequently growth did not take place and was therefore not detected, even though mycobacteria were attached to the polymer surface. This result was in good agreement with literature, which verified that quaternary ammonium moieties of antimicrobial compounds interacted with the mycobacterial cell wall due to the electrostatic force between the negatively charged mycobacterial outer membrane and the positively charged quaternary ammonium moiety of the polymer. This interaction subsequently damages the mycobacterial outer membrane structure and increases its permeability, leading to cell death.[17-20]

The affinity studies between *M. smegmatis* and the relevant functionalized SMI nanofibers at neutral pH were repeated using BCG as mycobacterium strain to determine whether there was a change in the interaction if BCG was used. Analysis of the SEM images suggested that BCG was captured onto the surfaces of all the functionalized nanofibers as detailed in Figure 5.1.

5.2.2 Affinity studies with BCG at low pH

The affinity studies between BCG and the relevant functionalized SMI nanofibers at neutral pH (described in section 5.2.1) were repeated at low pH to determine whether there was a change in the interaction between BCG and the relevant functionalized SMI nanofibers if the pH was lowered to 2 to simulate gastric conditions. These affinity studies were carried out by adjusting the pH of the BCG culture with the addition of concentrated hydrochloric acid, adding the modified polymer nanofibers as detailed in Figure 5.1 and incubating it at 37 °C for one hour. The polymer nanofibers were subsequently washed and visualized using SEM and FM. Analysis of the SEM and FM images suggested that there was no interaction between BCG and the surfaces of the SMI-Gluc/Man, SMI-BCML and SMI-Con A nanofibers as no BCG was captured onto the surfaces of these said polymer nanofibers. BCG was however captured onto the SMI-qC_{12} nanofibrous surface as indicated by wart-like structures visible on the SEM images and green and red stained mycobacteria on the FM images. BCG was visualized using fluorescence microscopy by staining the mycobacterium with two fluorescent nucleic acid-binding stains, namely propidium iodide and SYTO-9. Propidium iodide is a red dye that penetrates bacterial cells with damaged membranes and SYTO-9 is a green dye that penetrates all bacterial cells – those with intact membranes and those with damaged membranes. Viable bacterial cells with intact membranes are thus stained fluorescent green and dead cells with damaged membranes are stained fluorescent red.[21]

After the putative capture of BCG onto the surface of the SMI nanofibers functionalized with a C_{12} aliphatic quaternary ammonium moiety (Fig. 5.1(d)), the affinity studies were repeated at low pH using SMI nanofibers functionalized with a variety of N-alkylamines of varying aliphatic chain lengths and N-functionalities to ascertain which N-functionality/aliphatic chain length combination captured BCG the most effectively. Refer Figure 5.2 for the chemical structures of the SMI nanofibers functionalized with N-alkylamines of varying aliphatic chain lengths and N-functionalities used for the affinity studies with BCG at low pH.

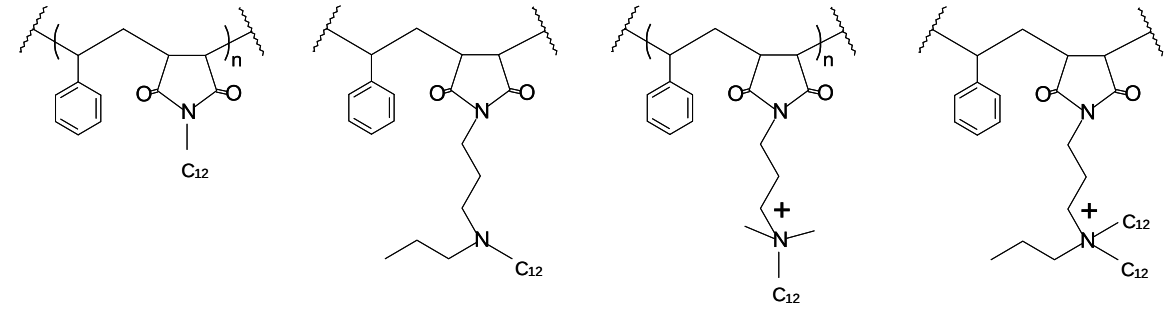

(a) SMI-C_{12} (b) SMI-tC_{12} (c) SMI-qC_{12} (d) SMI-qC_{24}

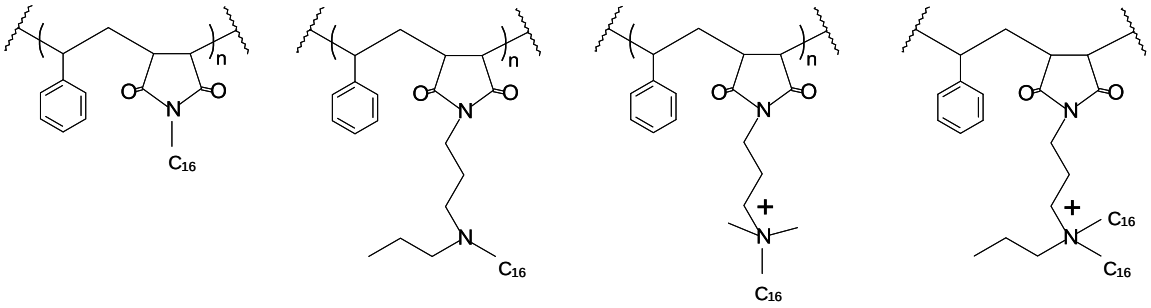

(e) SMI-C_{16} (f) SMI-tC_{16} (g) SMI-qC_{16} (h) SMI-qC_{32}

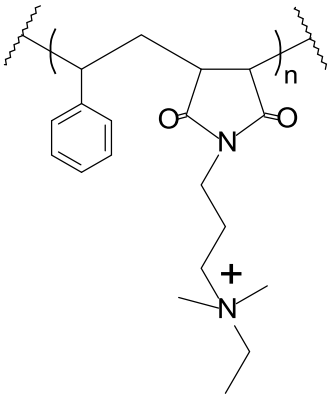

(i) SMI-qC_2

Figure 5.2 Chemical structures of the SMI nanofibers functionalized with N-alkylamines of varying aliphatic chain lengths and N-functionalities used for the affinity studies with BCG at low pH.

BCG captured onto the surfaces of these functionalized SMI nanofibers was visualized using SEM and FM. Analysis of the SEM and FM images indicated that BCG interacted strongly with SMI-qC_{12} and SMI-qC_{16} due to high quantities of BCG visible on the surfaces of these functionalized nanofibers, and weakly with SMI-tC_{12}, SMI-tC_{16}, SMI-qC_{24} and SMI-qC_{32} due to lower quantities of BCG visible on the surfaces of these functionalized polymer nanofibers. None of the other functionalized polymer nanofibers showed any interaction with BCG as no BCG was visible on the surfaces of the SMI-C_{12}, SMI-C_{16} or SMI-qC_2 nanofibers.

After the putative capture of BCG onto the surfaces of the SMI-qC_{12} and SMI-qC_{16} nanofibers, time and concentration studies were carried out to determine if the interaction between BCG and these functionalized nanofibers were dependent on these factors.

a) Time studies

These studies were carried out by incubating BCG with the SMI-qC_{12} and SMI-qC_{16} nanofibers at 37 °C and pH 2 for 15 min., 30 min., 45 min. and 60 min., respectively. The polymer nanofibers were removed after the specified time had lapsed and washed twice with PBS to remove any loosely adhered BCG onto the surface of the functionalized polymer nanofibers. SEM and FM were used to visualize the interaction between BCG and the functionalized nanofibers. Analysis of the SEM and FM images indicated that the interaction between BCG and the functionalized nanofibers appeared to be dependent on time as the number of BCG captured onto the SMI-qC_{12} and SMI-qC_{16} nanofibrous surface increased with an increase in incubation time. Further analysis of the SEM and FM images also indicated that the number of BCG captured onto the surface of SMI-qC_{12} nanofibers were higher than on the surface of the SMI-qC_{16} nanofibers after each specified time period.

b) Concentration studies

The concentration studies were carried out by incubating SMI-qC_{12} and SMI-qC_{16} nanofibers with decreasing concentrations of BCG, from approximately 10^8 BCG/mL to 10 BCG/mL, serially diluted 1:10, at 37 °C and pH 2 for one hour. SEM and FM were used to visualize the interaction between BCG and the surfaces of the functionalized nanofibers. Analysis of the SEM and FM images indicated that the interaction between BCG and the functionalized nanofibers appeared to be concentration dependent as the number of BCG captured onto the SMI-qC_{12} and SMI-qC_{16} nanofibrous surfaces decreased with decreasing concentration of BCG. Further analysis of the SEM images indicated that the surfaces of the SMI-qC_{12} and SMI-qC_{16} nanofibers were able to capture BCG at a concentration as low as 10 BCG/mL as wart-like structures that looked like clusters of aggregated BCG, were visible on the surfaces of these nanofibers at all the BCG concentrations. Further analysis of the FM images however indicated that the surfaces of the SMI-qC_{12} and SMI-qC_{16} nanofibers were only able to capture BCG at a concentration of 10^5 BCG/mL and higher. PCR was used as additional detection

method. This method indicated that the surface of the SMI-qC_{12} nanofibers were able to capture BCG at a concentration of 10 BCG/mL and higher. From these results it is quite evident that there appeared to be a significant discrepancy among the SEM and FM results and the PCR results. Further analysis of the FM images also indicated that the number of BCG captured onto the surface of SMI-qC_{12} nanofibers were higher than on the surface of the SMI-qC_{16} nanofibers at each BCG concentration level.

The results of the time and concentration studies indicated that the SMI-qC_{12} nanofibrous surface captured BCG more effectively than the surface of the SMI-qC_{16} nanofibers. It was therefore decided to use the SMI-qC_{12} nanofibers for the subsequent affinity studies with *M. tuberculosis* to determine whether the SMI-qC_{12} nanofibrous surface could capture *M. tuberculosis* at low pH.

5.2.3 Affinity studies with *M. tuberculosis* at low pH

The affinity studies between *M. tuberculosis* and the SMI-qC_{12} nanofibers were carried out at pH 2 to simulate gastric conditions. These affinity studies were done by incubating specific weights of SMI-qC_{12} nanofibers with defined volumes of acidified culture containing decreasing numbers of *M. tuberculosis* bacilli (approximately 10^8 *M. tuberculosis*/mL (*Mtb*/mL) to 10 *Mtb*/mL, serially diluted 1:10) at 37 °C for one hour. The polymer nanofibers were subsequently washed with PBS to remove any loosely adhered *M. tuberculosis* not properly captured onto the surfaces of the functionalized polymer nanofibers and visualized using FM and LM. SEM was not used as detection method as it was difficult to differentiate between mycobacteria and the polymer nanofibers due to the mycobacteria saturating the surface of the polymer nanofibers at high concentrations of *M. tuberculosis*. This was not a problem during the initial stage of the study, but as the quaternization reaction of the polymer was improved, the affinity between the mycobacteria and functionalized polymer nanofibers increased. This resulted in the appearance of the mycobacteria on the surface of the polymer nanofibers changing from wart-like structures to a ‘coating’ of mycobacteria. SEM was therefore no longer considered accurate enough to base conclusions on. Analysis of the FM and LM images indicated that the SMI-qC_{12} nanofibrous surface was able to capture *M. tuberculosis* at a concentration of 10^2 *Mtb*/mL and higher. PCR was used as an additional molecular detection method. This method indicated that the surface of the SMI-qC_{12} nanofibers was able to capture *M. tuberculosis* at a concentration of 10^4 *Mtb*/mL and higher, although faint bands were visible at lower concentrations. This result was unexpected as PCR is a detection method with high sensitivity and should therefore have shown bands at the lower concentration levels as well. There was therefore a slight discrepancy between the FM and LM results and the PCR results (see below for explanation).

5.3 Analysis of the interaction between mycobacteria and the functionalized SMI nanofibers

5.3.1 Analysis of the interaction between BCG and the functionalized SMI nanofibers at neutral pH

The interaction between BCG and the nanofibers of SMI-Man/Gluc, SMI-BCML, SMI-Con A and SMI-qC_{12} after incubation at neutral pH was visualized using SEM. The SEM images of the washed nanofibers of SMI-Man/Gluc, SMI-BCML, SMI-Con A and SMI-qC_{12} showed wart-like structures on the surface of all the fibers. Refer Figure 5.3(a) for a representative SEM image of the washed SMI-qC_{12} nanofibers after incubation with BCG at 37 °C and neutral pH for one hour and Figure 5.3(b) and 5.3(c) for a SEM image of BCG as positive control and washed SMI-qC_{12} nanofibers after incubation in PBS as negative control, respectively. (These images were captured at different magnification settings.) As these wart-like structures were not visible on the polymer nanofibers before BCG incubation, it was concluded that these wart-like structures could be BCG captured onto the surface of the functionalized polymer nanofibers.

(a)

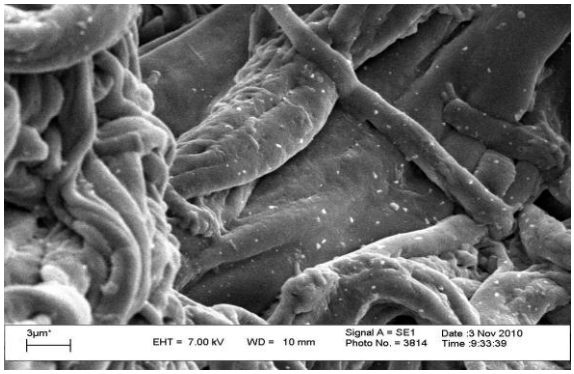

(b)

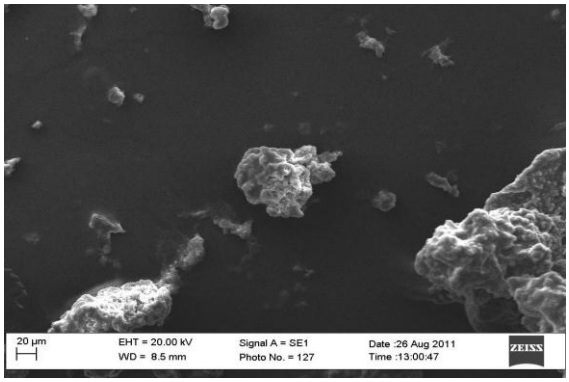

(c)

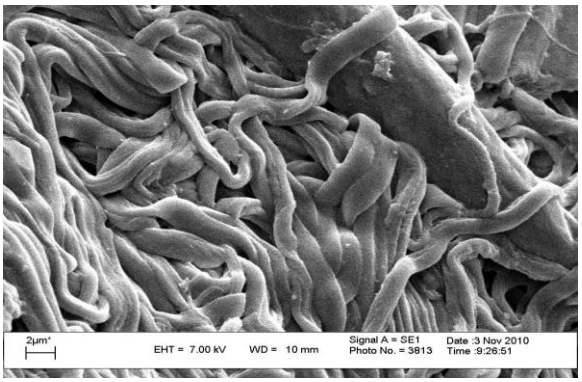

Figure 5.3 SEM images of (a) the washed SMI-qC_{12} nanofibers after incubation with BCG at 37 °C and neutral pH for one hour, (b) BCG as positive control and (c) washed SMI-qC_{12} nanofibers after incubation in PBS as negative control.

Refer Figure 5.4 for an enlargement of these wart-like structures and Figure 5.5 showing two of these wart-like structures that have started to detach from the surface of the polymer.

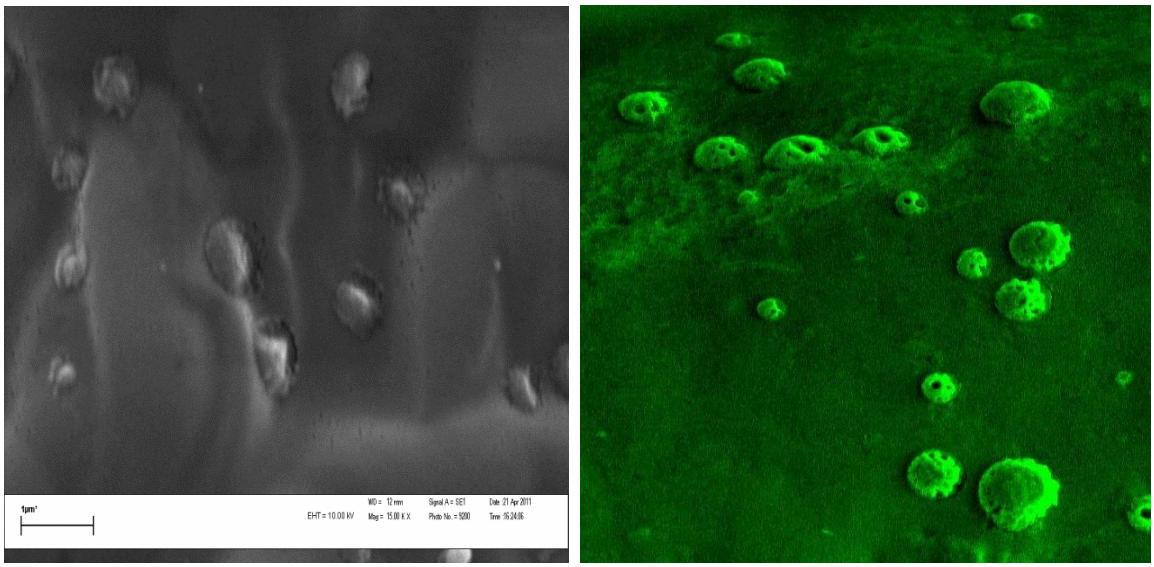

Figure 5.4 Enlargement of the wart-like structures.

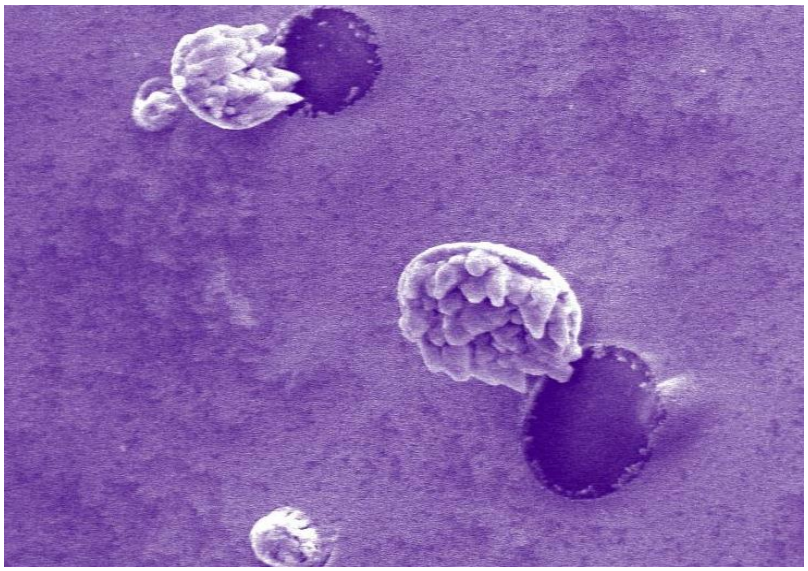

Figure 5.5 Two wart-like structures that have started to detach from the surface of the polymer, indicative of aggregated BCG (image was captured without a scale-bar).

As BCG is prone to aggregation due to the extreme hydrophobic character of the cell wall caused by the mycolic acids present in the BCG cell wall, these wart-like structures therefore appeared to be BCG clusters comprising aggregated BCG, with the individual BCG clearly visible as protrusions. The abundance of mycolic acids spread throughout the BCG cell wall is the primary reason for their tendency to aggregate.[22-25]

The SEM results therefore suggested that the nanofibers of SMI-Man/Gluc, SMI-BCML, SMI-Con A and SMI-qC_{12} seemed to be able to capture BCG at neutral pH.

5.3.2 Analysis of the interaction between BCG and the functionalized SMI nanofibers at low pH

The interaction between BCG and the nanofibers of SMI-Man/Gluc, SMI-BCML, SMI-Con A and SMI-qC_{12} after incubation at pH 2 was visualized using SEM and FM. The SEM images of the washed nanofibers of SMI-Man/Gluc, SMI-BCML and SMI-Con A did not show any wart-like structures, suggestive of aggregated BCG, on the surfaces of the nanofibers (results not shown). These wart-like structures were however present on the surface of the washed SMI-qC_{12} nanofibers. Refer Figure 5.6 for a representative SEM image of (a) the washed SMI-qC_{12} nanofibers after incubation with BCG at 37 °C and pH 2 for one hour and (b) washed SMI-qC_{12} nanofibers after incubation in PBS as negative control. (Refer Figure 5.3(b) for a SEM image of BCG as positive control.)

(a) (b)

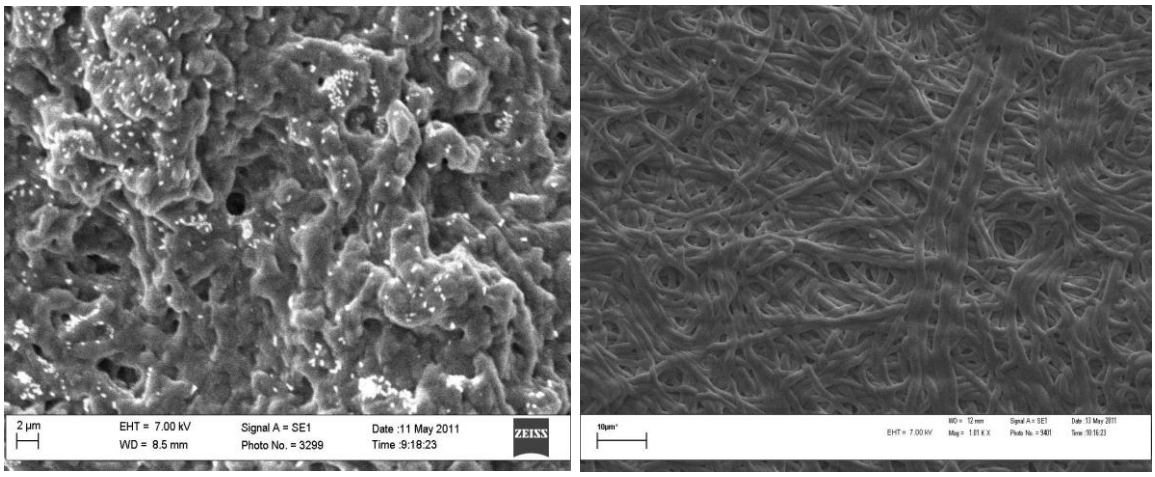

Figure 5.6 SEM images of (a) the washed SMI-qC_{12} nanofibers after incubation with BCG at 37 °C and pH 2 for one hour and (b) washed SMI-qC_{12} nanofibers after incubation in PBS as negative control.

The results of the SEM images were corroborated by FM images of the washed nanofibers of SMI-Man/Gluc, SMI-BCML, SMI-Con A and SMI-qC_{12}. Analysis of the FM images indicated that there was no BCG captured onto the surfaces of the washed nanofibers of SMI-Man/Gluc, SMI-BCML and SMI-Con A, whereas the FM image of the washed SMI-qC_{12} nanofibers showed high numbers of BCG captured onto the surface of these nanofibers, as indicated by the red and green stained microbes. Refer Figure 5.7 for representative FM images of the washed (a) SMI-Man, (b) SMI-Gluc, (c) SMI-BCML, (d) SMI-Con A and (e) SMI-qC_{12} nanofibers after incubation with BCG at 37 °C and pH 2 for one hour and Figure 5.7(f) and 5.7(g) for FM images of BCG as positive control and washed SMI-qC_{12} nanofibers after incubation in PBS as negative control, respectively.

(a)

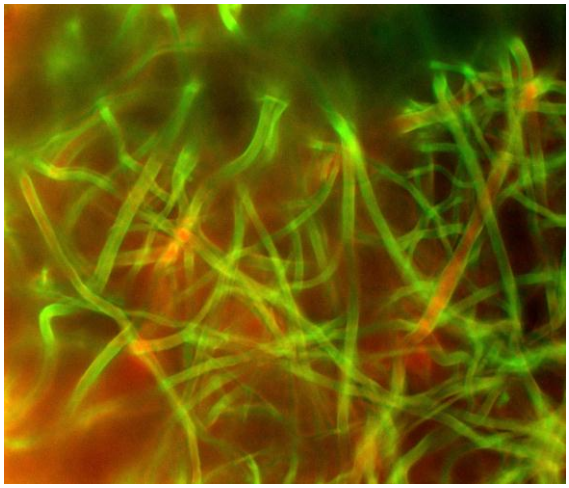

(b)

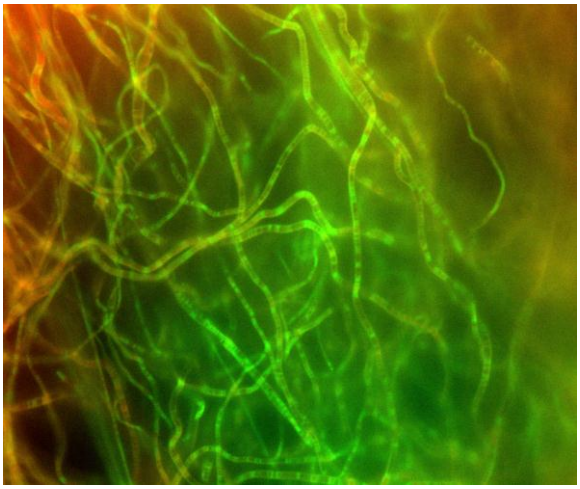

(c)

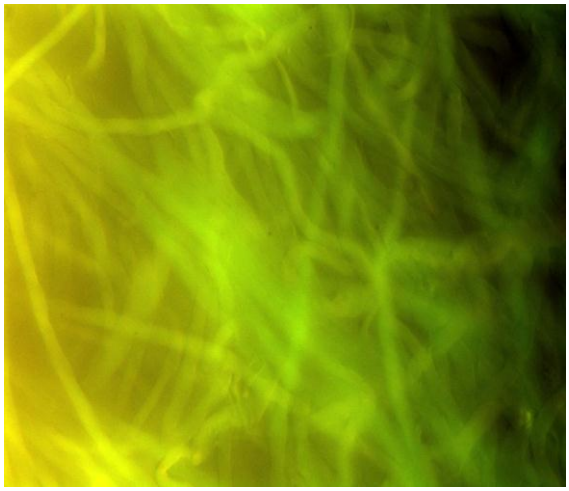

(d)

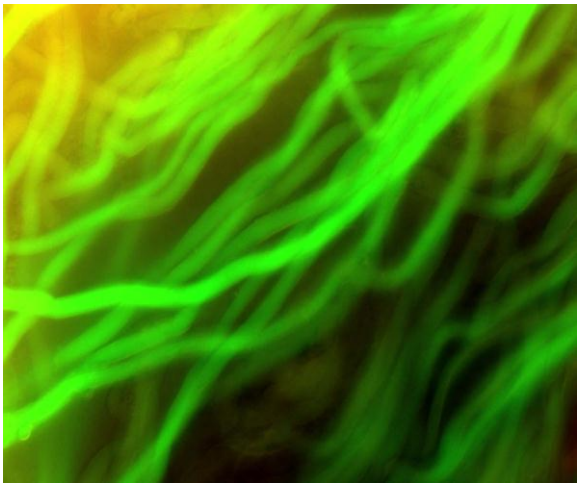

(e)

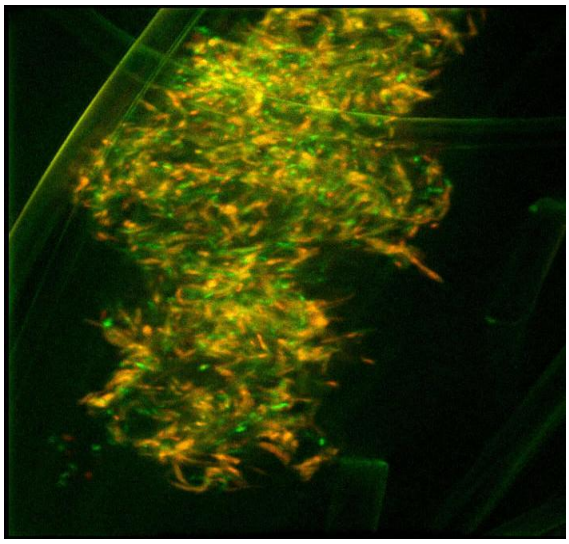

(f) (g)

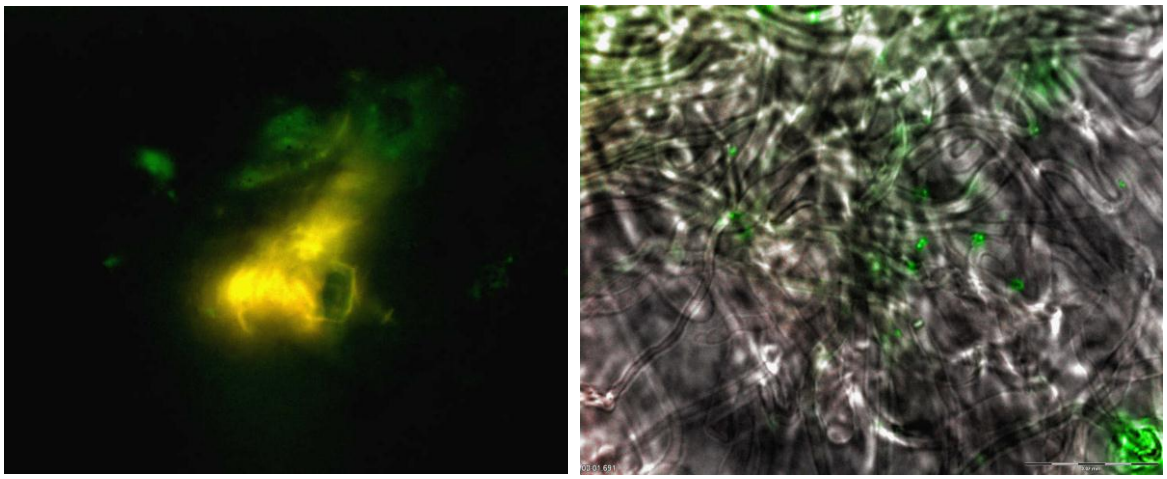

Figure 5.7 FM images of the washed (a) SMI-Man, (b) SMI-Gluc, (c) SMI-BCML, (d) SMI-Con A and (e) SMI-qC$_{12}$ nanofibers after incubation with BCG at 37 °C and pH 2 for one hour, (f) BCG as positive control and (g) washed SMI-qC$_{12}$ nanofibers after incubation in PBS as negative control.

From the results of the SEM and FM images, it is clear that only the SMI-qC$_{12}$ nanofibers were able to interact with BCG at low pH in such a manner that the bacilli remained bound despite washing with PBS. None of the other modified polymers was able to capture BCG onto the surface of their respective electrospun nanofibrous mats under acidic conditions.

These results may possibly be explained as follows for the different modified polymers:

SMI-Gluc and SMI-Man interacted with BCG at neutral pH due to the possibility that the modified polymer may have functioned as a glycopolymer, i.e. a synthetic polymer consisting of a non-carbohydrate backbone with carbohydrate units as pendants.[26] The incorporation of pendant saccharides into the polymer backbone leads to multivalent oligosaccharide ligands, resulting in enhanced protein binding affinity[27] between BCG and the modified polymer. Although the interaction between the protein and saccharides are usually weak, it is amplified by the multivalent effect of the saccharides clustered together along the polymer backbone.[28,29] The expectation was that the sugar-modified SMI polymer could function as a synthetic glycosaminoglycan-mimic and enable BCG binding to the surface of SMI-Gluc/Man via the heparin-binding haemagglutinin adhesin (HBHA),[30,31] PE-PGRS proteins (proteins with a conserved N-terminal Proline-Glutamic acid (PE) and C-terminal polymorphic Glycine-Cysteine rich repetitive sequence (PGRS))[32-34] and/or fibronectin-binding protein (FAP).[35,36] These proteins bind to sulfated carbohydrates, also called sulfated glycoconjugates.[30] A subsequent study by Menozzi however indicated that HBHA and PE-PGRS adhered specifically to sulfated carbohydrates as no significant adherence was observed when non-sulfated sugars such as dextran, mannose or galactose were used.[30]

The results of this study therefore indicated that the interaction between glucose and mannose of SMI-Gluc and SMI-Man and BCG at neutral pH may purely have been incidental and possibly occurred due to hydrogen-bonding interaction between the sugar-modified SMI polymer and the

amino acids of the cell surface proteins of BCG. As soon as the pH was lowered to 2, the interaction between BCG and the non-sulfated sugar molecules of SMI-Gluc/Man was not strong enough to facilitate interaction between BCG and the surface of the modified polymer nanofibers.[27,37]

SMI-Con A was able to interact with BCG at neutral pH and capture it onto the surface of the SMI-Con A nanofibers possibly due to Con A's mannose-binding properties.[38] The terminal mannose caps of lipoarabinomannan (LAM), a key component of the mycobacterial cell wall of BCG, act as mycobacterial ligands that can bind to Con A using hydrogen-bonds and Van Der Waals interactions.[39,40] This carbohydrate-protein interaction is only possible if the protein is present in its biologically active 3-D structure at the physiological pH of 7.2.[38,41,42] Con A is however susceptible to denaturation at a pH below 3. Denaturation is a process that causes a protein to lose its tertiary and secondary structure, thereby becoming biologically inactive and no longer able to perform its function. Con A thus loses its ability to recognize and bind to terminal mannose caps of BCG's cell wall LAM.[43-45] SMI-Con A therefore lost its ability to capture BCG at a pH below 3 most likely due to denaturation of Con A.

The interaction between SMI-qC_{12} and BCG could possibly be explained by looking at the ionic interaction between the negatively charged BCG cell wall and the positively charged quaternary ammonium moiety of the functionalized polymer, as well as the hydrophobic-hydrophobic interaction between the mycolic acids of the BCG cell wall and the aliphatic C_{12} hydrocarbon chains of the functionalized polymer. The cell wall of BCG is negatively charged at neutral pH due to surface exposed anionic components such as proteins, liposaccharides,[46] phosphatidylinositol mannosides (PIM), phosphatidyl ethanolamine (PE) and sulfolipids (SL).[3,47,48] At pH 2, the proteins and liposaccharides are protonated, but PIM, PE and SL remain negatively charged due to sulphate groups of the sulfolipids and the phosphodiester bonds of PIM and PE where the negative charge is stabilized through resonance. The ionic interaction between the negatively charged BCG cell wall and positively charged polymer is therefore independent of the pH. The same applies to the hydrophobic-hydrophobic interaction that is also not affected by pH.

Further analysis of the FM image of Figure 5.7 also indicated that some BCG stained red and some stained green when propidium iodide and SYTO-9 were used as fluorescent nucleic acid-binding stains. BCG that stained red is indicative of dead BCG and those stained green are indicative of viable BCG. These results indicated that SMI-qC_{12} seemed to have antimicrobial properties and killed or inactivated captured BCG. These results correlate well with literature where it has been reported extensively that quaternary ammonium compounds possess antimicrobial properties. The proposed mechanism of the antimicrobial action is based on the interaction between the positively charged ammonium groups of the cationic polymer and the multitude of anionic components on the cell surface such as proteins and liposaccharides, resulting in the disruption of the integrity of the outer membrane and changing the permeability of the cell membrane, thus weakening its barrier function.[19,49,50]

Based on these results, it was decided to investigate the interaction between BCG and SMI nanofibers functionalized with a variety of N-alkylamines of varying aliphatic chain lengths and N-functionalities (refer Figure 5.2 for relevant chemical structures) to ascertain which N-functionality/aliphatic chain length combination captured BCG the most effectively at low pH.

The interaction between BCG and the functionalized SMI nanofibers as illustrated schematically in Figure 5.2 after incubation at pH 2, was visualized using SEM and FM. Analysis of the SEM images of the washed polymer nanofibers indicated that BCG may have interacted with the nanofibrous surfaces of SMI-qC_{12} and SMI-qC_{16} as the wart-like structures, suggestive of BCG clusters, were only visible on these nanofibers. None of the other nanofibers showed any wart-like structures on their surfaces. Refer Figure 5.8 for representative SEM images of the washed nanofibers of (a) SMI-qC_{12} and (b) SMI-qC_{16} after incubation with BCG at 37 °C and pH 2 for one hour.

(a) (b)

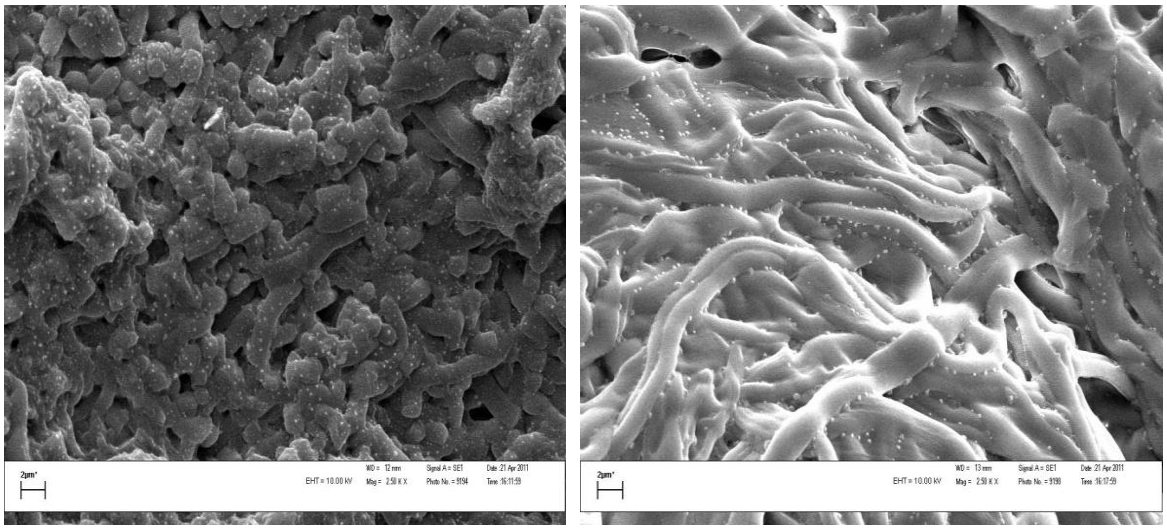

Figure 5.8 SEM images of the washed nanofibers of (a) SMI-qC_{12} and (b) SMI-qC_{16} after incubation with BCG at 37 °C and pH 2 for one hour.

Analysis of the FM images of the washed nanofibers indicated that BCG interacted with the nanofibrous surfaces of SMI-tC_{12}, SMI-tC_{16}, SMI-qC_{12}, SMI-qC_{16}, SMI-qC_{24} and SMI-qC_{32} as indicated by the red and green stained microbes on these nanofibers. Further analysis of the FM images also indicated that the concentration of BCG was higher on the nanofibers surface of SMI-qC_{12} and SMI-qC_{16}, compared to those of SMI-tC_{12}, SMI-tC_{16}, SMI-qC_{24} and SMI-qC_{32}. Refer Figure 5.9 for representative FM images of the washed nanofibers of (a) SMI-qC_{12}, (b) SMI-qC_{16}, (c) SMI-tC_{12}, (d) SMI-tC_{16}, (e) SMI-qC_{24} and (f) SMI-qC_{32} after incubation with BCG at 37 °C and pH 2 for one hour.

(a) (b)

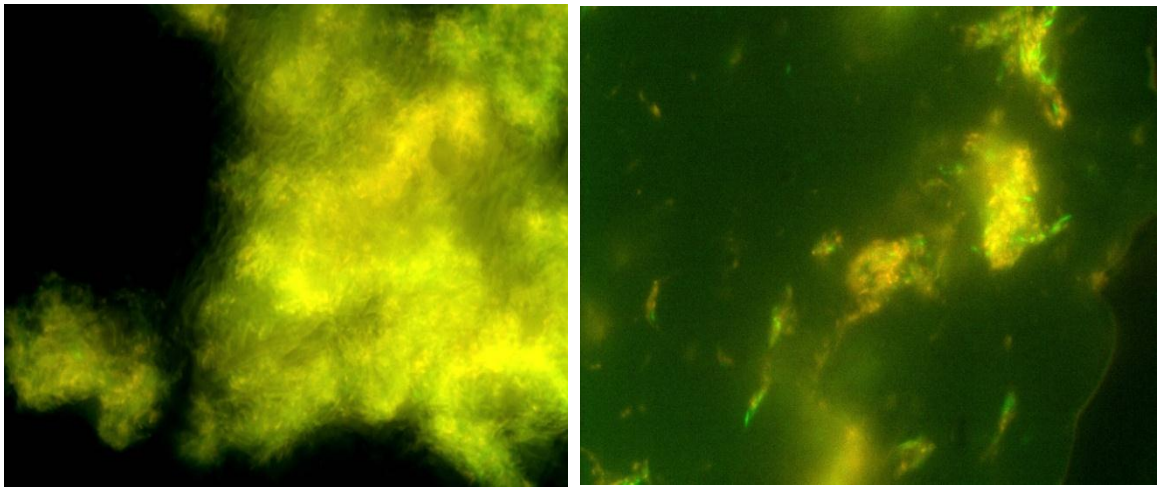

(c) (d)

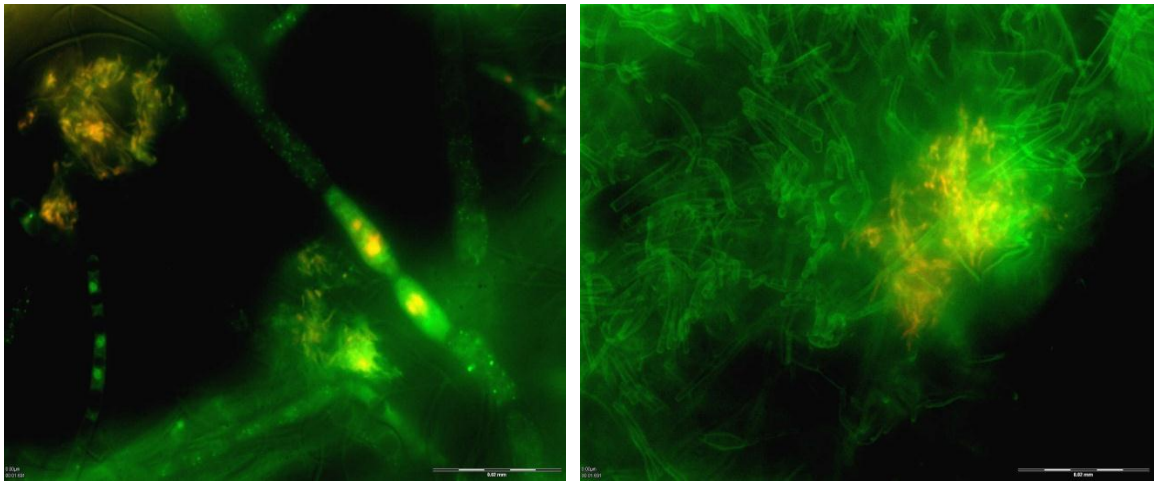

(e) (f)

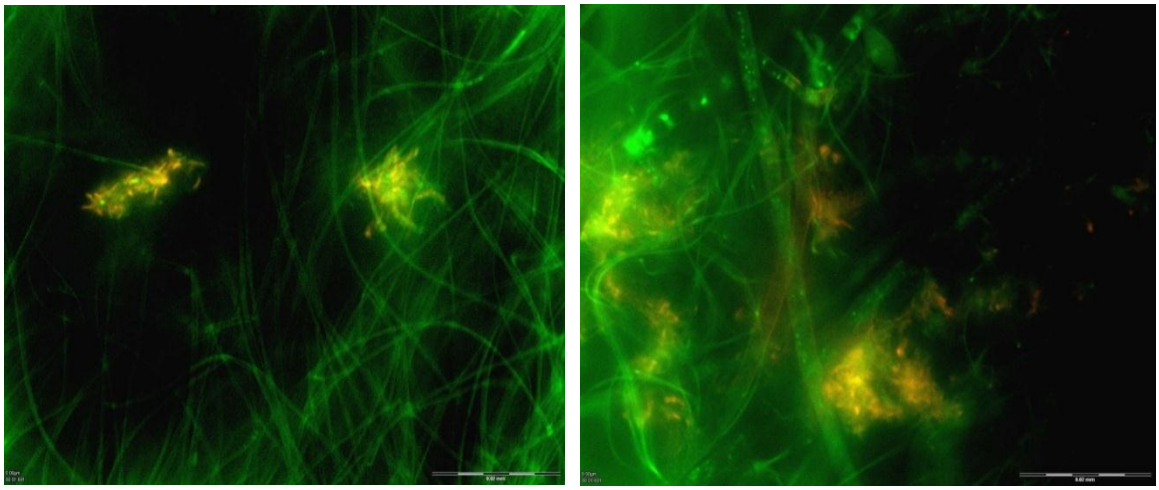

Figure 5.9 FM images of the washed nanofibers of (a) SMI-qC$_{12}$, (b) SMI-qC$_{16}$, (c) SMI-tC$_{12}$, (d) SMI-tC$_{16}$, (e) SMI-qC$_{24}$ and (f) SMI-qC$_{32}$ after incubation with BCG at 37 °C and pH 2 for one hour.

These results can be discussed by looking at the conversion percentages of the modified polymer, the average fiber diameter of the functionalized nanofibers, the synthetic route and the hydrophobic character of the modified polymer. Refer Table 5.1 for the conversion percentages of the modified polymer and average fiber diameter of the functionalized nanofibers.

Table 5.1 Conversion percentages of the modified polymer and average fiber diameter of the functionalized nanofibers

Modified polymer	Conversion %	Average fiber diameter (nm)	Strength of interaction with BCG
SMI-tC_{12}	81	746 ± 81	+
SMI-tC_{16}	84	752 ± 85	+
SMI-qC_{12}	87	625 ± 90	+++
SMI-qC_{16}	87	755 ± 429	++
SMI-qC_{24}	84	755 ± 148	+
SMI-qC_{32}	75	744 ± 91	+

The conversion percentages were calculated using the FTIR spectra of the respective modified SMI derivatives as documented in Chapter 3 and 4. This calculation was done using the ratio of the peak height of the styrene peak at 703 cm^{-1} and the anhydride carbonyl peak at 1774 cm^{-1}, before and after modification with the relevant surface-functionalization agent, and is described in detail in section 3.5.2(b) and 4.5.2(b) of Chapters 3 and 4, respectively.

It is evident from the results recorded in Table 5.1 that there is not a significant difference in the conversion percentages of the modified polymer or the average fiber diameter of the functionalized nanofibers, with the exception of SMI-qC_{16}, showing a big standard deviation on the average fiber diameter. SMI-qC_{12} and SMI-qC_{16} were modified with the highest conversion percentage, although not significant, and SMI-qC_{12} also had the lowest average fiber diameter.

Different synthetic routes were used to prepare the functionalized nanofibers detailed in Table 5.1: The SMI-qC_{12} and SMI-qC_{16} nanofibers were prepared by modifying the parent polymer, SMA, and thereafter electrospinning the modified polymer to yield the relevant functionalized nanofibers. SMI-tC_{12}, SMI-tC_{16}, SMI-qC_{24} and SMI-qC_{32} were prepared by electrospinning the parent polymer into nanofibers and thereafter surface-functionalizing the nanofibers to yield the relevant functionalized nanofibers. In view of the indication that the nanofibrous surfaces of SMI-qC_{12} and SMI-qC_{16} captured BCG more effectively than those of SMI-tC_{12}, SMI-tC_{16}, SMI-qC_{24} and SMI-qC_{32}, the conclusion could be drawn that the functionalized nanofibers prepared by first modifying the polymer and then electrospinning it yielded better BCG-capturing platforms than the post-electrospun surface-functionalization route. This assumption was however not supported by work done in this study, but not discussed in this study where P(St-*alt*-MAnh) was modified before electrospinning using *N,N*-didodecyl-*N*-propyl-propane-1,3-diamine (qC_{24} – refer Fig. 3.4(c)) and *N,N*-dihexadecyl-*N*-propyl-propane-1,3-diamine (qC_{32} – refer Fig. 3.4(d)), respectively, to yield SMI-qC_{24} and SMI-qC_{32}. qC_{24} and

qC_{32} modified P(St-*alt*-MAnh) with 76% and 75%, respectively. The modified polymers were electrospun to yield functionalized SMI nanofibers and were tested to ascertain if there was a difference in the number of BCG captured onto the surface of the functionalized SMI nanofibers that was modified before electrospinning. Analysis of the SEM and FM images indicated that there was not an increase in the number of BCG captured onto the surfaces of the SMI-qC_{24} and SMI-qC_{32} nanofibers, modified before electrospinning. These results therefore serve as confirmation that the synthetic route used to prepare the functionalized polymer nanofibers did not influence the results of the affinity studies with regard to the effectivity of the functionalized nanofibers as BCG-capturing platform.

As there was no significant difference with regard to conversion percentage, average fiber diameter or the synthetic route used to prepare the functionalized nanofibers, it would be expected that SMI-qC_{24} and SMI-qC_{32} be more effective BCG-capturing platforms due to the longer hydrocarbon chains attached to the quaternary ammonium moiety compared to SMI-qC_{12} and SMI-qC_{16}, resulting in SMI-qC_{24} and SMI-qC_{32} having a more hydrophobic character. It should therefore have captured BCG more effectively due to hydrophobic-hydrophobic interactions between the hydrophobic polymer and the mycolic acids spread throughout the BCG cell wall. However, the results of the affinity studies indicated otherwise. The FM results clearly indicated that the SMI-qC_{12} and SMI-qC_{16} nanofibrous surfaces were more effective capturing platforms for BCG than any of the other functionalized nanofibers. These results therefore indicate that the hydrophobicity due to the C_{24} and C_{32} hydrocarbon chains of SMI-qC_{24} and SMI-qC_{32} may have resulted in poor wetting of these functionalized nanofibers, thus preventing close contact with BCG. The nanofibers functionalized with shorter hydrocarbon chains, such as SMI-qC_{12} and SMI-qC_{16}, would wet better, ensuring better contact with BCG, which resulted in more BCG being captured onto the SMI-qC_{12} and SMI-qC_{16} nanofibrous surface. These results were supported by a study done by Roy *et al*.[51] who investigated the antibacterial activity of cellulose-g-(*poly*(2-dimethylamino)ethyl methacrylate) (PDMAEMA), quaternized with C_8-C_{16} alkyl groups. The results of the study indicated that the antibacterial activity diminished with an increase in alkyl chain length due to decreasing contact between the polymer and *E. coli* as a result of increasing hydrophobicity and decreasing wettability of the polymer.

In conclusion, the combination of ionic and hydrophobic interaction was thus strong enough to capture BCG onto the nanofibrous surfaces of SMI-tC_{12}, SMI-tC_{16}, SMI-qC_{12}, SMI-qC_{16}, SMI-qC_{24} and SMI-qC_{32}. Of these, SMI-qC_{12} and SMI-qC_{16} appeared to capture BCG most effectively. None of the other SMI nanofibers functionalized with just a C_{12} or C_{16} aliphatic hydrocarbon chain (SMI-C_{12} and SMI-C_{16}), or just a positively charged quaternary ammonium moiety without a long aliphatic hydrocarbon chain (SMI-qC_2) were able to capture BCG onto their respective surfaces. It was thus concluded that BCG was captured by a combination of a positive charged centre with a hydrophobic character, such as an aliphatic hydrocarbon chain. The hydrophobic moiety or positive charge moiety on its own was not sufficient for BCG capture.

a) Time studies

Time studies were carried out with BCG and SMI-qC_{12} and SMI-qC_{16} nanofibers to determine whether the interaction between BCG and these polymers were dependent on time. The interaction between BCG and SMI-qC_{12} and SMI-qC_{16}, respectively, after incubation with BCG at 37 °C and pH 2 for 15 min., 30 min., 45 min. and 60 min. were visualized using SEM and FM. Refer Figure 5.10 for the representative SEM images (left) and FM images (right) of the washed SMI-qC_{12} nanofibers after incubation with BCG at 37 °C and pH 2 for the specified time periods.

(a)

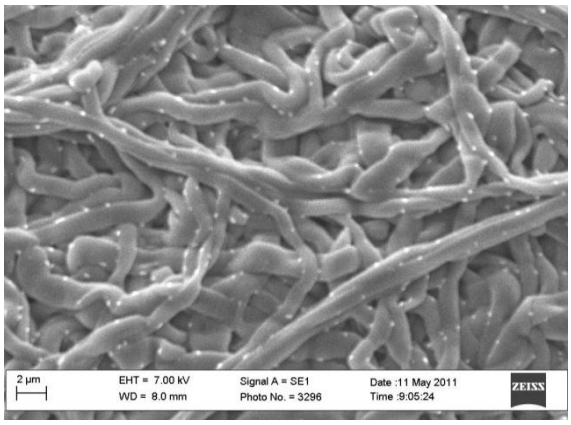

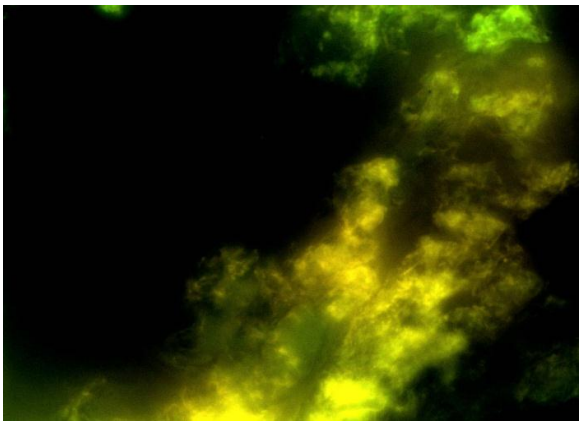

(b)

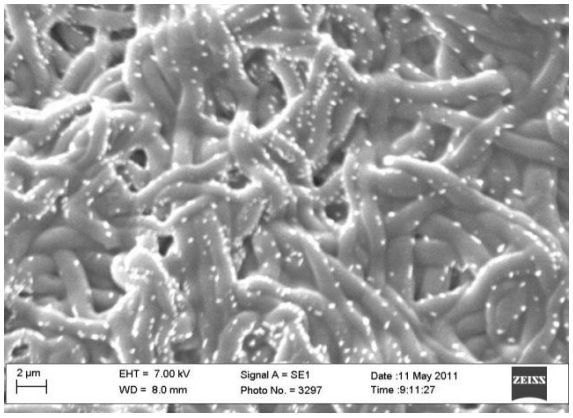

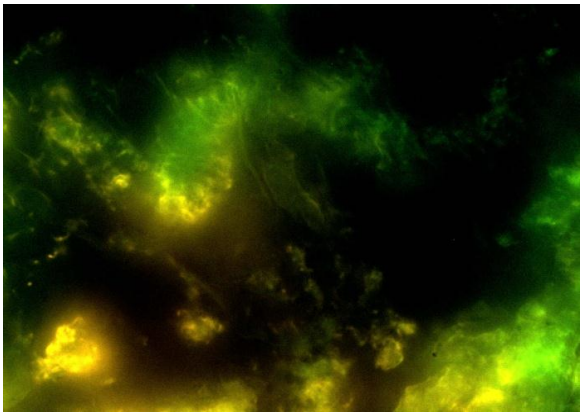

(c)

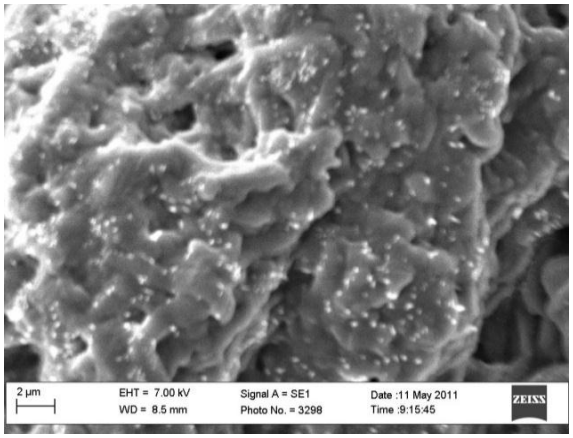

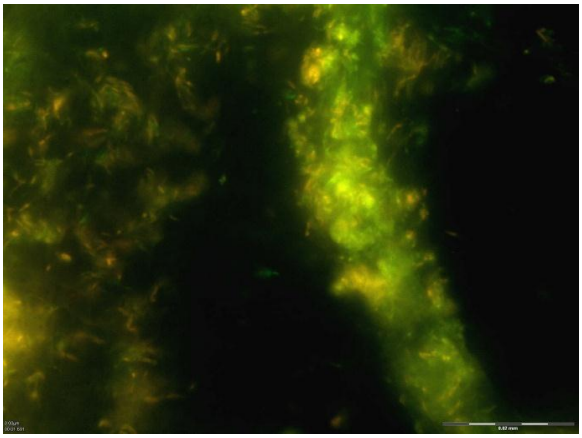

(d)

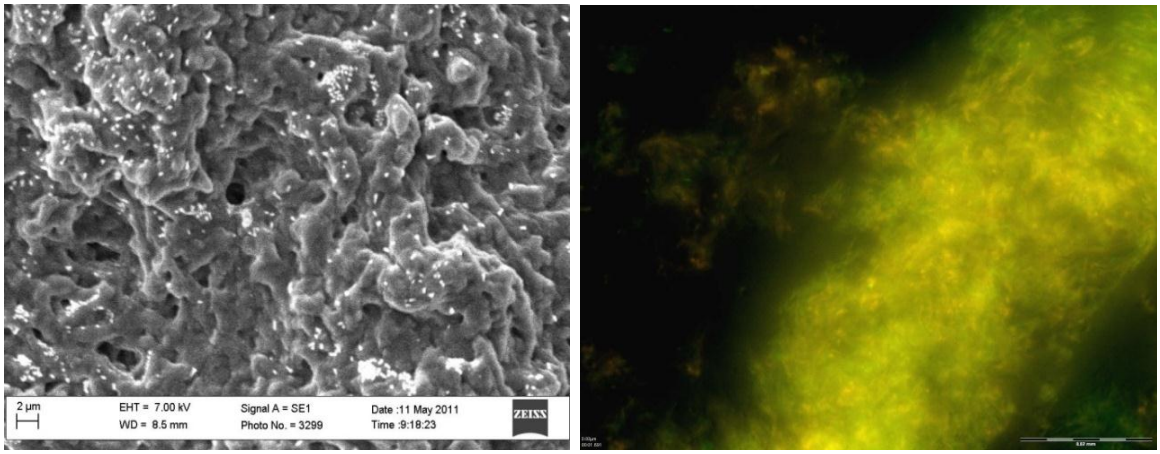

Figure 5.10 SEM images (left) and FM images (right) of the washed SMI-qC$_{12}$ nanofibers after incubation with BCG at 37 °C and pH 2 for (a) 15 min., (b) 30 min., (c) 45 min. and (d) 60 min.

Analysis of the SEM images (Figure 5.10 left) indicated that the number of BCG captured onto the surface of the SMI-qC$_{12}$ nanofibers appeared to increase with an increase in incubation time. These SEM results were confirmed by the FM images (Figure 5.10 right), which also indicated an increase in the number of BCG captured onto the surface of the SMI-qC$_{12}$ nanofibers with an increase in incubation time.

Based on the SEM and FM images of Figure 5.10, it can be concluded that the extent of interaction between BCG and the surface of the SMI-qC$_{12}$ nanofibers appeared to be a function of time. The longer the incubation time between BCG and the SMI-qC$_{12}$ nanofibers, the more BCG was captured onto the surface of these polymer nanofibers.

Analysis of the SEM and FM images of the washed SMI-qC$_{16}$ nanofibers after incubation with BCG at 37 °C and pH 2 for 15 min., 30 min., 45 min. and 60 min. showed a similar trend to that of the SMI-qC$_{12}$ nanofibers, with an increase in the number of BCG captured onto the surface of the SMI-qC$_{16}$ nanofibers with an increase in incubation time (results not shown). What was evident from the SEM and FM images of the time studies of SMI-qC$_{12}$ (Fig. 5.10), compared to that of SMI-qC$_{16}$, was that a higher number of BCG was captured onto the surface of the SMI-qC$_{12}$ nanofibers than on the SMI-qC$_{16}$ nanofibers at each specified time period. The surface of the SMI-qC$_{12}$ nanofibers therefore appeared to capture BCG more effectively than the surface of the SMI-qC$_{16}$ nanofibers.

b) Concentration studies

Concentration studies were also carried out with BCG and SMI-qC$_{12}$ and SMI-qC$_{16}$ nanofibers to determine whether the interaction between BCG and these polymers were dependent on the concentration of BCG. Interaction between SMI-qC$_{12}$ and SMI-qC$_{16}$, respectively, and decreasing concentrations of BCG at pH 2 were visualized using SEM and FM. Refer Figure 5.11 for the

representative SEM and FM images of the washed SMI-qC_{12} nanofibers, after incubation with decreasing concentrations of BCG at 37 °C and pH 2 for one hour.

(a) 10^8 BCG/mL

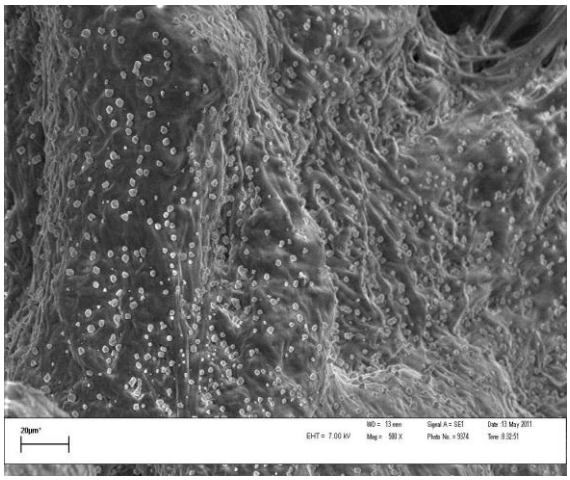

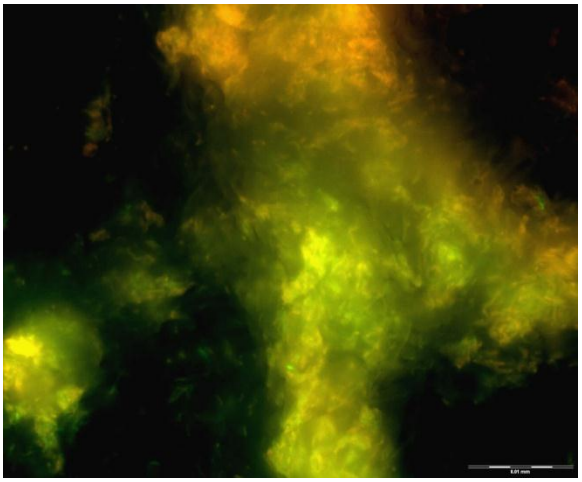

(b) 10^7 BCG/mL

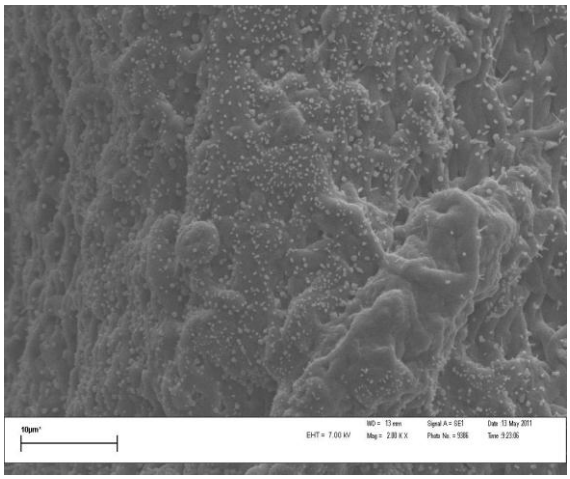

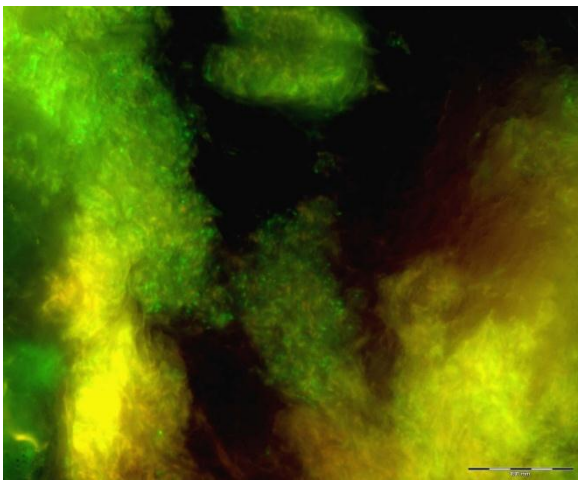

(c) 10^6 BCG/mL

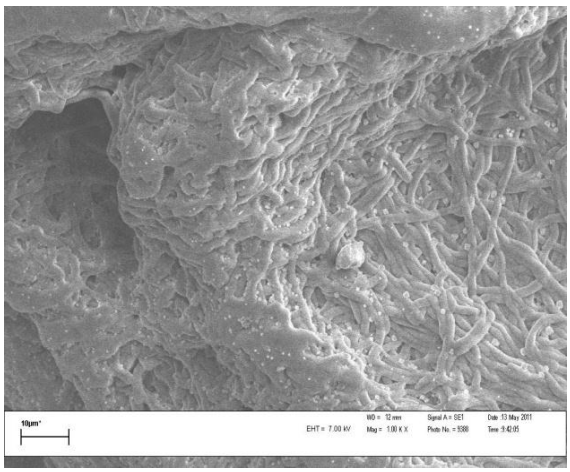

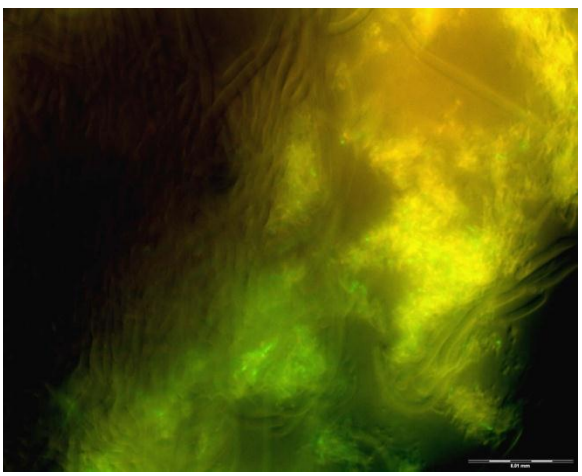

(d) 10^5 BCG/mL

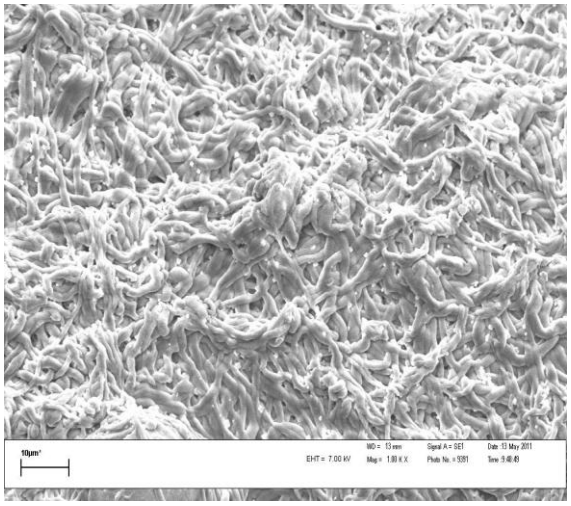

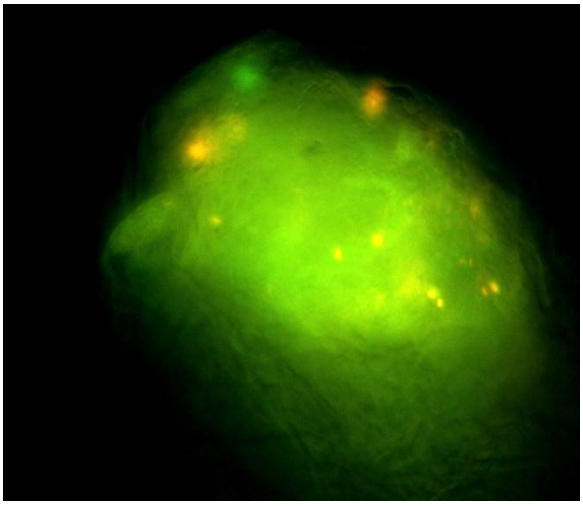

(e) 10^4 BCG/mL

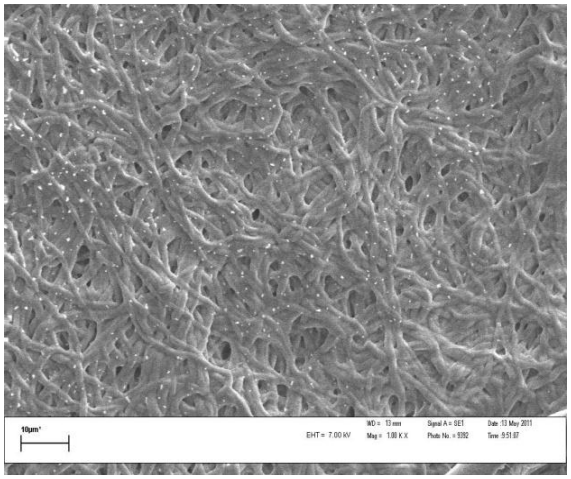

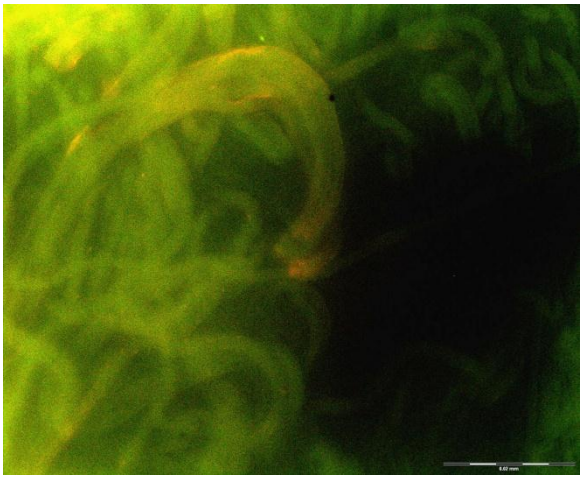

(f) 10^3 BCG/mL

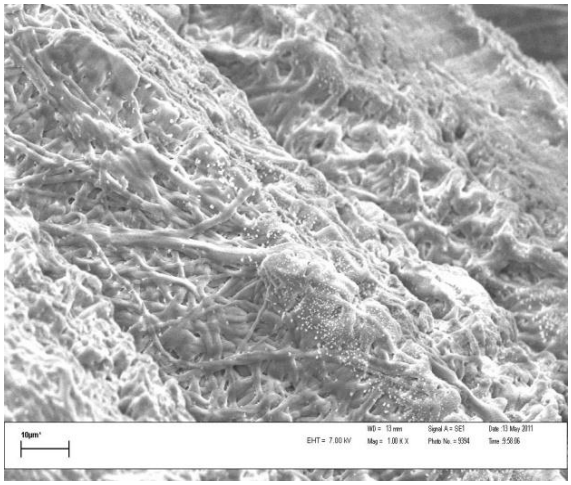

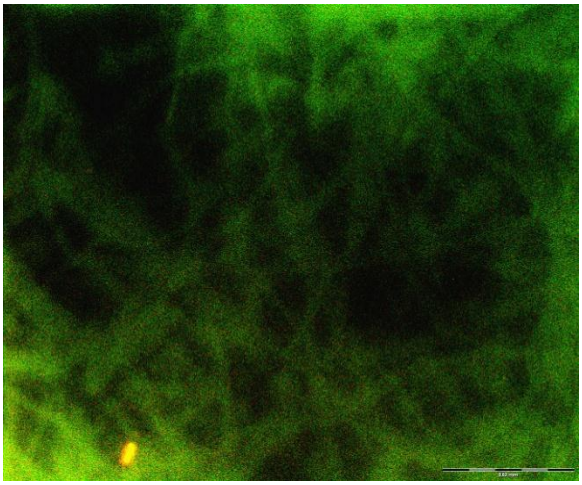

(g) 10^2 BCG/mL

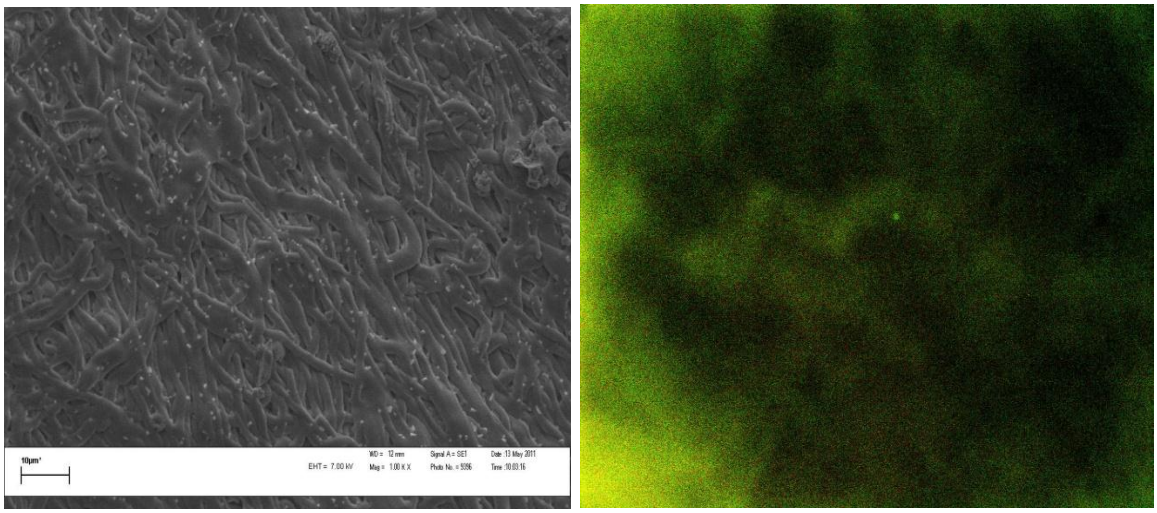

(h) 10 BCG/mL

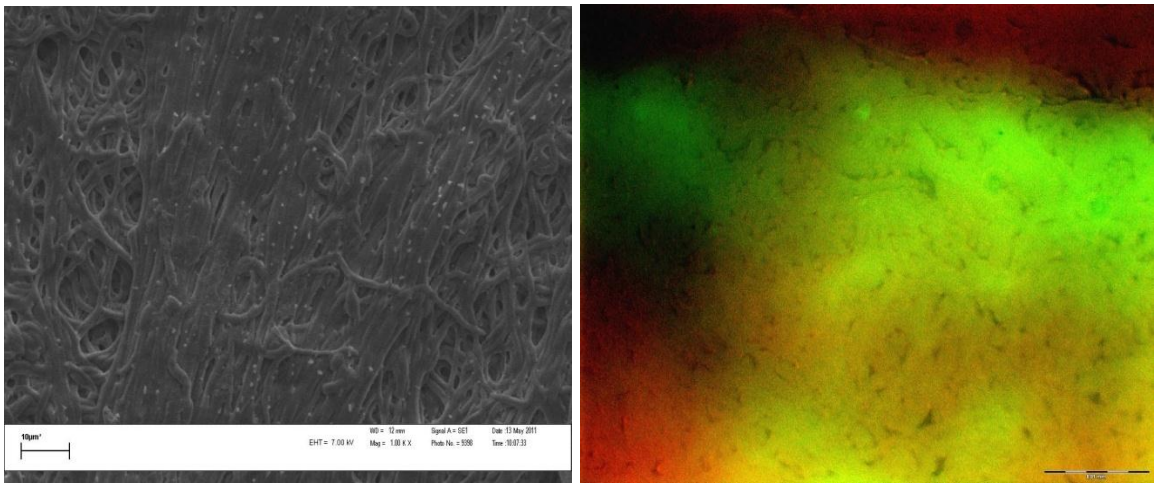

(i) PBS

Figure 5.11 SEM images (left) and FM images (right) of the washed SMI-qC$_{12}$ nanofibers after incubation with decreasing concentrations of BCG at 37 °C and pH 2 for one hour.

Analysis of the SEM images of Figure 5.11 indicated that the number of BCG captured onto the SMI-qC_{12} nanofibrous surface appeared to decrease with a decreasing concentration of BCG from approximately 10^8 BCG/mL to 10 BCG/mL. These SEM results did not correlate with the FM images of Figure 5.11. According to the FM images, no BCG was visibly captured onto the SMI-qC_{12} nanofibrous surface at a concentration below 10^5 BCG/mL. These FM results correlated well with literature in which it is documented that 5000-10 000 acid-fast bacilli/mL are required to give a positive microscopy result.[52-54]

Based on these results it is evident that there is not a good correlation between the SEM and FM results of the washed SMI-qC_{12} nanofibers after incubation with decreasing concentrations of BCG. Although there is not an accurate correlation between the SEM and FM results, it can be concluded that the extent of interaction between BCG and the SMI-qC_{12} nanofibers is indeed a function of concentration. The higher the concentration of BCG, the more BCG was captured onto the surface of the said polymer nanofibers.

Analysis of the SEM images of washed SMI-qC_{16} nanofibers after incubation with decreasing concentrations of BCG at 37 °C and pH 2 showed a similar trend to that of Figure 5.11, with a decrease in the number of BCG captured onto the surface of SMI-qC_{16} nanofibers with a decreasing concentration of BCG from approximately 10^8 BCG/mL to 10 BCG/mL. The FM images however indicated that the number of BCG captured onto the SMI-qC_{16} nanofibrous surface seemed to decrease with a decreasing concentration of BCG from 10^8 BCG/mL to 10^5 BCG/mL. No BCG was visibly captured onto the surface of the SMI-qC_{16} polymer nanofibers at a concentration below 10^5 BCG/mL (results not shown).

When comparing the FM images of the washed SMI-qC_{12} and SMI-qC_{16} nanofibers after incubation with decreasing concentrations of BCG, it is evident that more BCG appeared to have been captured onto the surface of the SMI-qC_{12} nanofibers than on the SMI-qC_{16} nanofibers. The surface of the SMI-qC_{12} nanofibers therefore appeared to capture BCG more effectively than that of SMI-qC_{16}.

The results of the time and concentration studies between BCG and the SMI-qC_{12} and SMI-qC_{16} nanofibers at pH 2 indicated that SMI-qC_{12} nanofibers captured BCG more effectively than the SMI-qC_{16} nanofibers. A possible explanation for this result may be that the increase in the alkyl chain length of SMI-qC_{16}, compared to SMI-qC_{12}, resulted in an increase in the hydrophobicity of the modified polymer, thus limiting the contact between BCG and the SMI-qC_{16} nanofibers due to poor wetting of the polymer by the BCG culture.

The extent of interaction between SMI-qC_{12} and BCG was also analysed using PCR. Refer Figure 5.12 for a representative image of the agarose gel analysis of the PCR products of BCG after the affinity study between SMI-qC_{12} and decreasing concentrations of BGC.

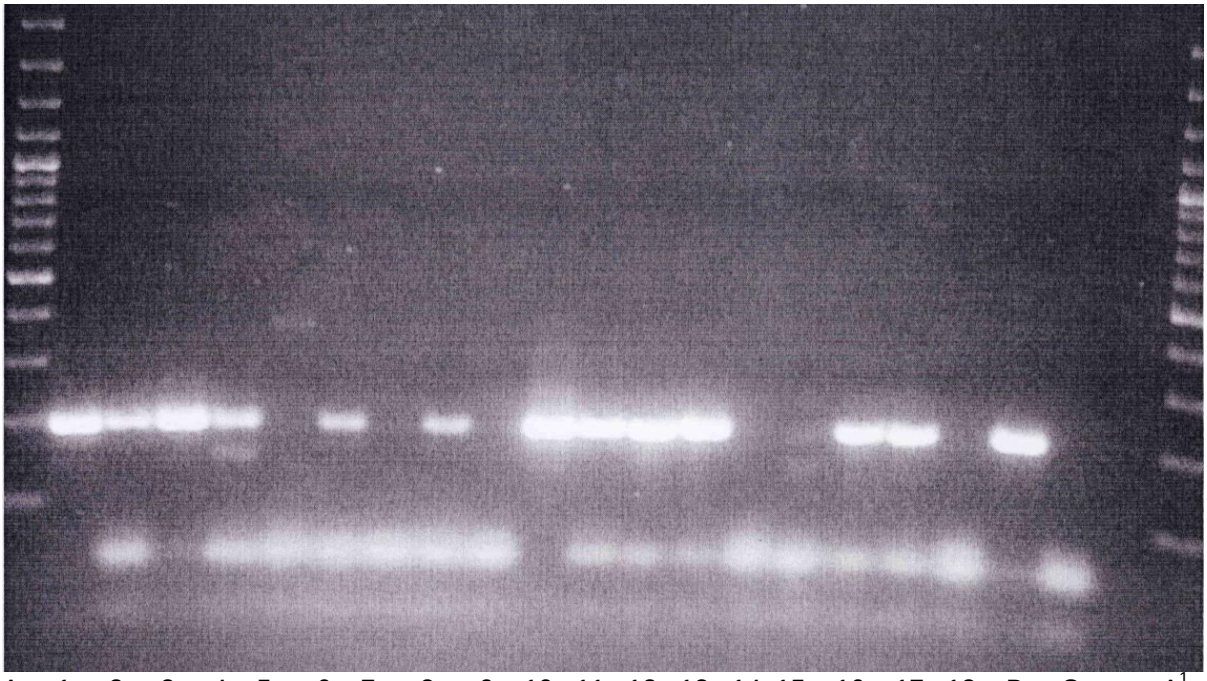

Figure 5.12 PCR products in a 2.5% agarose gel for BCG concentration studies. Lanes A and A[1] contain DNA 100 bp size marker, lane B contains lysed BCG as positive control and lane C contains H_2O as negative control. Numbered lanes contain the following PCR products of decreasing concentration of BCG incubated with SMI-qC_{12}: lanes 1 and 10, 10^8 cells; lanes 2 and 11, 10^7 BCG/mL; lanes 3 and 12, 10^6 BCG/mL; lanes 4 and 13, 10^5 BCG/mL; lanes 5 and 14, 10^4 BCG/mL; lanes 6 and 15, 10^3 BCG/mL; lanes 7 and 16, 10^2 BCG/mL; lanes 8 and 17, 10 BCG/mL; lanes 9 and 18, 0 cells.

The PCR gel shows clear and distinct bands at 196 bp for the presence of BCG at concentration levels of 10^8 BCG/mL to 10^5 BCG/mL for both sets, as well as 10^3 and 10 BCG/mL for the one set and 10^2 and 10 BCG/mL for the other set, indicating that SMI-qC_{12} was able to capture BCG at a concentration of 10 BCG/mL and higher. There are some bands in the duplicate sets that did not amplify properly. A possible explanation for this occurrence may be that the DNA of BCG was not properly released during the DNA purification procedure and was therefore not detected by PCR, or that the DNA was lost during the amplification process. Non-specific bands of primer dimers at approximately 50 bp were sometimes present on the gel that has no bearing on this study. These may be as a result of non-specific amplified products or the formation of primer dimers.

Based on these results, it was decided to use the SMI-qC_{12} nanofibers for the subsequent affinity studies with *Mycobacterium tuberculosis* (*M. tuberculosis)* at low pH to determine whether the SMI-qC_{12} nanofibrous surface could capture *M. tuberculosis.*

5.3.3 Analysis of the interaction between *M. tuberculosis* and SMI-qC$_{12}$ at low pH

Interaction between SMI-qC$_{12}$ and decreasing concentrations of *M. tuberculosis* after incubation at 37 °C and pH 2 was visualized using FM and conventional light microscopy with ZN staining (LM). PCR, a molecular detection method, was used as an alternative detection method. Refer Figure 5.13 for the representative FM images (left) and LM images (right) of the washed SMI-qC$_{12}$ nanofibers after incubation with decreasing concentrations of *M. tuberculosis* at 37 °C and pH 2 for one hour.

(a) 10^8 *M. tuberculosis*/mL

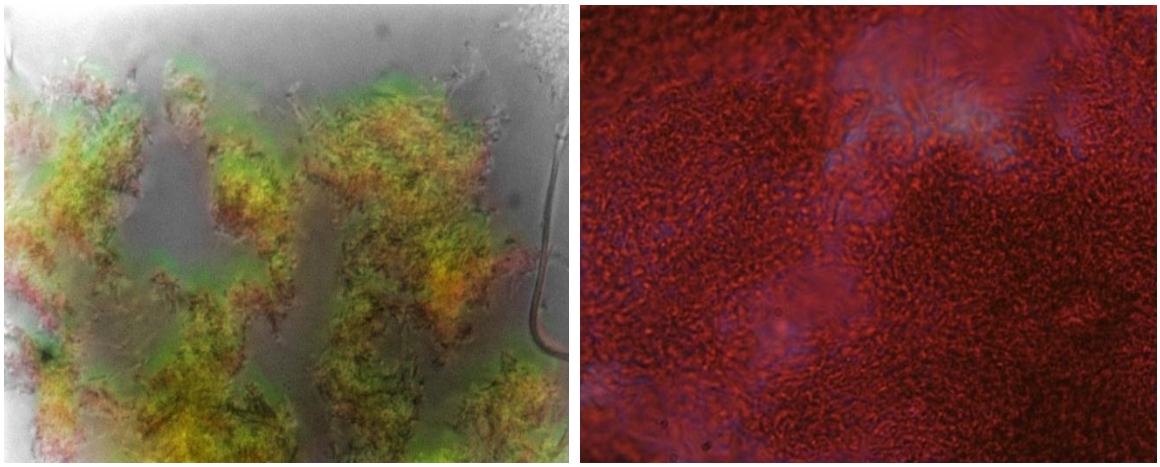

(b) 10^7 *M. tuberculosis*/mL

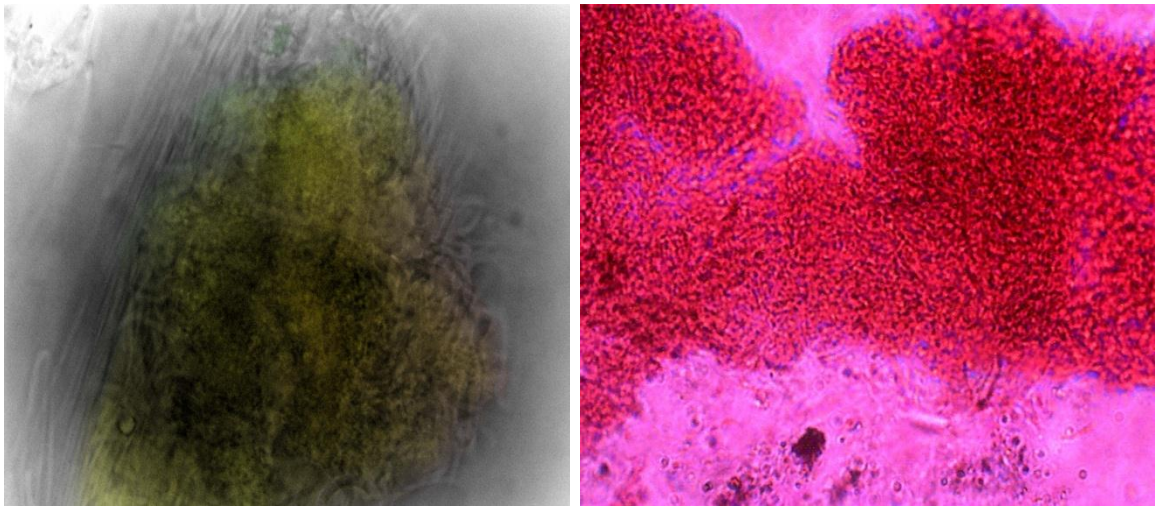

(c) 10^6 *M. tuberculosis*/mL

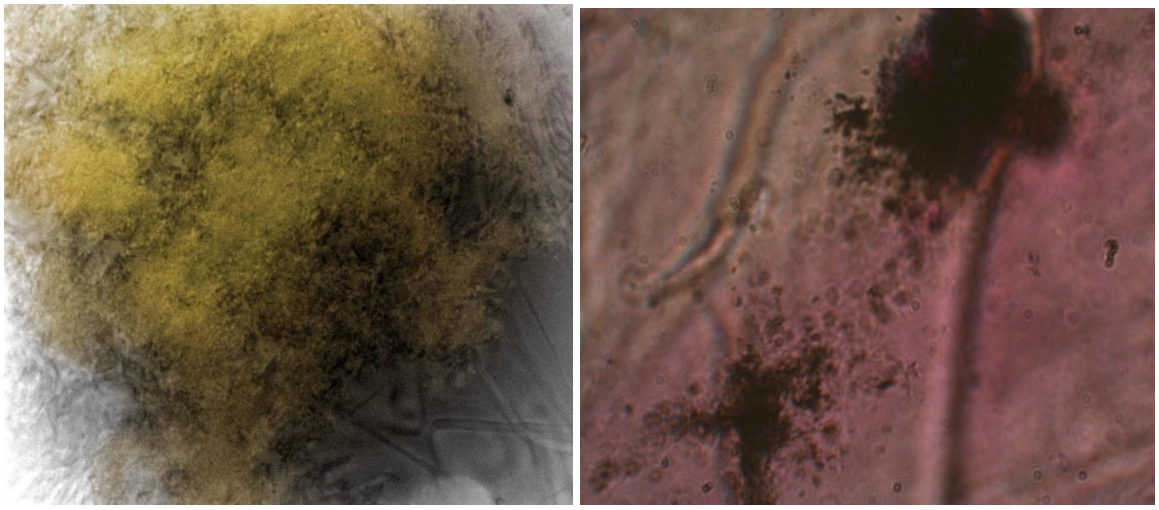

(d) 10^5 *M. tuberculosis*/mL

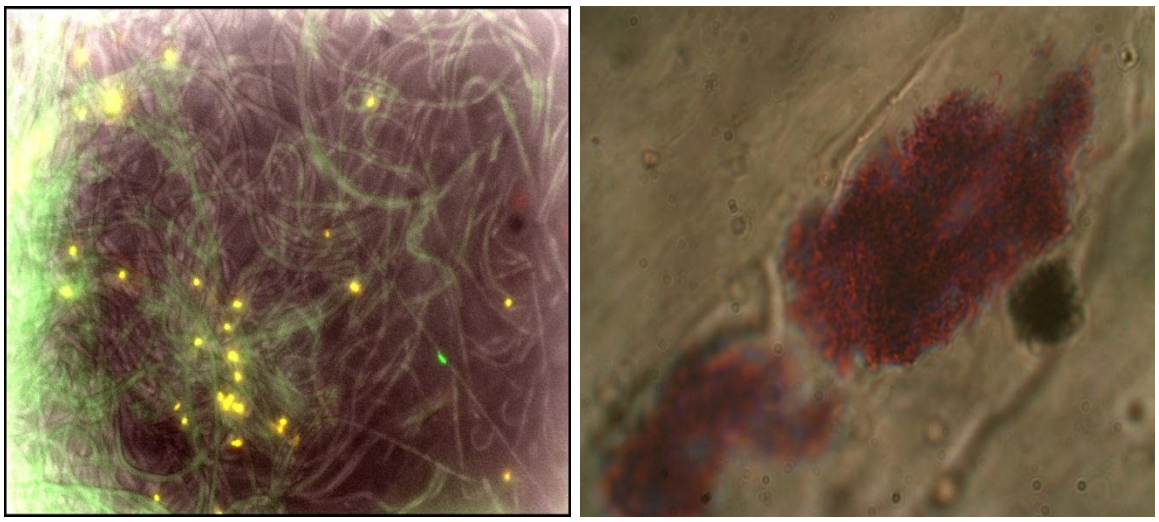

(e) 10^4 *M. tuberculosis*/mL

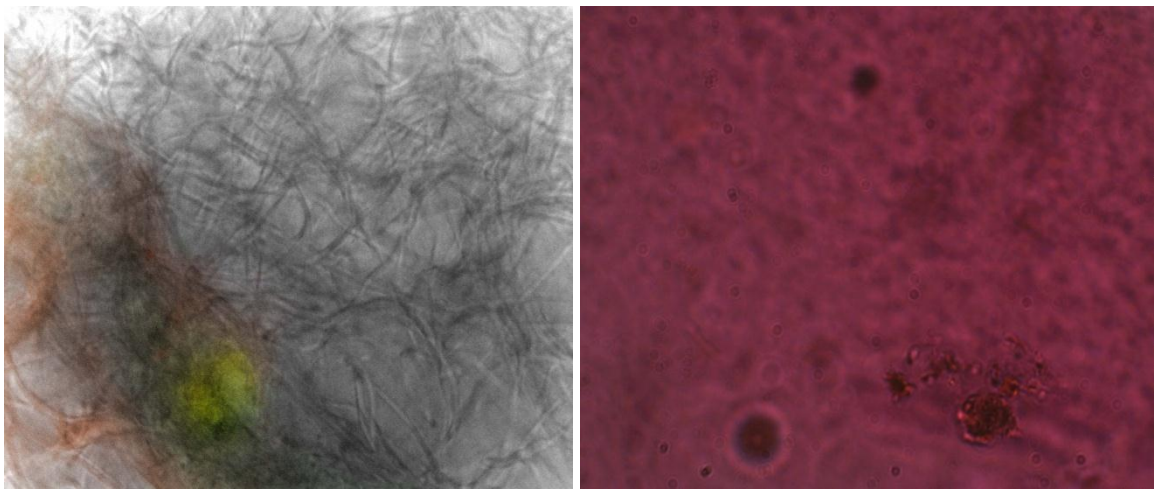

(f) 10^3 *M. tuberculosis*/mL

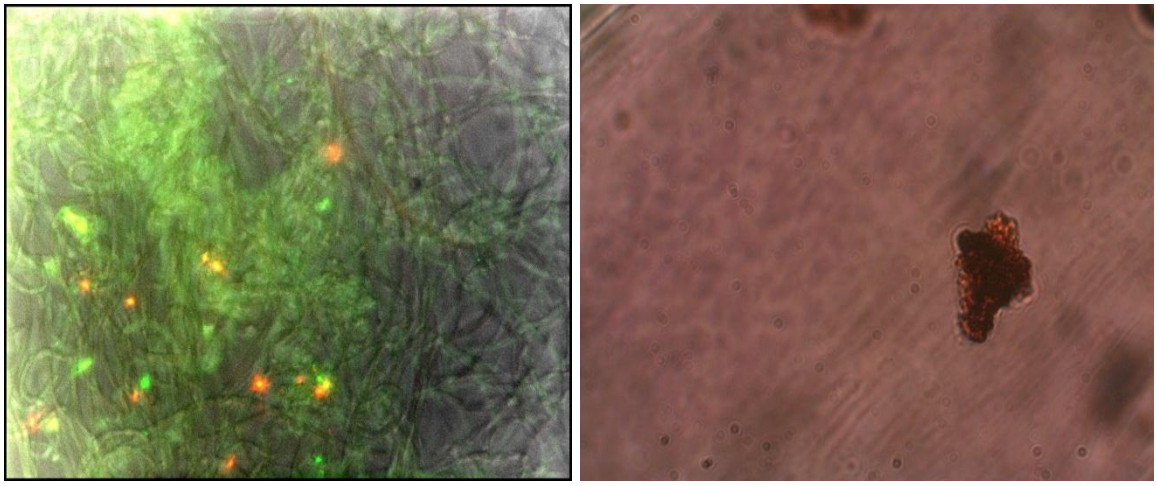

(g) 10^2 *M. tuberculosis*/mL

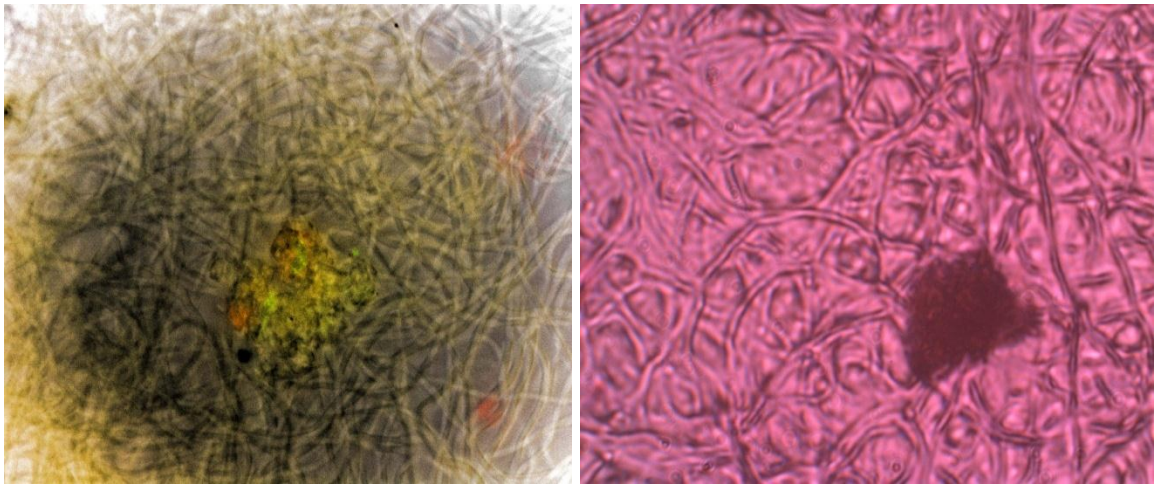

(h) 10 *M. tuberculosis*/mL

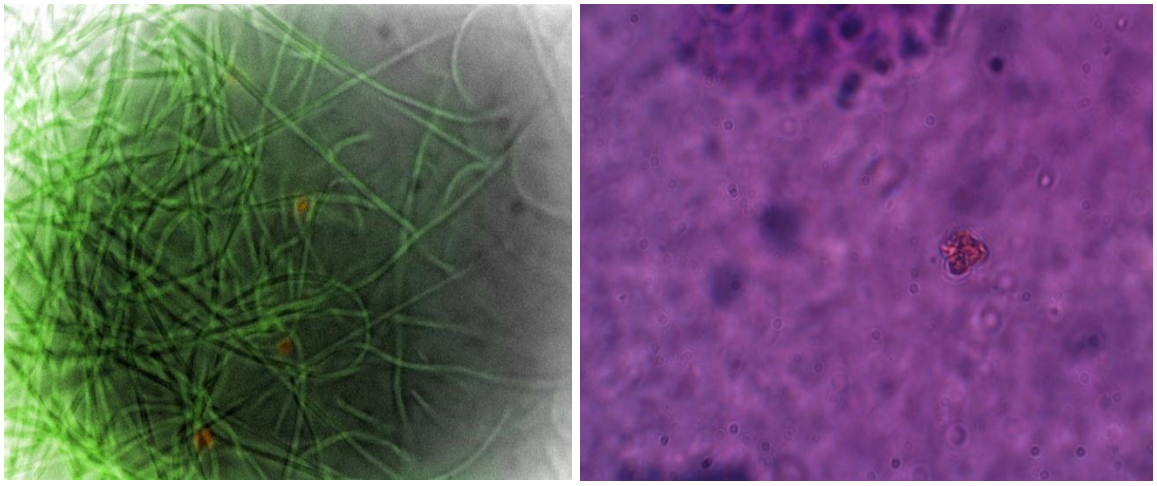

(i) PBS

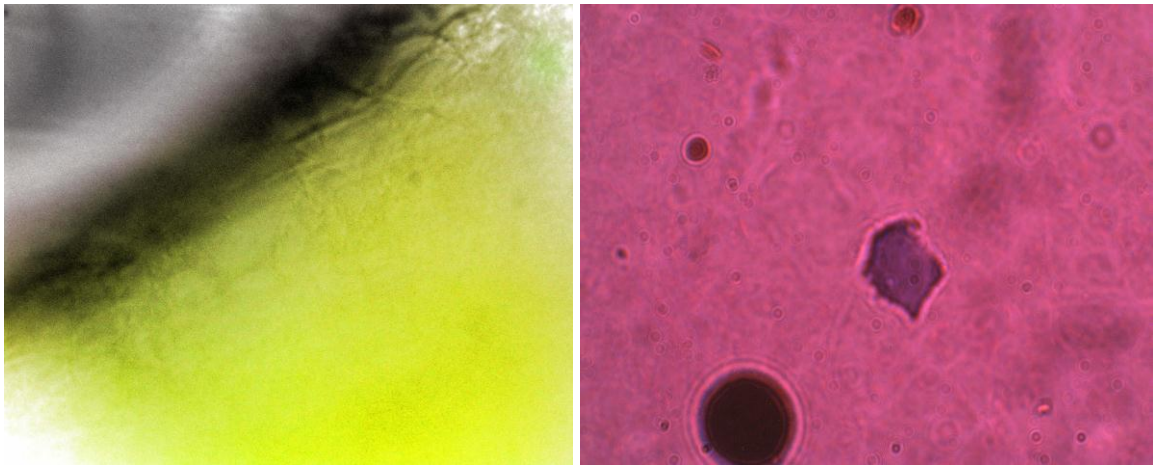

Figure 5.13 FM images (left) and LM images (right) of washed SMI-qC$_{12}$ nanofibers after incubation with decreasing concentrations of M. tuberculosis at 37 °C and pH 2 for one hour.

The FM images of the washed SMI-qC$_{12}$ nanofibers (Figure 5.13 left) indicated that *M. tuberculosis* was captured onto the surface of these nanofibers as indicated by the red and green stained microbes in Figure 5.13(a). Analysis of the FM images further indicated that the number of *M. tuberculosis* captured onto the SMI-qC$_{12}$ nanofibrous surface appeared to decrease with a decreasing concentration of *M. tuberculosis* from approximately 10^8 *Mtb*/mL to 10^2 *Mtb*/mL. According to the FM images, no *M. tuberculosis* was captured onto the surface of the SMI-qC$_{12}$ nanofibers at a concentration below 10^2 *Mtb*/mL. These results differ from literature where it is reported that 5000-10 000 acid-fast bacilli/mL are required to give a positive microscopy result.[52-54] A possible explanation for this result may be that the inclination of *M. tuberculosis* to clump together in clusters on the hydrophobic surface of the SMI-qC$_{12}$ nanofibers, made it easier for the microscope operator to see them. The microbes are not spread out and do not need to be identified individually. An alternative explanation may be that there were more than 100 bacilli/mL present.

The LM images of the washed SMI-qC$_{12}$ nanofibers (Figure 5.13 right) indicated that *M. tuberculosis* was captured onto the surface of the said nanofibers as evidenced by the dark pink stained microbes in Figure 5.13(a). Analysis of the LM images further indicated that the number of *M. tuberculosis* captured onto the SMI-qC$_{12}$ nanofibrous surface appeared to decrease with a decreasing concentration of *M. tuberculosis* from approximately 10^8 *Mtb*/mL to 10^2 *Mtb*/mL. According to the LM images, no *M. tuberculosis* was captured onto the SMI-qC$_{12}$ nanofibrous surface at a concentration below 10^2 *Mtb*/mL.

Based on these FM and LM results it can be concluded that *M. tuberculosis* can be captured onto the SMI-qC$_{12}$ nanofibrous surface due to ionic interaction between the negatively charged *M. tuberculosis* cell wall and the positively charged quaternary ammonium moiety of the functionalized polymer, as well as the hydrophobic-hydrophobic interaction between the mycolic acids of the *M. tuberculosis* cell wall and the aliphatic C$_{12}$ hydrocarbon chain of the functionalized polymer. This interaction is also a

function of concentration, i.e. the higher the concentration of *M. tuberculosis*, the more *M. tuberculosis* is captured onto the nanofibrous surface.

PCR was also used as diagnostic tool to determine the extent of interaction between *M. tuberculosis* and the surface of the SMI-qC_{12} nanofibers. Refer Figure 5.14 for a representative image of the agarose gel analysis of the PCR products of *M. tuberculosis* after the affinity study between SMI-qC_{12} and decreasing concentrations of *M. tuberculosis*.

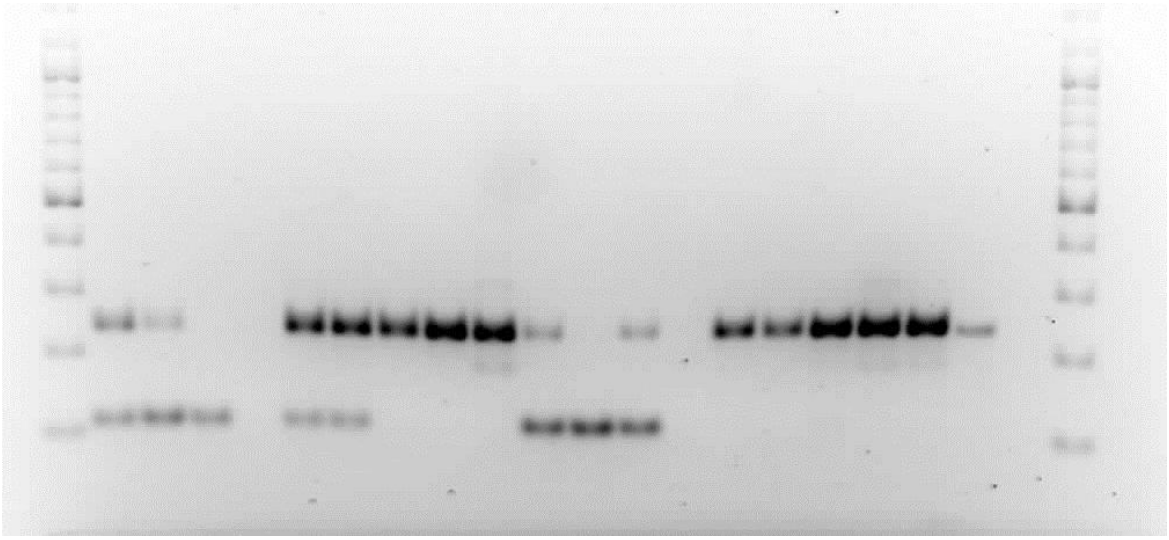

A 1 2 3 4 5 6 7 8 9 10 11 12 13 14 15 16 17 18 B C A^1

Figure 5.14 PCR products in a 2.5% agarose gel for M. tuberculosis concentration studies. Lanes A and A^1 contain DNA 100 bp size markers, lane B contains lysed M. tuberculosis as positive control and lane C contains H_2O as negative control. Numbered lanes contain the following PCR products of increasing concentration of M. tuberculosis incubated with SMI-qC_{12}: lanes 1 and 10, 0 cells; lanes 2 and 11, 10 Mtb/mL; lanes 3 and 12, 10^2 Mtb/mL; lanes 4 and 13, 10^3 Mtb/mL; lanes 5 and 14, 10^4 Mtb/mL; lanes 6 and 15, 10^5 Mtb/mL; lanes 7 and 16, 10^6 Mtb/mL; lanes 8 and 17, 10^7 Mtb/mL; lanes 9 and 18, 10^8 Mtb/mL.

The PCR gel shows clear and distinct bands at 235 bp for the presence of *M. tuberculosis* at concentration levels of 10^4 *Mtb*/mL to 10^8 *Mtb*/mL and faint bands at 10 *Mtb*/mL and 10^2 *Mtb*/mL, indicating that SMI-qC_{12} was able to capture *M. tuberculosis* at a concentration of 10 *Mtb*/mL and higher. There are some bands in the duplicate sets that did not amplify properly. A possible explanation for this occurrence may be that the DNA of *M. tuberculosis* was not properly released during the DNA purification procedure and was therefore not detected by PCR, or that the DNA was lost during the amplification process. The faint bands in lanes 1 and 10 at 235 bp may indicate some cross contamination during the DNA extraction process. Non-specific bands of primer dimers at approximately 115 bp were sometimes present on the gel. These may be as a result of non-specific amplified products or primer dimers.[55]

The bands on the PCR gel, correlating to *M. tuberculosis* DNA, also showed an increase in intensity from 10^4 *Mtb*/mL to 10^8 *Mtb*/mL, indicating an increase in the amount of *M. tuberculosis* DNA detected

through amplification. This result correlates well with the results from the FM and LM images that also showed an increase in the amount of *M. tuberculosis* captured by SMI-qC_{12} with an increase in the concentration level of *M. tuberculosis*.

In conclusion, the FM, LM and PCR results indicated that the SMI-qC_{12} nanofibrous surface was able to capture *M. tuberculosis* effectively at low pH conditions and that this interaction was concentration dependent.

5.3.4 Comparative affinity study using Entero-string and *M. tuberculosis*

Interaction between the Entero-string and decreasing concentrations of *M. tuberculosis* after incubation at 37 °C and pH 2 were evaluated using FM, LM and PCR. Figure 5.15 shows representative FM images of the washed Entero-string after incubation with decreasing concentrations of *M. tuberculosis* at 37 °C and pH 2 for one hour. LM images could not be taken as the string was saturated by the staining chemicals used in the ZN staining protocol and could therefore not be visualized using conventional light microscopy.

(a) 10^8 *M. tuberculosis*/mL

(b) 10^7 *M. tuberculosis*/mL

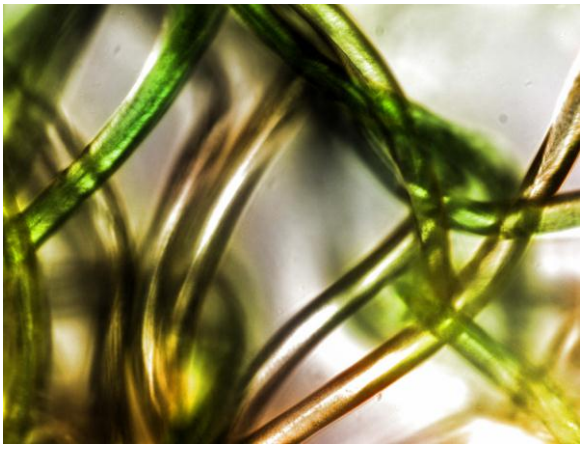

(c) 10^6 *M. tuberculosis*/mL

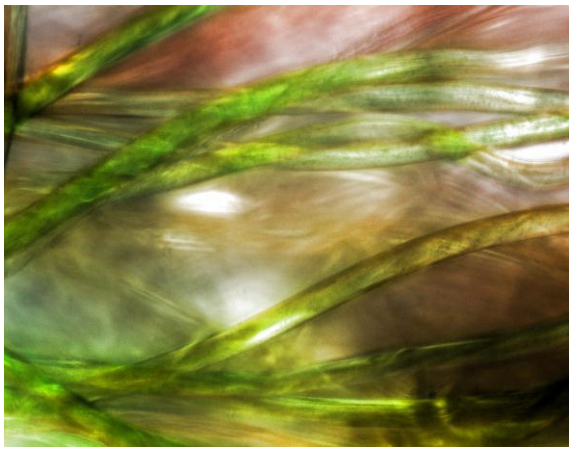

(d) 10^5 *M. tuberculosis*/mL

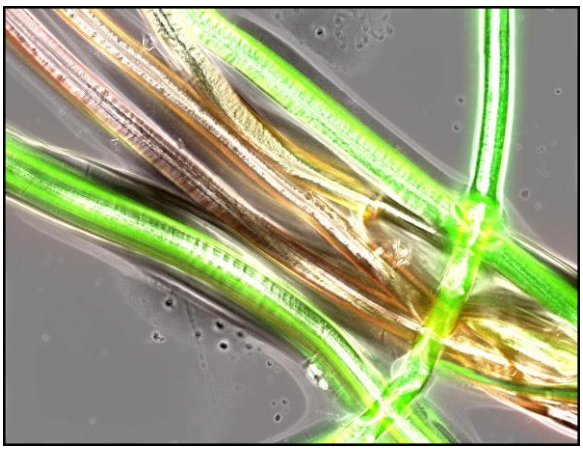

(e) 10^4 *M. tuberculosis*/mL

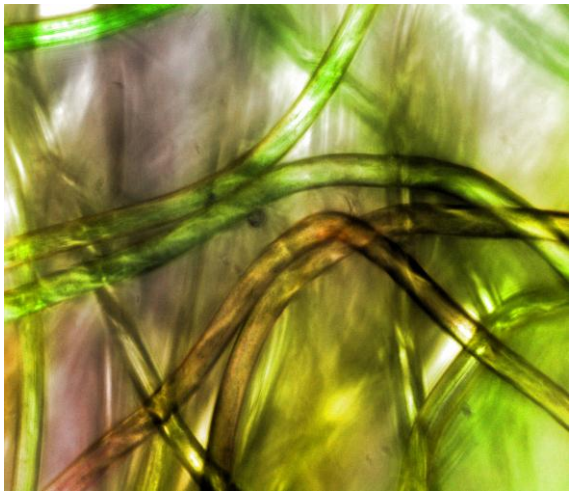

(f) 10^3 *M. tuberculosis*/mL

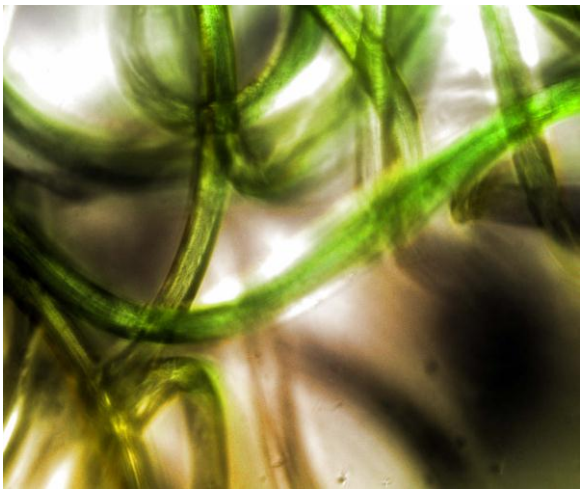

(g) 10^2 *M. tuberculosis*/mL

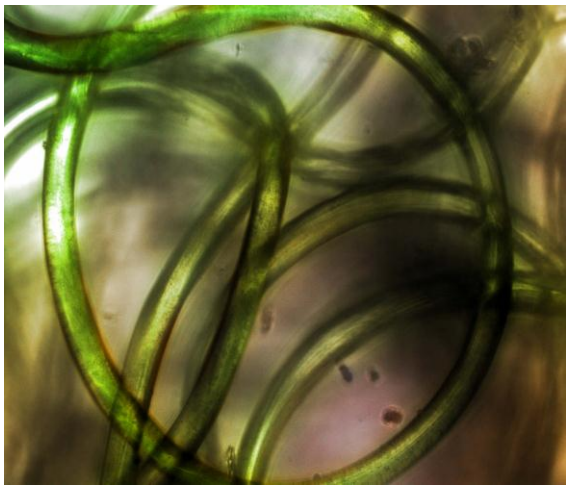

(h) 10 *M. tuberculosis*/mL

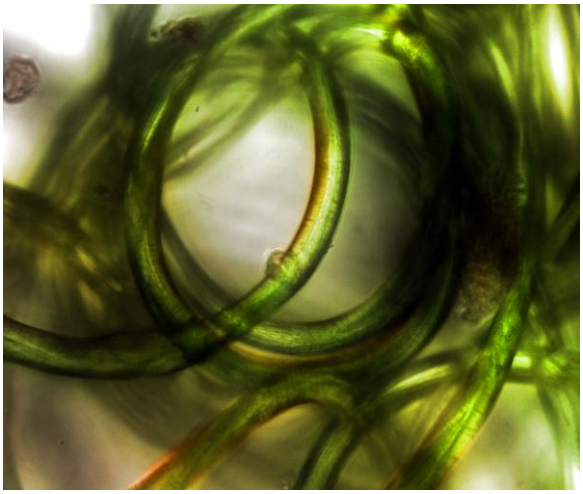

(i) PBS

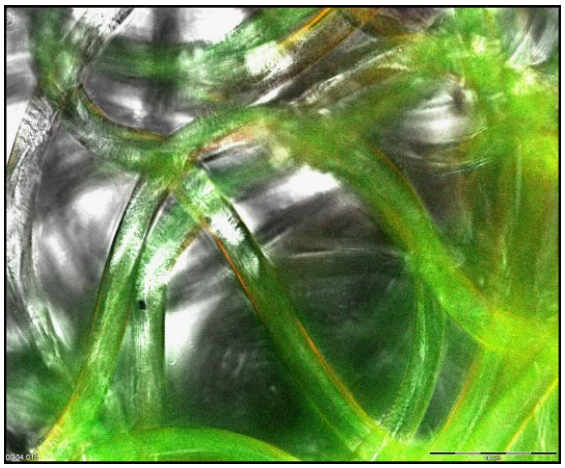

Figure 5.15 FM images of the washed Entero-string after incubation with decreasing concentrations of M. tuberculosis at 37 °C and pH 2 for one hour.

The FM images of the washed Entero-string (Figure 5.15) indicated that *M. tuberculosis* was not captured onto the surface of the Entero-string as no mycobacteria was visible on the FM images.

PCR was used as additional detection method to determine the extent of interaction between *M. tuberculosis* and the Entero-string. Refer to Figure 5.16 for a representative image of the agarose gel analysis of the PCR products of *M. tuberculosis* after the affinity study between the Entero-string and decreasing concentrations of *M. tuberculosis*.

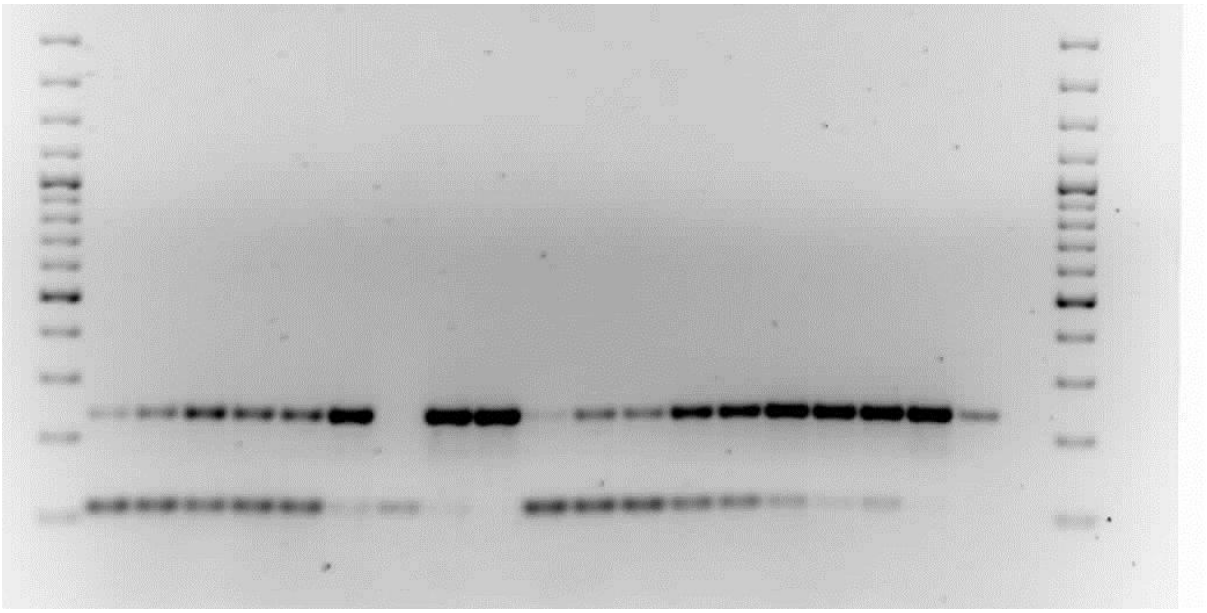

A 1 2 3 4 5 6 7 8 9 10 11 12 13 14 15 16 17 18 B C A^1

Figure 5.16 PCR products in a 2.5% agarose gel for M. tuberculosis concentration studies. Lanes A and A^1 contain DNA 100 bp size markers, lane B contains lysed M. tuberculosis as positive control and lane C contains H_2O as negative control. Numbered lanes contain the following PCR products of increasing concentration of M. tuberculosis incubated with the Entero-string: lanes 1 and 10, 0 cells; lanes 2 and 11, 10 Mtb/mL; lanes 3 and 12, 10^2 Mtb/mL; lanes 4 and 13, 10^3 Mtb/mL; lanes 5 and 14, 10^4 Mtb/mL; lanes 6 and 15, 10^5 Mtb/mL; lanes 7 and 16, 10^6 Mtb/mL; lanes 8 and 17, 10^7 Mtb/mL; lanes 9 and 18, 10^8 Mtb/mL.

The PCR gel shows clear and distinct bands at 235 bp for the presence of *M. tuberculosis* at concentration levels of 10 *Mtb*/mL to 10^8 *Mtb*/mL, indicating that the Entero-string was able to capture *M. tuberculosis* at a concentration of 10 *Mtb*/mL and higher. There is one band in the first set that did not amplify properly. A possible explanation for this occurrence may be that the DNA was lost during the amplification process. The faint bands in lanes 1 and 10 at 235 bp may indicate some cross contamination during the DNA extraction process. Non-specific bands of primer dimers at approximately 115 bp were sometimes present on the gel that has no bearing on this study. These may be as a result of primer dimers.[55] The bands on the PCR gel, correlating to *M. tuberculosis* DNA, also showed an increase in intensity from 10 *Mtb*/mL to 10^8 *Mtb*/mL, indicating an increase in the amount of *M. tuberculosis* DNA detected through amplification.

This PCR result did not correlate with the results from the FM images that showed that no *M. tuberculosis* was captured by the Entero-string at any of the *M. tuberculosis* concentration levels. A possible explanation for this result may be that there is a non-specific interaction between *M. tuberculosis* and the Entero-string, i.e. *M. tuberculosis* is not chemically captured by the string, but rather 'taken up' by the string when it swells in the aqueous environment containing the mycobacteria. As the *M. tuberculosis* was not attached to the string, it could not be detected when the Entero-string was imaged using FM, or the *M. tuberculosis* was not detected due to the microbes being spread out, making detection of individual microbes difficult.

In conclusion, the PCR results indicated that the Entero-string was able to capture *M. tuberculosis* at low pH conditions and that this interaction was concentration dependent.

5.4 Conclusion

BCG, used initially as non-pathogenic *M. tuberculosis*-mimic, was successfully captured onto the surfaces of SMI nanofibers, functionalized with amino sugars, an amino acid derivative, a protein and a C_{12} aliphatic quaternary ammonium group, respectively, at neutral pH. After the pH was decreased to 2 to simulate gastric conditions, BCG could only be captured onto the surface of the SMI nanofibers functionalized with a C_{12} aliphatic quaternary ammonium group, namely SMI-qC_{12}. This result prompted an investigation between BCG and SMI polymers, modified with a variety of N-alkylamines of varying aliphatic chain lengths and N-functionalities to determine which N-functionality/aliphatic chain length combination captured BCG most effectively. The SMI nanofibers functionalized with a C_{12} and C_{16} aliphatic tertiary amine group, as well as C_{12}, C_{16}, C_{24} and C_{32} aliphatic quaternary ammonium groups, captured BCG successfully. Of these, SMI-qC_{12} and SMI-qC_{16} proved more effective than the others. Subsequent concentration and time studies between SMI-qC_{12} and SMI-qC_{16} and BCG indicated that SMI-qC_{12} was the most effective BCG-capturing platform and that the extent of this interaction was dependent on incubation time and concentration of BCG. The successful capture of BCG onto the surfaces of the various functionalized nanofibers was visualized using SEM and FM. PCR was used as an additional detection method to evaluate the extent of interaction between SMI-qC_{12} and BCG.

Subsequent affinity studies between *M. tuberculosis* and SMI-qC_{12} indicated that SMI-qC_{12} successfully captured *M. tuberculosis* under low pH conditions. The successful capture of *M. tuberculosis* onto the SMI-qC_{12} nanofibrous surface was confirmed by FM, LM and PCR, with good correlation among the results of the different detection methods. The capturing effectivity of the SMI-qC_{12} nanofibers was also compared with that of the original Entero-string. Analysis of the PCR results of the two affinity studies indicated that SMI-qC_{12} and the Entero-string captured *M. tuberculosis* effectively at high concentrations of *M. tuberculosis* (10^4 *Mtb*/mL and higher). Further analysis of the PCR results however indicated that the Entero-string was able to capture *M. tuberculosis* more

effectively at the lower concentration levels than SMI-qC_{12}, or the *M. tuberculosis* DNA was released more quantitatively from the Entero-string during DNA purification than in the case of SMI-qC_{12}. On the other hand, analysis of the FM and LM results indicated that the captured *M. tuberculosis* on the surface of the SMI-qC_{12} nanofibers was more easily visualized using FM and LM than in the case of the Entero-string, as the FM images of the Entero-string did not show any captured *M. tuberculosis* and visualization of the captured mycobacteria using LM was not possible due to over-staining of the string polymer. The Entero-string therefore yielded better PCR results and the SMI-qC_{12} nanofibers yielded better FM and LM results.

The work discussed in this chapter therefore confirmed that SMA, modified with a C_{12} aliphatic quaternary ammonium moiety, successfully captured *M. tuberculosis* under low pH conditions through a combination of ionic interaction between the negatively charged *M. tuberculosis* cell wall and the positively charged quaternary ammonium moiety of the functionalized polymer, as well as hydrophobic interaction between the mycolic acids of the *M. tuberculosis* cell wall and the C_{12} hydrocarbon chain of the functionalized polymer. It was also confirmed that the extent of this interaction was dependent on the concentration level of *M. tuberculosis*. A variety of detection methods were used to verify this interaction, namely FM, LM and PCR, with good correlation among the results of these different detection methods.

5.5 Experimental

5.5.1 Analysis techniques

a) Scanning electron microscopy (SEM)

Images of the functionalized SMI fibers were obtained using a Leo® 1430VP Scanning Electron Microscope (SEM). The sample fibers were cut into approximately 1 cm x 1 cm squares and attached onto the SEM stub with double-sided carbon tape. The SEM stubs were then sputter coated with gold under vacuum prior to imaging. The images were analysed using an imaging analysis program, SEM Image Studio, to obtain data regarding the presence of mycobacteria on the surface of the SMI fibers.

b) Fluorescence microscopy (FM)

BCG: Images of the functionalized SMI fibers were obtained using an Olympus IX-81 microscope, coupled to an MT-20 Xenon burner. The samples were placed on a microscope slide and incubated with SYTO-9 nucleic acid and propidium iodide for 15 minutes. The samples were excited using a

Xenon-Arc burner (Olympus Biosystems GMBH) as light source, with the 472 nm or 572 nm excitation filter. Emission was collected using a UBG triple-bandpass emission filter cube.

***M. tuberculosis*:** Images of the functionalized SMI fibers were obtained using an Olympus IX-81 microscope, coupled to an MT-20 Xenon burner. The samples were placed on a microscope slide and incubated with SYTO-9 nucleic acid and propidium iodide for 15 minutes. The stained samples were returned to an eppendorf and heated in a heating block at 85 °C for 20 minutes. The stained samples were returned to a microscope slide and were excited using a Xenon-Arc burner (Olympus Biosystems GMBH) as light source, with the 472 nm or 572 nm excitation filter. Emission was collected using a UBG triple-bandpass emission filter cube.

c) Light microscopy (LM)

The polymer samples were fixed to a microscope slide with 2 drops of albumin fixative and heat set at 85 °C for 2 hours on a heating block. The polymers were covered with carbol fuchsin solution, heated from below using a lit cotton swap until steam started to rise from the slide, and left for 5 minutes. The stained polymers were carefully rinsed with water, taking care that the polymer remained on the slide. The stained polymers were subsequently destained with dilute hydrochloric acid for one minute and counter stained with methylene blue for two minutes. The stained polymers were carefully rinsed with water, taking care that the polymer remained on the slide. The stained slides were air-dried and the samples were viewed using a 100x oil immersion objective.

d) Polymerase chain reaction (PCR)

The primers used were as follows:

BCG: 5'-AAGCGGTTGCCGCCGACCGACC-3', 5'-CTGGCTATATTCCTGGGCCCGG-3' and 5'-GAGGCGATCTGGCGGTTTGGGG-3'.

M. tuberculosis: 5'-CAAGTTGCCGTTTCGAGCC-3', 5'-CAATGTTTGTTGCGCTGC-3' and 5'-GCTACCCTCGACCAAGTGTT-3'.[56]

The PCR reactions were carried out in a total volume of 25 µL, containing 1 µL DNA template, 1 x enzyme buffer, 3.5 mM $MgCl_2$, 4.0 mM dNTP's, 25 pmol of each primer and 0.5 U HotStarTaq DNA polymerase (Qiagen Germany). Amplification was initiated by incubation at 95 °C for 15 min., followed by 45 cycles at 94 °C for 0.5 min., 62 °C for 0.5 min., and 72 °C for 0.5 min. After the last cycle, the samples were incubated at 72 °C for 10 min. PCR amplification products were electrophoretically fractionated in 2.5% agarose in 1xTAE (pH 8·3) at 3·5 V/cm for 4 hours, and visualized by staining with ethidium bromide.

To minimise the risk of laboratory cross-contamination during the PCR amplification, each procedure (preparation of the PCR reaction mixes, the addition of the DNA, the PCR amplification and the electrophoretic fractionation) was conducted in physically separated rooms. Negative controls (water) were included to control for reagent contamination.[56]

5.5.2 Culture

a) BCG

One mL BCG (containing pJV 75 Amber) freezer stock was inoculated in 10 mL Middlebrook 7H9 medium containing 0.2% glycerol, 0.05% Tween-80, 10% ADC and 25 µg/ml kanamycin and grown to an optical density of 0.6-0.8, when measured at 600 nm in a spectrophotometer (OD_{600}). The cells were pelleted by centrifugation at 3000 x g for 10 minutes at 4 °C and resuspended in 10 mL Middlebrook 7H9 medium containing 0.2% glycerol and 10% ADC (no Tween). The centrifugation and resuspension steps were repeated. The cells were inoculated to approximate OD_{600} of 0.05 in 7H9 medium containing 0.2% glycerol, 10% ADC and 25 µg/mL kanamycin (no Tween) (50-100 mL cultures) and grown to approximate OD_{600} of 0.6-0.8 (as the cells clumped in the media without Tween it was difficult to take an accurate OD measurement).

b) *M. tuberculosis*

One mL H37Rv *M. tuberculosis* isolate (harbouring an rpoB531 mutation - confers rifampicin resistance) freezer stock was inoculated in 10 mL Middlebrook 7H9 medium containing 0.2% glycerol, 0.05% Tween-80, 10% ADC and grown to OD_{600} of 0.6-0.8. The cells were pelleted by centrifugation at 3000 x g for 10 minutes at 4 °C and resuspended in 10 mL Middlebrook 7H9 medium containing 0.2% glycerol and 10% ADC (no Tween). The centrifugation and resuspension steps were repeated. The cells were inoculated to approximate OD_{600} of 0.05 in Middlebrook 7H9 medium containing 0.2% glycerol, 10% ADC and 2 µg/mL rifampicin (no Tween) (2 x 50 mL cultures) and grown to approximate OD_{600} of 0.6-0.8 (as the cells clumped in the media without Tween it was difficult to take an accurate OD measurement, but 10-14 days of growth were sufficient to reach the specified OD).

5.5.3 Affinity studies with BCG at neutral pH

A 10 mL aliquot of BCG culture dispersion (pH ~ 7) was pipetted into a tube with a screw lid. A 10 mg piece of functionalized SMI nanofibrous mat was added to the BCG culture in the tube, taking care

that the polymer did not stick to the side of the tube and was moving freely in the culture. The tube was closed and incubated at 37 °C for one hour, whilst shaking. A tube with PBS, instead of BCG culture, was included as negative control. The polymer piece was subsequently removed and washed twice in PBS for 5 minutes and returned to a clean eppendorf tube. BCG-polymer interaction was determined using SEM as detection method.

5.5.4 Affinity studies with BCG at low pH

BCG culture dispersion was decanted from the tissue culture flask into a 250 mL Erlenmeyer flask, equipped with a magnetic stirrer bar. The pH of the BCG culture dispersion was adjusted to 2 by dripping concentrated HCl into the culture whilst stirring on a magnetic stirrer. A 10 mL aliquot of pH-adjusted BCG culture dispersion was pipetted into a tube with a screw lid. A tube with PBS, instead of BCG culture, was included as negative control. A 10 mg piece of functionalized SMI nanofibrous mat was added to the BCG culture in the tube, taking care that the polymer did not stick to the side of the tube and was moving freely in the liquid. The tube was closed and incubated at 37 °C for one hour, whilst shaking. The polymer piece was subsequently removed and washed twice in PBS for 5 minutes and returned to a clean eppendorf tube. BCG-polymer interaction was determined using SEM and FM as detection method.

5.5.5 Time studies with BCG at low pH

BCG culture dispersion was decanted from the tissue culture flask into a 250 mL Erlenmeyer flask, equipped with a magnetic stirrer bar. The pH of the BCG culture dispersion was adjusted to 2 by dripping concentrated HCl into the culture whilst stirring on a magnetic stirrer. A 10 mL aliquot of pH-adjusted BCG culture dispersion was pipetted into 4 tubes with screw lids. A tube with PBS, instead of BCG culture, was included as negative control. A 10 mg piece of functionalized SMI nanofibrous mat was added to each of the tubes, taking care that the polymer did not stick to the side of the tube and was moving freely in the liquid. The tubes were closed and incubated at 37 °C, whilst shaking. After 15 minutes of incubation time, the polymer was removed from one tube and washed twice in PBS for 5 minutes. After 30 minutes of incubation time, another polymer was removed from a tube and washed twice with PBS and returned to a clean eppendorf tube. The same procedure was followed after 45 minutes and 60 minutes of incubation time. BCG-polymer interaction was determined using SEM and FM as detection method.

5.5.6 Concentration studies with BCG at low pH

BCG culture dispersion was decanted from the tissue culture flask into a 250 mL Erlenmeyer flask, equipped with a magnetic stirrer bar. The pH of the BCG culture dispersion was adjusted to 2 by dripping concentrated HCl into the culture whilst stirring on a magnetic stirrer. The resulting pH-adjusted culture dispersion was diluted serially 1:10 in PBS, from approximately 10^8 BCG/mL to 10 BCG/mL. Aliquots of 10 mL of the final dispersion were pipetted into tubes with screw lids. A tube with PBS, instead of BCG culture, was included as negative control. A 10 mg piece of functionalized SMI nanofibrous mat was added to each of the tubes, taking care that the polymer did not stick to the side of the tube and was moving freely in the liquid. The tubes were closed and incubated at 37 °C for one hour, whilst shaking. The polymer pieces were subsequently removed and washed twice in PBS for 5 minutes and returned to a clean eppendorf tube. BCG-polymer interaction was determined using SEM, FM and PCR (after DNA extraction) as detection method.

PCR: DNA extraction:

Proteinase K (10 µL of 10 mg/mL) was added to each tube and incubated overnight at 42 °C. The tubes with polymer were removed from the oven and equal volumes of buffer 2 containing guanidine hydrochloride were added to each tube containing a washed polymer sample ~ 200 µL. NucliSENSE lysis buffer (1.6 mL) was added to each tube. After vortexing and incubating the tubes for 30 minutes, they were centrifuged and the polymer was removed.

The silica suspension was subsequently vortexed and a 50 µL aliquot was added to each of the lysed samples. Thereafter, the tubes were briefly vortexed immediately and left for 10 minutes without mixing. The tubes were centrifuged for 2 minutes at 1500g and the supernatant was carefully decanted. The silica was washed as follows:

- 400 µL **wash buffer 1** for 30 seconds,

- 500 µL **wash buffer 2** to each of the test tubes and wash for 30 seconds.

- 500 µL **wash buffer 2** to each of the test tubes and wash for 30 seconds.

- 500 µL **wash buffer 3** to each of the test tubes and wash for 15 seconds.

- 50 µL **elution buffer** onto the silica pellet in the micro tubes and close the caps.

The tubes were placed in the Thermoshaker and incubated for 5 minutes at 60 °C at 1400 rpm to elute any nucleic acid from the silica. Thereafter the tubes were placed in the miniMAG and the magnet was placed close to the silica to compact it. The supernatant containing the extracted nucleic acid was transferred to a fresh clean tube, properly marked. Care was taken not to transfer any silica particles.

The extracted nucleic acid was amplified using PCR: PCR stock solution was prepared as per 5.5.1(d). Two additional tubes were added, one with 2 µL of lysed BCG as positive control and one with RNA-nuclease free water as negative control. All the tubes were loaded into the DNA Thermal cycler and the machine was set to run for 45 cycles as per 5.5.1(d).

The presence of the PCR products were determined by electrophoresing 10 µL of the reaction product on a 2.5% agarose gel in 1XTAE buffer at 5 V/cm for 4 hours. 5 µL of a 100 bp DNA size marker was co-electrophoresed. The gel was stained with ethidium bromide (50 µL (10mg/mL stock solution) added to 1700 mL TAE buffer) and photographed under UV to visualize.

5.5.7 Concentration studies with *M. tuberculosis* at low pH

M. tuberculosis culture dispersion was decanted from the tissue culture flask into a tube and centrifuged at 3000 rpm for 15 minutes. The supernatant was discarded and the pellet was resuspended in pH 2-adjusted PBS (pH adjustment done using concentrated HCl) to a total volume of 50 mL. The resulting pH-adjusted culture dispersion was diluted serially 1:10 in pH 2-adjusted PBS, from approximately 10^8 *Mtb*/mL to 10 *Mtb*/mL. Aliquots of 10 mL of the final dispersion were pipetted into tubes with screw lids. A tube with PBS, instead of *M. tuberculosis* culture, was included as negative control. A 10 mg piece of polymer was added to each of the tubes, taking care that the polymer did not stick to the side of the tube and was moving freely in the culture. The tubes were closed and incubated at 37 °C for one hour, whilst shaking. The polymer piece was subsequently removed and washed twice in PBS for 5 minutes and returned to a clean eppendorf tube. *M. tuberculosis*-polymer interaction was determined using FM, LM and PCR (after DNA extraction) as detection methods.

The same DNA extraction procedure was followed as detailed in 5.5.6, using lysed *M. tuberculosis* as positive control.

5.6 References

1. Corrigan, D.L.; Paton, J.Y. *Breathe* **2007**, 3, 351-363.

2. Marais, B.J.; Pai, M. *Br. Med. J*. **2007**, *92*, 446-452.

3. Brennan, P.J. *Tuberculosis* **2003**, *83*, 91-97.

4. Kolattukudy, P.E.; Fernandes, N.D.; Azad, A.K.; Fitzmaurice, A.M.; Sirakova, T.D. *Mol. Microbiol.* **2003**, *24*, 263-270.

5. Maeda, N.; Nigou, J.; Herrmann, J.L.; Jackson, M.; Amara, A.; Lagrange, P.H.; et al. *J. Biol. Chem*. **2003**, *278*, 5513-5516.

6. Rezwan, M.; Lanéelle, M.A.; Sander, P.; Daffé, M. *J. Microbiol. Methods* **2007**, *68*, 32-39.

7. Tailleux, L.; Schwartz, O.; Herrmann, J.L.; Pivert, E.; Jackson, M.; Amara, A.; et al. *J. Exp. Med*. **2003**, *197*, 121-127.

8. Brosch, R.; Gordon, S.V.; Marmiesse, M.; Brodin, P.; Buchrieser, C.; Eiglmeier, K.; et al. *Proc. Natl. Acad. Sci. USA* **2002**, *99*, 3684-3689.

9. Geijtenbeek, T.B.H.; Van Vliet, S.J.; Koppel, E.A.; Sanchez-Hernandez, M.; et al. *J. Exp. Med*. **2003**, *197*, 7-17.

10. Van Kooyk, Y.; Geijtenbeek, T.B.H. *Nature Rev. Immunol.* **2003**, *3*, 697-709.

11. Nascimento, I.P.; Dias, W.O.; Mazzantini, R.P.; Miyaji, E.N.; Gamberini, M.; Quintilio, W.; et al. *Infect. Immun*. **2000**, *68*, 4877-4883.

12. Mikhailovich, V.; Lapa, S.; Gryadunov, D.; Sobolev, A.; Strizhkov, B.; Chernyh, N.; et al. *J. Clin. Microbiol.* **2001**, *39*, 2531-2540.

13. Malbruny, B.; Le Marrec, G.; Courageux, K.; Leclercq, R.; Cattoir, V. *Int. J. Tuberc. Lung Dis.* **2011**, *15*, 553-555.

14. Lemaire, J.F.; Casenghi, M. *J. Int. AIDS Soc.* **2010**, *13*, 1-7.

15. Kuhn, W.; Armstrong, D.; Atteberry, S.; Dewbrey, E.; Smith, D.; Hooper, N. *The Open Microbiology Journal* **2010**, *4*, 30-33.

16. Perkins, M.D.; Roscigno, G.; Zumla, A. *Lancet* **2006**, *367*, 942-943.

17. Cortesia, C.; Lopez, G.J.; de Waard, J.H.; Takiff, H.E. *J. Antimicrob. Chemother*. **2010**, *65*, 2574-2581.

18. Endo, Y.; Tani, T.; Kodama, M. *Appl. Environ. Microbiol*. **1987**, *53*, 2050-2055.

19. Kenawy, E.R.; Worley, S.; Broughton, R. *Biomacromolecules* **2007**, *8*, 1359-1384.

20. Yao, C.; Li, X.; Neoh, K.; Shi, Z.; Kang, E. *J. Membr. Sci.* **2008**, *320*, 259-267.

21. Boulos, L.; Prévost, M.; Barbeau, B.; Coallier, J.; Desjardins, R. *J. Microbiol. Methods* **1999**, *37*, 77-86.

22. Jarlier, V.; Nikaido, H. *FEMS Microbiol. Lett.* **1994**, *123*, 11-18.

23. Barry, C.E.; Lee, R.E.; Mdluli, K.; Sampson, A.E.; Schroeder, B.G.; Slayden, R.A.; et al. *Prog. Lipid Res*. **1998**, *37*, 143-179.

24. Ojha, A.K.; Baughn, A.D.; Sambandan, D.; Hsu, T.; Trivelli, X.; Guerardel, Y.; et al. *Mol. Microbiol.* **2008**, *69*, 164.

25. Dahl, J.L.; *Can. J. Microbiol*. **2005**, *51*, 277-281.

26. Albertin, L.; Stenzel, M.H.; Barner-Kowollik, C.; Foster, L.J.R.; Davis, T.P. *Macromolecules* **2005**, *38*, 9075-9084.

27. Baskaran, S.; Grande, D.; Sun, X.L.; Yayon, A.; Chaikof, E.L. *Bioconjugate Chem*. **2002**, *13*, 1309-1313.

28. Guan, R.; Sun, X.L.; Hou, S.; Wu, P.; Chaikof, E.L. *Bioconjugate Chem.* **2004**, *15*, 145-151.

29. Miura, Y. *J. Pol. Sci.* **2007**, *45*, 5031-5036.

30. Menozzi, F.D.; Rouse, J.H.; Alavi, M.; Laude-Sharp, M.; Muller, J.; Bischoff, R.; et al. *J. Exp. Med*. **1996**, *184*, 993-1001.

31. Middleton, A.M.; Chadwick, M.V.; Nicholson, A.G.; Dewar, A.; Groger, R.K.; Brown, E.J.; et al. *Respir. Med*. **2004**, *98*, 1203-1206.

32. Espitia, C.; Laclette, J.P.; Mondragon-Palomino, M.; Amador, A.; Campuzano, J.; Martens, A.; et al. *Microbiology* **1999**, *145*, 3487-3495.

33. David, G.; Bernfield, M. *Matrix Biol*. **1998**, *17*, 461-463.

34. Pethe, K.; Alonso, S.; Biet, F.; Delogu, G.; Brennan, M.J.; Locht, C.; et al. *Nature* **2001**, *412*, 190-194.

35. Abou-Zeid, C.; Ratliff, T.L.; Wiker, H.G.; Harboe, M.; Bennedsen, J.; Rook, G.A. *Infect. Immunol*. **1988**, *56*, 3046-3051.

36. Alteri, C.J.; Xicohténcatl-Cortes, J.; Hess, S.; Caballero-Olín, G.; Girón, J.A.; Friedman, R.L. *Proc. Natl. Acad. Sci.* **2007**, *104*, 5145-5150.

37. Delogu, G.; Brennan, M.J. *J. Bacteriol*. **1999**, *181*, 7464-7469.

38. Brewer, C.F.; Brown, III R.D. *Biochemistry (N Y)* **1979**, *18*, 2555-2562.

39. Nigou, J.; Gilleron, M.; Puzo, G. *Biochimie* **2003**, *85*, 153-166.

40. Naismith, J.H.; Field, R.A. *J. Biol. Chem*. **1996**, *271*, 972-976.

41. Swaminathan, C.P.; Surolia, N.; Surolia, A. *J. Am. Chem. Soc.* **1998**, *120*, 5153-5159.

42. Sato, K.; Imoto, Y.; Sugama, J.; Seki, S.; Inoue, H.; Odagiri, T.; et al. *Langmuir* **2005**, *21*, 797-799.

43. Auer, H.E.; Schilz, T. *Int. J. Pept. Protein Res*. **1984**, *24*, 569-579.

44. Arrondo, J.L.R.; Young, N.M.; Mantsch, H.H. *Biochim. Biophys. ACTA* **1988**, *952*, 261-268.

45. Chatterjee, A.; Mandal, D.K. *Biochim. Biophys. ACTA* **2003**, *1648*, 174-183.

46. Wilson, S.; Lane, A.; Rosedale, R.; Stanley, C. *Int. J. Tuberc. Lung Dis.* **2010**, *14*, 1164-1168.

47. Brennan, P.J. *Rev. Infect. Dis*. **1989**, *11*, 420-430.

48. Chatterjee, D. *Curr. Opin. Chem. Biol*. **1997**, *1*, 579-588.

49. Kim, C.H.; Choi, J.W.; Chun, H.J.; Choi, K.S. *Polymer Bulletin* **1997**, *38*, 387-393.

50. Qin, C.; Xiao, Q.; Li, H.; Fang, M.; Liu, Y.; Chen, X.; et al. *Int. J. Biol. Macromol*. **2004**, *34*, 121-126.

51. Roy, D.; Knapp, J.S.; Guthrie, J.T.; Perrier, S. *Biomacromolecules* **2007**, *9*, 91-99.

52. Graham, S.M. *Lancet Infect. Dis*. **2010**, *10*, 581-582.

53. Hesseling, A.C.; Schaaf, H.S.; Gie, R.P.; Starke, J.R.; Beyers, N. *Int. J. Tuberc. Lung Dis.* **2002**, *6*, 1038-1045.

54. Nicol, M.P.; Zar, H.J. *Paediatr. Respir. Rev.* **2011**, *12*, 16-21.

55. Mapstone, N.; Lynch, D.; Lewis, F.; Axon, A.; Tompkins, D.; Dixon, M.; et al. *J. Clin. Pathol*. **1993**, *46*, 540-543.

56. Warren, R.; Gey, P.N.C.; Barnard, M.; Hesseling, A.; Engelke, E.; De Kock, M.; et al. *Int. J. Tuberc. Lung Dis.* **2006***, 10,* 818-822.

Chapter 6: Conclusions and recommendations for future research

6.1 Conclusions

The synthesis and characterization of a variety of functionalized poly(styrene-*co*-maleimide) (SMI) nanofibers were presented in this thesis. All these functionalized SMI nanofibers were initially evaluated as a capturing platform for the bacillus Calmette-Guérin strain of *Mycobacterium bovis* (BCG) at different pH values. BCG was used as *M. tuberculosis*-mimic due to the pathogenicity of *M. tuberculosis*. One of these functionalized nanofibers was subsequently selected and evaluated as a capturing platform for *Mycobacterium tuberculosis* (*M. tuberculosis*) in a low pH environment. The main findings and recommendations are discussed in this chapter.

6.1.1 Polymer modification

Poly(styrene-*co*-maleic anhydride) (SMA) was modified with a variety of compounds to yield modified SMI derivatives and electrospun to produce functionalized polymer nanofibers. Some of the functionalized SMI nanofibers were prepared by surface-functionalization of the polymer nanofibers after electrospinning and some by modification of the polymer before electrospinning.

Two SMA copolymer grades were used for the surface-functionalization of the polymer nanofibers, namely a commercially available poly(styrene-*co*-maleic anhydride) (P(St-*co*-MAnh)) and an alternating poly(styrene-*alt*-maleic anhydride) (P(St-*alt*-MAnh)), successfully synthesized using conventional free radical copolymerization. P(St-*alt*-MAnh), with a 50% maleic anhydride content, was yielded with a dispersity of 2.7 and a weight average molecular weight (M_w) 128 000 g/mol.

P(St-*alt*-MAnh) and P(St-*co*-MAnh) were successfully electrospun into nanofibrous mats and characterized using scanning electron microscopy (SEM). Analysis of these SEM images indicated that nanofibers were produced with an average fiber diameter in the region of 680 nm.

These pristine P(St-*co*-MAnh) and P(St-*alt*-MAnh) nanofibers were subsequently successfully surface functionalized with a variety of surface-functionalization agents via nucleophilic acyl substitution. These surface-functionalization agents had a primary amine moiety that reacted with the maleic anhydride group of SMA through a ring-opening amidation reaction and comprised amino sugars (D-(+)-glucosamine (Gluc) and D-(+)-mannosamine (Man)), an amino acid derivative (N_α,N_α-bis(carboxymethyl)-L-lysine hydrate (BCML)), a protein (Concanavalin A (Con A)) and a variety of tertiary amines (*N*-dodecyl-*N*-propyl-propane-1,3-diamine (tC_{12}) and *N*-hexadecyl-*N*-propyl-propane-1,3-diamine (tC_{16})) and quaternary ammonium compounds (*N,N*-didodecyl-*N*-propyl-propane-1,3-diamine (qC_{24}) and *N,N*-dihexadecyl-*N*-propyl-propane-1,3-diamine (qC_{32})). Ring closure was successfully achieved through the application of heat and corresponding loss of water to yield SMI-Gluc, SMI-Man, SMI-BCML, SMI-Con A, SMI-tC_{12}, SMI-tC_{16}, SMI-qC_{24} and SMI-qC_{32}. The solvent

system for the surface-functionalization procedure varied for the P(St-*co*-MAnh) and P(St-*alt*-MAnh) nanofibers when the surface-functionalization agents were of low molar mass (< 284 g/mol), but became similar when the surface-functionalization agents increased in size due to the polar character of the surface-functionalization agent playing the dominant role, and not that of the polymer anymore. The P(St-*alt*-MAnh) nanofibers functionalized with BCML, tC_{12}, tC_{16}, qC_{24} and qC_{32} were further successfully crosslinked using a heat treatment step at 130 °C under vacuum. This heat treatment step rendered the functionalized P(St-*alt*-MAnh) nanofibers insoluble in water and was essential for the preservation of the P(St-*alt*-MAnh) nanofibrous structure when immersed in water for extended periods. The functionalized P(St-*co*-MAnh) nanofibers were already insoluble in water due to the hydrophobic nature of the polymer backbone and did not require an additional heat-induced crosslinking step.

The synthesized surface-functionalization agents were characterized using ^{1}H-NMR and ^{13}C-NMR spectroscopy. The successful functionalization of the P(St-*co*-MAnh) and P(St-*alt*-MAnh) nanofibers was confirmed with attenuated total reflectance Fourier transform infrared spectroscopy (ATR-FTIR). Results revealed that the P(St-*alt*-MAnh) nanofibers were surface-functionalized at higher conversion percentages than the P(St-*co*-MAnh) nanofibers, which indicated that the size of the surface-functionalization agent and the difference in spatial orientation between the alternating maleic anhydride units of P(St-*alt*-MAnh) and the maleic anhydride units of P(St-*co*-MAnh) played a significant role in the surface-functionalization reaction. SEM was used to confirm the preservation of the nanofibrous structure after functionalization. The average fiber diameter of the pristine SMA fibers increased slightly after surface-functionalization as a result of the covalent bond formed between the polymer and surface-functionalization agent. These increases were however only marginal and fell within the standard deviation of the measured average fiber diameter and were thus not considered significant.

P(St-*alt*-MAnh) was also successfully modified before electrospinning with a variety of N-alkylamine compounds via an amidization reaction. These N-alkylamine compounds comprised dodecylamine (C_{12}), hexadecylamine (C_{16}) and 3-(*N,N*-dimethylamino)-1-propylamine (tC). After heat-induced ring-closure, styrene-[*N*-dodecyl-maleimide] copolymer (SMI-C_{12}), styrene-[*N*-hexadecyl-maleimide] copolymer (SMI-C_{16}) and styrene-[*N*-3-(*N',N'*-dimethylamino)propyl maleimide] copolymer (SMI-tC) were successfully yielded. SMI-tC was used as precursor and underwent an additional substitution reaction with C_2, C_{12} and C_{16} bromoalkane compounds to yield SMI derivatives, modified with an aliphatic quaternary ammonium moiety with various aliphatic chain lengths, namely styrene-[*N*-3-(*N*'-ethyl-*N',N'*-dimethylammonium) propyl maleimide] copolymer (SMI-qC_2), styrene-[*N*-3-(*N*'-dodecyl-*N',N'*-dimethylammonium) propyl maleimide] copolymer (SMI-qC_{12}) and styrene-[*N*-3-(*N*'-hexadecyl-*N',N'*-dimethylammonium) propyl maleimide] copolymer (SMI-qC_{16}). These modified SMI polymers were subsequently successfully electrospun to yield nanofibers with an average fiber diameter in the region of 580-755 nm. The SMI-qC_2, SMI-qC_{12} and SMI-qC_{16} nanofibers were further successfully crosslinked using heat treatment at 130 °C under vacuum to preserve the nanofibrous structure of the electrospun modified SMI polymer when immersed in water for prolonged periods.

The successful modification of P(St-*alt*-MAnh) was confirmed with ^{1}H-NMR and ^{13}C-NMR spectroscopy and the electrospun nanofibers were characterized using ATR-FTIR and SEM.

6.1.2 Affinity studies

Affinity studies were conducted between the different functionalized SMI nanofibers and two mycobacterium strains, namely BCG and *M. tuberculosis,* to determine whether the mycobacteria could be captured onto the surface of the modified SMI nanofibers in a low pH environment.

a) BCG

BCG, used initially as non-pathogenic *M. tuberculosis*-mimic, was successfully captured onto the surfaces of the SMI nanofibers, functionalized with amino sugars (SMI-Gluc/Man), an amino acid derivative (SMI-BCML), a protein (SMI-Con A) and a C_{12} aliphatic quaternary ammonium group (SMI-qC_{12}), respectively, at neutral pH. After the pH was decreased to two to simulate gastric conditions, BCG was successfully captured onto the surface of the SMI-qC_{12} nanofibers.

This result prompted an investigation between BCG and the SMI nanofibers, modified with a variety of N-alkylamines of varying aliphatic chain lengths and N-functionalities to determine which N-functionality/aliphatic chain length combination captured BCG most effectively. The SMI nanofibers functionalized with a C_{12} and C_{16} aliphatic tertiary amine group, namely SMI-tC_{12} and SMI-tC_{16}, as well as a C_{12}, C_{16}, C_{24} and C_{32} aliphatic quaternary ammonium group, namely SMI-qC_{12}, SMI-qC_{16}, SMI-qC_{24} and SMI-qC_{32}, captured BCG successfully. Of these, SMI-qC_{12} and SMI-qC_{16} proved more effective than the others did. Subsequent concentration and time studies between SMI-qC_{12} and SMI-qC_{16}, respectively, and BCG revealed that SMI-qC_{12} was the most effective BCG-capturing platform and that the extent of this interaction was dependent on incubation time and concentration of BCG.

The successful capture of BCG onto the surfaces of the various functionalized nanofibers was confirmed by SEM and FM. Analysis of these SEM and FM images also revealed that BCG aggregated into clusters and interacted as such with the SMI-qC_{12} nanofibrous surface. This interaction between BCG and SMI-qC_{12} is due to the ionic interaction between the negatively charged BCG cell wall and the positively charged quaternary ammonium moiety of the functionalized polymer, as well as the hydrophobic-hydrophobic interaction between the mycolic acids of the BCG cell wall and the aliphatic C_{12} hydrocarbon chains of the functionalized polymer. Analysis of the FM images further revealed that SMI-qC_{12} has antimicrobial properties as indicated by the colour of the mycobacteria captured onto the nanofibrous surface when stained for FM imaging.

The results of the affinity studies between the functionalized nanofibers and BCG also indicated that the synthetic route used to prepare the functionalized polymer nanofibers did not influence the outcome of the affinity studies with regard to the effectivity of the functionalized nanofibers as BCG-capturing platform.

Finally, it appeared as if the polymer used for the nanofibrous capturing platform must not be too hydrophobic in character as this caused poor wetting of the functionalized nanofibers, thus preventing close contact with the mycobacteria and a reduction in the capture effectivity of the polymer nanofibers.

b) *Mycobacterium tuberculosis*

Subsequent affinity studies between *M. tuberculosis* and SMI-qC_{12} at pH 2 indicated that *M. tuberculosis* was successfully captured onto the nanofibrous surface of SMI-qC_{12} under low pH conditions. The successful capture of *M. tuberculosis* onto the SMI-qC_{12} nanofibrous surface was confirmed by fluorescence microscopy (FM), light microscopy (LM) and polymerase chain reaction (PCR), with good correlation among the results of the different detection methods. The interaction between *M. tuberculosis* and SMI-qC_{12} is due to the same reasons as for BCG's interaction with SMI-qC_{12} and the extent of this interaction was dependent on the concentration level of *M. tuberculosis*.

The detection of *M. tuberculosis* using FM and LM as detection methods was simplified by the tendency of *M. tuberculosis* to clump together in clusters on the hydrophobic surface of the SMI-qC_{12} nanofibers. The microbes were not spread out and did not need to be identified individually. As a result of this clustering, FM and LM are therefore feasible detection methods to image *M. tuberculosis* on the surface of the SMI-qC_{12} nanofibers, even at relative low concentration of *M. tuberculosis*.

6.2 Recommendations for future research

The results presented in this study indicated the potential of the SMI nanofibers functionalized with a C_{12} aliphatic quaternary ammonium moiety as a capturing platform for *M. tuberculosis*. Further development and optimization of the capturing polymer however need to be considered and will require further research. These can be summarized as follows:

In terms of the modified polymer:

- The results of the affinity studies indicated that the polymer used for the capturing platform should not be too hydrophobic, as this appears to reduce the effective wetting of the polymer nanofibers to ensure close contact with the mycobacteria. Although good results were

obtained with SMI-qC_{12}, it is worth investigating the effect of quaternization done with a C_8 or C_{10} hydrocarbon chain on the interaction between *M. tuberculosis* and the relevant functionalized polymer. There may be an interplay between the wettability of the capturing polymer nanofibers and the degree of hydrophobicity required to facilitate mycobacterial capture.

- The results of some of the affinity studies created the impression that there may be low affinity between the mycobacteria and the SMI-qC_{12} nanofibrous surface at low concentration levels of the mycobacteria. This phenomenon will have to be investigated and the polymer modification adapted if necessary. A polymer modified with a combination of C_8/C_{10} and C_{12} hydrocarbon chains may be a possible way of increasing the interaction between the mycobacteria and the modified polymer's nanofibrous surface, whilst still maintaining a certain degree of hydrophobicity.
- Preliminary tests indicated low cytotoxicity for SMI-qC_{12} nanofibrous mats. Low cytotoxicity is crucial considering the potential use of the polymer, i.e. as a key component in an *M. tuberculosis* specimen collection device. For biomedical applications of SMI-q$C_{12,}$ further tests are required using Methylthiazol Tetrazolium (MTT) assays to confirm the biocompatibility of SMI-qC_{12}.

In terms of the detection methods:

- Although there was good correlation among the results of FM, LM and PCR, the results were not identical, as the PCR did not show amplification at all the low concentration levels of *M. tuberculosis*, whilst FM and LM showed captured *M. tuberculosis* on the surface of the SMI-qC_{12} nanofibers at these low concentration levels of *M. tuberculosis*. A possible reason for this result may be that the *M. tuberculosis* DNA was not properly released during the DNA extraction and purification process, which affected the amplification results more significantly at the lower concentration levels where there is less DNA than at the higher concentration levels. Further work is therefore required to optimize the DNA extraction and purification process to ensure that all the *M. tuberculosis* DNA is released from the polymer nanofibers for detection using PCR.

In terms of the *M. tuberculosis* specimen collection device:

- The development of an *M. tuberculosis*-capturing polymer, spun as nanofibers, is the first step towards the design of an *M. tuberculosis* specimen collection device. Although a design for the *M. tuberculosis* specimen collection device has been proposed, a working prototype of this device must still be completed and tested.

Acknowledgements

First and most importantly, I would like to thank God for putting me on this road and blessing me with this opportunity! I know that He gave me strength and guidance in times of despair and the belief that I can do this. He blessed me with the gift of life and the enjoyment thereof.

To my supervisor, Bert Klumperman, your guidance, support and encouragement during this time of study were invaluable. You were a great supervisor, always available for a short meeting and quick turnaround times on e-mails. Thank you so much!

To Rob Warren, your time and effort spent with me, teaching me the wonderful ways of molecular biologists is more appreciated than I can say. You were always willing and ready to help and provide guidance when needed. I thank you for your endless assistance, critical thinking and constructive criticism.

From a financial viewpoint, I would like to thank the University of Stellenbosch, National Research Foundation and CRDF for financial support.

Aan Johan Malherbe, jy is die eerste persoon by wie ek kom aanklop het vir hulp omdat ek so verroes was in die laboratorium. Baie dankie vir jou geduld, tyd, hulp en ondersteuning. Dankie vir die heerlike geselsies, jou vaste vertroue in my vermoëns en die verrassings e-posse van jou met stukkies inligting wat ek kon gebruik in my studie.

Aan Adine, baie dankie vir jou ondersteuning in hierdie tyd wat ek besig was met my studie. Ek besef ek het soms geskitter in my afwesigheid, maar jy het altyd verstaan en geduld gehad.

Many thanks to Gareth Arnott for allowing me to do my synthetic work in his laboratory while the Polymer Science building was being renovated.

I would like to take this opportunity to thank the following people for their contributions to this project:

Ben Loos (and Lize Engelbrecht) for their input and effort to get the best FM images. Thank you!

Madeleine Frazenberg for SEM analysis and her special effort to get me some stunning images.

Elsa Malherbe for your willingness to help and special effort to forward the spectra as quickly as possible. I always think about you on a Friday!

Mae Newton-Foot and Carol van Reenen for all the BCG cultures that you have grown for me. It is much appreciated.

Osama Bshena for his assistance, encouragement and fruitful discussions for which I am deeply grateful. You have evened out many bumps in my road!

Erinda Cooper, Aneli Fourie, Deon Koen, Calvin Maart and Jim Motshweni for their commitment to ensuring that everything runs like a well-oiled machine.

Aan Danie, baie dankie vir jou eindelose ondersteuning en vaste vertroue in my. Dankie vir jou simpatieke oor as dinge nie so goed gegaan het nie. En dankie vir die ure wat jy spandeer het om my werk te proeflees. Ek waardeer dit meer as wat woorde kan sê. Jy is my anker!

Aan Michele, wat elke laboratorium waar ek gewerk het ken omdat jy na skool saam moes teruggaan lab toe omdat “iets” nog nie klaar was nie. Baie dankie vir jou eindelose geduld, gogga!

Laastens, wil ek my ouers bedank vir julle onvoorwaardelike liefde, ondersteuning en geloof in my. Julle het vir geen oomblik getwyfel in my vermoëns nie. Ek is lief vir julle!